Insights into the evolution of Late Cretaceous metatherian mammals of North America: interpreting feeding ecologies using quantitative analyses

Alexandria L. Brannick

A dissertation

submitted in partial fulfillment of the

requirements for the degree of

Doctor of Philosophy

University of Washington

2021

Reading Committee:

Gregory P. Wilson Mantilla, Chair

Sharlene E. Santana

Christian A. Sidor

Program Authorized to Offer Degree:

Biology

University of Washington

Abstract

Insights into the evolution of Late Cretaceous metatherian mammals of North America: interpreting feeding ecologies using quantitative analyses

Alexandria L. Brannick

Chair of the Supervisory Committee:
Dr. Gregory P. Wilson Mantilla
Department of Biology

Metatherian mammals (the stem-based clade of extant marsupials and their closest relatives) were important members of North American communities during the Late Cretaceous: they were both taxonomically rich and numerically abundant. Previous studies have mostly focused on taxonomic diversity measures, which provide important information regarding ecosystem dynamics, but less attention has been devoted to understanding the ecology of this group of mammals. This dissertation seeks to add to our growing knowledge of both the anatomy and associated ecologies (i.e., ecomorphology) that North American metatherians possessed during the Late Cretaceous. I specifically focus on interpreting diet and feeding ecology because the fossil record of North American metatherians is mainly composed of teeth and tooth bearing elements. In the first study, I describe rare, new cranial fossils of the metatherian *Alphadon*

halleyi that were discovered at the Egg Mountain locality (Montana, USA). These specimens represent some of the most complete cranial material for any North American metatherian. My co-authors and I use this new anatomical information to score previously unknown characters for *A. halleyi* and subsequently conduct a phylogenetic analysis in order to reassess the phylogenetic relationships among metatherians. Our results conflict with recent phylogenetic analyses and demonstrate that the place of origin of Marsupialia (crown marsupials) remains elusive.

The remaining two studies of this dissertation concentrate on the ecomorphology of North American metatherians. My co-authored study of the evolution of durophagy (hard-object feeding) in stagodontid metatherians utilizes a relatively new method that quantifies biomechanical properties of the dentary (jaw). We apply beam theory to estimate bending force capabilities of dentaries of stagodontids and other metatherians. We find that the jaws of the two species of the stagodontid *Eodelphis* had different bending force profiles from each other and from the durophagous stagodontid *Didelphodon*. The jaw of *E. browni* was not adapted toward withstanding bending forces associated with durophagous habits, whereas the jaw of *E. cutleri* was adapted toward withstanding mediolateral bending forces associated with durophagy. However, the jaw of *E. cutleri* lacked other dorsoventral buttressing associated with exceptionally high bite forces of *Didelphodon*. Our results imply that Cretaceous metatherians had a wide range of feeding behaviors and some morphological changes associated with durophagy evolved twice within this clade, independently in *E. cutleri* and *Didelphodon*.

Finally, my co-authored study on the dental ecomorphology of North American Late Cretaceous metatherians aims to take a more synoptic approach at examining the dental morphology of these animals. We use three-dimensional dental topographic analysis to predict the diets of metatherians to try to understand macroevolutionary patterns in dental morphology

and dietary diversity. Although our results show that dental disparity and dietary diversity did not significantly change throughout the Late Cretaceous and that most metatherians were insectivorous, we also found that metatherians occupied a wide range of dietary niches. Metatherians were also arguably the most dietarily diverse of any mammalian clade of the Late Cretaceous. Our results also indicate that this ecological diversification was more correlated in time with the Cretaceous Terrestrial Revolution and the mid-Cretaceous taxonomic diversification of angiosperms. Overall, this dissertation serves to bolster our knowledge of ecological roles metatherians filled during the Late Cretaceous in North America. My results reinforce the concept that different proxies, when available, should be used to better infer ecology and further demonstrate that metatherians were more ecologically diverse than previously appreciated.

TABLE OF CONTENTS

LIST OF FIGURES

CHAPTER 2: NEW CRANIAL SPECIMENS OF *ALPHADON HALLEYI*, SAHNI 1972 FROM EGG MOUNTAIN AND THEIR IMPLICATIONS FOR METATHERIAN EVOLUTION

CHAPTER 3: NEW SPECIMENS OF THE LATE CRETACEOUS METATHERIAN *EODELPHIS* AND THE EVOLUTION OF HARD-OBJECT FEEDING IN THE STAGODONTIDAE

CHAPTER 4: DENTAL ECOMORPHOLOGY AND MACROEVOLUTIONARY PATTERNS OF LATE CRETACEOUS NORTH AMERICAN METATHERIANS

LIST OF TABLES

ACKNOWLEDGEMENTS

There are many people—family, friends, and colleagues—I would like to thank. My dissertation would not have been possible without all of them. I would first like to thank my advisor, Greg Wilson Mantilla, for his continued support and guidance throughout my graduate career. He afforded me many research opportunities and for that, I'm infinitely thankful. His diligence and carefulness throughout the process of conducting research, as well as his emphasis on the importance of being able to clearly communicate science, has made me a better scientist, writer, and communicator. He took a chance on me by taking me on as a graduate student after meeting me at the 2013 SVP meeting—I've learned so much from him since then. I also would like to thank my other committee members, Sharlene Santana, Christian Sidor, and Tracy Popowics, for their support. Both their input and advice on my work were vital to my development as a scientist. Additionally, I am immensely grateful to Karen Petersen and Casey Self. I had the pleasure of being a TA for Karen many times and during those courses, she fostered my love of teaching. She allowed me to explore who I wanted to be as an instructor and instilled in me the importance of pedagogy. She became one of my closest mentors and her willingness to listen and provide advice—on everything from implementing new teaching practices to navigating mental health—has made an everlasting positive impact on me. Plus, we always had a lot of fun in her classes too! I also was a TA for Casey several times. She helped me further develop my skills as an instructor. Her dedication to her students and education is contagious. I was able to help design course material for her Human Anatomy course when classes switched to being online during 2020–2021, and that was a pivotal experience for me in my teaching career.

I am extremely fortunate to have had several other academic cheerleaders throughout my PhD journey. It was an absolute honor to work with and get to know Bill Clemens, who passed away at the end of 2020. Not only was he a giant in the world of paleontology with an endless vat of knowledge, but he was incredibly kind and generous as well. Being my advisor's advisor, Bill treated all of Greg's graduate students as if they were his own—he was invested in all our successes. I will always cherish my memories of him checking in on me during my visits to the UCMP, sharing photos of fossil mammal teeth with each other, and tromping around the Montana outcrops together with the rest of the field crew. I'm also grateful to Dave Varricchio for his guidance and support. He let me crash his fieldwork operation at Egg Mountain for two summers and I gained invaluable field experience there. Learning about the history of the site from him was a highlight for me. It has been awesome to work with him on so many different avenues of research regarding the fossil material from this incredible locality. Jason Moore caught me up to speed on the geology of Egg Mountain during my first field trip there, and it was always fun to catch up and talk Egg Mountain when we ran in to each other at conferences. I also became quick friends with William Freimuth at Egg Mountain, and it has been wonderful collaborating with him on the Egg Mountain projects. Mark Goodwin, Randy Irmis, and Tadesse Alemu were amazingly patient with me during our fieldwork trip to Ethiopia together. Their support and encouragement were extremely valuable to me during that experience. I learned a lot from them about the intricacies of conducting fieldwork in a place other than the USA. Robin O'Keefe and Julie Meachen were my advisors during my master's degree—without them, I would have never made it to UW. Robin had me dive head-first into a big research project and let me figure out how to get things done. This experience better prepared me for my PhD research. Julie has been a close mentor to me; she guided me through my first data collection trip

as a master's student and she's always been there to provide advice whenever I needed it—even after I moved on to UW. Finally, the Lafayette College Geology Department is the first place I ever genuinely felt like a scientist. The faculty there are amazing and incredibly dedicated to their undergraduates—it is truly a special place to be a student. More specifically, Lawrence Maliconico, Kira Lawrence, and Dave Sunderlin were all Lafayette professors that inspired me to apply to graduate school. The field experiences in my Structural Geology and Geology of the National Parks classes with Dr. M. sparked my love of field work. Kira gave me my first opportunity to participate in a research project (beyond required classwork) and guided me through the steps of properly conducting research for the first time. Dave served as my undergraduate thesis advisor and allowed me to meld both of those worlds—fieldwork and lab research—together. While working with him, I first experienced what true ownership of the research work I completed felt like. All those experiences were critical in my development as a scientist. I would have never considered continuing on to graduate school if it wasn't for them and their continued support. Furthermore, there have been many other colleagues (who subsequently became my friends) that I have interacted with over the years that made me a better researcher and a better person. I will deeply miss seeing all of them at the annual SVP meetings and catching up—thank you for everything.

The UW Biology community has also been hugely supportive. With the help of the UW Biology staff, my research and teaching experiences were possible. Specifically, I'd like to thank Marissa Heringer, Eddie Sabiniano, Sarah O'Hara, Yen Lai, Hayato Kosai, Dave Hurley, Brianna Divine, Michele Conrad, Krista Clouser, Davis Chong, John Parks, Ben Wiggins, and Gretchen Shirley-Bellande for all of their help. Additionally, Ben Kerr was an amazing Graduate Program Chair while I was a graduate student. The great folks at Friday Harbor Labs also helped

my research become a reality. Many thanks to Adam Summers for access to the CT scanner at FHL, and to Karly Cohen, Kayla Hall, Jonathan Huie, and Mo Turner for CT scanner training/troubleshooting and for letting me crash with them during my CT scanning trips to FHL. I am also grateful to everyone at the Burke Museum of Natural History and Culture for all their help. Jeff Bradley, Meredith Rivin, Ron Eng, and Katie Anderson assisted me in all my collections-based adventures. Michael Holland, Kelsie Abrams, Bruce Crowley, and John Alexander aided in essential fossil preparation work that was necessary for my research. Liz Nesbitt, Chris Sidor, Caroline Strömberg, and Greg Wilson Mantilla answered all my curatorial questions and provided me with essential guidance in museum operations as well. The Paleolunch seminar group was also great fun to be a part of too! J. Sean Yeung, Michelle Hickner, Timothy Cox, and Katie Stanchek provided guidance on CT scanning and/or performed CT scans that were essential for my research. I am also grateful to Ally Kinahan who assisted me in post-processing CT scans.

My research would not have been possible without the funding support from the National Science Foundation (grant 1325365 [EAR] to D. J. Varricchio, G. P. Wilson, and J. Conrad), the Evolving Earth Foundation Student Grant (grant #A132982 to A. L. Brannick and G. P. Wilson), the Paleontological Society N. Gary Lane Award, the Margo and Tom Wyckoff UW Biology Department Award, the Walter and Margaret Sargent UW Biology Department Award, the Transmitting Science Scholarship, the Society of Vertebrate Paleontology Jackson Travel Award, and the UW Graduate and Professional Student Senate Travel Grant. I am also indebted to the WRF-Hall Fellowship from the UW Biology Department which enabled me to participate in the Pacific Science Center Science Communication Program. I am also grateful to the folks at

the Pacific Science Center for providing me with valuable pedagogy lessons and for assisting me in creating my own hands-on activity to be used at museum events.

Much of my research relied on obtaining museum specimens that I needed for direct observations or to CT scan. Many thanks to the following people and associated institutions for their help in making this happen: Patricia Holroyd (University of California Museum of Paleontology); Michael Caldwell, Richard Fox, Howard Gibbins, Aaron LeBlanc, and Tiago Simões (University of Alberta Laboratory of Vertebrate Paleontology); Randall Irmis and Carolyn Levitt (Utah Museum of Natural History); Eric Sargis, Marylin Fox, and Chris Norris (Yale Peabody Museum); Richard Cifelli and Jennifer Larsen (Sam Noble Oklahoma Museum of Natural History); Janet Gillette, David Gillette, Amber King, and Elaine Hughes (Museum of Northern Arizona); and John Scannella and Amy Atwater (Museum of the Rockies). I am also grateful to Christian de Muizon and Sandrine Ladevèze for hosting me during my trip to the Muséum national d'Histoire naturelle where I had the opportunity to make direct anatomical observations of many South American metatherian taxa.

I spent most of my summers as a graduate student doing fieldwork in and around Jordan, Montana. I am grateful to the many people and ranchers of Jordan for their hospitality and access to their properties so that a bunch of "bone diggers" could look for and collect fossils. And for all their help and enthusiasm with getting those fossils into our trucks too! I will miss visiting each year. Jordan, MT is also where the DIG Field School takes place. Being a part of the DIG was one of the most paramount experiences I had as a graduate student. I loved every second of it. I am thankful to have met so many amazing K–12 educators from all over the country (and Canada too!). Being able to provide these educators with an interactive, hands-on field experience that they could bring back to their students just makes my heart sing. It was also great

being able to visit so many classrooms and be a part a of the DIG fossil “sorting parties”. The DIG instructors are downright incredible as well. Working with all the DIG instructors improved my teaching and communication skills. I had an absolute blast working with all of you! Instructors from institutions other than UW include, but are not limited to: Tom Tobin, Courtney Sprain, Isabel Fendley, Mark Watrin, Ben Rodwell, Garry Norman, Corinna Casey, and Adam Smith. I can’t say thank you enough to all the DIG instructors for making the DIG program incredibly special. A special thank you goes to Richard Meyn. He was one of the first DIG participants (before I started at UW) and has come back to Jordan, MT each summer as a member of our field crew. He has been instrumental in our fieldwork operations and has served as a great camp manager during the DIG program. I had the opportunity to be on multiple prospecting projects with Richard, and I learned so many life lessons from him. In addition to working for the DIG out in the field, I also had the opportunity to work on DIG related materials back in Seattle at the Burke Museum. I’m incredibly grateful to Greg for providing the funding that allowed me to do so. Thanks also to Katharine Canning and Devin Leatherman (Burke Education team) with whom I worked with on redesigning DIG Box lessons and creating DIG Box instructional videos.

I’m so thankful to have been a part of the UW Biology graduate student and postdoc community. I’ve learned so much from everyone, beyond biology-related topics. There are too many people to name, but the UW Biology grads that I’ve gotten to know are a selfless, passionate group of people, and they continue to inspire me. Thank you for your patience, time, and work—especially outside of the realm of academia. I was also incredibly lucky to share an office with Stephanie Smith, Hannah Jordt, Itzue Caviedes-Solis, Jake Cooper, Luke Weaver, and Jordan Claytor in Kincaid Hall. I treasure the moments where we chatted about life, work,

and everything else together. The current and former paleo-group grads outside of the Wilson Mantilla lab—Brandon Peecook, Chuck Beightol, Savannah Olroyd, Zoe Kulik, Regan Dunn, Elisha Harris, Camilla Crifo, Will Brightly, Alex Lowe, Elena Stiles, Steven Lautzenheister, and Abby Vander Linden—are unequivocally amazing. It's been an honor to be a part of such a powerhouse paleo group. A special thank you also goes to Brandon Peecook for being a great mentor and friend.

I would like to thank three undergraduates/postbacs in particular that enriched my time as a graduate student: Natalie Toews, Amanda Peng, and Henry Fulghum. I had a lot of fun working with Natalie and Amanda on side projects and prospecting teams! Some of the funniest moments I can remember that happened in the field were with them. Natalie's optimism shines so brightly that it's difficult to ever feel down around her. She's so driven and it was awesome to work with her on our diel activity pattern project. Amanda is tenacious and exceptionally creative, and she effortlessly motivates all those around her. It was a pleasure to TA with her for the paleo field course. Her work as the Wilson Mantilla Lab manager was also vital to lab operations, which included my own research, and I'm extremely grateful to her for all her hard work during that time. I would like to extend special thanks to Henry as well. I am lucky to have worked with Henry in many different facets: teaching, fieldwork, collections work, and research. Henry is one of the hardest workers I've ever known, and he always puts others before himself. He played a critical role in data collection for two of my dissertation chapters—I can't thank him enough for that—and he was an amazing lab manager as well. He is the human embodiment of joy; he's also incredibly kind and empathetic as well. I sincerely admire all three of these people a great deal and they each have inspired me in their own ways. I'm so fortunate to have met them and I'm privileged to call each one of them my friend. Thanks for everything!

I think some of the most important and influential people grad students interact with during graduate school are their fellow labmates. I was lucky enough to have the best of them. I would not have finished my dissertation without each and every one of my labmates. Besides providing me with invaluable input and suggestions on my research, they all helped me grow into the person I am today. Lauren DeBey taught me how to be confident in myself and to not be afraid to ask questions; her generosity in assisting me with job searches and preparation has been overwhelming. Meng Chen never hesitates to help anyone, and he also urged me not to give up on coding (no small feat!). It was fun to share my first grad school office with him too. Dave DeMar taught me the ropes of fieldwork and helped me with my phylogenetic analysis too. He taught me the importance of thoroughness and attention to detail. Jonathan Calede has a huge heart. His dedication to his students resonated with me and inspired my own teaching style. He also helped me with analyses and editing, but more importantly, his encouragement—especially in the last few months of working on my dissertation—gave me the energy I really needed. Stephanie Smith was one of the first friends I made after moving to Seattle. Through leading by example, she taught me to always be true to myself and remember to always have fun. She provided me with vital assistance in conducting analyses and endless amounts of advice on navigating grad school and life. Luke Weaver is just a magnetic person who is exceedingly dedicated to everything he does. We braved the very literal storms of both Egg Mountain and the Terry Badlands together, and the many metaphorical storms of graduate school too. He taught me to remember there is life outside of work, and that the people you surround yourself with is what really matters. Paige Wilson is the unsung glue that has held the Wilson Mantilla lab together. She's utterly selfless and has spearheaded important changes to both lab and fieldwork operations through her dedication to ensuring everyone's safety and comfort. I joke that she is

“my moral compass”, but in all seriousness I look up to Paige a lot. Jordan Claytor is effortlessly graceful; he is also incredibly driven and resilient. His immense generosity and service to both the UW Biology Department and the lab made a huge impact on me and how I view the world. I also appreciate all the opossum Tik Toks he sent me when it was crunch time for me. Dave Grossnickle has been, what I consider, an unofficial committee member and an important mentor to me. He’s steadfast in his work and always ready for a laugh with his perfectly timed puns. My time as a graduate student would not have been the same without my labmates—I had (and still do have) so much fun with all of them! I’m proud and honored to call them some of my closest friends. A million thanks to each of them for all their help, guidance, and support. And thanks to them especially for never giving up on me and teaching me to not give up on myself. I’m a better person for having met and learned from all of you.

A very special thank you to Cooper French and Megan Whitney. Cooper, Meg, and I started at UW at the same time, and we became close friends fast. Cooper is an incredibly thoughtful, careful, and kind person. He taught me how to change my oil and improve my birding abilities. Engaging in philosophical debates with him has continuously sharpened my logic skills too. Our chats over coffee and hot chocolate kept me sane throughout this entire process. Meg is an undeniably remarkable person—fierce, generous, fun, and all-around badass. Meg knows everything I’d like to say to her here, but it can be wholeheartedly summarized by the following phrase: I love you so much, I would never eat your leftover pizza. Meg and Cooper have both seen me at my lowest lows and my highest highs. And through it all, we’ve become even closer friends. I love them both dearly.

My family has been instrumental in all my successes and I’m extremely fortunate to have this support system. Their support never faltered when I told them I wanted to be a

paleontologist. It still didn't waiver when I told them I was moving to West Virginia, and then to Seattle, to try to achieve this dream. I'm also lucky to have people in my life that I consider family through my partner, Brody; Tyler, Sharon, Tim, Scot, Brandon, and Claire have given me an extra support system I never expected to have when I first moved to Washington. Additionally, although it may sound silly, my family's dogs—Zoe, Sherlock, and Rogue—provided wordless support and constant love that I needed more than I realized until now. My sisters, Samantha and Sydney, are just amazing. I admire them both so much and love that we have unbreakable sibling bonds with each other. My brother-in-law, Chris, has also been someone I can always turn to and I'm so thankful to have a close relationship with him too. My nieces, Scarlett and Layla, have kept me grounded and have provided me with endless giggles and fun. My Mom and Dad are the loveliest people ever and are the reason why I've made it as far as I have. "Thank you" doesn't even begin to cover how much I appreciate them and all their support. Finally, my partner, Brody, has been my rock. His unwavering love, support, patience, and confidence in me kept me going throughout this entire process. He's one of the most genuine people I've ever met and I'm enormously grateful to have him in my life. I cherish all the adventures we've been on together so far and I'm looking forward to many more. Thank you, Brody, for everything.

DEDICATION

I dedicate this body of work to my parents, Janet and Michael Brannick. Their guidance and support sustained me throughout my PhD journey. They've always encouraged me to follow my dreams. I'm grateful that I can always lean on them when I need a laugh and seek their advice when I need help. Their zest for life is contagious, and I strive to emulate this attitude. Without them, this dissertation would have never happened. I am eternally grateful to them for everything.

CHAPTER 1: INTRODUCTION

Extant mammals can be categorized into three major groups—monotremes (e.g., echidnas, platypus), placentals (e.g., primates, canids, whales) and marsupials (e.g., kangaroos, opossums, quolls). The marsupials are a charismatic group commonly recognized by the presence of an abdominal pouch (marsupium) in which their young continue to develop in after birth (although, not all marsupials possess the external covering of the marsupium; e.g., Smith and Keyte, 2020). Although enigmatic, extant marsupials are not as taxonomically rich (~400 species of marsupials vs. >5,000 species of placentals) or as geographically wide-ranging (marsupials are only found in only the Neotropics and Australasia, with the exception of *Didelphis virginiana*) as their placental contemporaries. However, this imbalance between the two therian (node-based clade that includes living marsupials, placentals, and their most recent common ancestor) clades did not always favor eutherians (the stem-based clade of extant placentals and their closest relatives; Sereno, 2006; O'Leary et al., 2013). During the Late Cretaceous (ca. 100–66 million years ago [Ma]), metatherians (the stem-based clade of extant marsupials and their closest relatives; e.g., Rougier et al., 1998; Sereno, 2006; Beck, in review) were evolutionarily successful. They occupied all northern landmasses and possibly some southern ones (Rougier et al. 1998; Krause, 2001; Kielan-Jaworowska et al., 2004; Martin et al., 2005; Vullo et al., 2009; Averianov et al., 2010; Williamson et al., 2014; Goin et al., 2016). They were also numerically abundant, making up as much as 45% of all mammalian fossil individuals within local faunas (e.g., Cifelli, 2004; Wilson, 2014), and were often in higher abundance than eutherians. Finally, Late Cretaceous metatherians were

taxonomically rich (Bennett et al., 2018; Williamson et al., 2014) and occupied a wider range of dietary ecologies (Brannick et al., in review) than coincident eutherians.

Several studies have highlighted the taxonomic richness of Late Cretaceous metatherians (e.g., Williamson et al. 2012; Williamson et al., 2014; Wilson et al., 2016; Cohen et al., 2020; Beck, in press). However, the precise phylogenetic relationships among early metatherians are unclear. This is mainly because many taxa are known only from fossil teeth (Kielan-Jaworowska et al., 2004; Williamson et al., 2014). Skulls and postcrania are scarce, particularly among North American taxa. Of the 68 North American species known, relatively complete skulls have been described for only one taxon: *Didelphodon vorax* (Wilson et al., 2016). In turn, many phylogenetic analyses of early metatherians have either excluded many North American taxa (e.g., Horovitz and Sánchez-Villagra, 2003; Horovitz et al., 2009; de Muizon et al., 2018; de Muizon and Ladevéze, 2020) or only included craniodental data (e.g., Rougier et al., 2004, 2015; Williamson et al., 2014; Wilson et al., 2016; Cohen et al., 2020).

Chapter 2 of this dissertation reassesses the phylogenetic relationships among metatherians and is centered on the raw data for morphological phylogenetic analyses—anatomical information. In this chapter, I add to the growing collection of anatomical data for North American taxa by describing newly discovered skulls of *Alphadon halleyi* from the Egg Mountain locality (Montana, USA). These incredible specimens represent the most complete skull material for this taxon and some of the most complete material for any North American marsupialiform from the Cretaceous (with the exception being *Didelphodon*; Wilson et al., 2016). For this study, I utilized micro-computed tomography to uncover anatomical details that would otherwise be impossible to discern without risking

serious damage to the fossils. With these new data, I updated character scores for *Alphadon* and subsequently performed a phylogenetic analysis.

As with the uncertainty surrounding metatherian phylogenetic relationships, questions regarding the paleoecology of these animals still remain. As stated above, postcranial fossils of early metatherians are rare and the few examples of postcrania are almost exclusively known for Asiatic and South American taxa. Thus, interpretations of locomotor diversity and substrate use for these taxa are limited (e.g., Szalay, 1994; Szalay and Trofimov, 1996; Argot, 2001; Argot, 2002; Argot, 2003 Szalay and Sargis, 2006; DeBey and Wilson, 2017). Similar to many phylogenetic analyses, most paleoecological studies have used the abundant dental record and they subsequently focus on reconstructing feeding ecology. Many of these studies are largely qualitative in nature; hypotheses regarding the diets of fossil taxa usually stem from tooth shape comparisons between the fossil taxa and modern taxa with known diets. For example, *Glasbius* has broad-basined, bunodont molars which have prompted interpretations that it was frugivorous (Clemens, 1966; Clemens, 1979), whereas the molars of *Nanocuris* indicate adaptation to carnivory, as they are elongated, buccolingually compressed, and have an exaggerated postvallum-prevallid shearing crest as well as a reduced talonid (Fox et al., 2007; Wilson and Riedel, 2010).

A few other studies have taken more quantitative approaches to examining feeding ecologies in metatherians. For example, Wilson (2013) used 2D geometric morphometrics to quantify the morphological disparity of mammalian (including metatherian) teeth immediately before and after the Cretaceous-Paleogene (K-Pg) boundary. He found that metatherians exploited a wide range of body sizes and feeding ecologies in the Lancian, but

that local extinction contributed to a loss in ecological endmembers within the Hell Creek mammalian fauna. Similarly, Grossnickle and Newham (2016) investigated dental morphological disparity through time on a global scale and found that metatherian disparity increased throughout the Late Cretaceous. Wilson et al. (2016) employed a number of different techniques, including estimating bite force, canine bending strength, and mandibular bending strength, to infer that *Didelphodon* was a powerful omnivore with durophagous (hard-object) capabilities. Nonetheless, studies using methods that quantify morphological data to infer feeding ecology—especially those with broader taxonomic sampling of Metatheria— are lacking.

In *Chapter 3*, I focus on one clade of metatherians, the Stagodontidae. Of the recognized species of the stagodontid genus *Eodelphis*, *E. cutleri* is larger and has a more robust dentary, more inflated premolars, and third premolars specialized for crushing, whereas *E. browni* is smaller and more gracile. These differences have led to the hypothesis that an *E. cutleri*-like ancestor gave rise to *Didelphodon*, which has been previously interpreted as a durophagous predator-scavenger. I test this hypothesis and investigate the evolution of durophagy within the stagodontids by examining dentary shape, as opposed to dental morphology. I implement beam theory to quantify the biomechanical properties of the dentary of stagodontids and other metatherians. I also use the resulting force profiles to further constrain the feeding behavior of these taxa.

Chapter 4 seeks to broaden the phylogenetic scope of interpreting metatherian dietary ecology and elucidate macroevolutionary patterns regarding metatherian ecomorphological diversification. In this chapter, I examine the dental ecomorphologies of a comprehensive sample of North American Late Cretaceous metatherians by employing

three-dimensional dental topographic analysis to predict diet. The application of this method has been underutilized for metatherian taxa, as many of studies that implement dental topographic analysis have focused on placentals (mostly primates; e.g., Evans et al., 2007; Boyer, 2008; Winchester et al., 2014). Additionally, no other dental ecomorphology study has exclusively focused on the dietary diversification of metatherians within a phylogenetic context. I also provide a new hypothesis regarding the timing of early metatherian ecological diversification in this chapter.

Chapter 5 consists of concluding remarks and a summary of the main conclusions of the three studies included in my dissertation.

Overall, this dissertation provides novel insights into the evolution of metatherians. First, it highlights the importance of more complete Cretaceous-aged metatherian specimens, particularly from North America, and the persistent instability of the metatherian phylogenetic tree. It also demonstrates the significance of examining different ecomorphological units (i.e., dental morphology, dentary morphology, and likely cranial morphology) in concert with each other to better infer likely feeding ecologies. Finally, this dissertation shows that quantitative methods reliably predict diet and can be used to investigate macroevolutionary patterns of fossil taxa. Future studies should seek to continue adding anatomical data for North American metatherians and investigate paleoecology within a phylogenetic framework (as it improves) to advance our understanding of the evolution of Metatheria.

1.1 REFERENCES CITED

Archibald, D. 2011. Extinction and radiation: how the fall of dinosaurs led to the rise of Mammals. The Johns Hopkins University Press, Baltimore, Maryland

Argot, C. 2001. Functional-adaptive anatomy of the forelimb in the Didelphidae, and the paleobiology of the Paleocene marsupials *Mayulestes ferox* and *Pucadelphys andinus*. Journal of Morphology, 247(1):51–79. doi:Doi 10.1002/1097-4687(200101)247:1<51::Aid-Jmor1003>3.0.Co;2-#.

Argot, C. 2002. Functional-adaptive analysis of the hindlimb anatomy of extant marsupials and the paleobiology of the Paleocene marsupials *Mayulestes ferox* and *Pucadelphys andinus*. Journal of Morphology, 253:76–108

Argot, C. 2003. Functional-adaptive anatomy of the axial skeleton of some extant marsupials and the paleobiology of the paleocene marsupials *Mayulestes ferox* and *Pucadelphys andinus*. Journal of Morphology, 255(3):279–300. doi:10.1002/jmor.10062

Beck, R. M. D. In press. Current understanding of the phylogeny of Metatheria: A review. In F. J. Goin, and A. M. Forasiepi (Eds.), New World marsupials and their extinct relatives: 100 million years of evolution: Springer.

Bennet, C.V., Upchurch, P., Goin, F.J., and Goswami, A. 2018. Deep time diversity of metatherian mammals: implications for evolutionary history and fossil-record quality. Paleobiology, 44(2):171-198. DOI: 10.1017/pab.2017.34

Boyer, D.M. 2008. Relief index of second mandibular molars is a correlate of diet among prosimian primates and other euarchontan mammals. Journal of Human Evolution, 55:1118-1137. doi:10.1016/j.jhevol.2008.08.002

Brannick, A. L., Fulghum, H. Z., Grossnickle, D. M., and Wilson Mantilla, G. P. In review. Dental ecomorphology and macroevolutionary patterns of North American Late Cretaceous metatherians.

Cifelli, R.L. 2004. Marsupial mammals form the Albian–Cenomanian (Early–Late Cretaceous) Boundary, Utah. Bulletin of the American Museum of Natural History, 285:62-79 http://dx.doi.org/10.1206/0003-0090(2004)285<0062:C>2.0.CO;2

Clemens, W.A. 1966. Fossil mammals of the type Lance Formation Wyoming. Part II. Marsupialia. University of California Publications in Geological Sciences, 62:1-122

Clemens, W.A. 1979. Marsupialia, p. 192-220. In Lillegraven, J.A., Kielan-Jaworowska, Z. and Clemens, W.A. (eds.), Mesozoic mammals: the first two-thirds of mammalian history. University of California Press, Berkeley, California

Cohen, J.E. 2018. Earliest divergence of stagodontid (Mammalia: Marsupialiformes) feeding strategies from the Late Cretaceous (Turonian) of North America. Journal of Mammalian Evolution. DOI 10.1007/s10914-017-9382-0

Cohen, J.E., Davis, B.M., and Cifelli, R.L. 2020. Geologically oldest Pediomyoidea (Mammalia, Marsupialiformes) from the Late Cretaceous of North America, with implications for taxonomy and diet of earliest Late Cretaceous mammals. Journal of Vertebrate Paleontology. DOI:10.1080/02724634.2020.1835935

de Muizon, C. and Ladevèze, S. 2020. Cranial anatomy of *Andinodelphys cochabambensis*, a stem metatherian from the early Palaeocene of Bolivia. Geodiversitas, 42(30):597–739

de Muizon, C. et al. 2018. *Allqokirus australis* (Sparassodonta, Metatheria) from the early Palaeocene of Tiupampa (Bolivia) and the rise of the metatherian carnivorous radiation in South America. Geodiversitas, 40(16):363–459

DeBey L.B. and Wilson, G.P. 2017. Mammalian distal humerus fossils from eastern Montana, USA with implications for the Cretaceous-Paleogene mass extinction and the adaptive radiation of placentals. Palaeontologia Electronica 20.3.49A:1-92. palaeoelectronica.org/content/2017/1983-mammal-humeri-across-the-k-pg

Evans, A.R., Wilson, G.P., Fortelius, M., and Jernvall, J. 2007. High-level similarity of dentitions in carnivorans and rodents. Nature, 445:78-81. https://doi.org/10.1038/nature05433

Fox, R. C., Scott, C. S., and Bryant, H. N. 2007. A new, unusual therian mammal from the Upper Cretaceous of Saskatchewan, Canada. Cretaceous Research, 28:821-829

Grossnickle, D.M. and Newham, E. 2016. Therian mammals experience an ecomorphological radiation during the Late Cretaceous and selective extinction at the K–Pg boundary. Proceedings of the Royal Society B, 283:20160256. http://dx.doi.org/10.1098/rspb.2016.0256

Horovitz, I. and Sánchez-Villagra, M. R. 2003. A morphological analysis of marsupial mammal higher-level phylogenetic relationships. Cladistics, 19:181–212

Horovitz, I., Martin, T., Bloch, J., Ladevèze, S., Kurz, C., and Sánchez-Villagra, M. R. 2009. Cranial anatomy of the earliest marsupials and the origin of opossums. PLoS ONE, 4(12): e8278

Morales-García, N.M., Gill, P.G., Janis, C.M., and Rayfield, E.J. 2021. Jaw shape and mechanical advantage are indicative of diet in Mesozoic mammals. Communications Biology, https://doi.org/10.1038/s42003-021-01757-3

O'Leary, M. A., Bloch, J. I., Flynn, J. J., Gaudin, T. J., Giallombardo, A., Giannini, N. P., et al. (2013). The placental mammal ancestor and the post-K-Pg radiation of placentals. Science, 339(6120):662–667. doi:10.1126/science.1229237

Rougier, G. W., Davis, B. M., and Novacek, M. J. 2015. A deltatheroidan mammal from the Upper Cretaceous Baynshiree Formation, eastern Mongolia. Cretaceous Research, 52:167–177

Rougier, G.W., Wible, J.R., and Novacek, M. J. 1998. Implications of Deltatheridium specimens for early marsupial history. Nature, 396:459-463. https://doi.org/10.1038/24856

Rougier, G. W., Wible, J. R., and Novacek, M. J. 2004. New specimens of *Deltatheroides cretacicus* (Metatheria, Deltatheroida) from the Late Cretaceous of Mongolia. Bulletin of Carnegie Museum of Natural History, 36(1): 245–266

Sereno, P. C. 2006. Shoulder girdle and forelimb in multituberculates: evolution of parasagittal forelimb posture in mammals. In M. T. Carrano, T. J. Gaudin, R. W. Blob, & J. R. Wible (Eds.), Amniote paleobiology: perspectives on the evolution of mammals, birds, and reptiles pp. 315–366. Chicago: University of Chicago Press.

Smith, K.K. and Keyte, A.L. 2020. Adaptations of the marsupial newborn: birth as an extreme environment. The Anatomical Record, 303:235–249

Szalay, F.S. 1994. Evolutionary history of the marsupials and an analysis of osteological characters. Cambridge University Press, New York

Szalay, F.S. and Sargis, E.J. 2006. Cretaceous therian tarsals and the metatherian-eutherian dichotomy. Journal of Mammalian Evolution, 13:171-210

Szalay, F.S. and Trofimov, B.A. 1996. The Mongolian Late Cretaceous *Asiatherium*, and the early phylogeny and paleobiology of Metatheria. Journal of Vertebrate Paleontology,

16(3):474–509

Williamson, T. E., Brusatte, S. L., and Wilson, G. P. 2014. The origin and early evolution of metatherian mammals: The Cretaceous record. ZooKeys, 76(465):1-76

Williamson, T. E., Brusatte, S. L., Carr, T. D., Weil, A., and Standhardt, B. R. 2012. The phylogeny and evolution of Cretaceous-Paleogene metatherians: cladistic analysis and description of new early Paleocene specimens from the Nacimiento Formation, New Mexico. Journal of Systematic Paleontology, 10(4):625–651

Wilson, G.P., 2014. Mammalian extinction, survival, and recovery dynamics across the Cretaceous-Paleogene boundary in northeastern Montana, USA, Geological Society of America Special Paper 503, p. 1-28. In Wilson, G.P., Clemens, W.A., Horner, J.R., and Hartman, J.H. (eds.), Through the End of the Cretaceous in the Type Locality of the Hell Creek Formation in Montana and Adjacent Areas, doi:10.1130/2014.2503(15)

Wilson, G. P., and Riedel, J. A. 2010. New specimen reveals deltatheroidan affinities of the North American Late Cretaceous mammal *Nanocuris*. Journal of Vertebrate Paleontology, 30(3):872–884

Winchester, J.M., Boyer, D.M., St. Clair, E.M., Gosselin-Ildari, A.D., Cooke, S.B., and Ledogar, J.A. 2014. Dental topography of platyrrhines and prosimians: convergence and contrasts. American Journal of Physical Anthropology, 153:29-44. DOI: 10.1002/ajpa.22398

CHAPTER 2: NEW CRANIAL SPECIMENS OF *ALPHADON HALLEYI*, SAHNI 1972 FROM EGG MOUNTAIN AND THEIR IMPLICATIONS FOR METATHERIAN EVOLUTION

2.1 INTRODUCTION

Extant marsupials are neither as taxonomically rich (~340 species of marsupials vs. >5,000 species of placentals) nor as geographically wide-ranging as extant placental mammals (Sánchez-Villagra 2013). However, during the Late Cretaceous, metatherians (the stem-based clade that includes marsupials and their closest therian relatives) were more evolutionarily successful than eutherians (the stem-based clade that includes placentals and their closest therian relatives): they were geographically widespread (Rougier et al. 1998; Krause 2001; Kielan-Jaworowska et al. 2004; Martin et al. 2005; Vullo et al. 2009; Averianov et al. 2010; Williamson et al. 2014; Goin et al. 2016), numerically abundant in local faunas (e.g., Cifelli 2004; Wilson 2014), taxonomically rich (e.g., Archibald 2011; Williamson et al. 2014; Wilson et al. 2016; Bennett et al. 2018), and had greater dental morphological diversity (Archibald 2011; Brannick et al. submitted). Metatherians in North America then experienced a significant decline in taxonomic diversity during the Cretaceous-Paleogene (K-Pg) mass extinction event (ca. 66 million years ago [Ma]), such that only two families, the Peradectidae and Herpetotheriidae, occur in Paleogene deposits (Clemens 1979; Cifelli and Davis 2003; Kielan-Jaworowska et al. 2004; Wilson 2014; Williamson and Lofgren 2014; Williamson et al. 2014).

Previous work has focused on the taxonomic diversity, geographic distribution, temporal range, and diet of early metatherians (see Williamson et al. 2014 for review), but important

questions regarding other aspects of their paleoecology and their phylogenetic relationships remain. These gaps in our understanding are in part due to the fossil record of early metatherians, which consists mostly of isolated teeth and fragmentary jaws (Kielan-Jaworowska et al. 2004). Cranial and postcranial fossils are very rare, particularly for Late Cretaceous North American (NA) Marsupialiformes (the clade that includes metatherians more closely related to Marsupialia than to Deltatheroida; Vullo et al. 2009; Williamson et al. 2014). The most complete cranial specimens known belong to Paleogene South American taxa (e.g., *Pucadelphys*, *Mayulestes*, and *Andinodelphys*; Marshall et al. 1995; de Muizon 1998; Macrini et al. 2007; de Muizon and Ladevèze 2020). The lack of skeletal data for Cretaceous NA taxa has hampered a better understanding of the phylogenetic relationships among NA stem marsupialiforms, impeded a broad assessment of the patterns of metatherian taxonomic evolution, and hindered our understanding of the paleoecological evolution of these early marsupial relatives.

Until recently, cladistic analyses of metatherians commonly showed a tree topology in which an early split separated Late Cretaceous Asian and NA stem taxa from Paleogene South American (SA) stem taxa with crown marsupials nested within the SA clade (e.g., Rougier et al. 1998). The nesting of Marsupialia within the SA group is congruent with the current distribution of living marsupials—almost all extant marsupials live in South America and Australasia (although *Didelphis virginiana* has a range that extends into the Nearctic region of North America, it likely originated in the Neotropics; Kirsch et al. 1993; Dias and Perini 2018)— and our current understanding of marsupial dispersal events from South America to Antarctica and Australia (e.g., Goin et al. 2016).

More complete scoring of cladistic characters for one Cretaceous metatherian brought this scenario into question. Indeed, the study by Wilson and colleagues (2016) of relatively

complete cranial fossils of the North American stem marsupialiform *Didelphodon vorax* led to the scoring of 34 previously unscored characters and the revision of seven scores out of 164 characters for this taxon (*Didelphodon vorax* = 86% characters scored). The strict consensus tree that resulted from their cladistic analysis showed a substantial change in topology from earlier trees (e.g., Rougier et al. 2004). Although the tree of Wilson et al. (2016) is congruent with previous analyses in separating NA and SA stem marsupialiforms into different clades, it differs in showing crown marsupials nested within the NA stem marsupialiform clade. This result implies that by the Santonian to early Paleocene (ca. 85–65 Ma), crown marsupials either originated in North America or their closest marsupialiform relatives dispersed from North America to South America and crown marsupials evolved soon after. With such a dramatic change in topology after adding anatomical data for one taxon, it begs the question of how updating morphological information for other taxa might further alter the tree topology. The lack of consensus within the metatherian tree solicits further testing of the results of Wilson et al. (2016). Improving the stability and robusticity of the metatherian phylogeny is contingent upon the discovery and detailed study of more complete cranial and postcranial fossils—especially of Mesozoic taxa.

Here, we describe new skull material (four crania and two dentaries) of the Late Cretaceous NA stem marsupialiform *Alphadon halleyi* recovered from the Egg Mountain locality. This locality is located ~25 km west of Choteau, Teton County, northwestern Montana, USA (Fig. 2.1). It is in the upper part of the Two Medicine Formation, which is Campanian in age (ca. 75.5 Ma; Rogers et al. 1993). Previous work on the locality has described the sedimentology, interpreted the depositional environment, placed it in a geochronological framework, and studied the taphonomy (e.g., Lorenz and Gavin 1984; Shelton 2007; Varricchio

et al. 2010; Freimuth and Varricchio 2019; Weaver et al. 2020; Freimuth et al. 2021). The quarry is 16.5 m stratigraphically above a bentonite horizon dated to 76.305 ± 0.1404 Ma (Varricchio et al. 2010; recalibrated by Fowler [2017] using plagioclase); consistent with assignment to the Judithian North American land mammal 'age' ([NALMA]; Rogers 1990, 1998; Shelton 2007; Varricchio et al. 2010). The sediments of Egg Mountain are calcareous mudstones and siltstones as well as micritic limestones that are well indurated (Lorenz and Gavin 1984). The sedimentary rock units lack clear bedding planes and primary sedimentary structures, most likely due to bioturbation (Lorenz and Gavin 1984; Freimuth and Varricchio 2019). The 1.5m stratigraphic interval of the Egg Mountain quarry has been divided into three main lithologic units (see Weaver et al. 2020 for details). Unit 1—the lowermost unit of the quarry—is a micritic limestone that is roughly laterally continuous throughout the quarry (Weaver et al. 2020). Unit 2 is ~1-m-thick grey calcareous siltstone that overlies Unit 1. It also has interfingering micritic limestone lenses that are of a similar lithology to Unit 1 (Weaver et al. 2020). Unit 3 overlies Unit 2 and is a thin (20–30 cm) micritic limestone (Weaver et al. 2020). Because the sedimentary rock units of the Egg Mountain quarry are generally massive, stratigraphic positions of fossils were recorded in association with jackhammer passes—stratigraphically parallel cuts at ~11-cm deep intervals (Weaver et al. 2020; Freimuth et al. 2021; Fig. 2.1).

The Egg Mountain locality (Museum of the Rockies site TM-006) has been widely recognized for the preservation of dinosaur egg clutches (Horner 1984, 1987; Varricchio et al. 1997, 1999). This site has also yielded shed dinosaur teeth (Scofield 2018), root traces and insect cocoons (Martin and Varricchio 2011), a shell fragment of the turtle *Adocus* (Scofield 2018), mammalian skulls and partial skeletons (e.g., Wilson and Varricchio 2014; Weaver et al. 2020), nearly complete skeletons of the oldest North American iguanomorph, *Magnuviator*

ovimonsensis (DeMar et al. 2017), and other squamates (DeMar, person. comm.). Only two mammalian taxa have thus far been identified from Egg Mountain—a multituberculate, *Filikomys primaevus* (Weaver et al. 2020; previously identified as *Cimexomys judithae* by Montellano et al. 2000), and a marsupialiform, *Alphadon halleyi* (Montellano 1988; Wilson and Varricchio 2014; Freimuth et al. 2021). Most of the substantial collection of well-preserved mammal fossils from this site has not yet been described (but see the comprehensive study of *Filikomys primaevus* by Weaver et al. 2020).

The genus *Alphadon* has been considered an important taxon in determining phylogenetic relationships among Cretaceous stem marsupialiforms and crown marsupials due to its geologic age range and its conservative dental morphology (Clemens 1968). Thus, we provide a detailed description of the new skull fossils of *Alphadon halleyi* from Egg Mountain and incorporate the resulting anatomical data into a phylogenetic analysis to reevaluate the phylogenetic relationships within Metatheria.

2.2 INSTITUTIONAL ABBREVIATIONS—AMNH, American Museum of Natural History, New York, New York, USA.; **MOR**, Museum of the Rockies, Bozeman, Montana, USA

2.3 TERMINOLOGY AND MEASUREMENTS

We follow Wible (2003) for cranial osteology terminology and Kielan-Jaworowska et al. (2004) for dental terminology. The postcanine dental formula for Metatheria has been re-interpreted as P1/p1, P2/p2, P4/p4, DP5/dp5, M1/m1, M2/m2, and M3/m3 (Luckett 1993; O'Leary et al. 2013), but we use the conventional terminology of three premolars and four molars for practical purposes.

2.4 MATERIALS AND METHODS

2.4.1 Fieldwork and Preparation

All *Alphadon halleyi* specimens described here were collected during the 2010–2016 field seasons at Egg Mountain (Teton County, Montana, USA). Weaver et al. (2020) and Freimuth et al. (2021) provide details regarding specimen excavation and stratigraphic position mapping. MOR 10911 and MOR 10913 were found at jackhammer pass (JHP) 7, whereas MOR 10912 was found at JHP 5 (Fig. 2.1). MOR 10912 and MOR 10913 were manually prepared by J.P. Cavigelli in Casper, WY and MOR 10911 was manually prepared by J. Alexander in Seattle, WA.

2.4.2 Micro-computed Tomography (μCT)

Many of these specimens are encased in hard rock that is difficult to mechanically prepare without severe risk of damage to the fossils. To mitigate this risk and to aid our morphological descriptions, we created three-dimensional (3D) virtual models of the specimens described here. MOR 10912a–d and 10913a were μCT scanned at the University of Washington on a North Star Imaging X5000 CT scanner with a Feinfocus FXE (11164478) X-ray source and Perkin Elmer (XRD 1620/1621 AM/AN) detector. MOR 10911 was μCT scanned by T. Cox at Seattle Children's Hospital on a Skyscan 1076. See 2.11: Appendix 1 for scan parameter details. We post-processed and created three-dimensional virtual reconstructions derived from μCT data using Avizo Lite software (ThermoFisher Scientific, version 9.2). All measurements were taken on virtually reconstructed elements in Fiji (Schindelin et al. 2012) using the Line tool and Measure function. Dental measurements follow Lillegraven (1969). All measurements were

taken three times and then averaged; they are millimeters (mm) and rounded to the nearest hundredth of a millimeter.

2.4.3 Phylogenetic Analysis

To assess the phylogenetic relationships of *Alphadon* with other metatherians, we conducted a cladistic analysis using a data matrix derived from Rougier et al. (2015), Wilson et al. (2016) and Cohen et al. (2020). Our data matrix includes 54 taxa (13 outgroup taxa, 10 deltatheroidans and 31 marsupialiforms) and 164 characters (67 dental, 86 cranial, and 11 mandibular; 11 ordered characters; 2.11: Appendix 2). We scored 14 previously unscored characters for *Alphadon* from direct observations of the physical specimens described here, as well as μCT image and 3D digital models of the same specimens (2.11: Appendix 5). We assembled our data matrix in Mesquite (Maddison and Maddison 2018) and then used the software program Tree Analysis Using New Technology (TNT; Goloboff et al. 2008) to conduct our cladistic analysis (2.11: Appendices 3–4). We subjected our data matrix to a new technology search using the sectorial, ratchet, drift and tree-fusing strategies with 500 minimum length trees (Goloboff 1999; Nixon 1999). Bremer supports were calculated by retaining trees suboptimal by ten steps.

2.5 RESULTS AND DISCUSSION

2.5.1 Systematic Paleontology

MAMMALIA Linnaeus, 1758

THERIA Parker and Haswell, 1897

METATHERIA Huxley, 1880

MARSUPIALIFORMES Vullo, Gheerbrant, de Muizon, & Nréaudeau 2009

"ALPHADONTIDAE" Marshall, Case, & Woodburne 1990

ALPHADON, Simpson 1927

ALPHADON HALLEYI, Sahni 1972

Holotype—AMNH 77367: a lower molar. The holotype was found at the Clambank Hollow locality in the upper portion of the Judith River Formation (Judithian; Late Cretaceous), Chouteau County, Montana.

Referred Specimens— MOR 10911, a partial skull (Figs. 2.2–2.3; 2.11: Appendix 5); MOR 10912a, a partial cranium (Fig. 2.4; 2.11: Appendix 5); MOR 10912b, a partial cranium with associated upper dentition (Figs. 2.5–2.6; 2.11: Appendix 5); MOR 10912c, a partial cranium with associated upper dentition (Figs. 2.7–2.8; 2.11: Appendix 5); MOR 10912d, a partial left dentary with associated lower dentition (Figs. 2.7, 2.9; 2.11: Appendix 5); and MOR 10913a, a partial cranium (Figs. 2.10–2.12; 2.11: Appendix 5).

Locality data—All referred specimens were found at the MOR locality TM-006, Egg Mountain, Two Medicine Formation (Judithian: Late Cretaceous), Montana.

Diagnosis—"Small species of *Alphadon* the same size or slightly smaller than *A*. *lulli*; upper molar cusp B large, cusp C small (much smaller than in *A*. *marshi*), cusp D large but smaller than B and low ridge present in cusp E position; cusp A large, separated from B by a significant notch; cusp B close to paracone; paracone and metacone nearly equal in size (paracone is larger than metacone in *A. lulli*) and separated by a wide valley (not as narrow as in *A*. *lulli*); lower molar hypoconulids more separate than in *A*. *lulli*; lower molars smaller, talonids

proportionately smaller, and paraconid more anteriorly projecting than *A. wilsoni*" (Rigby and Wolberg 1987, p. 55); "as well: metasylar wing prominent, postmetacingulum more posteriorly than labially directed on M1–M3, ectoflexus more broadly open than on other M3s referred to *Alphadon sensu lato*" (Johanson 1996:171). Montellano (1992) also states that paraconule and metaconule are positioned closer to the protocone and more separated from the paracone and metacone in *Alphadon halleyi* than in other species of *Alphadon* s.l., but this condition has not been found consistently (Johanson 1996).

General skull anatomy remarks— The specimens described herein include the anterior region of the cranium and part of the rostrum; the braincase is not preserved in any of these specimens. Almost all specimens underwent some manner of postmortem deformation. MOR 10911 and MOR 10912c underwent mediolateral compression, so the view of the palate is obscured. MOR 10912a underwent dorsoventral compression and shearing, thus positions of the orbital bones are difficult to determine. An intensive taphonomic study of Egg Mountain specimens led to the hypothesis that MOR 10912a–d and MOR 10913a represent regurgitated gastric pellets of the theropod *Troodon* (Freimuth et al. 2021). The taphonomic study of MOR 10911 is outside the scope of this paper; however, MOR 10911 shares preservational aspects consistent with regurgitalites as well (e.g., the braincase is not preserved, teeth and teeth bearing elements are preserved, lack of associated postcrania).

Nasal— Fragmentary nasals are present in MOR 10913a (Figs. 2.10–2.11; 2.11: Appendix 5) and more complete nasals are present in MOR 10912a (Fig. 2.4; 2.11: Appendix 5). In dorsal view, the nasals contact the frontals, lacrimals, maxillae, and premaxillae. As seen in MOR 10913a, the most posterior portion of the nasals is somewhat diamond-shaped and achieves maximum width at the contact with the lacrimal, maxilla, and frontal. The nasals

terminate posteriorly dorsal to the M3. From the point of maximum width, the nasals begin to taper anteriorly toward the midline dorsal to M1. MOR 10912a is crushed, but sutures are visible; this specimen shows that the nasals extend anterior to the canine, as in most living didelphids and fossil metatherians (Voss and Jansa 2009; Wilson et al. 2016).

Premaxilla— The anatomy anterior to the canine is only preserved in MOR 10912a (Fig. 2.4; 2.11: Appendix 5). Additionally, MOR 10912a is crushed, making a description of the 3D shape of the snout (i.e., broad vs. narrow) impossible. The posterior border of the facial process contacts the maxilla vertically and the nasal dorsally. Although the deformation of this specimen makes it difficult to see, it appears that a thin posterodorsal process tapers between the nasal and maxilla to its termination dorsal to the canine, much like the condition seen in *Andinodelphys cochabambensis* and *Mayulestes ferox* (de Muizon 1998; de Muizon and Ladevèze 2020). The alveolar and palatal processes are not preserved in this specimen.

Maxilla— Portions of the maxilla are preserved in all five specimens included here. Overlapping elements are morphologically consistent, but we also note a few differences between the specimens. Like other metatherians, the facial process of the maxilla forms the dorsolateral wall of the rostrum (de Muizon et al. 2018). An infraorbital foramen (IOF) is present on the lateral aspect of the facial process. In MOR 10911 (Figs. 2.2–2.3; 2.11: Appendix 5) and MOR 10912b (Fig. 2.5; 2.11: Appendix 5), this foramen has a slightly more posterior position than what is observable in *Allqokirus* (dorsal to the embrasure between P2 and P3; de Muizon et al. 2018), but anterior to the location seen in *Didelphodon* (dorsal to the P3–M1 embrasure; Wilson et al. 2016). Instead, the foramen location is more similar in position to some specimens of *Andinodelphys*, where the foramen is generally dorsal to the posterior root of P3 but also overhangs the anterior root of P3 (de Muizon et al. 2018). The IOF in MOR 10912a is positioned

slightly more anterior than the other two specimens; it's dorsal to the P2–P3 embrasure, as in *Allqokirus* (Fig. 2.4; 2.11: Appendix 5). There is also a small nutrient foramen dorsal to the posterior edge of the anterior root of P3 in MOR 10912a. Posterodorsally, the maxilla extends between the nasal and lacrimal, and has a small contact with the frontal. The frontal-maxilla contact is not as clear as in MOR 10913a as in MOR 10912a, but it is still present. From the frontal-maxilla suture, the posterior edge of the maxilla then contacts the lacrimal and extends anteriorly, then anteroventrally. The maxilla contacts the jugal near the ventral rim of the orbit dorsal to the M1-M2 embrasure, and the edge of the maxilla-jugal suture extends posteroventrally. The maxilla also contributes to the anterior zygomatic root dorsal to M2–M4.

In MOR 10912a and MOR 10913a, the triangle-shaped orbital plate is formed by the maxilla. In MOR 10912a (Fig. 2.4; 2.11: Appendix 5), the orbital floor is dorsal to the M1 and extends posteriorly, whereas in MOR 10913a (Fig. 2.11; 2.11: Appendix 5), the orbital floor appears to be dorsal to the M2. There is some slight dorsoventral deformation of the orbit in MOR 10913a which may account for this difference in position of the orbital floor. The posterior edge of the orbital floor is not preserved in any of these specimens.

Due to the mediolateral crushing of MOR 10911, MOR 10912a, and MOR 10912c, much of the palatal process of the maxilla is obscured. As a consequence, we cannot determine the presence of any palatal fenestrae. MOR 10912b preserves a small, undeformed portion of the palatal process, but does not preserve enough bone medially to determine the presence of palatal fenestrae; the posterior most portion of the palatal process is missing.

Palatine— The palatine is not preserved in most of the specimens included here. Only the most posterolateral portion of the palatine is preserved in MOR 10912a (Fig. 2.4; 2.11: Appendix 5). MOR 10912a underwent shearing deformation and compression, such that the

palatine is crushed into the orbit. An oval-shaped foramen is present that is either the sphenopalatine foramen or the minor palatine foramen—the deformation of this specimen makes this determination difficult.

Lacrimal— The lacrimal forms the anterior rim of the orbit. The facial process of the lacrimal is semicircular, although, the lacrimal-jugal suture is fairly straight in MOR 10913a (Fig. 2.12; 2.11: Appendix 5). The facial process contacts the maxilla anteriorly, the jugal ventrally, and the frontal dorsally. The lacrimal foramen is circular to slightly ovoid, although the lacrimal foramen in MOR 10913a is deformed dorsoventrally. MOR 10913a (2.11: Appendix 5) and MOR 10911 (Fig. 2.3; 2.11: Appendix 5) have one distinct lacrimal canal, whereas MOR 10912a (Fig. 2.4; 2.11: Appendix 5) has two distinct canals that are subequal in size with one directly dorsal to the other. The lacrimal foramina in MOR 10912a are relatively smaller than the single foramen in the other specimens. However, intraspecific variation in the number of lacrimal foramina is also present in didelphids (Sánchez-Villagra and Asher 2002; Wible 2003; Voss and Jansa 2009).

Both MOR 10912a and MOR 10913a also preserve the orbital process of the lacrimal. The orbital process forms the anteromedial wall of the orbit, but, due to preservation, it is unclear if other bones contribute to this wall. The orbital process contacts the frontal and lacrimal posteriorly. The orbital process also contributes to the dorsal border of the maxillary foramen, which is visible in MOR 10913a; the remaining borders of the maxillary foramen are formed by the maxilla and possibly the palatine (although the palatine is not preserved in MOR 10913a).

Jugal—Only the anterior portion that contributes to the ventral rim of the orbit of the jugal is preserved. The anterior edge of the jugal and jugal-lacrimal suture is dorsal to the M1-M2 embrasure. From the jugal-lacrimal suture, the contact of the jugal with the maxilla arcs

broadly in a posterolateral direction. Although the contribution of the jugal to the anterior zygomatic root is preserved, much of the jugal that contributes to the zygomatic arch is not.

Frontal—Fragments of the frontals are present in both MOR10912a and MOR 10913a. Anteriorly, the contact between the frontals and nasals is W-shaped, much like in *Pucadelphys andinus* (Marshall et al., 1995). The frontal makes a small contact with the maxilla, wedged between the nasal and lacrimal. The frontal-lacrimal contact is almost horizontal dorsally and nearly vertical laterally. Most of the orbitotemporal fossa is not preserved, so contacts between the frontal and cranial bones (e.g., alisphenoid, palatine, parietal, etc.) that form this area of the skull cannot be determined. However, MOR 10912a and MOR 10913a preserve part of the frontal process that contributes directly to the medial wall of the orbit. The frontal process contributing to the orbit in MOR 10913a curves medially, but this is most likely due to dorsoventral compression deformation. MOR 10913a also preserves a distinct foramen near the edge of the supraorbital margin of the frontal that opens anteroventrally, which most likely is the foramen for the frontal diploic vein (Fig. 2.12; 2.11: Appendix 5). In dorsal view, the posterior portion of the frontal constricts medially (postorbital constriction) and then expands laterally near the most posterior edge. There is no evidence for a postorbital process and the supraorbital margin appears smooth.

Dentary— Fragments of the dentary are preserved in MOR 10911 (Figs. 2.2–2.3; 2.11: Appendix 5) and MOR 10912d (Figs. 2.7, 2.9; 2.11: Appendix 5). Anterior to the molar arcade, including the symphyseal region, the corpus is not preserved in either specimen (MOR 10911, anterior to the m3 and MOR 10912d, anterior to m2). From what is preserved of the corpus, the ventral margin is straight, but becomes convex ventrally below the m4, much like the condition seen in *Allqokirus*. There is no apparent retromolar space posterior to the m4. This is also the

condition in *Allqokirus* and the extant *Didelphis* but is different from the condition seen in *Andinodelphys*, *Pucadelphys*, and the extant *Monodelphis* (Wible 2003) and *Metachirus* (Voss and Jansa 2009). The digital model of MOR 10911 revealed that on the medial of the dentary, there is distinct groove extending from the ramus onto the corpus, and along the corpus for as long as the specimen is preserved. This is the mylohyoid groove (Bensley 1902), where the neurovascular bundle containing the mylohyoid nerve and artery rested; this groove has also been observed in other fossil metatherian taxa including, *Pucadelphys* (Marshall et al. 1995), *Mayulestes* (de Muizon 1998), *Allqokirus* (de Muizon et al. 2018), and *Andinodelphys* (de Muizon and Ladevèze 2020). There are no mental foramina visible on the corpora preserved.

Most of the ramus, including the coronoid, condyloid and angular process, are also missing in both specimens. Only a fragment of the anterior edge of the coronoid process is preserved in MOR 10911. More of the coronoid process is preserved in MOR 10912d, such that the most anterior portion of a shallow masseteric fossa is present.

Upper dentition—MOR 10913a is the only specimen associated with an incisor (I1?) (Fig. 2.11; 2.11: Appendix 5). The incisor is only visible in the digital model derived from μCT data; it is isolated and floating within the rock matrix. The tooth does not appear to have a distinct mesiostyle (anterior angle) or distostyle (posterior angle); it is fairly styliform. The apex of the crown is pointed, and the crown has a scoop-like morphology, in which the crown curves posterolingually. As such, we estimate this to be an upper first incisor, although it is difficult to determine if any wear is present from the digital model. The single root is long, but the exact position of the root-crown junction on the digital model is challenging to ascertain.

Upper canines are present in MOR 10912a, MOR 10912b, MOR 10912c and MOR 10913a. The upper right canine in MOR 10912a is complete and unworn except for some slight

apical wear, whereas the left canine is broken halfway down the crown such that the apex is missing. In MOR 10912b, the right canine has a fair amount of wear on the apex and mesial aspect, which may have been formed by attritional wear with the lower opposing canine. MOR 10912c preserves a complete right canine as well; on the surface of the specimen itself, it appears as though there is some slight apical wear, but the μCT scan shows that the apex is intact. MOR 10913a includes an isolated upper canine but it is broken and missing part of the root. The upper canines are simple and unicuspid with a single root; no accessory cusps are present. The apex is slightly recurved such that it is approximately ventral to the posterior border of the alveolus. The medial aspect is slightly less rounded than the lateral aspect. There is a shallow groove on the lateral aspect of the canine in MOR 10912c, like *Andinodelphys* but it is not as pronounced as in *Allqokirus*.

Three, double-rooted upper premolars are present and increase in size from P1 to P3; P1 is considerably smaller than P2 and P3 (Table 2.1). All upper premolars are oriented parallel to the axis of the tooth row, and each bears a single triangular cusp. Each premolar is transversely compressed (ovoid occlusal outline) and is longer than they are wide.

In lateral view, the apex of P1 is ventral to the anterior edge of the posterior root. P1 is close to the canine but it is not appressed such that the anterior root is lateral to the posterolateral edge of the canine as in *Andinodelphys*. The anterior edge is slightly convex, whereas the posterior edge is almost straight—a condition also seen also in *Allqokirus*, *Mayulestes*, and *Pucadelphys* (Marshall et al. 1995; de Muzion 1998; de Muizon et al. 2018). The posterior root is more robust than the anterior root. There is not an anterobasal cusp, but a small posterobasal cusp is present. Posterior to P1, a small diastema is visible.

P2 is larger than P1, but only slightly smaller than P3. It is slightly higher than the occlusal plane of the molars. Both anterobasal and posterobasal cusps are present, but the anterobasal cusp is much smaller than the posterobasal cusp. The apex of P2 is ventral to posterior edge of the anterior root—the anterior edge is not as convex as the condition seen in P2 but is almost straight instead. In lateral view, the posterior edge of the main cusp extends posteroventrally and then becomes concave at the base. In occlusal view, the posterior portion (dorsal to the posterior root) is wider than the anterior portion.

P3 is the largest and most robust of the three premolars. P3 shares many morphological features with P2. The apex of main cusp is higher than the occlusal plane of the molars, taller than P2, and ventral to the posterior edge of the anterior root. The anterior edge of the main cusp is mostly straight, whereas the posterior edge—which forms a sharp crest— extends posteroventrally to meet the posterobasal cusp. The anterobasal cusp is smaller and distinctly lower in the occlusal plane than the posterobasal cusp; a cingulum extends posterolabially from the anterobasal cusp for half of the anterior root. The posterobasal cusp is heel-like in shape. Small cingula extend on both labial and lingual sides of the posterobasal cusp as well. Much like P2, the posterior portion of P3 is wider than the anterior portion.

The upper molar morphology is consistent with previous descriptions and the diagnosis of *Alphadon halleyi* (e.g., Rigby and Wolberg 1987; Montellano 1992; Johanson 1996). The original diagnosis of *A. halleyi* (Sahnii 1972; maintained by Montellano 1992 and Cifelli 1990) does not accurately distinguish it from other species of *Alphadon* (Johanson 1996). Rigby and Wolberg (1987) and Johanson (1996) both revised the diagnosis to include more distinctive upper molar features. Johanson (1996) notes that the presence of a metastylar wing (distal stylar shelf) that is transversely wider (and more posterolabially directed) than the mesial stylar shelf is

diagnostic of *A*. *halleyi*. A metastylar wing that is transversely wider than the mesial stylar shelf is consistently observed in all of these specimens, especially in the M2s and M3s. Other diagnostic features include a broadly open ectoflexus on the M3s and a list of specific relative sizes and positions of the stylar cusps. Specifically, stylar cusp C is the smallest stylar cusp in *A*. *halleyi*, whereas stylar cusp B (stylocone) is the largest stylar cusp. The specimens described here follow these stylar cusp specifications, but we did notice some variability in the size of stylar cusp C. Stylar cusp C is more prominent on the M2s and M3s, whereas it is minute to the point where it is difficult to discern on the M1s—specifically in MOR 10911. This is most likely due to the resolution of the μCT scan, as details of the upper dentition of this specimen can only be viewed in the digital model. In all specimens, the paraconule and metaconule are closer to the protocone than to the paracone and metacone—another feature of *A*. *halleyi*, although this state is not found consistently (Montellano 1992; Johanson 1996). Almost all teeth lie within the observed size range found in *A. halleyi*; a few teeth are slightly larger than previously recorded ranges (Montellano 1992), but they are within the observed size range of *A*. *sahnii* (Table 2.1). We follow the recommendation of Johanson (1996) and consider *A*. *sahnii* a junior synonym of *A*. *halleyi*.

Lower dentition—Although the holotype of this species is a lower molar, Sahni (1972) did not include any lower molar features in the original diagnosis of *A*. *halleyi*, apart from mentioning that it is "smaller than *Alphadon praesagus* but larger than *A*. *lulli* from the Lance Formation." Although much of the discussion surrounding species classification within the Alphadontidae focuses on upper molar characteristics, Rigby and Wolberg (1987) revised the diagnosis of *A*. *halleyi* and attempted to include useful lower molar features; yet, the lower molar characteristics they included mainly rely on comparisons to *A*. *lulli* (now classified as

Protalphadon lulli) and *A. wilsoni* (a taxon that has subsequently had specimens referred to as both *A. marshi* and *A. jasoni*).

Only MOR 10911 (Fig. 2.3; 2.11: Appendix 5) and MOR 10912d (Figs. 2.7, 2.9; 2.11: Appendix 5) preserve lower dentition; however, no lower premolars are preserved. MOR 10911 is a fragmentary dentary and preserves the complete right molar arcade, m1–m4, whereas MOR 10912d, another fragmentary dentary, only preserves the left m2–m4. The morphology of these specimens is consistent with previously described lower molars of *A. halleyi* (Sahni 1972; Fox 1979; Rigby and Wolberg 1987; Cifelli 1990; Montellano 1992, 1988) and the dimensions of the specimens described here fall within the known size range of *A. halleyi* (Table 2.1). The protoconid is the tallest trigonid cusp; it is located anteriorly to the metaconid. The paraconid is anterior to the protoconid and medial to both the protoconid and metaconid. The metaconid is more anteroposteriorly elongated than the paraconid. The cristid obliqua extends from the hypoconid to the posterior wall of the trigonid ventral to the notch separating the protoconid and metaconid—an orientation characteristic of *Alphadon* (Sahni 1972; Montellano 1992). The hypoconid is the most robust talonid cusp. The entoconid and hypoconulid are twinned; the entoconid is anterolingual to the hypoconulid. Contra to most previous descriptions, the trigonid width is slight larger than the talonid width in all specimens; however, because other features characteristics of *A. halleyi* are present in the specimens, we classify them as such.

2.5.2 Phylogenetic Analysis Results

We obtained six equally parsimonious trees (tree length = 617, consistency index = 0.355, and retention index = 0.670; Fig. 2.13; 2.11: Appendices 6–9). Our strict consensus tree is consistent with recent analyses (e.g., Wilson et al. 2016; Cohen et al. 2020) in several ways.

Marsupialia is recovered as a monophyletic group that includes *Mimoperadectes–Peradectes* + *Herpetotherium* (Wilson et al., 2016). Additionally, stagodontids are recovered as a monophyletic group, as in previous studies (e.g., Wilson et al. 2016; Cohen et al.2020). The Bremer support for the sister taxa *Fumodelphodon*+ *Didelphodon* is high, whereas the support for *Hoodootherium* + *Eodelphis* + *Fumodelphodon* + *Didelphodon* clade is only moderate. As in previous studies (e.g., Williamson et al. 2012; Williamson et al. 2014; Wilson et al. 2016; Cohen et al. 2020), *Glasbius* is most closely related to the pediomyid taxa, and *Dakotadens* + *Scalaridelphys* + *Aquiladelphis* form the Aquiladelphidae clade (Cohen et al. 2020). In contrast, alphadontids do not form a monophyletic group; our results show *Alphadon* as the sister taxon to *Albertatherium*, but *Turgidodon* as more closely related to the Aquiladelphidae clade.

Although a number of similarities are present between our results and previous analyses, our strict consensus tree bears some striking differences. First, our results show the Maastrichtian Mongolian specimen, the so-called "Gurlin Tsav Skull' (GTS), nested within Stagodontidae (*Pariadens* is considered a stagodontid, although this designation has been debated [e.g., Fox and Naylor 2006]) (Fig. 2.13). This is interesting because this specimen has consistently grouped with SA Paleogene stem taxa (e.g., *Mayulestes* and *Andinodelphys*) in most other analyses. However, de Muizon and Ladevèze (2020) also recovered GTS as a sister taxon to *Eodelphis* and *Didelphodon* and that clade as sister group to Sparassodonta. On one hand, the relationship between GTS and stagodontids has been questioned because it relies mostly on dental features, such as a well-developed upper molar postmetacrista, which might represent convergent adaptations for carnivory (e.g., Fox and Naylor 1995; de Muizon and Lange-Badré 1997; Wilson et al. 2016; de Muizon and Ladevèze 2020). Our low consistency index indicates that homoplasy is common in our tree and is likely the reason for the current placement of GTS. On the other

hand, if GTS is indeed closely related to other stagodontids, as suggested by Marshall et al. (1990), its position may indicate a biogeographic link between Asia and North America during the Late Cretaceous. Laurasian dispersal events have been hypothesized for other terrestrial vertebrate groups, including dinosaurs (Evans et al. 2013), mammals (Kielan-Jaworowska 1975; Cifelli 2000), and lizards (Nydam 2013)—including the basal iguanomorph *Magnuviator ovimonsensis* from the Egg Mountain locality (DeMar et al. 2017)—so the phylogenetic position of GTS might indicate a Laurasian dispersal event of stagodontids.

The phylogenetic placements of borhyaenids and *Holoclemensia* also differ from previous analyses. Borhyaenids—an extinct group of carnivorous sparassodonts found in South America—have consistently grouped with other South American taxa (e.g., *Jaskhadelphys*, *Pucadelphys*) in previous studies (e.g., Rougier et al. 1998; Wilson et al. 2016). However, our results place borhyaenids as the earliest branching marsupialiform; this topology has a Bremer support of two. The synapomorphies associated with the separation of borhyaenids from other marsupialiforms are mostly dental features, which, again, are prone to homoplasy (de Muizon and Lange-Badré 1997). This position of borhyaenids may be due to biases created by treating this clade as a single operational taxonomic unit (OTU) (de Muizon and Ladevèze 2020). Other analyses (e.g., de Muizon and Ladevèze 2020; Engelman et al. 2020) that have focused on sparassodonts and used individual borhyaenid species as OTUs recover borhyaenid as a sister group to other South American stem taxa.

Contrary to the accepted position of borhyaenids, the phylogenetic position of the Aptian-Albian-aged *Holoclemensia* has been contentious (Beck in press). The original description (Slaughter 1968) and subsequent studies (e.g., Wilson and Riedel 2010; Luo et al. 2011; Rougier et al. 2015; Bi et al. 2015; Wilson et al. 2016) place it at the base of Metatheria.

However, other studies have placed this taxon outside of Theria altogether (Cifelli 1993) or considered it a tribotherian (Kielan-Jaworowska et al. 2004); others still consider *Holoclemensia* as a eutherian (Vullo et al. 2009; Averianov et al. 2010; Davis and Cifelli 2011). Our results fall in line with these latter studies and designate *Holoclemensia* as a eutherian or stem-eutherian (Fig. 2.13). The position of *Holoclemensia* is unclear and its phylogenetic position will remain unstable until more data can be garnered (Beck in press).

Finally, our strict consensus tree indicates that the relationships between crown marsupials, NA marsupialiforms, and SA marsupialiforms are ambiguous. All of these major groups form a polytomy. This contrasts with the resulting phylogenetic tree from Wilson et al. (2016), which dramatically altered the placement of crown marsupials within marsupialiforms—a topology has been upheld by subsequent other studies (e.g., Cohen et al. 2020; de Muizon and Ladevèze 2020). Although these new specimens of *Alphadon* provided novel data that contribute to our understanding of the morphology of Cretaceous metatherians, our phylogenetic results are not as clear. Though our resulting tree upholds the dichotomy between NA and SA marsupialiforms, the relationship of crown marsupials to these older taxa is ambiguous.

2.6 CONCLUSIONS

The metatherian skull material from Egg Mountain represents the most well-known specimens of *Alphadon halleyi* and some of the most complete crania of any North American Cretaceous metatherians (only *Didelphodon* has more complete material known). Here, we report novel morphological data for *Alphadon*, mostly in relation to the premolars and bones of the rostrum. General anatomical comparisons to other metatherian skulls are complicated by the deformation of the Egg Mountain specimens. However, a few critical observations can be made.

In comparison to *Didelphodon*—the only other skull material of a North American metatherian currently known—the nasals project more anteriorly (MOR 10912a; Fig. 2.4). *Alphadon halleyi* has a more slender, elongated rostrum than *Didelphodon*. The slim rostrum morphology of *A. halleyi* is more similar to the Paleogene South American taxa, including *Pucadelphys* and *Andinodelphys* (e.g., de Muizon et al. 2018). An *A. halleyi* specimen with an intact premaxilla and incisor arcade would aid in further rostrum comparisons with South American taxa, including the morphology of the ventral orientation angle of the alveolar process of the premaxilla (de Muizon et al. 2018: figure 15). Additionally, MOR 10911, MOR 10912a, and MOR 10913a hint at the large size of the orbit relative to rest of the cranium. The anterior portion of the orbit is preserved in these specimens, and we hypothesize that the orbit of *A. halleyi* is larger relative to the overall cranium than in *Didelphodon*. More complete orbital anatomy may be able to reveal dial activity patterns of *A. halleyi*, but we postulate that the animal probably had nocturnal habits based on its relatively large orbit. Furthermore, Brannick et al. (submitted) determined that *A. halleyi* was a soft-insect specialist. Future studies should focus on biomechanical and functional aspects of the cranial anatomy and utilize methodologies such as bite force estimations (e.g., Wilson et al. 2016) and bending strength of the dentary (e.g., Wilson et al. 2016; Brannick and Wilson 2020). As more complete fossil material for North American metatherians is discovered, more in-depth comparisons to other metatherian taxa can be made, autapomorphies for *A. halleyi* can be determined, and the ecology of *Alphadon halleyi* can further be inferred.

Using these new anatomical data, we updated the phylogenetic character scores for *Alphadon* and reexamined the phylogenetic relationships among metatherians. Our results demonstrate the presence of instability across the metatherian tree. However, pediomyids and

stagodontids are recovered as in previous studies, indicating they are robust, monophyletic groups. The relatively recent change in the phylogenetic placement of Marsupialia (being nested within a North American marsupialiforms clade instead of South American marsupialiform clade; Wilson et al. 2016) has been consistent across recent studies. Our results demonstrate the high instability in resolution between crown marsupials, North American marsupialiforms and South American marsupialiforms. We recover Marsupialia as a polytomy that includes both North American and South America groups. Thus, the place of origin of crown marsupials remains elusive. Yet, our study exhibits the importance of new, extraordinary fossil discoveries and incorporating subsequent anatomical details into phylogenetic analyses so that we can revise and improve our understanding of metatherian evolution.

2.7 ACKNOWLEDGEMENTS

We thank the Museum of the Rockies for allowing us to study these *Alphadon* specimens and J. Scannella and A. Atwater for access to specimens. We are grateful to T. Cox and J. S. Yeung for assistance in CT scanning operations and H. Z. Fulghum for assistance in post-processing of CT scans. We thank T. Cox and UW Children's Hospital as well as UW Computed Tomography Facility for access to CT scanners. We also thank D. DeMar, Jr. for his assistance and guidance in the use of TNT. We are grateful to C. de Muizon and S. Ladevèze for museum assistance and aid in confirming direct observations of South American metatherian taxa. We thank B.T. Hovatter, M. R. Whitney, J. J. Calede, B. R. Peecook, E. M. Edwards, S. Santana, C. Sidor, and T. Popowics for helpful feedback that improved this manuscript. This project was funded by NSF grant 1325365 (EAR) to D. J Varricchio, G. P Wilson, and J. Conrad and Evolving Earth grant #A132982 to A. L. Brannick and G. P. Wilson.

2.8 REFERENCES CITED

Averianov, A. O., Archibald, D., and Ekdale, E. G. 2010. New material of the Late Cretaceous Deltatheroidan mammal *Sulestes* from Uzbekistan and phylogenetic reassessment of the metatherian-eutherian dichotomy. Journal of Systematic Paleontology, 8(3):301–330. https://doi.org/10.1080/14772011003603499

Beck, R. M. D. In press. Current understanding of the phylogeny of Metatheria: a review. In F.J. Goin and A.M. Forasiepi (eds), New World marsupials and their extinct relatives: 100 million years of evolution. Springer.

Bennet, C. V., Upchurch, P., Goin, F. J., and Goswami, A. 2018. Deep time diversity of metatherian mammals: implications for evolutionary history and fossil-record quality. Paleobiology, 44(2):171-198. DOI: 10.1017/pab.2017.34

Bensley, B. A. 1902. On the identification of the Meckelian and mylohyoid grooves in the jaws of Mesozoic and Recent mammals. University of Toronto Studies, Biological Series, 3:75–82

Bi, S., Jin, X., Li, S., and Du, T. 2015. A new Cretaceous metatherian mammal from Henan, China. PeerJ, 3:e896. doi: 10.7717/peerj.896

Brannick, A. L., Fulghum, H. Z., Grossnickle, D. M., and Wilson Mantilla, G. P. submitted. Dental ecomorphology and macroevolutionary patterns of Late Cretaceous North American metatherians.

Cifelli, R. L. 1990. Cretaceous mammals of southern Utah. I. Marsupials from the Kaiparowits Formation (Judithian). Journal of Vertebrate Paleontology, 10:332–345

Cifelli, R. L. 2000. Cretaceous mammals of Asia and North America. Paleontological Society of Korea Special Publication 4:49–84.

Cifelli, R. L. and Davis, B. M. 2003. Marsupial Origins. Science 302:1899–1900

Cifelli, R.L. 1993. Theria of metatherian-eutherian grade and the origin of marsupials. In: F. S. Szalay, M. J. Novacek, and M. C. McKenna (eds.), Mammal phylogeny, volume 1: Mesozoic differentiation, multituberculates, monotremes, early therians, and marsupials. pp. 205–215. New York: Springer-Verlag

Clemens, W. A. (eds.), Mesozoic mammals: the first two-thirds of mammalian history. University of California Press, Berkeley, California

Clemens, W. A. 1968. A mandible of *Didelphodon vorax* (Marsupialia, Mammalia). Los Angeles County Museum Contributions in Science, 133:1–11

Clemens, W. A. 1979. Marsupialia, p. 192-220. In: Lillegraven, J. A., Kielan-Jaworowska, Z. and W. A. Clemens (eds.), Mesozoic mammals: the first two-thirds of mammalian history. pp. 192–220. University of California Press, Berkeley, California.

Davis, B. M. and Cifelli, R. L. 2011. Reappraisal of the tribosphenidan mammals from the Trinity Group (Aptian–Albian) of Texas and Oklahoma. Acta Palaeontologica Polonica, 56(3):441–462

de Muizon, C. 1998. *Mayulestes ferox,* a borhyaenoid (Metatheria, Mammalia) from the early Palaeocene of Bolivia. Phylogenetic and palaeobiologic implications. Geodiversitas, 20(1):19–142

de Muizon, C. 1999. Marsupial skulls from the Deseadan (late Oligocene) of Bolivia and phylogenetic analysis of the Borhyaenoidea (Marsupialia, Mammalia). Geobios, 32(3):483–509. https://doi.org/10.1016/S0016-6995(99)80022-9

de Muizon, C. and Ladevèze, S. 2020. Cranial anatomy of *Andinodelphys cochabambensis*, a stem metatherian from the early Palaeocene of Bolivia. Geodiversitas, 42(30):597–739

de Muizon, C. and Lange-Badré, B. 1997. Carnivorous dental adaptations in marsupials and placentals and phylogenetical reconstruction. Lethaia, 30: 351–366. https://doi. org/10.1111/j.1502-3931.1997.tb00481.x

de Muizon, C., Ladevèze, S., Selva, C., Vignaud, R., and Goussard, F. 2018. *Allqokirus australis* (Sparassodonta, Metatheria) from the early Palaeocene of Tiupampa (Bolivia) and the rise of the metatherian carnivorous radiation in South America. Geodiversitas, 40(16):363–459

DeMar, D. G. Jr, Conrad, J. L., Head, J. J., Varricchio, D. J. and Wilson, G. P. 2017. A new Late Cretaceous iguanomorph from North America and the origin of New World Pleurodonta (Squamata, Iguania). Proceedings of the Royal Society B, 284:e20161902

Dias, C.A.R. and Perini, F. A. 2018. Biogeography and early emergence of the genus *Didelphis* (Didelphimorphia, Mammalia). Zoologica Scripta, 47:645–654

Engelman, R. K., Flynn, J. J., Wyss, A. R., and Croft, D. A. 2020. *Eomakhaira molossus*, A New Saber-Toothed Sparassodont (Metatheria: Thylacosmilinae) from the Early Oligocene (?Tinguiririan) Cachapoal Locality, Andean Main Range, Chile. American Museum Novitates, 3957. https://doi.org/10.1206/3957.1

Evans, D., D. Larson, and P. J. Currie. 2013. A new dromaeosaurid (Dinosauria: Theropoda) with Asian affinities from the latest Cretaceous of North America. Naturwissenschaften, 100:1041–1049

Fox, R. C. and Naylor, B. G. 1995. The relationships of the Stagodontidae, primitive North American Late Cretaceous mammals. In Sun A. and Wang Y. (eds) Sixth Symposium on Mesozoic Terrestrial Ecosystems and Biota. China Ocean Press, Beijing: 247-250

Fox, R. C. and Naylor, B. G. 2006. Stagodontid marsupials from the Late Cretaceous of Canada and their systematic and functional implications. Acta Palaeontologica Polonica, 51(1):13–36

Freimuth, W. J. and Varricchio, D. J. 2019. Insect trace fossils elucidate depositional environments and sedimentation at a dinosaur nesting site from the Cretaceous (Campanian) Two Medicine Formation of Montana. Palaeogeography, Palaeoclimatology, Palaeoecology, 534:109262

Freimuth, W. J., Varricchio, D. J., Brannick, A. L., Weaver, L. N., and Wilson Mantilla, G. P. 2021. Mammal-bearing gastric pellets potentially attributable to *Troodon formosus* at the Cretaceous Egg Mountain locality, Two Medicine Formation, Montana, USA. Paleontology, doi: 10.1111/pala.12546

Goin, F. J., Woodburne, M. O., Zimicz, A. N., Martin, G. M., and Chornogubsky, L. 2016. A brief history of South American metatherians: evolutionary contexts and intercontinental dispersals. Springer, Dordrecht Heidelberg New York London

Goloboff, P. A. 1999. Analyzing large data sets in reasonable times: solutions for composite optima. Cladistics 15, 415–428

Goloboff, P. A., Farris, J. S. and Nixon, K. C. 2008. TNT, a free program for phylogenetic analysis. Cladistics 24, 774–786

Goloboff, P. A., Farris, J. S., Nixon, K. C., 2008. TNT, a free program for phylogenetic analysis. Cladistics, 24:774–786

Horner, J. R. 1984. The nesting behavior of dinosaurs. Scientific American 250:130–137

Horner, J. R. 1987. Ecological and behavioral implications derived from a dinosaur nesting site in S. J. Czerkas and E. C. Olson (eds.) Dinosaurs Past and Present, Vol II. Natural History

Museum of Los Angeles County, Los Angeles, pp. 51–63

Horovitz, I., Martin, T., Bloch, J., Ladevèze, S., Kurz, C., and Sánchez-Villagra, M. R. 2009. Cranial anatomy of the earliest marsupials and the origin of opossums. PLoS ONE, 4(12): e8278

Johanson, Z. 1996. Revision of the Late Cretaceous North American marsupial genus *Alphadon*. Palaeontographica Abteilung A: Palaeozoologie-Stratigraphie, 242(4):127–184

Kielan-Jaworoska, Z., Cifelli, R. L., and Luo, Z. 2004. Mammals from the age of dinosaurs: origins, evolution, and structure. Columbia University Press, New York

Kielan-Jaworowska, Z. 1975. Late Cretaceous Mammals and Dinosaurs from the Gobi Desert: Fossils excavated by the Polish-Mongolian Paleontological Expeditions of 1963–71 cast new light on primitive mammals and dinosaurs and on faunal interchange between Asia and North America. American Scientist, 63(2):150–159

Kirsch, J. A., Bleiweiss, R. E., Dickerman, A. W., and Reig, O. A. 1993. DNA/DNA hybridization studies of carnivorous marsupials. III. Relationships among species of *Didelphis* (Didelphidae). Journal of Mammalian Evolution, 1(1):75–97

Krause, D. W. 2001. Fossil molar from a Madagascan marsupial. Nature, 412:497–498. https://doi.org/10.1038/35087649

Lillegraven, J. A. 1969. Latest Cretaceous mammals of upper part of Edmonton Formation of Alberta, Canada, and review of marsupial-placental dichotomy in mammalian evolution. The University of Kansas Paleontological Contributions, Article 50

Lorenz, J. C. and Gavin, W. 1984. Geology of the two medicine formation and the sedimentology of a dinosaur nesting ground. 175–186. In McBane, J.D. and Garrioson, P.B. (eds). Montana Geological Society 1984 field conference guidebook. Montana

Geological Society

Luckett, W. P. 1993. In Mammal Phylogeny: Mesozoic Differentiation, Multituberculates, Monotremes, Early Therians, and Marsupials (eds. F. S. Szalay, M. J. Novacek, and M. C. McKenna). Springer, New York. pp. 182–204

Luo, Z.-X., Yuan, C. X., Meng, Q. J., and Ji, Q. 2011. A Jurassic eutherian mammal and divergence of marsupials and placentals. Nature, 476(7361): 442–445 doi:10.1038/nature10291

Macrini, T. E., de Muizon, C., Cifelli, R. L., and Rowe, T. 2007. Digitial endocast of *Pucadelphys andinus*, a Paleocene metatherian. Journal of Vertebrate Paleontology, 27(1):99–107

Maddison, W. P. and Maddison, D. R. 2015. Mesquite: a modular system for evolutionary analyses. Version 3.10. http://www.mesquiteproject.org

Marshall, L. G., and de Muizon, C. 1995. Part II. The skull. Pp. 21–90, in Pucadelphys andinus (Marsupialia, Mammalia) from the Early Paleocene of Bolivia (L.G. Marshall, C. de Muizon, and D. Sigogneau-Russell, eds.). Mémoires du Muséum National d'Histoire Naturelle, 165

Marshall, L. G., Case, J. A., and Woodburne, M. O. 1990. Phylogenetic relationships of the families of marsupials. In: Genoways, H.H. (ed.) Current Mammalogy. Plenum Press, New York: 433-505

Martin, A. J. and Varricchio, D. J. 2011. Paleoecological utility of insect trace fossils in dinosaur nesting sites of the Two Medicine Formation (Campanian), Choteau, Montana. Historical Biology, 23(1):15–25

Martin, J. E. et al. 2005. A new European marsupial indicates a Late Cretaceous high-latitude

transatlantic dispersal route. Journal of Mammalian Evolution, 12(3/4):495–511

Montellano, M. 1998. Alphadon halleyi (Didelphidae, Marsupilia) from the Two Medicine Formation (Late Cretaceous, Judithian) of Montana. Journal of Vertebrate Paleontology 8(4):378–382

Montellano, M., Weil, A., and Clemens, W. A. 2000. An exceptional specimen of *Cimexomys judithae* (Mammalia: Multituberculata) from the Campanian Two Medicine Formation of Montana, and the phylogenetic status of *Cimexomys*. Journal of Vertebrate Paleontology 20(2):333–340

Nixon, K. C. 1999. The parsimony ratchet, a new method for rapid parsimony analysis. Cladistics 15, 407–414

Nydam, R. L. 2013. Squamates from the Jurassic and Cretaceous of North America. Palaeobiodiversity and Palaeoenvironments, 93:535–565

O'Leary, M. A. et al. 2013. The Placental Mammal Ancestor and the Post K-Pg Radiation of Placentals. Science, 339:662–667

Rigby, J. K., Jr. and Wolberg, D. L. 1987. The therian mammalian fauna (Campanian) of Quarry 1, Fossil Forest study area, San Juan Basin. Geological Society of America, Special Paper 209:51–79

Rogers, R. R. 1990. Taphonomy of Three Dinosaur Bone Beds in the Upper Cretaceous Two Medicine Formation of Northwestern Montana: Evidence for Drought Related Mortality. PALAIOS 5(5):394–413

Rogers, R. R. 1998. Sequence analysis of the Upper Cretaceous Two Medicine and Judith River Formations, Montana: nonmarine response to the Claggett and Bearpaw marine cycles. Journal of Sedimentary Research 68(4):615–631

Rogers, R. R., Swisher, C. C., and Horner, J. R. 1993. Ar/Ar age and correlation of the non-marine Two Medicine Formation (Upper Cretaceous), northwestern Montana. Canadian Journal of Earth Sciences, 30:1066–1075

Rougier, G. W., Davis, B. M., and Novacek, M. J. 2015. A deltatheroidan mammal form the Upper Cretaceous Baynshiree Formation, eastern Mongolia. Cretaceous Research, 52:167–177

Rougier, G. W., Wible, J. R., and Novacek, M. J. 1998. Implications of Deltatheridium specimens for early marsupial history. Nature, 396:459-463. https://doi.org/10.1038/24856

Sahni, A. 1972. The vertebrate fauna of the Judith River Formation. Bulletin American Museum of Natural History, 147:321–412

Sánchez-Villagra, M. R. 2013. Why are there fewer marsupials than placentals? On the relevance of geography and physiology to evolutionary patterns of mammalian diversity and disparity. Journal of Mammal Evolution, 20:279–290. DOI 10.1007/s10914-012-9220-3

Sánchez-Villagra, M. R. and Asher, R. J. 2002. Cranio-sensory adaptations in small faunivorous semiaquatic mammals, with special reference to olfaction and the trigeminal system. Mammalia, 66:93–109

Schindelin, J. et al. 2012. Fiji: an open-source platform for biological-image analysis. Nature Methods, 9(7), 676–682. doi:10.1038/nmeth.2019

Scofield, G. B. 2018. Analysis of hadrosaur teeth from Egg Mountain Quarry, a diffuse microsite locality, upper Cretaceous, Two Medicine Formation, northwest Montana. Unpublished MSc thesis, Montana State University, Bozeman, 138 pp

Shelton, J. A. 2007. Application of sequence stratigraphy to the nonmarine Upper Cretaceous Two Medicine Formation, Will Creek Anticline, northwestern Montana (Masters Thesis).

Montana State University

Slaughter, B. H. 1968. Earliest known marsupials. Science, 162:254–255

Varricchio, D. J, Borkowski, J. J., and Horner, J. R. 1997. Nest and egg clutches of the dinosaur *Troodon formosus* and the evolution of avian reproductive traits. Nature, 385:247–250

Varricchio, D. J. and Trueman, C. N. 1999. A nesting trace with eggs for the Cretaceous theropod dinosaur *Troodon formosus*. Journal of Vertebrate Paleontology, 19:91–100

Varricchio, D. J. et al. 2010. Tracing the Manson impact event across the Western Interior Cretaceous Seaway. The Geological Society of America. Special Paper 465:269–299

Voss, R. S. and Jansa, S. A. 2009. Phylogenetic relationships and classification of didelphid marsupials, an extant radiation of New World metatherian mammals. Bulletin of the American Museum of Natural History, 322

Vullo, R., Gheerbrant, E., de Muizon, C., and Néraudeau, D. 2009. The oldest modern therian mammal from Europe and its bearing on stem marsupial paleobiology. Proceedings of the National Academy of Sciences, 106(47):19910–19915 https://doi.org/10.1073/pnas.0902940106

Weaver, L. N., Varricchio, D. J., Sargis, E. J., Chen, M., Freimuth, W. J. and Wilson Mantilla, G. P. 2021. Early mammalian social behavior revealed by multituberculates from a dinosaur nesting site. Nature Ecology & Evolution, 5:32–37

Wible, J. R. 2003. On the cranial osteology of the short-tailed opossum *Monodelphis brevicaudata* (Didelphidae, Marsupialia). Annals of Carnegie Museum, 72(3):137–202

Williamson, T. E. and Lofgren, D. L. 2014. Late Paleocene (Tiffanian) metatherians from the Goler Formation, California. http://dx.doi.org/10.1080/02724634.2013.804413

Williamson, T. E., Brusatte, S. L., and Wilson, G. P. 2014. The origin and early evolution of

metatherian mammals: The Cretaceous record. ZooKeys, 76(465):1–76. https://doi.org/10.3897/zookeys.465.8178

Wilson, G. P. and Riedel, J. A. 2010. New specimen reveals deltatheroidan affinities of the North American Late Cretaceous mammal *Nanocuris*. Journal of Vertebrate Paleontology, 30(3):872–884

Wilson, G. P., 2014. Mammalian extinction, survival, and recovery dynamics across the Cretaceous-Paleogene boundary in northeastern Montana, USA, Geological Society of America Special Paper 503, p. 1–28. In Wilson, G.P., Clemens, W.A., Horner, J.R., and Hartman, J.H. (eds.), Through the End of the Cretaceous in the Type Locality of the Hell Creek Formation in Montana and Adjacent Areas, doi:10.1130/2014.2503(15)

Wilson, G. P., Ekdale, E. G., Hoganson, J. W., Calede, J. J., and Vander Linden, A. 2016. A large carnivorous mammal from the Late Cretaceous and the North American origin of marsupials. Nature Communications, 7:13734. https://doi.org/10.1038/ncomms13734

2.9 FIGURES

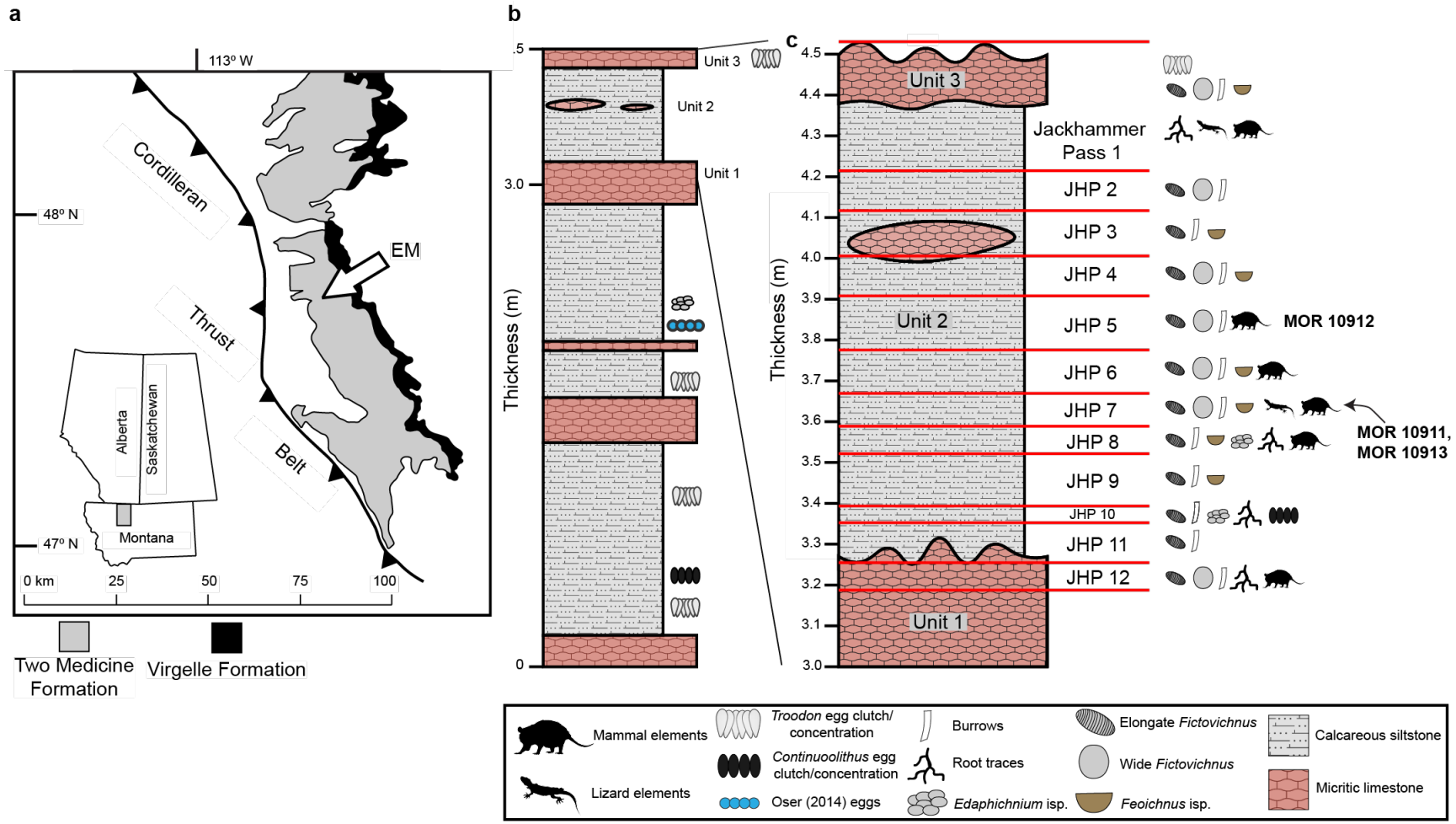

Figure 2.1 Geography and geology at the Egg Mountain locality (Museum of the Rockies Tm-006). **A,** Map of the field area at the Willow Creek Anticline, Two Medicine Formation near Choteau, MT, USA. The Egg Mountain locality is indicated with the arrow.

B, Schematic stratigraphic section measured at the Egg Mountain locality. **C,** The top 1.5 m of the main quarry; schematic jackhammer passes are superimposed over the stratigraphy. Specimens are assigned to jackhammer passes to track their stratigraphic position and the level at which specimens occur within a jackhammer pass is approximate. Jackhammer passes are stratigraphically parallel cuts that proceeded at ~11 cm in thickness. MOR 10912 was located within jackhammer pass 5 whereas both MOR 10911 and MOR 10913 were located within jackhammer pass 7. Figure modified from Weaver et al. 2020 and Freimuth et al. 2021. Lizard silhouette by Ghedo and T. Michael Keesey (https://creativecommons.org/licenses/by-sa/3.0/). Abbreviations: **EM,** Egg Mountain; **JHP,** jackhammer pass.

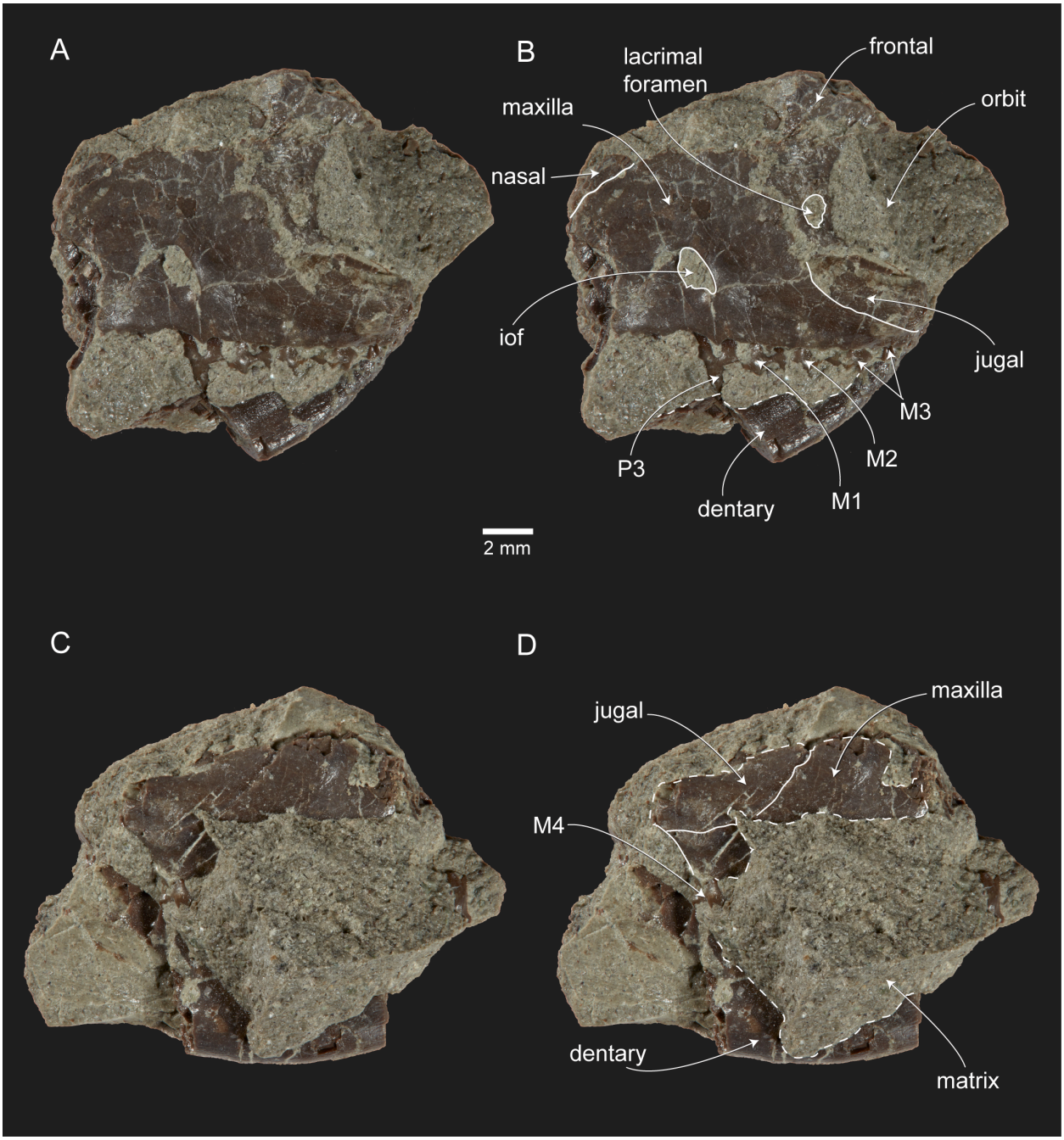

Figure 2.2. MOR 10911, incomplete maxillae with associated lower right m1–m4 of *Alphadon halleyi*. **A,** Left lateral view. **B,** Left lateral view with accompanying labels. **C,** Right lateral view. **D,** Right lateral view with accompanying labels. Abbreviations: **iof,** infraorbital foramen.

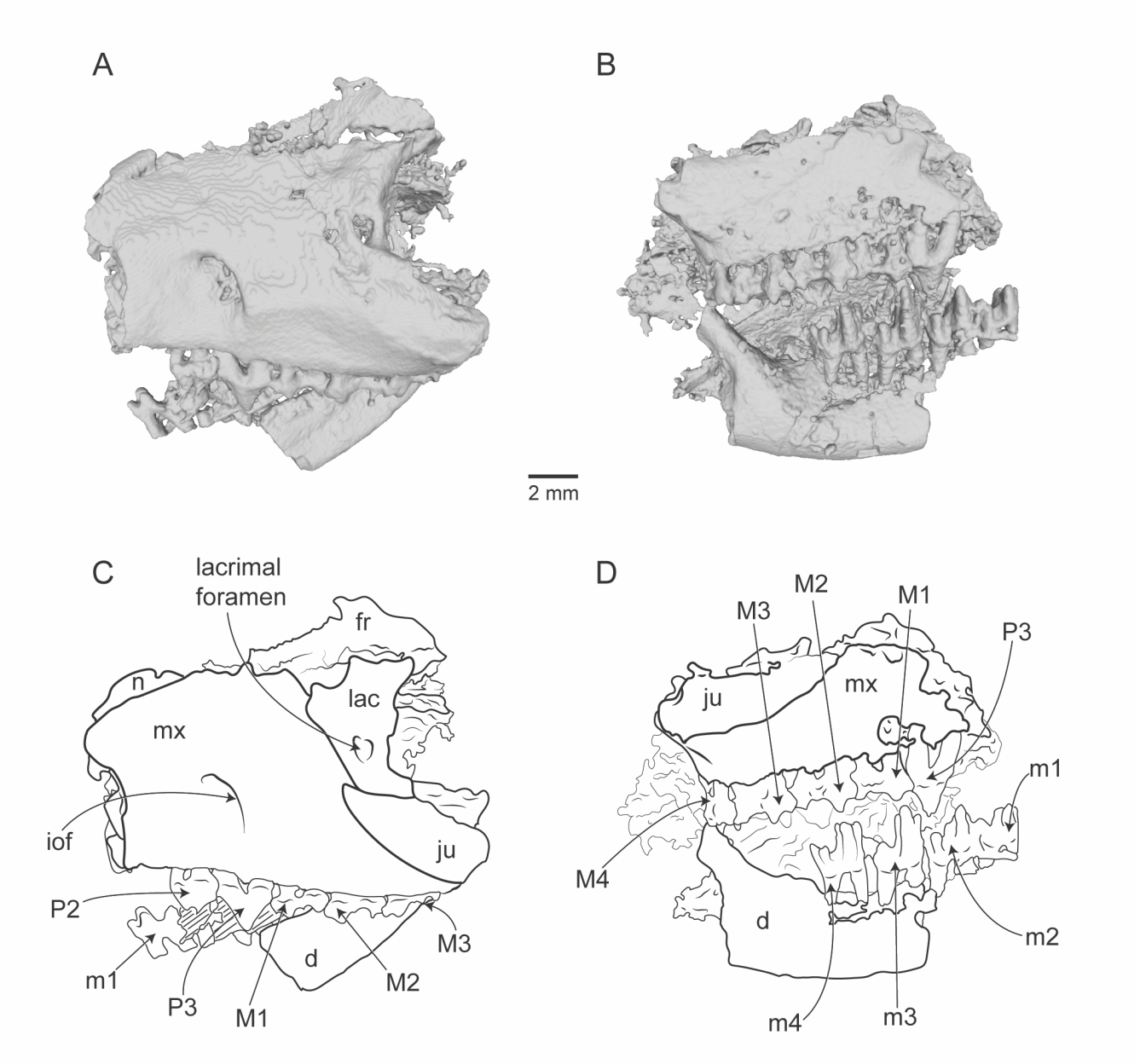

Figure 2.3. MOR 10911, incomplete maxillae with associated lower right m1–m4 of *Alphadon halleyi*. **A,** Digital model in left lateral view. **B,** Digital model in right lateral view. **C,** Accompanying line drawing to **A** in left lateral view. **D,** Accompanying line drawing to **B** in right lateral view. Abbreviations: **d,** dentary; **fr,** frontal; **iof,** infraorbital foramen; **ju,** jugal; **lac,** lacrimal; **mx,** maxilla.

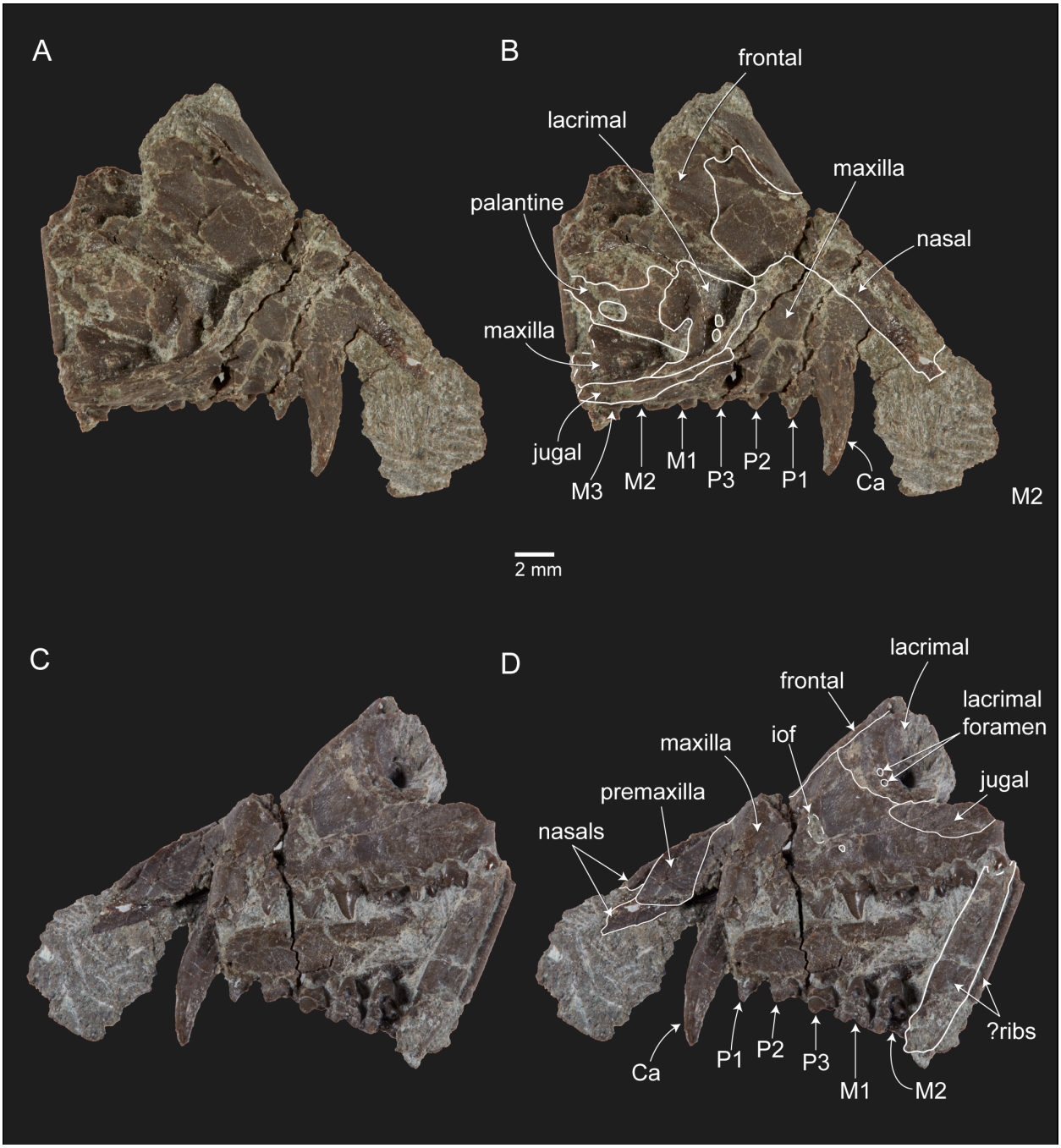

Figure 2.4. MOR 10912a, a partial skull of *Alphadon halleyi*. **A,** Right lateral view. **B,** Right lateral with accompanying labels. **C,** Left lateral and occlusal views. **D,** Left lateral and occlusal views with accompanying labels. Abbreviations: **Ca,** canine; **iof,** infraorbital foramen.

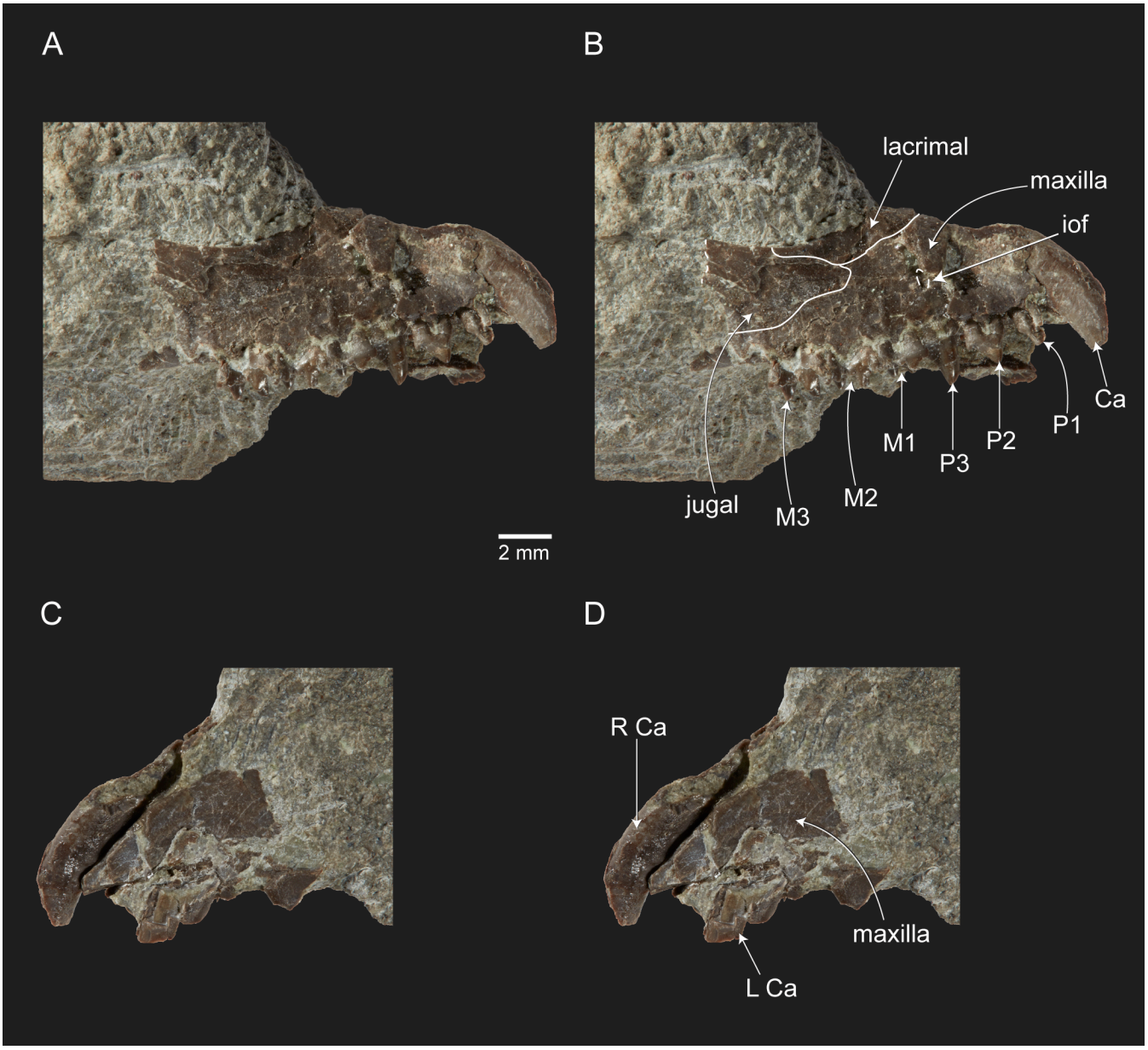

Figure 2.5. MOR 10912b, a right maxilla with associated dentition of *Alphadon halleyi*. **A,** Right lateral view. **B,** Right lateral view with accompanying labels. **C,** Left lateral view. **D,** Left lateral view with accompanying labels. Abbreviations: **Ca,** canine; **iof,** infraorbital foramen. Right (R) and left (L) are labeled to denote side of dentition.

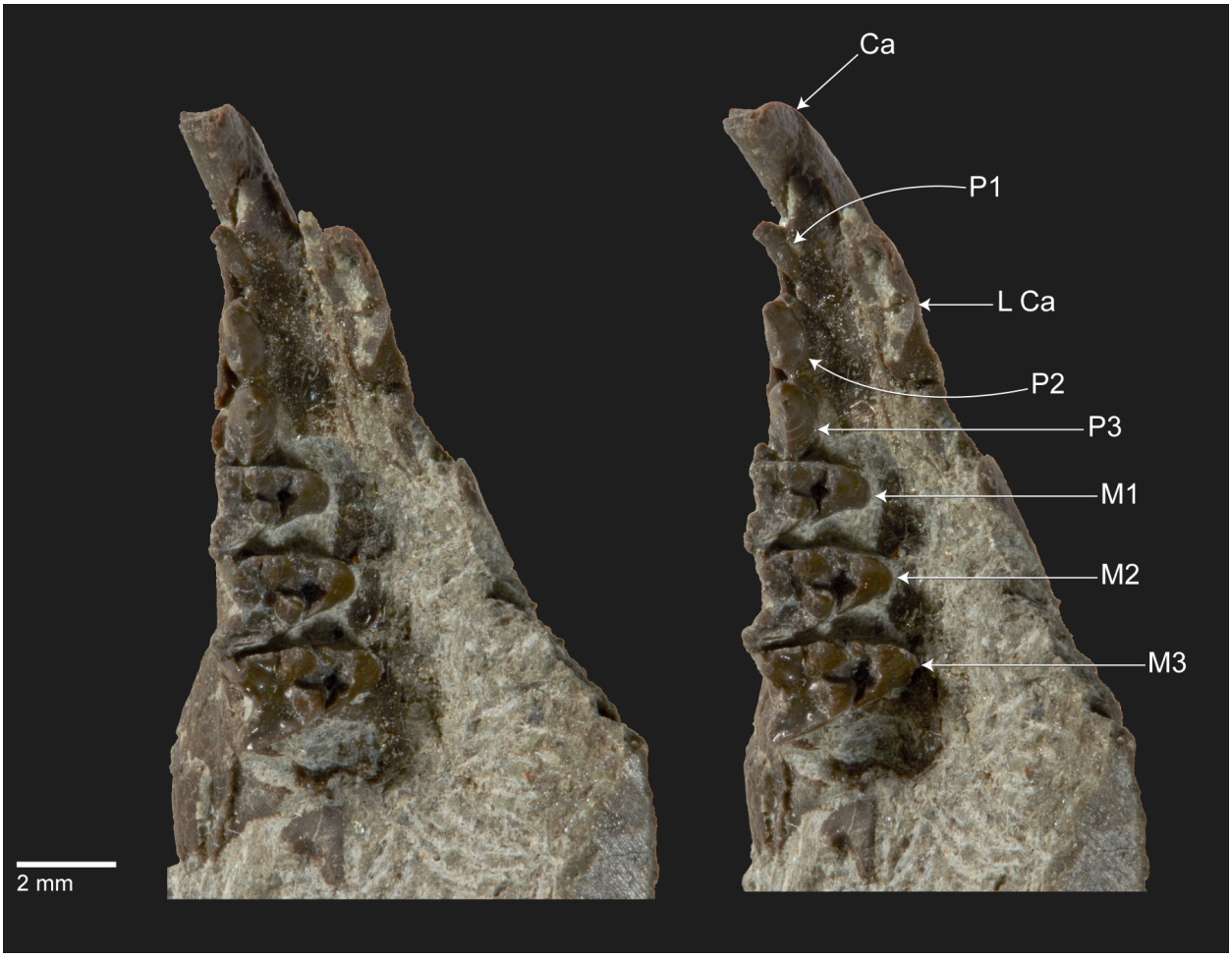

Figure 2.6. MOR 10912b of *Alphadon halleyi* in occlusal stereopair. Abbreviations: **Ca,** canine.

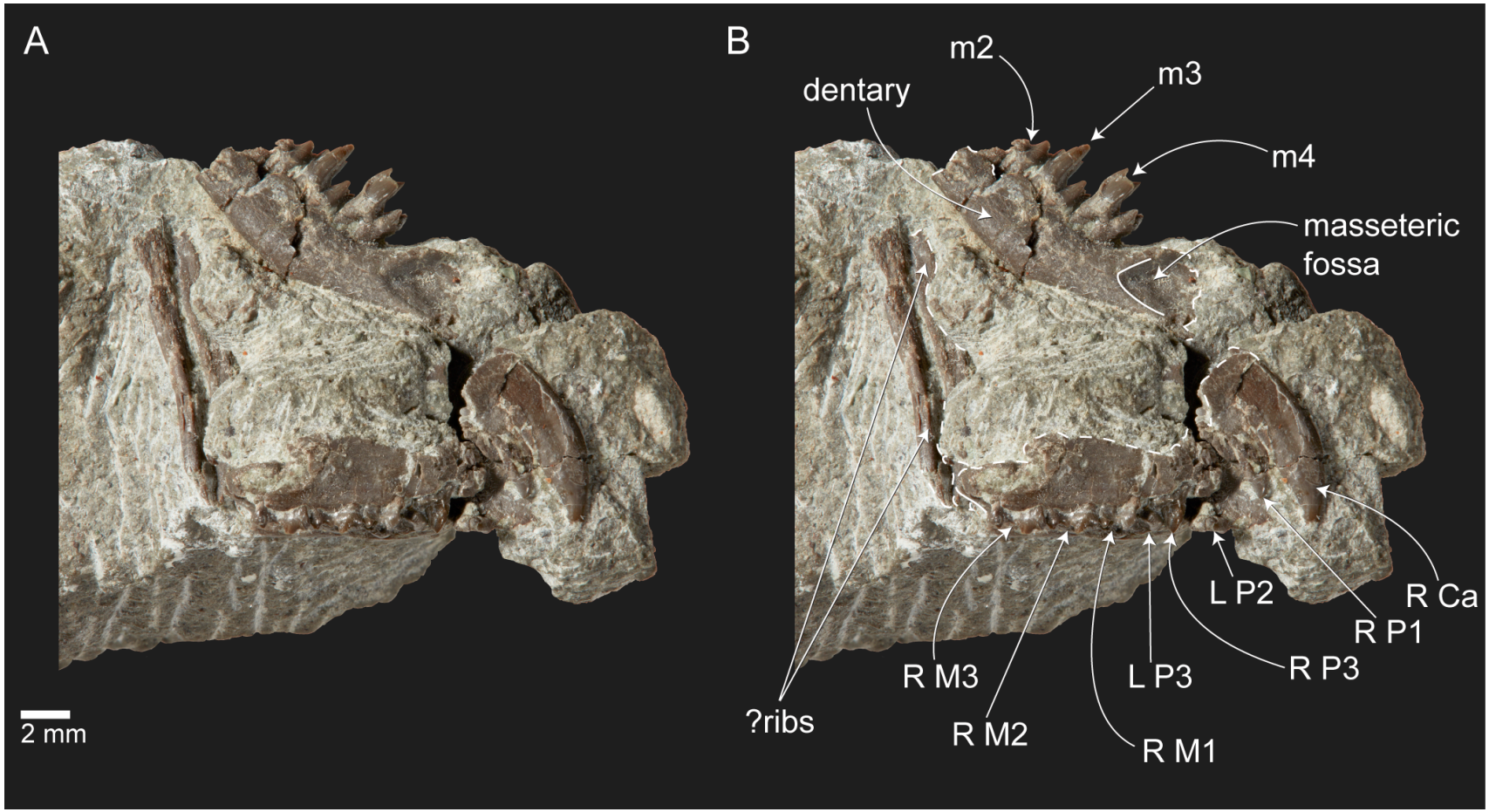

Figure 2.7. MOR 10912c, a partial skull with associated upper dentition, and MOR 10912d, a partial left dentary with associated dentition, of *Alphadon halleyi*. **A,** Lateral view. **B,** Lateral view with accompanying labels. Abbreviations: **Ca,** canine; **mx,** maxilla. Right (R) and left (L) are labeled to denote side of dentition

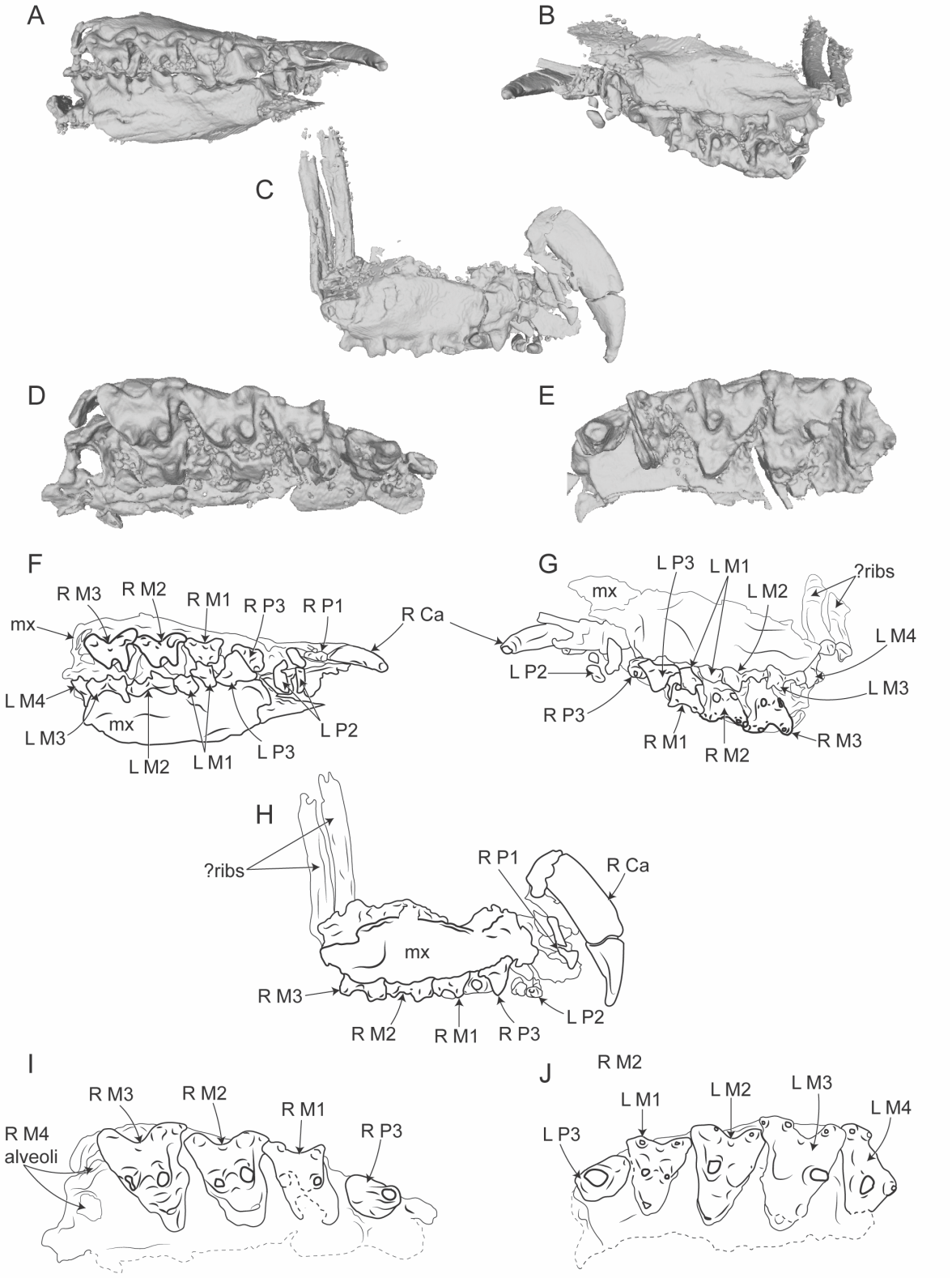
A
B
C
D
E
F
R M3
R M2
R M1
R P3
R P1
R Ca
mx
L M4
L M3
mx
L P2
L M2
L M1
L P3
G
L P3
L M1
?ribs
mx
L M2
L M4
L P2
L M3
R P3
R M1
R M2
R M3
H
?ribs
R P1
R Ca
mx
R M3
L P2
R M2
R M1
R P3
I
R M3
R M2
R M1
R P3
R M4
alveoli
J
R M2
L M1
L M2
L M3
L M4
L P3

Figure 2.8. Digital models of MOR 10912c, a partial skull of *Alphadon halleyi*. **A, F,** Digital model in ventral view and associated line drawing. **B, G,** Digital model in left lateral view and associated line drawing. **C, H,** Digital model in right lateral view and associated line drawing. **D, I,** Digital model of right molar row and associated line drawing. **E, J,** Digital model of left molar row and associated line drawing. Right (R) and left (L) are labeled to denote side of dentition.

Figure 2.9. MOR 10912d, lower m2–m4, of *Alphadon halleyi* in occlusal stereopair.

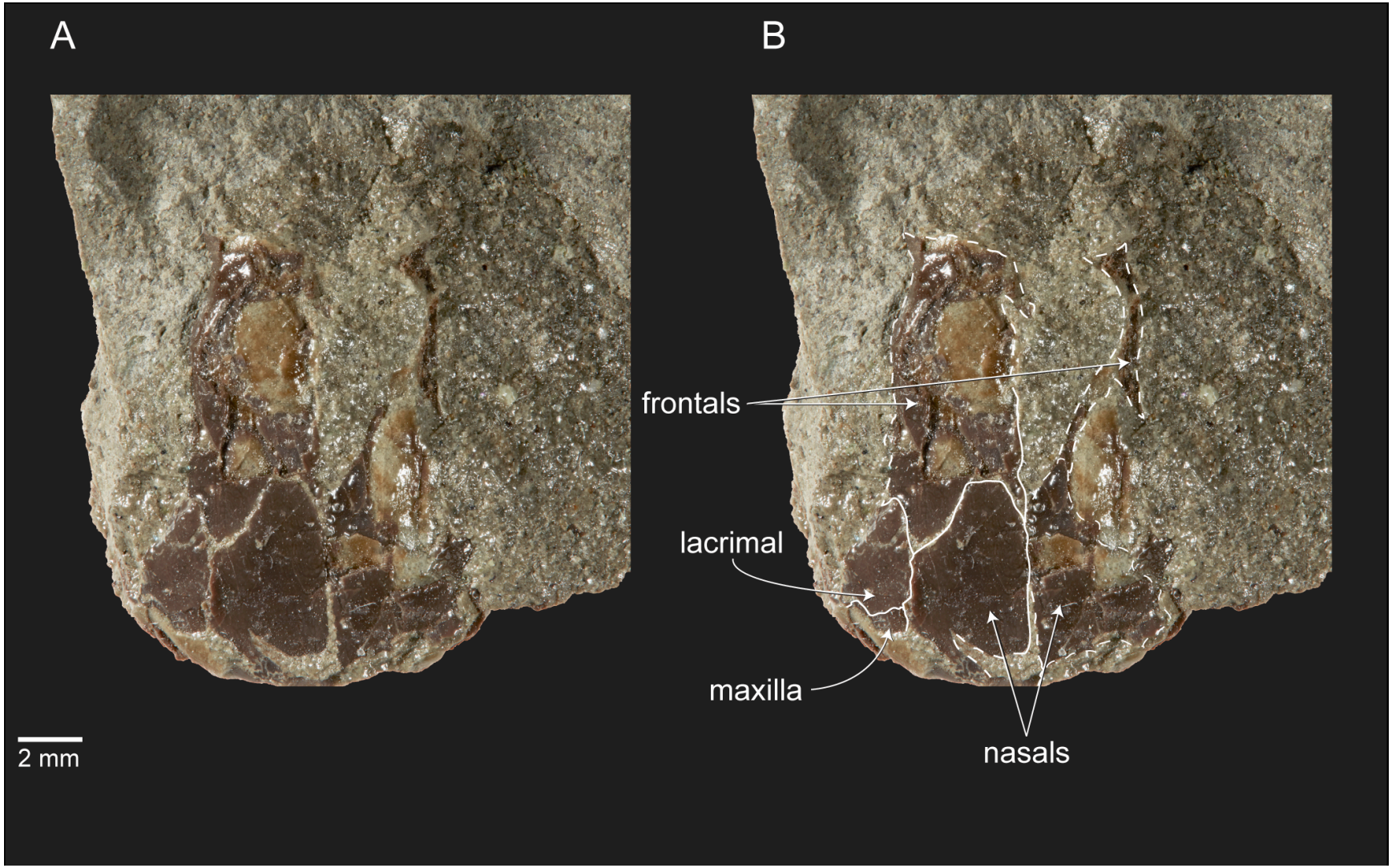

Figure 2.10. MOR 10913a, a partial skull, of *Alphadon halleyi*. **A,** Dorsal view. **B,** Dorsal view with accompanying labels.

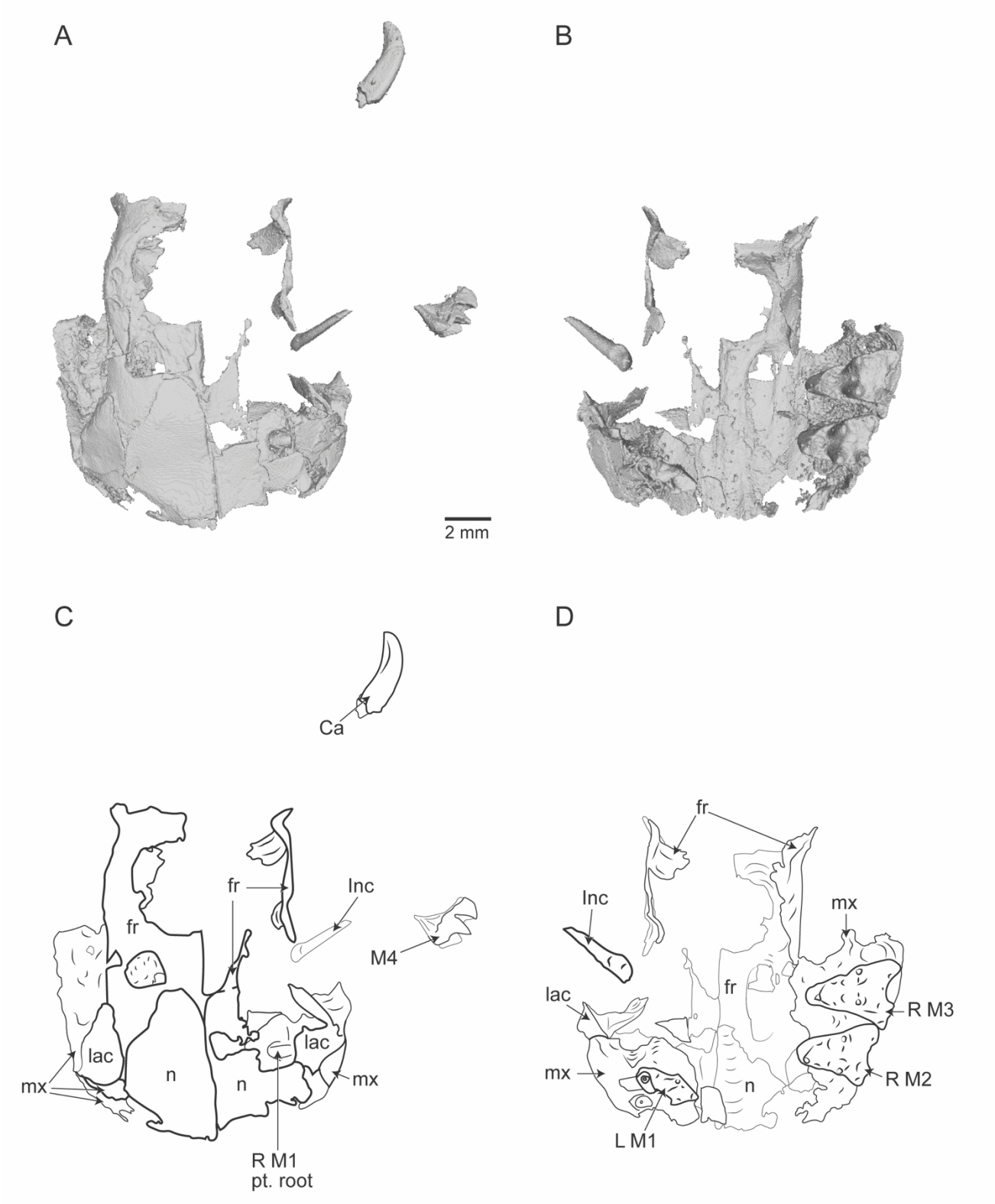
A
B
2 mm
C
Ca
fr
Inc
M4
fr
lac
n
n
lac
mx
mx
R M1
pt. root
D
fr
Inc
mx
lac
fr
R M3
mx
R M2
n
L M1

Figure 2.11. MOR 10913a, a partial skull, of *Alphadon halleyi*. **A,** Digital model of cranial elements in dorsal view. **B,** Digital model of cranial elements in ventral view. **C,** Accompanying line drawing in dorsal view. **D,** Accompanying line drawing in ventral view. Abbreviations: **Ca,** canine; **d,** dentary; **fr,** frontal; **Inc,** incisor; **lac,** lacrimal; **mx,** maxilla; **n,** nasal. Right (R) and left (L) are labeled to denote side of dentition.

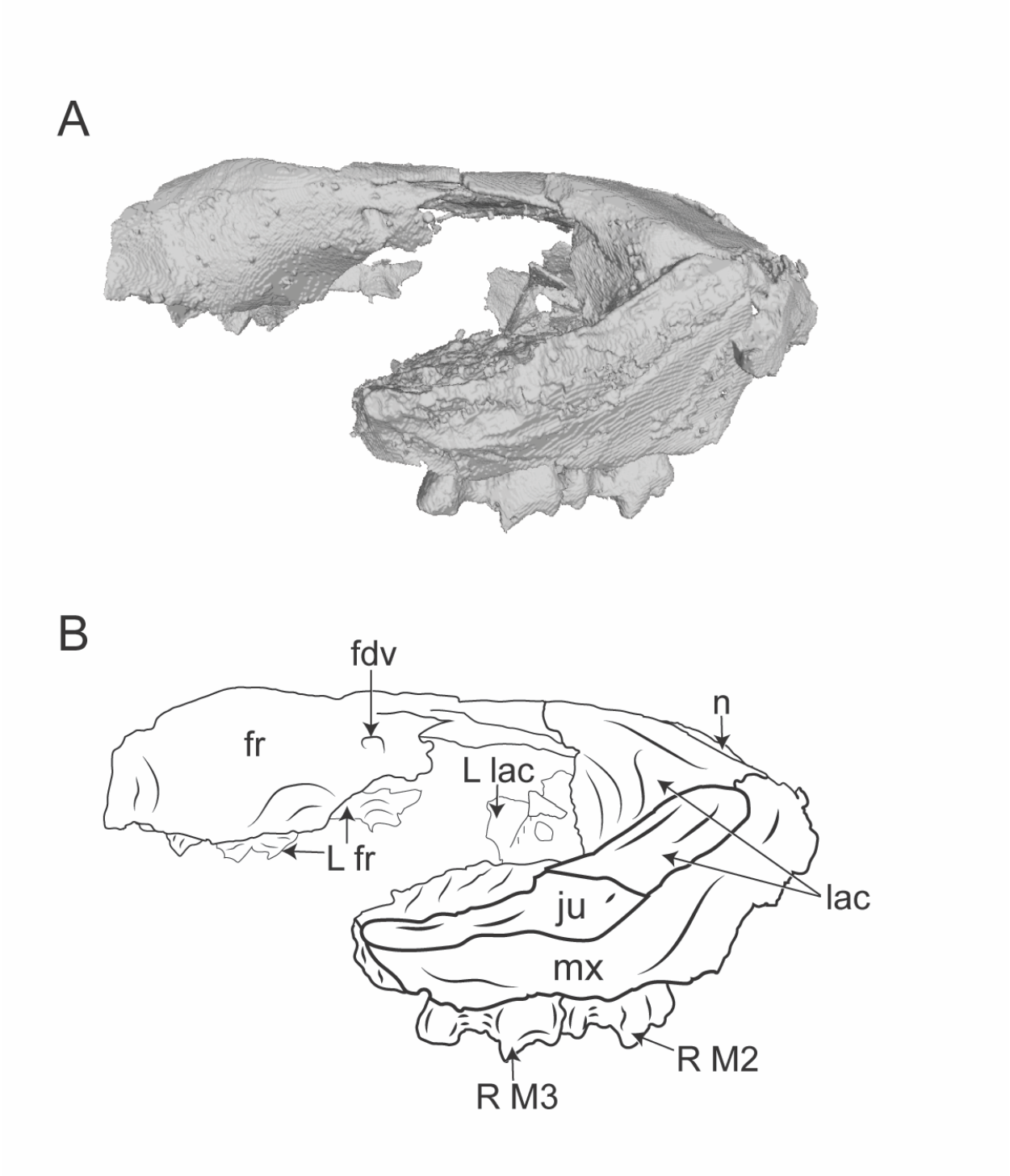

Figure 2.12. MOR 10913a, a partial skull, of *Alphadon halleyi*. **A,** Digital model in right lateral view. **B,** Accompanying line drawing in right lateral view. Abbreviations: **fdv,** foramen for the

frontal diploic vein; **fr,** frontal; **ju,** jugal; **lac,** lacrimal; **mx,** maxilla; **n,** nasal. Left (L) lacrimal and frontal are labeled for clarity.

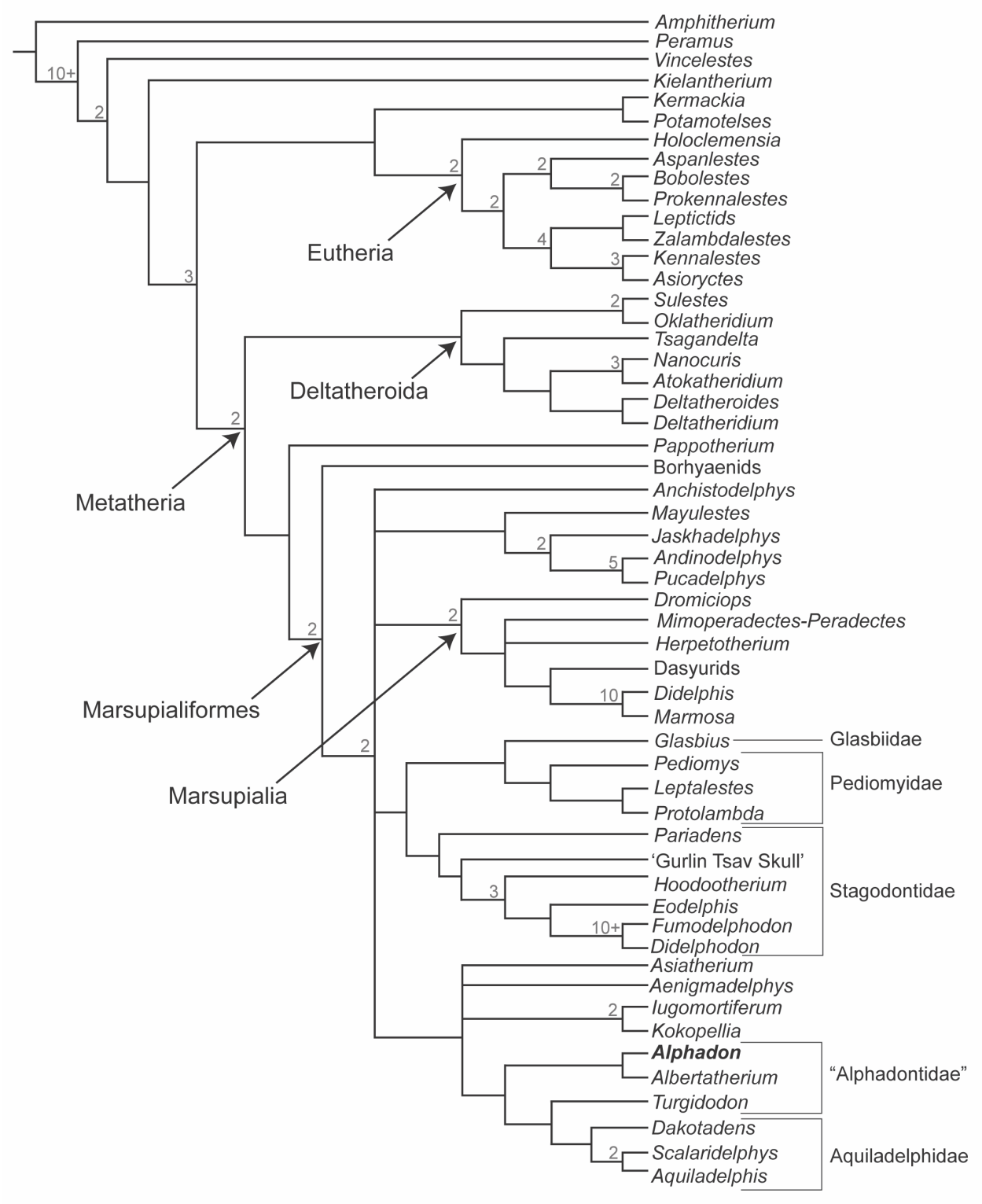

Figure 2.13. Strict consensus of six equally parsimonious trees (tree length = 617; consistency index = 0.355; and retention index = 0.670) following a phylogenetic analysis of 54 taxa and 164

characters. Bremer support values greater than one are shown above the node in gray. *Alphadon* is in boldface type. The position of Eutheria is marked as such provided that *Holoclemensia* is indeed a eutherian. It is possible that *Holoclemensia* is a stem eutherian; in this case, Eutheria would be designated to only include the most inclusive clade containing *Aspanlestes* + *Kennalestes*.

2.10 TABLES

Table 2.1. Dental measurements for specimens of *Alphadon halleyi*. L, length; W, width; MW, mesial width; DW, distal width; W-Tri, trigonid width; W-Tal, talonid width; OR, observed range; AVG, average; SD, standard deviation; CV, coefficient of variation. All measurements in mm. The asterisk denotes specimens where CT scans were difficult to segment—we consider these estimated dental measurements. These measurements were still included in summary statistics. The degree symbol denotes specimens for which measurements from left and right sides were averaged for summary statistics.

		MOR 10911*°		**MOR 1012a°**		**MOR 10912b**		**MOR 10912c*°**		**MOR 10912d**		**MOR 10913a**		**OR**	**AVG**	**SD**	**CV**
		left	right	left	right	left	right	left	right	left	right	left	right				
P1	L	–	–	0.89	1.02	–	–	–	0.81	–	–	–	–	0.81–1.00	0.92	0.10	0.11
	W	–	–	0.44	0.44	–	–	–	0.41	–	–	–	–	0.39–0.44	0.41	0.03	0.06
P2	L	1.68	–	1.42	1.42	–	1.50	1.40	–	–	–	–	–	1.40–1.68	1.50	0.13	0.09
	W	0.68	–	0.65	0.67	–	0.76	–	–	–	–	–	–	0.66–0.76	0.70	0.05	0.08
P3	L	1.70	2.19	1.76	1.48	–	1.74	1.71	1.89	–	–	–	–	1.62–2.00	1.78	0.13	0.08
	W	0.90	0.94	0.81	0.95	–	0.94	1.02	0.93	–	–	–	–	0.88–0.98	0.93	0.04	0.04
M1	L	1.99	2.00	1.74	1.71	–	1.93	1.77	1.46	–	–	–	–	1.62–2.00	1.81	0.18	0.10
	MW	2.03	1.93	1.71	2.09	–	2.15	2.08	–	–	–	–	–	1.90–2.15	2.03	0.11	0.05
	DW	2.35	2.29	2.18	2.35	–	2.33	2.22	–	–	–	–	–	2.22–2.33	2.28	0.05	0.02

		MOR 10911*°		MOR 1012a°		MOR 10912b		MOR 10912c*°		MOR 10912d		MOR 10913a		OR	AVG	SD	CV
		left	right	left	right	left	right	left	right	left	right	left	right				
M2	L	2.03	2.16	–	2.13	–	1.99	2.02	1.96	–	–	–	2.29	1.99–2.29	2.10	0.12	0.06
	MW	2.23	2.44	2.24	2.65	–	2.67	2.68	2.38	–	–	–	2.67	2.33–2.67	2.53	0.15	0.06
	DW	2.81	2.95	2.77	2.95	–	2.77	3.04	2.91	–	–	–	2.93	2.77–2.97	2.88	0.08	0.03
M3	L	2.20	2.27	2.15	–	–	2.15	2.24	2.16	–	–	–	2.44	2.15–2.44	2.24	0.12	0.05
	MW	2.59	2.75	2.49	2.90	–	3.13	3.03	2.92	–	–	–	3.08	2.67–3.13	2.91	0.22	0.07
	DW	3.07	3.10	2.96	3.09	–	2.93	3.26	3.28	–	–	–	3.36	2.93–3.36	3.13	0.18	0.06
M4	L	1.76	1.73	1.68	–	–	–	1.74	–	–	–	–	1.62	1.62–1.74	1.69	0.06	0.04
	MW	2.39	2.99	2.71	–	–	–	–	–	–	–	–	3.14	2.69–3.14	2.85	0.26	0.09
	DW	2.01	2.14	1.91	–	–	–	–	–	–	–	–	2.44	1.91–2.44	2.14	0.27	0.13
m1	L	–	1.76	–	–	–	–	–	–	–	–	–	–	–	–	–	–
	W-Tri	–	0.99	–	–	–	–	–	–	–	–	–	–	–	–	–	–
	W-Tal	–	1.06	–	–	–	–	–	–	–	–	–	–	–	–	–	–
m2	L	–	1.86	–	–	–	–	–	–	–	–	–	–	–	–	–	–
	W-Tri	–	1.27	–	–	–	–	–	–	–	–	–	–	–	–	–	–
	W-Tal	–	1.14	–	–	–	–	–	–	1.24	–	–	–	1.14–1.24	1.19	0.07	0.06
m3	L	–	2.17	–	–	–	–	–	–	2.31	–	–	–	2.17–2.31	2.24	0.10	0.04
	W-Tri	–	1.51	–	–	–	–	–	–	1.52	–	–	–	1.51–1.52	1.52	0.01	0.01

		MOR 10911*°		MOR 1012a°		MOR 10912b		MOR 10912c*°		MOR 10912d		MOR 10913a		OR	AVG	SD	CV
		left	right	left	right	left	right	left	right	left	right	left	right				
	W-Tal	–	1.19	–	–	–	–	–	–	1.31	–	–	–	1.19–1.31	1.25	0.09	0.07
m4	L	–	2.19	–	–	–	–	–	–	2.24	–	–	–	2.19–2.24	2.21	0.04	0.02
	W-Tri	–	1.40	–	–	–	–	–	–	1.44	–	–	–	1.40–1.44	1.42	0.02	0.02
	W-Tal	–	1.00	–	–	–	–	–	–	1.02	–	–	–	1.00–1.02	1.01	0.01	0.01

2.11 APPENDICES

Appendix 1: Scanner information and settings for all specimens

Specimen number	Scanner	Voltage (kV)	Current (uA)	Image pixel size (um)
MOR 10911	Skyscan 1076	100	100	34. 42
MOR 10912a	North Star Imaging X5000	93	330	19.16
MOR 10912b	North Star Imaging X5000	128	160	36.2
MOR 10912c	North Star Imaging X5000	128	160	36.2
MOR 10912d	North Star Imaging X5000	128	160	36.2
MOR 10913a	North Star Imaging X5000	120	315	24.4

Appendix 2: Phylogenetic character list and scores for *Alphadon*

The character list and descriptions combination from Wilson et al. (2016) is listed below; characters 1–156 are from Rougier et al. (2015), characters 157–162 are from Horovitz et al. (2009), and characters 163–164 are from Wilson et al. (2016). Scores for *Alphadon* are listed below each character description; new and revised scores are underlined. We treated eleven characters as ordered (characters 1, 4, 7, 12, 14, 35, 36, 50, 51, 52, and 116); all others were unordered.

General Dentition (7 characters)

1. Number of premolars – five (0), four (1), three (2), or less than three (3). Ordered.

***Alphadon* = 2**

2. Premolar cusp form – sharp, uninflated (0) or inflated, with apical wear strongly developed (1).

***Alphadon* = 0**

3. Tall, trenchant premolar – in last premolar position (0), in penultimate premolar position (1), or absent (2). [Upper dentition considered when possible]

***Alphadon* = 0**

4. Number of molars – more than four (0), four (1), or three (2). Ordered.

***Alphadon* = 1**

5. Molar cusp form – sharp, gracile (0) or inflated, robust (1).

***Alphadon* = 0**

6. Size of molars increasing posteriorly – absent (0), moderate posterior increase (1), or marked posterior increase (2). [All molars considered in lower jaw, and all but the last considered in upper jaw]

***Alphadon* = 1**

7. Number of postcanine tooth families – eight or more (0), seven (1), or less than seven (2). Ordered.

***Alphadon* = 1**

Upper Dentition (34 characters)

8. Number of upper incisors – five (0) or less than five (1).

***Alphadon* = ?**

9. First upper incisor – enlarged, anteriorly projecting, separated from I2 by small diastema (0), subequal or smaller than remaining incisors, without diastema (1), or lost (2).

***Alphadon* = ?**

10. Number of roots on upper canine – two (0) or one (1).

***Alphadon* = 1**

11. First upper premolar – erect, without diastema (0), erect, with a short diastema (1), or procumbent, separated by diastema (2).

***Alphadon* = 1**

12. Penultimate upper premolar protocone – absent (0), small lingual bulge (1), or with an enlarged basin (2). Ordered.

***Alphadon* = 0**

13. Number of roots on penultimate upper premolar – two (0) or three (1).

***Alphadon* = 0**

14. Last upper premolar – simple (0), complex, with small protocone (1), or molariform (2). Ordered.

***Alphadon* = 0**

15. Upper molar shape – as long as wide, or longer (0) or wider than long (1).

***Alphadon* = 1**

16. Upper molar outline in occlusal view – does (0) or does not (1) approach isosceles triangle.

***Alphadon* = 1**

17. Stylar shelf – uniform in width, 50% or more of total transverse width (0), uniform in width, but less than 50% of total transverse width (1), slightly reduced labial to paracone (2), strongly reduced labial to paracone (3), or strongly reduced or absent (4). [penultimate molar considered when present]

***Alphadon* = 1**

18. Metastylar area on penultimate upper molar – large (0) or reduced (1).

***Alphadon* = 0**

19. Deep ectoflexus – present only on penultimate molar (0), on penultimate and preceding molar (1), or strongly reduced or absent (2).

***Alphadon* = 1**

20. Stylar cusp A – distinct, but smaller than B (0), subequal to larger than B (1), or very small to indistinct (2). [penultimate molar considered when available]

***Alphadon* = 0**

21. Preparastyle – absent (0) or present (1).

***Alphadon* = 0**

22. Stylar cusp B size relative to paracone – smaller but distinct (0), vestigial to absent (1), or subequal (2).

***Alphadon* = 0**

23. Stylar cusp C – absent (0) or present (1).

***Alphadon* = 1**

24. Stylar cusp D – absent (0), smaller or subequal to B (1), or larger than B (2).

***Alphadon* = 1**

25. Stylar cusp E – directly lingual to D or D position (0), distal to D (1), or small to indistinct (2).

***Alphadon* = 2**

26. Preparacingulum – absent (0), interrupted between stylar margin and paraconule (1), or continuous (2). [penultimate molar considered when available]

***Alphadon* = 2**

27. Metacone size relative to paracone – noticeably smaller (0), slightly smaller (1), or subequal to larger (2).

***Alphadon* = 2**

28. Metacone position relative to paracone – labial (0), approximately at same level (1), or lingual (2).

***Alphadon* = 1**

29. Metacone and paracone shape – conical (0) or subtriangular, with labial face flat (1).

***Alphadon* = 1**

30. Metacone and paracone bases – adjoined (0) or separated (1).

***Alphadon* = 1**

31. Centrocrista – straight (0) or V-shaped (1).

***Alphadon* = 0**

32. Salient postmetacrista – weakly developed (0) or strongly developed, with paraconid enlarged and metaconid reduced on lower molars (1).

***Alphadon* = 0**

33. Preprotocrista – does not (0) or does (1) extend labially past base of paracone (double rank prevallum/postvallid shearing).

***Alphadon* = 1**

34. Postprotocrista – does not (0) or does (1) extend labially past base of metacone (double rank prevallum/postvallid shearing).

***Alphadon* = 1**

35. Conules – absent (0), small, without cristae (1), or strong, labially placed, with wing-like cristae (2). Ordered.

***Alphadon* = 2**

36. Protocone on upper molars – lacking (0), small, without trigon basin (1), small, with distinct trigon basin (2), somewhat expanded anteroposteriorly (3), or with posterior portion expanded (4). Ordered.

***Alphadon* = 3**

37. Procumbent protocone – absent (0) or present (1).

***Alphadon* = 1**

38. Protocone height – low (0) or tall, approaching para- and/ or metacone height (1).

***Alphadon* = 1**

39. Protocingula – absent (0) or pre- and/or postcingulum present (1).

***Alphadon* = 0**

40. Lingual root position – supporting paracone (0) or supporting trigon (1).

***Alphadon* = 1**

41. Last upper molar width relative to penultimate upper molar – subequal (0) or smaller (1).

***Alphadon* = 0**

Lower Dentition (22 characters)

42. Number of lower incisors – four (0) or less than four (1).

***Alphadon* = 0**

43. Staggered lower incisor – absent (0) or present (1).

***Alphadon* = 0**

44. Roots on lower canine – biradiculated (0) or uniradiculated (1).

***Alphadon* = 1**

45. First lower premolar – oriented in line with jaw axis (0) or oblique (1).

***Alphadon* = 0**

46. Second lower premolar – smaller than third premolar (0) or larger (1).

***Alphadon* = 0**

47. Last lower premolar – simple (0), complex, with a partial trigonid and/or talonid (1), or molariform (2). Ordered.

***Alphadon* = 0**

48. Trigonid configuration – open, with paraconid anteromedial (0), more acute, with paraconid more posteriorly placed (1), or anteroposteriorly compressed (2).

***Alphadon* = 1**

49. Lower molar talonid – small heel (0) or multicuspidated basin (1).

***Alphadon* = 1**

50. Talonid width relative to trigonid – very narrow, subequal to base of metaconid, developed lingually (0), narrower (1), or subequal to wider (2). Ordered.

***Alphadon* = 2**

51. Lower molar cristid obliqua – incomplete, with distal metacristid present (0), complete, attaching below notch in metacristid (1), or complete, labially placed, at base of protoconid (2). Ordered.

***Alphadon* = 1**

52. Hypoconulid – absent (0), in posteromedial position (1), or lingually placed and ‘‘twinned’’ with entoconid (2). Ordered.

***Alphadon* = 2**

53. Hypoconulid of last molar – short and erect (0) or tall and sharply recurved (1).

***Alphadon* = 0**

54. Entoconid – absent (0), smaller than (1), or subequal to larger than hypoconid and/or hypoconulid (2).

***Alphadon* = 2**

55. Labial postcingulid – absent (0) or present (1).

***Alphadon* = 1**

56. Paraconid and metaconid – metaconid at extreme lingual margin (0) or aligned (1).

***Alphadon* = 1**

57. Metacristid orientation to lower jaw axis – oblique (0) or transverse (1).

***Alphadon* = 1**

58. First lower molar paraconid, low and confluent with precingulid – absent (0) or present (1).

***Alphadon* = 0**

59. Protoconid height – tallest cusp on trigonid (0) or subequal to para- and/or metaconid (1).

***Alphadon* = 0**

60. Paraconid height relative to metaconid – taller (0), subequal (1), or shorter (2). [molars other than the first considered when available]

***Alphadon* = 2**

61. Last lower molar size relative to penultimate lower molar – subequal (0) or smaller or lost (1).

***Alphadon* = 0**

62. Rotation of last lower molar during eruption – absent (0) or present (1).

***Alphadon* = 1**

63. Space between last lower molar and coronoid process – present (0) or absent (1).

***Alphadon* = 0**

Tooth Replacement (3 characters)

64. Deciduous incisors – present (0) or absent (1).

***Alphadon* = 1**

65. Deciduous canine – present (0) or absent (1).

***Alphadon* = 1**

66. Replacement of dP1/dp1 and dP2/dp2 – present (0) or absent (1).

***Alphadon* = 1**

Lower jaw (11 characters)

67. Masseteric fossa – restricted dorsally by crest reaching condyle (0) or extended ventrally to lower margin of dentary (1).

***Alphadon* = 1**

68. Posterior shelf of masseteric fossa – absent (0) or present (1).

***Alphadon* = 1**

69. Convex ventral margin behind tooth row continuous to condyle – absent (0) or present (1).

***Alphadon* = 0**

70. Labial mandibular foramen – present (0) or absent (1).

***Alphadon* = 1**

71. Condyle shape – ovoid (0) or cylindrical (1).

***Alphadon* = 1**

72. Condyle position relative to tooth row – above (0) or very high (1)

***Alphadon* = 0**

73. Lower jaw angle – posteriorly directed (0), medially inflected (1), or posteroventrally directed (2).

***Alphadon* = 1**

74. Mandibular foramen – below (0) or posterior to anterior edge of coronoid process (1).

***Alphadon* = 1**

75. Meckelian groove – present (0) or absent (1).

***Alphadon* = 1**

76. ‘‘Coronoid’’ facet – present (0) or absent (1).

***Alphadon* = 1**

77. Two large mental foramen, one under second and third premolar and the other under first and second molar – absent (0) or present (1).

***Alphadon* = 1**

Cranium (79 characters)

78. Septomaxilla – present (0) or absent (1).

***Alphadon* = ?**

79. Premaxilla, palatal process – does not (0) or does reach nearly or to canine alveolus (1).

***Alphadon* = ?**

80. Premaxilla, facial process – does not (0) or does reach the nasal (1).

***Alphadon* = 1**

81. Lateral margin of paracanine fossa – formed by maxilla (0) or maxilla and premaxilla (1).

***Alphadon* = 0**

82. Exit(s) of infraorbital canal – multiple (0) or single (1).

***Alphadon* = 1**

83. Flaring of cheeks behind infraorbital foramen, as seen in ventral view – present (0) or absent (1).

***Alphadon* = 1**

84. Naso-frontal suture with medial process of frontals wedged between nasals – present (0) or absent (1).

***Alphadon* = 0**

85. Nasal foramina – present (0) or absent (1).

***Alphadon* = 1**

86. Frontal-maxillary contact – absent (0) or present (1).

***Alphadon* = 1**

87. Lacrimal tubercle – present (0) or absent (1).

***Alphadon* = 1**

88. Lacrimal foramen exposed on face – present (0) or absent (1).

***Alphadon* = 0**

89. Lacrimal foramen number – double (0) or single (1).

***Alphadon* = 0&1**

90. Preorbital length relative to postorbital length – two-thirds or more (0) or less than two-thirds (1).

***Alphadon* = ?**

91. Maxillary-jugal contact bifurcated – absent (0) or present (1).

***Alphadon* = 0**

92. Zygomatic arch – stout (0) or delicate (1).

***Alphadon* = 0**

93. Palatal vacuities – absent (0) or present (1).

***Alphadon* = 1**

94. Palatal expansion behind last molar – absent (0) or present (1).

***Alphadon* = ?**

95. Postpalatine torus – absent (0) or present (1).

***Alphadon* = ?**

96. Palate and basicranium at same level, connected by broad choanal ridges – absent (0) or present (1).

***Alphadon* = ?**

97. Minor palatine (postpalatine) foramen – small (0) or large, with thin, posterior bony bridge (1).

***Alphadon* = ?**

98. Palatine reaches infraorbital canal – present (0) or absent (1).

***Alphadon* = ?**

99. Pterygoids contact on midline – present (0) or absent (1).

***Alphadon* = ?**

100. Pterygopalatine crests – present (0) or absent (1).

***Alphadon* = ?**

101. Ectopterygoid process of alisphenoid – absent (0) or present (1).

***Alphadon* = ?**

102. Optic foramen – absent (0) or present (1).

***Alphadon* = ?**

103. Orbitotemporal canal – present (0) or absent (1).

***Alphadon* = ?**

104. Transverse canal – absent (0) or present (1).

***Alphadon* = ?**

105. Carotid foramen – within basisphenoid (0) or between basisphenoid and petrosal (1).

***Alphadon* = ?**

106. Dorsum sellae – tall (0) or low (1).

***Alphadon* = ?**

107. Alisphenoid canal – absent (0) or present (1).

***Alphadon* = ?**

108. Anterior lamina exposure on lateral braincase wall – present (0), rudimentary (1), or absent (2).

***Alphadon* = ?**

109. Cavum epiptericum – floored by petrosal (0), petrosal and alisphenoid (1), primarily or exclusively by alisphenoid (2), or primarily open as piriform fenestra (3).

***Alphadon* = ?**

110. Exit for maxillary nerve relative to alisphenoid – behind (0) or within or in front (1).

***Alphadon* = ?**

111. Foramen ovale composition – in petrosal (anterior lamina) (0), between petrosal and alisphenoid (1), in alisphenoid or between alisphenoid and squamosal (2).

***Alphadon* = ?**

112. Foramen ovale – on lateral wall of braincase (0) or on ventral surface of skull (1).

***Alphadon* = ?**

113. Squama of squamosal – absent (0) or present (1).

***Alphadon* = ?**

114. Position of jaw articulation relative to fenestra vestibuli – at same level (0) or in front (1).

***Alphadon* = ?**

115. Glenoid fossa shape – concave, open anteriorly (0) or trough-like (1).

***Alphadon* = ?**

116. Glenoid process of jugal – present, with articular facet (0), present, without facet (1), or absent (2). Ordered.

***Alphadon* = ?**

117. Glenoid process of alisphenoid – absent (0) or present (1).

***Alphadon* = ?**

118. Postglenoid process – absent (0) or present (1).

***Alphadon* = ?**

119. Postglenoid-suprameatal vascular system – absent (0), present, below squamosal crest (1), or present, above squamosal crest (2).

***Alphadon* = ?**

120. Postglenoid foramen – absent (0), present, behind postglenoid process (1), or present, medial to postglenoid process (2).

***Alphadon* = ?**

121. Alisphenoid tympanic process – absent (0) or present (1).

***Alphadon* = ?**

122. Epitympanic wing medial to promontorium – absent (0), flat (1), undulated (2), or confluent with bulla (3).

***Alphadon* = ?**

123. Tympanic aperture of hiatus Fallopii – in roof through petrosal (0), at anterior edge of petrosal (1), or absent (2).

***Alphadon* = ?**

124. Prootic canal – long and vertical (0), short and vertical (1), short and horizontal (2), or absent (3).

***Alphadon* = ?**

125. Position of sulcus for anterior distributary of transverse sinus relative to subarcuate fossa – anterolateral (0) or posterolateral (1).

***Alphadon* = ?**

126. Lateral flange – parallels length of promontorium (0), restricted to posterolateral corner (1), or greatly reduced or absent (2).

***Alphadon* = ?**

127. Stapedial ratio – rounded, less than 1.8 (0) or elliptical, more than 1.8 (1).

***Alphadon* = ?**

128. Complete wall separating cavum supracochleare from cavum epiptericum – absent (0) or present (1).

***Alphadon* = ?**

129. Coiling of cochlea – less than 360° (0) or 360° or greater (1).

***Alphadon* = ?**

130. Rostral tympanic process of petrosal, on posteromedial aspect of promontorium – absent or low ridge (0), tall ridge, occasionally contacting ectotympanic (1).

***Alphadon* = ?**

131. Paroccipital process (sensu Wible and Hopson, 1993) orientation and shape – vertical (0), slanted, projecting anteroventrally as flange towards back of promontorium (1), or indistinct to absent (2).

***Alphadon* = ?**

132. Caudal tympanic process of petrosal development – tall wall behind postpromontorial recess (0), tall wall decreasing in height markedly medially (1), or notched between stylomastoid notch and jugular foramen (2).

***Alphadon* = ?**

133. Crista interfenestralis and caudal tympanic process of the petrosal connected by curved ridge – absent (0) or present (1).

***Alphadon* = ?**

134. ‘‘Tympanic process’’ – absent (0) or present (1).

***Alphadon* = ?**

135. Tall paracondylar (‘‘paroccipital’’) process of exoccipital (sensu Evans and Christensen, 1979) – absent (0) or present (1).

***Alphadon* = ?**

136. Rear margin of auditory region – marked by a steep wall (0) or extended onto a flat surface (1).

***Alphadon* = ?**

137. Fossa incudis – continuous with (0) or separated from (1) epitympanic recess.

***Alphadon* = ?**

138. Epitympanic recess – with small contribution to posterolateral wall by squamosal (0) or with extensive contribution to lateral wall by squamosal (1).

***Alphadon* = ?**

139. Stapedius fossa – twice the size of fenestra vestibuli (0) or small and shallow (1).

***Alphadon* = ?**

140. Hypotympanic sinus – absent (0), formed by squamosal, petrosal, and alisphenoid (1), or formed by alisphenoid and petrosal (2).

***Alphadon* = ?**

141. Medial process of squamosal in tympanic cavity – absent (0) or present (1).

***Alphadon* = ?**

142. Ectotympanic – ring-like (0), fusiform (1), or expanded (2).

***Alphadon* = ?**

143. Foramina for temporal rami – on petrosal (0), on parietal and/or squama of squamosal (1), or absent (2).

***Alphadon* = ?**

144. Posttemporal canal – large (0), small (1), or absent (2).

***Alphadon* = ?**

145. Foramen for ramus superior of stapedial artery – on petrosal (0), on petrosal-squamosal suture (1), or absent (2).

***Alphadon* = ?**

146. Transpromontorial sulcus – present (0) or absent (1).

***Alphadon* = ?**

147. Sulcus for stapedial artery – present (0) or absent (1).

***Alphadon* = ?**

148. Deep groove for internal carotid artery excavated on anterior pole of promontorium – absent (0) or present (1).

***Alphadon* = ?**

149. Jugular foramen size relative to fenestra cochleae – subequal (0) or larger (1).

***Alphadon* = ?**

150. Jugular foramen – confluent with (0) or separated from (1) opening for inferior petrosal sinus.

***Alphadon* = ?**

151. Inferior petrosal sinus – intrapetrosal (0), between petrosal, basisphenoid, and basioccipital (1), or endocranial (2).

***Alphadon* = ?**

152. Ascending canal – intramural (0), intracranial (1), or absent (2).

***Alphadon* = ?**

153. Internal acoustic meatus – deep, with thick prefacial commissure (0) or shallow, with thin prefacial commissure (1).

***Alphadon* = ?**

154. Mastoid-squamosal fusion – absent (0) or present (1).

***Alphadon* = ?**

155. Interparietal – absent (0) or present (1).

***Alphadon* = ?**

156. Dorsal margin of foramen magnum – formed by exoccipitals (0) or by exoccipitals and supraoccipital (1).

***Alphadon* = ?**

From Horovitz et al. 2009 (6 characters)

157. Upper incisor arcade shape*– U-shape (0), broad V-shape (1), or long, narrow V-shape (2). (Ch. 158 of Horovitz et al. 2009 but unordered)

***Alphadon* = ?**

158. Posterior-most point of premaxillo-nasal contact – anterior or at the canine (0) or posterior to the canine (1). (Ch. 178 of Horovitz et al. 2009)

***Alphadon* = 0**

159. Fossa subarcuata –smaller than its aperture (i.e., conical shape) (0) or larger than its aperture (i.e., spherical shape) (1). (Ch. 221 of Horovitz et al. 2009)

***Alphadon* = ?**

160. Deep and large fossa for the tensor tympani muscle excavated on the anterolateral aspect of promontorium, creating a battered ventral surface of the promontorium – absent (0) or present (1). (Ch. 229 of Horovitz et al. 2009)

***Alphadon* = ?**

161. Broad shelf of bone surrounding fenestra cochleae and making a separation between it and aqueductus cochleae – absent (0) or present (1). (Ch. 233 of Horovitz et al. 2009)

***Alphadon* = ?**

162. Mastoid exposure – large (0), narrow (1), or reduced pars mastoidea, internal to the braincase and wedged between the squamosal and exoccipital (2). (Ch. 239 of Horovitz et al. 2009)

***Alphadon* = ?**

Characters from Wilson et al. 2016 (2 characters)

163. Internarial process of the premaxilla – absent (0) or present (1).

***Alphadon* = ?**

164. Anterior-most extent of the nasal – anterior to or at the canine (0) or posterior or to the canine (1).

***Alphadon* = 0**

Appendix 3: Phylogenetic character scores for *Alphadon halleyi* specimens included in this study

The character scores for each of the *Alphadon halleyi* specimens described in this study are listed below. The "MOR Composite" scores were used for the phylogenetic analysis— it is the updated scores from this study in combination with the scores for *Alphadon* from Wilson et al. (2016). Polymorphic entry is coded as: A = [0&1].

MOR 10911
?00101????000111010001l2?2111001123l1010??????112l202?110020?0???????????1??????
?????101?0??

MOR 10912a
20010?1??1100011l??00?11???111001123l101?????????????????????????????????????10??
011100?0??0?????

MOR 10912b
2001011???100011101000112221110011231101??
???????0??

MOR 10912c
2001011??1?000111010001122211100??231101??
??

MOR 10912d
????01??1121202111?020?0???1?????1?1??????????
??

MOR 10913a
???10????1????111010001l2?2111001123l1010????????????????????????????????????1?
0?1101?0??

MOR Composite
2001011??1100011101000112221110011231101000100011212021110020101111101101111l?
?101101110A?001???0?????
0

Appendix 4: Phylogenetic NEXUS input

Below is the nexus file format exported from Mesquite that was used for the phylogenetic analysis.

```
#NEXUS
[written Tue Jul 27 12:48:13 PDT 2021 by Mesquite  version 3.10 (build 765)
at Alexandrias-MacBook-Pro.local/127.0.0.1]

BEGIN TAXA;
	DIMENSIONS NTAX=54;
	TAXLABELS
		Amphitherium Peramus Vincelestes Kielantherium Potamotelses
Kermackia Holoclemensia Pappotherium Deltatheridium Deltatheroides
Tsagandelta Oklatheridium Sulestes Atokatheridium Nanocuris Gurlin Pariadens
Kokopellia Anchistodelphys Iugomortiferum Aenigmadelphys Didelphodon
Eodelphis Pediomys Albertatherium Alphadon Turgidodon Glasbius Asiatherium
Mayulestes Borhyaenids Pucadelphys Andinodelphys Jaskhadelphys Marmosa
Didelphis Dasyurids Dromiciops Prokennalestes Bobolestes Asioryctes
Kennalestes Zalambdalestes Aspanlestes Leptictids Fumodelphodon Hoodootherium
Aquiladelphis Scalaridelphys Dakotadens Protolambda Leptalestes
Herpetotherium 'Mimo_Peradectes'
	;

END;


BEGIN CHARACTERS;
```

```
      DIMENSIONS  NCHAR=164;
      FORMAT DATATYPE = STANDARD GAP = - MISSING = ? SYMBOLS = "  0 1 2 3 4 5
6 7 8 9";
      CHARSTATELABELS
            1 Number_of_premolars /  five four three less_than_three, 2
Premolar_cusp_form /  uninflated
inflated_with_apical_wear_strongly_developed, 3 'Tall, trenchant premolar' /
last_premolar_position penultimate_premolar_position absent, 4
Number_of_molars /  more_than_four four three, 5 Molar_cusp_form /  'sharp,
gracile' inflated_robust, 6 Size_of_molars_increasing_posteriorly /  absent
moderate_posterior_increase marked_posterior_increase, 7
Number_of_postcanine_tooth_families /  eight_or_more seven less_than_seven, 8
Number_of_upper_incisors /  five less_than_five, 9 First_upper_incisor /
'enalrged, anteriorly projecting, separated from I2 by small diastea'
subequal_of_smaller_than_remaining_incisors_without_diastema lost, 10
Number_of_roots_on_upper_canine /  two one, 11 First_upper_premolar /
erect_without_diastema erect_with_short_diastema 'procumbent, separated by
diastema', 12 Penultimate_upper_premolar_protocone /  absent
small_lingual_bulge enlarged_basin, 13
Number_of_roots_on_penultimate_upper_premolar /  two three, 14
Last_upper_premolar /  simple 'complex, with small protocone' molariform, 15
Upper_molar_shape /  'as long as wide, or longer' wider_than_long, 16
Upper_molar_outline_in_occlusal_view /  approaches_isoceles_triangle
does_not_approach_isoceles_triangle, 17 Stylar_shelf /  'uniform in width,
50% or more of total transverse width' 'uniform in width, but less than 50%
of total transverse width' slightly_reduced_labial_to_paracone
strongly_reduced_labial_to_paracone strongly_reduced_or_absent, 18
Metastylar_area_on_penultimate_upper_molar /  large reduced, 19
```

Deep_ectoflexus / present_only_on_penultimate_molar
on_penultimate_and_preceding_molar strongly_reduced_or_absent, 20
Stylar_cusp_A / distinct_but_smaller_than_B subequal_to_larger_than_B
very_small_to_indistinct, 21 Preparastyle / absent present, 22 Stylar_cusp_B
/ smaller_but_distinct vetigial_to_absent subequal, 23 Stylar_cusp_C /
absent present, 24 Stylar_cusp_D / absent smaller_of_subequal_to_B
larger_than_B, 25 Stylar_cusp_E / directly_lingual_to_D_or_D_position
distal_to_D small_to_indistinct, 26 Preparacingulum / absent
interrupted_between_stylar_margin_and_paraconule continuous, 27
Metacone_size_relative_to_paracone / moticeably_smaller slightly_smaller
subequal_to_larger, 28 Metacone_position_relative_to_paracone / labial
approximately_at_same_level lingual, 29 Metacone_and_paracone_shape /
conical subtriangular_with_labial_face_flat, 30 Metacone_and_paracone_bases /
adjoined separated, 31 Centrocrista / straight 'V-shaped', 32
Salient_postmetacrista / weakly_developed
strongly_developed_with_paracnoid_enlarged_and_metaconid_reduced_on_lower_mol
ars, 33 Preprotocrista / does_not_extend_labially_past_base_of_paracone
does_extend_labially_past_base_of_paracone, 34 Postprotocrista /
does_not_extend_labially_past_base_of_metacone
does_extend_labially_past_base_of_metacone, 35 Conules / absent
small_without_cristae 'strong, labially placed, with wing-like cristae', 36
Protocone_on_upper_molars / lacking small_without_trigon_basin
small_with_distinct_trigon_basin somewhat_expanded_anteroposteriorly
with_posterior_portion_expanded, 37 Procumbent_protocone / absent present,
38 Protocone_height / low 'tall, approaching para-and/or metacone height',
39 Protocingula / absent 'pre- and/or postcingulum present', 40
Lingual_root_position / supporting_paracone supporting_trigon, 41
Last_upper_molar_width_relative_to_penultimate_upper_molar / subequal

smaller, 42 Number_of_lower_incisors / four less_than_four, 43 Staggered_lower_incisor / absent present, 44 Roots_on_lower_canine / biradiculated uniradiculated, 45 First_lower_premolar / oriented_in_line_with_jaw_axis oriented_oblique_with_jaw_axis, 46 Second_lower_premolar / smaller_than_third_premolar larger_than_third_premolar, 47 Last_lower_premolar / simple 'complex with a partial trigonid and/or talonid' molariform, 48 Trigonid_configuration / 'open, with paraconid anteromedial' more_acute_with_paraconid_more_posteriorly_placed anteroposteriorly_compressed, 49 Lower_molar_talonid / small_heel multicuspidated_basin, 50 Talonid_width_relative_to_trigonid / 'very narrow, subequal to base of metaconid, developed lingually' narrower subequal_to_wider, 51 Lower_molar_cristid_obliqua / incomplete_with_distal_metacristid_present complete_attaching_below_notch_in_metacristid 'complete, labially placed at base of protoconid', 52 Hypoconulid / absent posteromedial_position lingually_placed_and_twinned_with_entoconid, 53 Hypoconulid_of_last_molar / short_and_erect tall_and_sharply_recurved, 54 Entoconid / absent 'smaller than hyponid and/or hypoconulid' 'subequal to larger than hypoconid and/or hypoconulid', 55 Labial_postcingulid / absent present, 56 Paraconid_and_metaconid / metacoind_at_extreme_lingual_margin aligned, 57 Metacristid_orientation_to_lower_jaw_axis / oblique transverse, 58 'First lower molar paraconid, low and confluent with precingulid' / absent present, 59 Protoconid_height / tallest_cusp_on_trigonid 'subequal to para- and/or metaconid', 60 Paraconid_height_relative_to_metaconid / taller subequal shorter, 61 Last_lower_molar_size_relative_to_penultimate_lower_molar / subequal smaller_or_lost, 62 Rotation_of_last_lower_molar_during_eruption / absent present, 63 Space_between_last_lower_molar_and_coronoid_process /

present absent, 64 Deciduous_incisors / present absent, 65 Deciduous_canince / present absent, 66 'Deplacement of dP1/dp1 and dP2/dp2' / present absent, 67 Masseteric_fossa / restricted_dorsally_by_crest_reaching_condyle extended_ventrally_to_lower_margin_of_dentary, 68 Posterior_shelf_of_masseteric_fossa / absent present, 69 Convex_ventral_margin_behind_tooth_row_continuous_to_condyle / absent present, 70 Labial_mandibular_foramen / present absent, 71 Condyle_shape / ovoid cylindrical, 72 Condyle_position_relative_to_tooth_row / above very_high, 73 Lower_jaw_angle / posteriorly_directed medially_inflected posteroventrally_directed, 74 Mandibular_foramen / below posterior_to_anterior_edge_of_coronoid_process, 75 Meckelian_groove / present absent, 76 Coronoid_facet / present absent, 77 'Two large mental foramen, one under second and third premolar and the other under the first and second molar' / absent present, 78 Septomaxilla / present absent, 79 'Premaxilla, palatal process' / does_not_reach_canine_alveolus does_reach_nearly_or_to_canine_alveolus, 80 Premaxilla_facial_process / does_not_reach_nasal does_reach_nasal, 81 Lateral_margin_of_paracanine_fossa / formed_by_maxilla formed_by_maxilla_and_premaxilla, 82 'Exit(s) of infraorbital canal' / multiple single, 83 'Flaring of cheeks behind infraorbital foramen, as seen in ventral view' / present absent, 84 'Naso-frontal suture with medial process of frontals wedged between nasals' / present absent, 85 Nasal_foramina / present absent, 86 'Frontal–maxillart contact' / absent present, 87 Lacrimal_tubercle / present absent, 88 Lacrimal_foramen_exposed_on_face / present absent, 89 Lacrimal_foramen_number / double single, 90 Preorbital_length_relative_to_postorbital_length / '2/3 or more' 'less than 2/3', 91 'Maxillary–jugal contact bifurcated' / absent present, 92 Zygomatic_arch / stout delicate, 93 Palatal_vacuities / absent present, 94

Palatal_expansion_behind_last_molar / absent present, 95 Postpalatine_torus / absent present, 96 'Palate and basicranium at same level, connected by broad choanal ridges' / absent present, 97 'Minor palatine (postpalatine) foramen' / small large_with_thin_posterior_bony_bridge, 98 Palatine_reaches_infraorbital_canal / present absent, 99 Pterygoids_contact_on_midline / present absent, 100 Pterygopalatine_crests / present absent, 101 Ectopterygoid_process_of_alisphenoid / absent present, 102 Optic_foramen / absent present, 103 Orbitotemporal_canal / present absent, 104 Transverse_canal / absent present, 105 Carotid_foramen / within_basisphenoid between_basisphenoid_and_petrosal, 106 Dorsum_sellae / tall low, 107 Alisphenoid_canal / absent present, 108 Anterior_lamina_exposure_on_lateral_braincase_wall / present rudimentary absent, 109 Cavum_epiptericum / floored_by_petrosal floored_by_petrosal_and_alisphenoid primarily_or_exclusively_floored_by_alisphenoid primarily_open_as_piriform_fenestra, 110 Exit_for_maxillary_nerve_relative_to_alisphenoid / behind within_or_in_front, 111 Foramen_ovale_composition / 'in pterosal (anterior lamina)' between_petrosal_and_alisphenoid in_alisphenoid_or_between_alisphenoig_and_squamosal, 112 Foramen_ovale / on_lateral_wall_of_braincase on_ventral_surface_of_skull, 113 Squama_of_squamosal / absent present, 114 Position_of_jaw_articulation_relative_to_fenestra_vestibuli / at_same_level in_front, 115 Glenoid_fossa_shape / 'concave, open anteriorly' 'trough-like', 116 Glenoid_proces_of_jugal / 'present, with articular facet' present_without_facet absent, 117 Glenoid_process_of_alisphenoid / absent present, 118 Postglenoid_process / absent present, 119 'Postglenoid-suprameatal vascular system' / absent present_below_squamosal_crest

present_above_squamosal_crest, 120 Postglenoid_foramen / absent present_behind_postglenoid_process present_medial_to_postgelnoid_process, 121 Alisphenoid_tympanic_process / absent present, 122 Epitympanic_wing_medial_to_promontorium / absent flat undulated confluent_with_bulla, 123 Tympanic_aperture_of_hiatus_Fallopii / in_roof_through_petrosal at_anterior_edge_of_petrosal absent, 124 Prootic_canal / long_and_vertical short_and_vertical short_and_horizontal absent, 125 Position_of_sulcus_for_anterior_distributary_of_transverse_sinus_relative_to_ subarcuate_fossa / anterolateral posterolateral, 126 lateral_flange / parallels_length_of_promontorium restricted_to_posterolateral_corner greatly_reduced_or_absent, 127 Stapedial_ratio / 'rounded, less than 1.8' 'elliptical, more than 1.8', 128 Complete_wall_separating_cavum_supracochleare_from_cavum_epiptericum / absent present, 129 Coiling_of_cochlea / less_than_360∫ 360∫_or_greater, 130 'Rostral tympanic process of petrosal, on posteromedial aspect of promontorium' / absent_or_low_ridge 'tall ridge, occasionally contacting ectotympanic', 131 'Paroccipital process (sensu Wible and Hopson, 1993) orientation and shape' / vertical 'slanted, projecting anteroventrally as flange towards back of promontorium' indistinct_to_absent, 132 Caudal_tympanic_process_of_petrosal_development / tall_wall_behind_postpromontorial_recess tall_wall_decreasing_in_heigh_markedly_medailly notched_between_stylomastoid_notch_and_jugular_foramen, 133 Crista_interfenestralis_and_caudal_tympanic_process_of_the_petrosal_connected _by_curved_ridge / absent present, 134 Tympanic_process / absent present, 135 'Tall paracondylar (paroccipital) process of exoccipital (sensu Evans and Christensen, 1979)' / absent present, 136 Rear_margin_of_auditory_region /

marked_by_a_steep_wall extended_onto_a_flat_surface, 137 Fossa_incudis /
continuous_with_epitympanic_recess separated_from_epitympanic_recess, 138
Epitympanic_recess /
with_small_contribution_to_posterolateral_wall_by_squamosal
with_extensive_contribution_to_lateral_wall_by_squamosal, 139 Stapedius_fossa
/ twice_the_size_of_fenestra_vestibuli small_and_shallow, 140
Hypotympanic_sinus / absent 'formed by squamosal, petrsoal, and alisphenoid'
formed_by_alisphenoid_and_petrosal, 141
Medial_process_of_suqmosal_in_tympanic_cavity / absent present, 142
Ectotympanic / 'ring-like' fusiform expanded, 143 Foramina_for_temporal_rami
/ on_petrosal 'on parietal and/or squama of squamosal' absent, 144
Posttemporal_canal / large small absent, 145
Foramen_for_ramus_superior_of_stapedial_artery / on_petrosal 'on petrosal-
squamosal suture' absent, 146 Transpromontorial_sulcus / present absent, 147
Sulcus_for_stapedial_artery / present absent, 148
Deep_groove_for_internal_carotid_artery_excavated_on_anterior_pole_of_promont
orium / absent present, 149
Jugular_foramen_size_relative_to_fenestra_cochleae / subequal larger, 150
Jugular_foramen / confluent_with_opening_for_inferior_petrosal_sinus
separated_from_opening_for_inferior_petrosal_sinus, 151
Inferior_petrosal_sinus / intrapetrosal 'between petrosal, basisphenoid, and
basioccipital' endocranial, 152 Ascending_canal / intramural intracranial
absent, 153 Internal_acoustic_meatus / deep_with_thick_prefacial_commissure
shallow_with_thin_prefacial_commissure, 154 'Mastoid-squamosal fusion' /
absent present, 155 Interparietal / absent present, 156
Dorsal_margin_of_foramen_magnum / formed_by_exoccipitals
formed_by_exoccipitals_and_supraoccipital, 157 Upper_incisor_arcade_shape /
'U-shape' 'broad V-shape' 'long, narrow V-shape ', 158 'Posterior-most point

of premaxillo-nasal contact' / anterior_or_at_the_canine
posterior_to_the_canine, 159 Fossa_subarcuata / 'smaller than its aperture
(i.e., conical shape)' 'larger than its aperture (i.e., spherical shape)',
160 'Deep and large fossa for the tensor tympani muscle excavated on the
anterolateral aspect of promontorium, creating a battered ventral surface of
the promontorium' / absent present, 161
Broad_shelf_of_bone_surrounding_fenestra_cochleae_and_making_a_separation_bet
ween_it_and_aqueductus_cochleae_ / absent present, 162 Mastoid_exposure_ /
large narrow 'reduced pars mastoidea, internal to the braincase and wedged
between the squamosal and exoccipital ', 163
Internarial_process_of_the_premaxilla / absent present, 164 'Anterior-most
extent of the nasal' / anterior_to_or_at_the_canine
posterior_or_to_the_canine ;

MATRIX

Amphitherium

0020000110?000??0??0?000??00???0??00???000000000000?000010200100000000000000
000001010010?0?000?0??
??????????

Peramus

0012000??10000000012000000010000??00???0000100100001000000000?0???0000?021001
??
??????????

Vincelestes

3002102100000000002200010021000000010001110100000001000000011?1??010000001100
000000000010100000000000000000000000000000000000000000000000?000000000000
0000000000

Kielantherium

1??1000???????1000(01)21000220110011001000l????0?(01)0100100000001?0??????0?

??1000??

???????????????

Potamotelses

????00????????00112200002101010000021001??????01101010000?011?????????????

??

??????????

Kermackia

?0??00????????111?(01)000002101000000121001??????12110101000?020?1???????????

??

?????????????

Holoclemensia

?01201??????0?11012100111211010010130001O?????12111101001012l?????????????????

??

??????????

Pappotherium

???10?????????11001000012201110010120001O??????11101?1010?01?????????????????

??

??????????

Deltatheridium

200102111120001101120000221100011012000111110000100101010000111?1110011011111

111010010000100000?10??????????21???1?1(01)0121?12212011010000?00?00??212110011

200????000???

Deltatheroides

2001021??1?000110012000022110001101200011l?10000100101010000l?1???1??1???1111

?1?010???????0??

??????????

Tsagandelta

2??10(12)1?????????????????????????1???????????110?11001??010?001?0???10?1?011
111???
????????????

Oklatheridium

???102????????11011(02)000022110001101 2??011?????11101?1010000?????????????
??
????????????

Sulestes

2001021??10?00110112000022110001101200011111100111010101000 01?0???10?1??11(01
)11?1??11??000????0????0?????????????????????????22?20110??00??0?0?????1110?11
20????????0???

Atokatheridium

???(12)02????????1100120000221100011012100 1??????01001?0010000?????????????
??
????????????

Nanocuris

???1011???????110??200002211000110(01)21001???11??011010001000 01?1??????1???1
11???
????????????

Gurlin

200102111120001110100201122201011023000 10?????????????????????????????????
111010010000100110011??00101?022121111001211 3???2??110100?0?1?11?21?111????00
0001???011

Pariadens

???102????????012?1000112221010111130101???????112(12)2021100100????????????
??
????????????

Kokopellia

2001011???????101?(01)20000221101001123?101??011001121112100001O?0???1??1???1

11???

????????????

Anchistodelphys

???1011??????11101000(01)(01)2222010011231101??????1121212100102O??????????

??

??????????????

Iugomortiferum

????11????????001??2000022210100112311O1??????1121202101002O??????????????

??

??????????

Aenigmadelphys

20?1011??????1120200001221111001123110I?????001111212101?000??????????????

??

??????????

Didelphodon

2121121??1?10111201(02)0201222201011024110101?1101212220211101O0?0??111111011

111?????1????????01??????????????22???1110010I?21212011010O?011110?212110?10

201??01000011

Eodelphis

21211211?1?000112012020022220101102311010111100212120211101O0?0??111111011111

????????????001?????????????????????111001(12)1?????????????00???(12)??(12)1?

????????1???????0??

Pediomys

2001011????00011300000(01)22222010011241101O??1100112220211100201O???1111?(01

)11111????1????????0111?1?????1????22??????????(12)?21212011001O0??100(12)??

(12)12110?11200??????????

Albertatherium

???101???????11101000(01)12221110011231101??????11212?2111?12?????????????

??

????????????

Alphadon

2001011??11000111010001122211100112311010001000112120211100201011111011011111

??101101110(01)?001??

??????0?????0

Turgidodon

2101111????000111010001122210100112311O1???1?0011212?21110020?0?????????????

?????1?????????????????????????22??????????1??12120110O?00?0010(12)??(12)12110

0?121???????????

Glasbius

2001101????00011101000(01)2222(12)0100112411111??11101122202111012l?1????????

???111??

??????????????

Asiatherium

2021011??1100011(12)00100022211010011230011O???000112120210100207?0???10010111

111??1?10010100100111010??0??????2(012)1(12)?1110?1211????0?10010000???(12)?

2?0?110011?????????????

Mayulestes

200101100120001110110001222201011023100100111001112211101001O?0?????????????1

11111011000010001101001O??00?021111111011?10113?20?10100000O111?1??111111?0

0101?10100

Borhyaenids

2001021111(12)000111010000022220101102210010111100111121111O000?0??110011011

1111111101100111000001101110100?022111111001210113120110100010010110l(12)2111

11120010O?????00

Pucadelphys

2001011001200011100102112122111010241101001110011222121010120?0???11011011111
1010100110001000110 10?100100?021111111011110112120110000000001 01?222111111210
?100111000

Andinodelphys

2001011001200011100002112222111010231101001 1?00112221111 10120?0???110??01??1?
101010111???1000110??1100110??2(12)111111011(12)10112?201100(01)00?001?01??22
11111?210??00011000

Jaskhadelphys

????01????????111010021122211111101311 01??????????????????????????????????????
??
??????????

Marmosa

2001011001200011200202111222111010031101001101011222020110020101111111111111 10
1110111111001001110111100110102211111101111111212011120001000120021211001121 0
1110????00

Didelphis

2001011001200011200202111122111010031101001101011222020110020101111111111111 10
1110111111011001110111100110102211111101111111212011120001000120021211001121 0
1010100100

Dasyurids

2001011111000011201202102222111010030101111100011222021111020101111111111111 10
111(01)1011110110011110011001101022111111011211112120111200010101202222110011
2101101????00

Dromiciops

2021011011000011201201002222010010041101100100011212020111021?011111111011111
1010111111001001110011100100102212111101121131 3?21?1020000000?202222110001210
1?00100000

Prokennalestes

0012000??01102111000100112010000111300010000000111011100100 20?0???0000?021001

???011??????0?0?????????0????11???1????????101010010(12)200?00100??(01)10000

0?0010??????????

Bobolestes

0012000??????1111011100220100001123000100010111111111001002 0?0???001?021001

??

??????????

Asioryctes

1012001010021211400101002201000011230101000000021111110010020?0???00010021111

1010110101010110010100111 00??023120110101120103?21110221101010001 12?100001(01

)10012????00

Kennalestes

1012001?10021211400111002201000011230111010000021111110010020 00??00001?021111

?01011010?0100100101001110???02312?110?011201?30211102211 01??000112?100001(01

)100???????00

Zalambdalestes

1012001120021211402201002111010001230101110100221221010010120?0???000(01)0101

111101010010010001 00(01)0110111000?023120110(12)01(12)201130211102211010100 01

111100001(01)10012????00

Aspanlestes

0012000??01102114000110021110100112311110??1?112121101001012000???00000021111

?0??1????????0????????????????????????????????10201011???00????0????10110??100?

??????????

Leptictids

1012001121021211402201002111010011240111010101221211110010120000001001112111 0

1010111110110110010101111001112212011120111011302111022000101010012100011111 0

112?????00

Fumodelphodon

21211?1??????1?????????????????????????????????00212??2111010?????????????????

??

??????????

Hoodootherium

21201?1??????0??????0?????2??0?0?1?131001?0???00212??2111?10?????????????????

??

??????????

Aquiladelphis

21?11?1???????11202000112212010011241111O?????01122?0211??01?????????????????

??

??????????

Scalaridelphys 21?11?1???????112020001122220100 1(0

1)241101??????011222?2111001?????????????0????????????????????????????????

??

Dakotadens

????1????????1110200011222201001012110 1??????11222?200??01?????????????????

??

??????????

Protolambda

21?11?1????0?011302101022222010011241101O?????0212220211?0010?????????????????

??

??????????

Leptalestes

20?10?1????0?011302101022222000011241101O?????0212220211?0020?????????????????

??

??????????

```
      Herpetotherium   20010110?120001120120011222211101O(0
1)3110100110001121202111002O?????1111101?1111?1?111?1?0?0001?????????????22?
2??????1??1103?2?01112O???0??2???22110??121???20100l?0
      'Mimo_Peradectes'2011011??120001110120011222201011O(0
1)311010011100111(0
1)201(01)110000?????????????????????110??100000???????????10??22?11????????111
2120111120???0??20??12110??121?????1001??

;

END;
BEGIN ASSUMPTIONS;
      TYPESET * UNTITLED   =  unord:  2 -  3 5 -  6 8 -  11 13 15 -  34 37 -
49 53 -  115 117 -  164, ord:  1 - 7\3 12 14 35 -  36 50 -  52 116;

END;
```

Appendix 5: All digital models are available via MorphoSource.org.

Digital models include:

1. Digital model of MOR 10911 cranium and dentary (.stl) created using Avizo Lite software (unconstrained smoothing= 2)
2. Digital model of only the cranium of MOR 10911 (.stl) created using Avizo Lite software (unconstrained smoothing= 2)
3. Digital model of only the dentary and associated lower dentition of MOR 10911 (.stl) created using Avizo Lite software (unconstrained smoothing= 2)
4. Digital model of MOR 10912a (.stl) created using Avizo Lite software (unconstrained smoothing= 2)
5. Digital model of the right upper post-canine dentition of MOR 10912a (.stl) created using Avizo Lite software (unconstrained smoothing= 2)
6. Digital model of the left upper post-canine dentition of MOR 10912a (.stl) created using Avizo Lite software (unconstrained smoothing= 2)
7. Digital model of MOR 10912b (.stl) created using Avizo Lite software (unconstrained smoothing= 2)
8. Digital model of MOR 10912c (.stl) created using Avizo Lite software (unconstrained smoothing= 2)
9. Digital model of the right upper post-canine dentition of MOR 10912c (.stl) created using Avizo Lite software (unconstrained smoothing= 2)
10. Digital model of the left upper post-canine dentition of MOR 10912c (.stl) created using Avizo Lite software (unconstrained smoothing= 2)

11. Digital model of MOR 10912d (.stl) created using Avizo Lite software (unconstrained smoothing= 2)
12. Digital model of MOR 10913a (.stl) created using Avizo Lite software (no smoothing). DOI: 10.17602/M2/M369759

Appendix 6: TNT output from phylogenetic analysis and strict consensus tree

```
Reading from C:\Users\Owner\Desktop\Alpha phylo--with
Dave\Alphadon_July262021_Brannick_diss.tnt
Matrix (164x54, 16 states). Memory required for data:   0.26 Mbytes
Space for 99999 trees in memory
Constraints is OFF
Random seed is 1
0 trees in memory
Repl. Algor.     Tree        Score       Best Score   Time       Rearrangs.
499   FUSE       9           ------      617          0:20:18
5,727,874,754
Completed search.
Total rearrangements examined: 5,727,874,754.
No target score defined.  Best score hit 500 times.
Best score: 617.  6 trees retained.
Time 1218.24 secs.
```

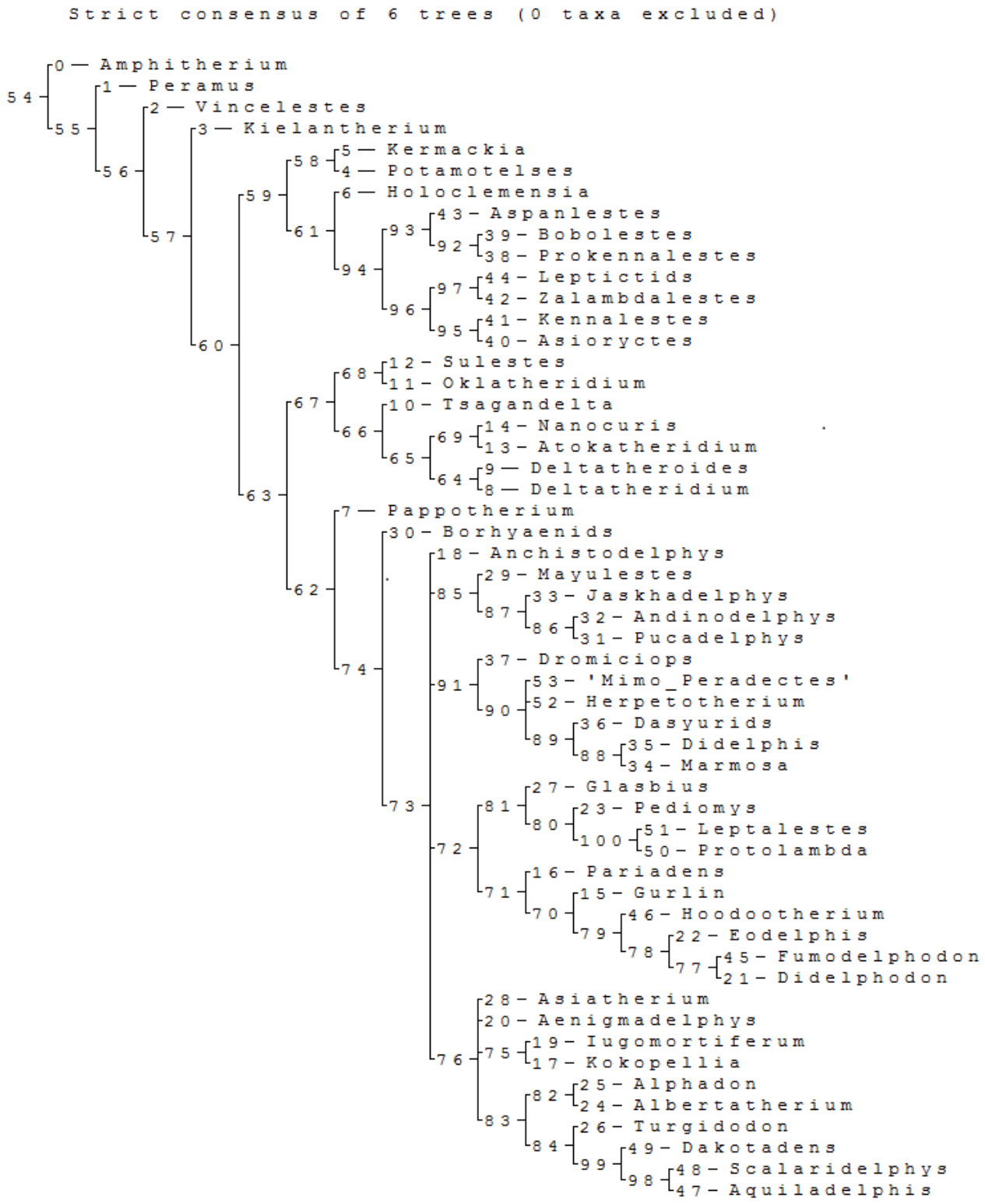
Strict consensus of 6 trees (0 taxa excluded)
0 — Amphitherium
1 — Peramus
2 — Vincelestes
3 — Kielantherium
5 — Kermackia
4 — Potamotelses
6 — Holoclemensia
43 — Aspanlestes
39 — Bobolestes
38 — Prokennalestes
44 — Leptictids
42 — Zalambdalestes
41 — Kennalestes
40 — Asioryctes
12 — Sulestes
11 — Oklatheridium
10 — Tsagandelta
14 — Nanocuris
13 — Atokatheridium
9 — Deltatheroides
8 — Deltatheridium
7 — Pappotherium
30 — Borhyaenids
18 — Anchistodelphys
29 — Mayulestes
33 — Jaskhadelphys
32 — Andinodelphys
31 — Pucadelphys
37 — Dromiciops
53 — 'Mimo_Peradectes'
52 — Herpetotherium
36 — Dasyurids
35 — Didelphis
34 — Marmosa
27 — Glasbius
23 — Pediomys
51 — Leptalestes
50 — Protolambda
16 — Pariadens
15 — Gurlin
46 — Hoodootherium
22 — Eodelphis
45 — Fumodelphodon
21 — Didelphodon
28 — Asiatherium
20 — Aenigmadelphys
19 — Iugomortiferum
17 — Kokopellia
25 — Alphadon
24 — Albertatherium
26 — Turgidodon
49 — Dakotadens
48 — Scalaridelphys
47 — Aquiladelphis

Appendix 7: Metatherian synapomorphies

The TNT output of synapomorphies common among the 6 equally parsimonious trees from the parsimony analysis of our data matrix is listed. Note: TNT (and the list below) uses a character numbering scheme that starts with 0 instead of 1, but in Appendix 1 our character numbering scheme starts with 1. For the list of characters and character states, also see Appendix 1. Node numbers refer to nodes in the strict consensus tree—see Appendix 4.

```
Amphitherium :
  All trees:
    No autapomorphies:

Peramus :
  All trees:
    Char. 9: 0 --> 1
    Char. 46: 0 --> 1
    Char. 76: 0 --> 1

Vincelestes :
  All trees:
    Char. 0: 1 --> 3
    Char. 4: 0 --> 1
    Char. 6: 01 --> 2
    Char. 8: 1 --> 0
    Char. 18: 1 --> 2
    Char. 23: 0 --> 1
    Char. 26: 0 --> 2
    Char. 40: 0 --> 1
    Char. 59: 0 --> 1
    Char. 84: 1 --> 0

Kielantherium :
  All trees:
    Char. 20: 0 --> 1
    Char. 28: 0 --> 1
    Char. 31: 0 --> 1

Potamotelses :
  All trees:
    Char. 14: 1 --> 0
    Char. 15: 1 --> 0
    Char. 34: 1 --> 0
    Char. 59: 2 --> 1

Kermackia :
  All trees:
    Char. 19: 2 --> 0
    Char. 60: 1 --> 0
```

```
Holoclemensia :
  All trees:
    Char. 5: 0 --> 1
    Char. 22: 0 --> 1
    Char. 23: 0 --> 1
    Char. 24: 2 --> 1

Pappotherium :
  All trees:
    Char. 28: 0 --> 1
    Char. 59: 0 --> 1

Deltatheridium :
  All trees:
    Char. 17: 0 --> 1

Deltatheroides :
  All trees:
    No autapomorphies:

Tsagandelta :
  All trees:
    No autapomorphies:

Oklatheridium :
  All trees:
    No autapomorphies:

Sulestes :
  All trees:
    No autapomorphies:

Atokatheridium :
  All trees:
    No autapomorphies:

Nanocuris :
  All trees:
    Char. 5: 2 --> 1
    Char. 49: 0 --> 1

Gurlin :
  All trees:
    Char. 24: 2 --> 1
    Char. 121: 2 --> 3
    Char. 147: 0 --> 1

Pariadens :
  All trees:
    Char. 14: 1 --> 0
    Char. 22: 0 --> 1
    Char. 27: 2 --> 1
    Char. 34: 2 --> 1
    Char. 56: 1 --> 0
```

```
Kokopellia :
  All trees:
    Char. 51: 2 --> 1
    Char. 56: 1 --> 0
    Char. 59: 2 --> 1
  Some trees:
    Char. 26: 2 --> 1
    Char. 52: 0 --> 1

Anchistodelphys :
  All trees:
    Char. 56: 1 --> 0
    Char. 57: 0 --> 1
  Some trees:
    Char. 33: 0 --> 1
    Char. 52: 0 --> 1

Iugomortiferum :
  All trees:
    Char. 4: 0 --> 1
    Char. 14: 1 --> 0
  Some trees:
    Char. 26: 12 --> 2

Aenigmadelphys :
  All trees:
    Char. 28: 0 --> 1
    Char. 49: 2 --> 1
    Char. 59: 2 --> 0
  Some trees:
    Char. 16: 1 --> 2
    Char. 18: 01 --> 2
    Char. 52: 0 --> 1

Didelphodon :
  All trees:
    Char. 46: 0 --> 1

Eodelphis :
  All trees:
    Char. 23: 1 --> 0
    Char. 50: 2 --> 1

Pediomys :
  All trees:
    No autapomorphies:

Albertatherium :
  All trees:
    Char. 58: 0 --> 1

Alphadon :
  All trees:
    No autapomorphies:
```

```
Turgidodon :
  All trees:
    No autapomorphies:

Glasbius :
  All trees:
    Char. 4: 0 --> 1
    Char. 5: 1 --> 0
    Char. 38: 0 --> 1
    Char. 40: 0 --> 1
    Char. 45: 0 --> 1
    Char. 60: 0 --> 1
    Char. 62: 0 --> 1

Asiatherium :
  All trees:
    Char. 19: 0 --> 1
    Char. 23: 1 --> 2
    Char. 36: 1 --> 0
    Char. 37: 1 --> 0
    Char. 38: 0 --> 1
  Some trees:
    Char. 2: 0 --> 2

Mayulestes :
  All trees:
    Char. 19: 0 --> 1
    Char. 37: 1 --> 0
    Char. 49: 2 --> 1
    Char. 59: 2 --> 1
    Char. 80: 0 --> 1
    Char. 98: 1 --> 0
    Char. 123: 2 --> 3
    Char. 142: 2 --> 1
    Char. 157: 0 --> 1
    Char. 161: 0 --> 1

Borhyaenids :
  All trees:
    Char. 31: 0 --> 1
    Char. 52: 0 --> 1
    Char. 80: 0 --> 1
    Char. 88: 0 --> 1
    Char. 95: 0 --> 1
    Char. 123: 2 --> 3
    Char. 134: 0 --> 1
    Char. 147: 0 --> 1
    Char. 148: 0 --> 1
    Char. 154: 0 --> 1

Pucadelphys :
  All trees:
    Char. 19: 0 --> 1
    Char. 25: 2 --> 1
    Char. 35: 3 --> 4
```

```
    Char. 83: 1 --> 0

Andinodelphys :
  All trees:
    Char. 103: 0 --> 1
    Char. 137: 0 --> 1
  Some trees:
    Char. 55: 0 --> 1

Jaskhadelphys :
  All trees:
    Char. 27: 2 --> 1
    Char. 34: 2 --> 1

Marmosa :
  All trees:
    No autapomorphies:

Didelphis :
  All trees:
    Char. 25: 2 --> 1
    Char. 155: 1 --> 0

Dasyurids :
  All trees:
    Char. 7: 0 --> 1
    Char. 10: 2 --> 0
    Char. 23: 1 --> 0
    Char. 36: 1 --> 0
    Char. 40: 0 --> 1
    Char. 41: 0 --> 1
    Char. 57: 0 --> 1
    Char. 82: 1 --> 0
    Char. 95: 0 --> 1
    Char. 136: 0 --> 1
    Char. 157: 0 --> 1

Dromiciops :
  All trees:
    Char. 2: 0 --> 2
    Char. 10: 2 --> 0
    Char. 21: 0 --> 1
    Char. 23: 1 --> 0
    Char. 35: 3 --> 4
    Char. 40: 0 --> 1
    Char. 42: 1 --> 0
    Char. 54: 1 --> 0
    Char. 57: 0 --> 1
    Char. 60: 0 --> 1
    Char. 78: 1 --> 0
    Char. 121: 1 --> 3
    Char. 123: 2 --> 3
    Char. 126: 0 --> 1
    Char. 149: 1 --> 0
  Some trees:
```

```
    Char. 130: 1 --> 2

Prokennalestes :
  All trees:
    Char. 21: 1 --> 0
    Char. 23: 0 --> 1
    Char. 24: 2 --> 1
    Char. 34: 2 --> 1
    Char. 43: 1 --> 0
    Char. 46: 1 --> 0
    Char. 50: 1 --> 0

Bobolestes :
  All trees:
    Char. 17: 0 --> 1

Asioryctes :
  All trees:
    Char. 41: 1 --> 0
    Char. 90: 0 --> 1

Kennalestes :
  All trees:
    Char. 20: 0 --> 1
    Char. 38: 0 --> 1

Zalambdalestes :
  All trees:
    Char. 32: 1 --> 0
    Char. 40: 0 --> 1
    Char. 50: 1 --> 2
    Char. 72: 2 --> 0
    Char. 82: 1 --> 0
    Char. 97: 0 --> 1

Aspanlestes :
  All trees:
    Char. 25: 2 --> 1
    Char. 36: 0 --> 1
    Char. 38: 0 --> 1
    Char. 49: 1 --> 2
    Char. 146: 0 --> 1

Leptictids :
  All trees:
    Char. 9: 0 --> 1
    Char. 35: 3 --> 4
    Char. 38: 0 --> 1
    Char. 45: 0 --> 1
    Char. 66: 0 --> 1
    Char. 70: 0 --> 1
    Char. 76: 1 --> 0
    Char. 83: 0 --> 1
    Char. 85: 0 --> 1
    Char. 90: 0 --> 1
```

```
    Char. 98: 0 --> 1
    Char. 104: 0 --> 1
    Char. 106: 0 --> 1
    Char. 108: 3 --> 2
    Char. 114: 0 --> 1
    Char. 139: 0 --> 1
    Char. 145: 1 --> 0
    Char. 148: 0 --> 1
    Char. 149: 0 --> 1
    Char. 154: 0 --> 1

Fumodelphodon :
  All trees:
    No autapomorphies:

Hoodootherium :
  All trees:
    Char. 3: 1 --> 0
    Char. 34: 2 --> 1

Aquiladelphis :
  All trees:
    Char. 26: 2 --> 1
    Char. 38: 0 --> 1

Scalaridelphys :
  All trees:
    No autapomorphies:

Dakotadens :
  All trees:
    Char. 33: 1 --> 0
    Char. 34: 2 --> 1
    Char. 35: 3 --> 2
    Char. 54: 1 --> 0
    Char. 55: 1 --> 0

Protolambda :
  All trees:
    Char. 1: 0 --> 1
    Char. 4: 0 --> 1
    Char. 59: 2 --> 1

Leptalestes :
  All trees:
    Char. 29: 1 --> 0

Herpetotherium :
  All trees:
    Char. 122: 1 --> 0
    Char. 123: 2 --> 3
    Char. 127: 1 --> 0
  Some trees:
    Char. 156: 0 --> 2
```

```
'Mimo_Peradectes' :
  All trees:
    Char. 2: 0 --> 1
    Char. 31: 0 --> 1
    Char. 49: 2 --> 1
    Char. 59: 2 --> 0
    Char. 83: 1 --> 0
    Char. 143: 2 --> 1
  Some trees:
    Char. 16: 2 --> 1
    Char. 44: 0 --> 1
    Char. 53: 2 --> 1

Node 55 :
  All trees:
    No synapomorphies

Node 56 :
  All trees:
    Char. 0: 0 --> 1
    Char. 35: 0 --> 1
    Char. 39: 0 --> 1
    Char. 41: 0 --> 1
    Char. 60: 0 --> 1

Node 57 :
  All trees:
    Char. 14: 0 --> 1
    Char. 24: 0 --> 2
    Char. 25: 0 --> 2
    Char. 48: 0 --> 1

Node 58 :
  All trees:
    Char. 16: 0 --> 1
    Char. 25: 2 --> 1
    Char. 32: 1 --> 0
    Char. 36: 0 --> 1

Node 59 :
  All trees:
    Char. 46: 0 --> 1
    Char. 59: 0 --> 2

Node 60 :
  All trees:
    Char. 15: 0 --> 1
    Char. 34: 0 --> 1
    Char. 35: 1 --> 2
    Char. 49: 0 --> 1
    Char. 53: 0 --> 1
    Char. 75: 0 --> 1
    Char. 76: 0 --> 1

Node 61 :
```

```
  All trees:
    Char. 35: 2 --> 3
    Char. 50: 0 --> 1
    Char. 56: 0 --> 1

Node 62 :
  All trees:
    Char. 19: 2 --> 0

Node 63 :
  All trees:
    Char. 0: 1 --> 2
    Char. 5: 0 --> 2
    Char. 9: 0 --> 1
    Char. 42: 0 --> 1
    Char. 44: 0 --> 1
    Char. 55: 0 --> 1
    Char. 61: 0 --> 1
    Char. 64: 0 --> 1
    Char. 65: 0 --> 1
    Char. 70: 0 --> 1
    Char. 78: 0 --> 1
    Char. 114: 0 --> 1
    Char. 124: 0 --> 1
    Char. 144: 0 --> 2
    Char. 146: 0 --> 1
    Char. 149: 0 --> 1
    Char. 151: 0 --> 2

Node 64 :
  All trees:
    Char. 44: 1 --> 0

Node 65 :
  All trees:
    Char. 47: 1 --> 0
    Char. 62: 0 --> 1

Node 66 :
  All trees:
    Char. 49: 1 --> 0

Node 67 :
  All trees:
    Char. 26: 0 --> 1
    Char. 31: 0 --> 1
    Char. 40: 0 --> 1

Node 68 :
  All trees:
    Char. 17: 0 --> 1

Node 69 :
  All trees:
    Char. 36: 0 --> 1
```

```
    Char. 53: 1 --> 0

Node 70 :
  All trees:
    Char. 21: 0 --> 2
    Char. 33: 1 --> 0

Node 71 :
  All trees:
    Char. 5: 1 --> 2
    Char. 31: 0 --> 1
    Char. 59: 2 --> 0

Node 72 :
  All trees:
    Char. 50: 1 --> 2
    Char. 68: 0 --> 1
    Char. 136: 0 --> 1

Node 73 :
  All trees:
    Char. 5: 2 --> 1
    Char. 35: 2 --> 3
    Char. 37: 0 --> 1
    Char. 41: 1 --> 0
    Char. 49: 1 --> 2
    Char. 59: 0 --> 2
    Char. 67: 0 --> 1
    Char. 93: 0 --> 1
    Char. 94: 0 --> 1
  Some trees:
    Char. 53: 1 --> 2

Node 74 :
  All trees:
    Char. 16: 0 --> 1
    Char. 26: 0 --> 2
    Char. 27: 1 --> 2
    Char. 34: 1 --> 2
    Char. 36: 0 --> 1
    Char. 50: 0 --> 1
    Char. 51: 1 --> 2
    Char. 54: 0 --> 1
    Char. 56: 0 --> 1

Node 75 :
  All trees:
    Char. 15: 1 --> 0
    Char. 19: 0 --> 2
    Char. 23: 1 --> 0

Node 76 :
  All trees:
    Char. 27: 2 --> 1
  Some trees:
```

```
    Char. 10: 2 --> 1
    Char. 42: 1 --> 0
    Char. 86: 0 --> 1

Node 77 :
  All trees:
    Char. 13: 0 --> 1

Node 78 :
  All trees:
    Char. 41: 0 --> 1

Node 79 :
  All trees:
    Char. 1: 0 --> 1
    Char. 2: 0 --> 2
    Char. 4: 0 --> 1

Node 80 :
  All trees:
    Char. 16: 1 --> 3

Node 81 :
  All trees:
    Char. 23: 1 --> 2
    Char. 35: 3 --> 4

Node 82 :
  All trees:
    Char. 28: 0 --> 1

Node 83 :
  All trees:
    Char. 22: 0 --> 1
  Some trees:
    Char. 55: 0 --> 1

Node 84 :
  All trees:
    Char. 1: 0 --> 1
    Char. 4: 0 --> 1

Node 85 :
  All trees:
    Char. 50: 1 --> 2
  Some trees:
    Char. 8: 1 --> 0
    Char. 52: 0 --> 1
    Char. 108: 2 --> 1
    Char. 147: 0 --> 1
    Char. 148: 0 --> 1
    Char. 159: 0 --> 1

Node 86 :
  All trees:
```

```
    Char. 18: 1 --> 0

Node 87 :
  All trees:
    Char. 21: 0 --> 2
    Char. 22: 0 --> 1
    Char. 28: 0 --> 1
    Char. 30: 0 --> 1

Node 88 :
  All trees:
    Char. 8: 1 --> 0
    Char. 18: 1 --> 0
    Char. 24: 2 --> 1
    Char. 45: 0 --> 1
    Char. 54: 1 --> 0
    Char. 118: 2 --> 1
    Char. 141: 2 --> 0
    Char. 143: 2 --> 1
    Char. 156: 0 --> 1

Node 89 :
  All trees:
    Char. 21: 0 --> 2
    Char. 50: 1 --> 2
    Char. 71: 0 --> 1
    Char. 76: 1 --> 0
  Some trees:
    Char. 130: 1 --> 2

Node 90 :
  All trees:
    Char. 22: 0 --> 1
    Char. 103: 0 --> 1
    Char. 129: 0 --> 1
    Char. 161: 0 --> 1

Node 91 :
  All trees:
    Char. 19: 0 --> 2
    Char. 34: 2 --> 0
    Char. 68: 0 --> 1
    Char. 86: 0 --> 1
    Char. 139: 1 --> 2
    Char. 154: 0 --> 1
  Some trees:
    Char. 16: 1 --> 2
    Char. 44: 1 --> 0

Node 92 :
  All trees:
    Char. 16: 4 --> 1
    Char. 47: 2 --> 1
    Char. 74: 1 --> 0
    Char. 75: 1 --> 0
```

```
Node 93 :
  All trees:
    Char. 0: 1 --> 0
    Char. 10: 0 --> 1
    Char. 20: 0 --> 1
    Char. 125: 2 --> 1

Node 94 :
  All trees:
    Char. 16: 0 --> 4
    Char. 21: 0 --> 1
    Char. 33: 0 --> 1
    Char. 34: 1 --> 2
    Char. 60: 1 --> 0

Node 95 :
  All trees:
    Char. 43: 1 --> 0

Node 96 :
  All trees:
    Char. 11: 1 --> 2
    Char. 12: 0 --> 1
    Char. 108: 1 --> 3
    Char. 123: 2 --> 3
    Char. 126: 0 --> 1
    Char. 135: 0 --> 1

Node 97 :
  All trees:
    Char. 8: 1 --> 2
    Char. 25: 2 --> 1
    Char. 49: 1 --> 2
    Char. 71: 0 --> 1
    Char. 122: 0 --> 1

Node 98 :
  All trees:
    Char. 16: 1 --> 2
    Char. 35: 3 --> 4

Node 99 :
  All trees:
    Char. 18: 1 --> 2
    Char. 27: 1 --> 2
    Char. 50: 1 --> 2
    Char. 59: 2 --> 1

Node 100 :
  All trees:
    Char. 19: 0 --> 1
    Char. 21: 0 --> 1
    Char. 47: 1 --> 2
```

Appendix 8: Resulting Majority Rule Consensus Tree

Below is the resulting TNT output tree for a majority rule consensus tree with a 50% cutoff.

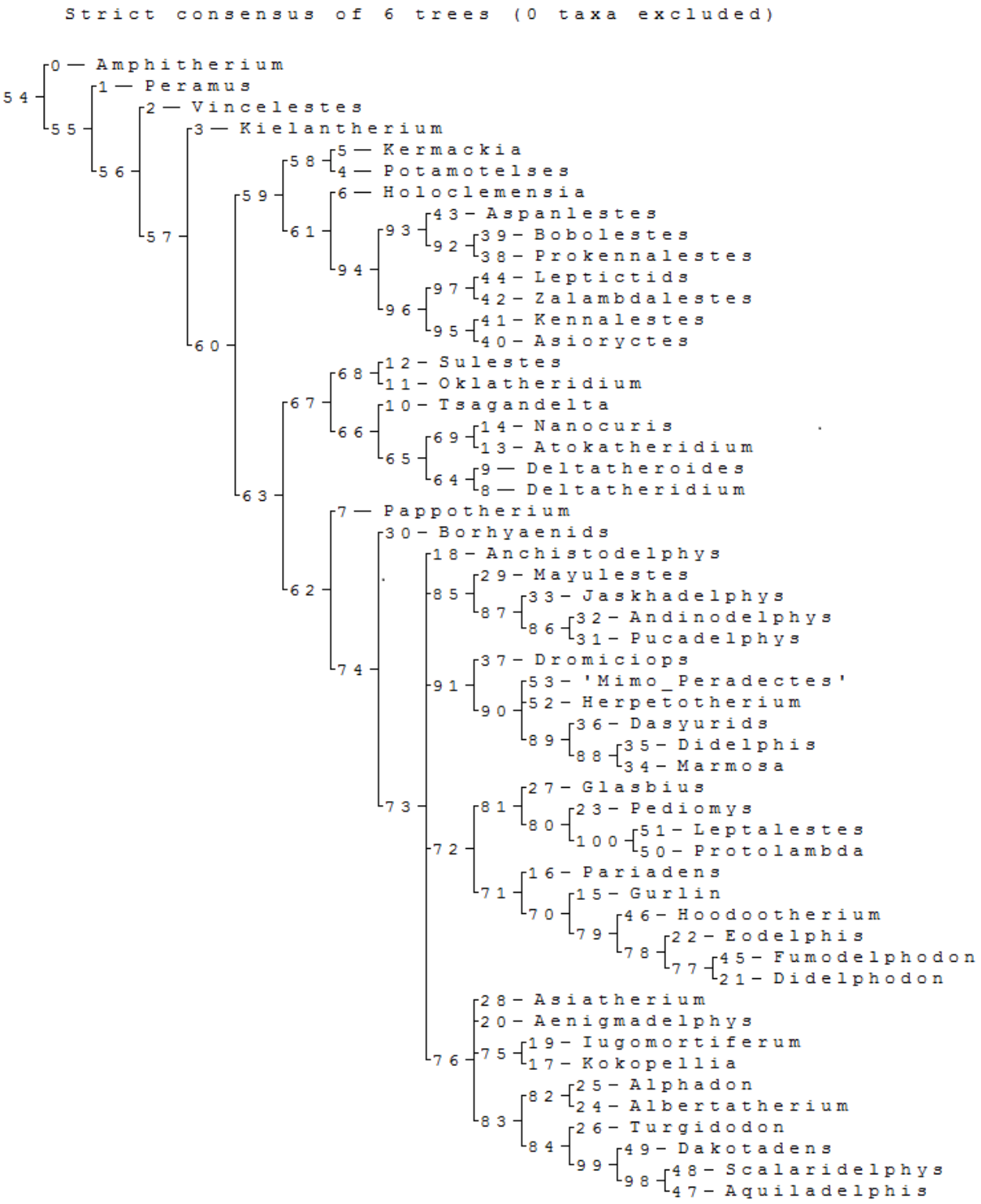

Appendix 9: Strict Consensus Tree with mapped synapomorphies.

Below is the resulting strict consensus tree with select synapomorphies mapped at associated nodes from our TNT output.

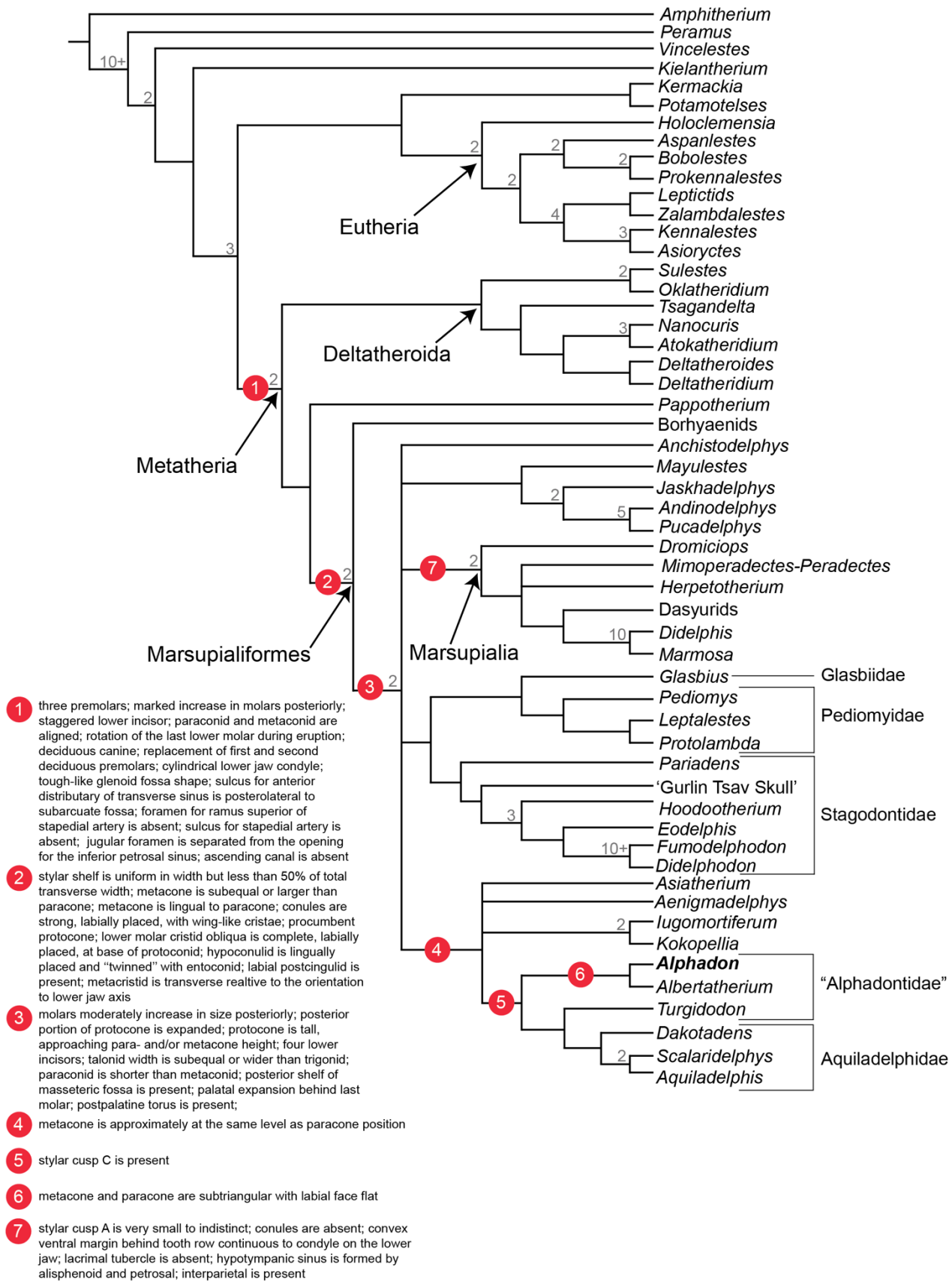

1 three premolars; marked increase in molars posteriorly; staggered lower incisor; paraconid and metaconid are aligned; rotation of the last lower molar during eruption; deciduous canine; replacement of first and second deciduous premolars; cylindrical lower jaw condyle; tough-like glenoid fossa shape; sulcus for anterior distributary of transverse sinus is posterolateral to subarcuate fossa; foramen for ramus superior of stapedial artery is absent; sulcus for stapedial artery is absent; jugular foramen is separated from the opening for the inferior petrosal sinus; ascending canal is absent

2 stylar shelf is uniform in width but less than 50% of total transverse width; metacone is subequal or larger than paracone; metacone is lingual to paracone; conules are strong, labially placed, with wing-like cristae; procumbent protocone; lower molar cristid obliqua is complete, labially placed, at base of protoconid; hypoconulid is lingually placed and "twinned" with entoconid; labial postcingulid is present; metacristid is transverse realtive to the orientation to lower jaw axis

3 molars moderately increase in size posteriorly; posterior portion of protocone is expanded; protocone is tall, approaching para- and/or metacone height; four lower incisors; talonid width is subequal or wider than trigonid; paraconid is shorter than metaconid; posterior shelf of masseteric fossa is present; palatal expansion behind last molar; postpalatine torus is present;

4 metacone is approximately at the same level as paracone position

5 stylar cusp C is present

6 metacone and paracone are subtriangular with labial face flat

7 stylar cusp A is very small to indistinct; conules are absent; convex ventral margin behind tooth row continuous to condyle on the lower jaw; lacrimal tubercle is absent; hypotympanic sinus is formed by alisphenoid and petrosal; interparietal is present

CHAPTER 3: NEW SPECIMENS OF THE LATE CRETACEOUS METATHERIAN *EODELPHIS* AND THE EVOLUTION OF HARD-OBJECT FEEDING IN THE STAGODONTIDAE

Brannick, A.L., and Wilson, G.P., 2020. New Specimens of the Late Cretaceous Metatherian *Eodelphis* and the Evolution of Hard-Object Feeding in the Stagodontidae: Journal of Mammalian Evolution. doi: 10.1007/s10914-018-9451-z

3.1 AUTHOR CONTRIBUTIONS

ALB and GPW conceived of the project. ALB collected bending strength measurements, conducted analyses, made figures, and wrote the main body of the manuscript; GPW contributed to the manuscript.

3.2 ABSTRACT

The Stagodontidae include the largest metatherians known from the Cretaceous of North America. Of the recognized species of the stagodontid genus *Eodelphis*, *E. cutleri* is larger and has a more robust dentary, more inflated premolars, and third premolars specialized for crushing, as opposed to the more gracile *E. browni*. These differences have led to the hypothesis that an *E. cutleri*-like ancestor gave rise to *Didelphodon*—another, mostly younger, stagodontid, which has been interpreted as a durophagous predator-scavenger. If correct, *E. cutleri* would be expected to show more morphological adaptation toward durophagy than *E. browni* does. Here, we describe two new dentary fossils referable to *E. browni* and test the evolutionary hypothesis by applying

beam theory to estimate bending force capabilities of 22 dentaries of Cretaceous stagodontids and other metatherians. The resulting diversity of bending force profiles of the sampled dentaries implies that Cretaceous metatherians had a wide range of feeding behaviors. Among the stagodontids, *E. cutleri* has a mediolateral bending force profile of the dentary that is more similar to that of *Didelphodon* than it is to that of *E. browni*; whereas its dorsoventral bending force profile is more similar to that of *E. browni*. These results indicate that anteriorly the dentary of *E. cutleri* was capable of resisting high torsional stresses from hard-object feeding but lacked other dorsoventral buttressing associated with exceptionally high bite forces of *Didelphodon*. Our results imply that some morphological changes associated with durophagy evolved twice within this clade, independently in *E. cutleri* and *Didelphodon*.

3.3 INTRODUCTION

The Metatheria, the stem-based clade of living marsupials and their closest relatives (Rougier et al. 1998), achieved substantial taxonomic and morphological diversity during the Late Cretaceous (ca. 100–66 million years ago [Ma]; Kielan-Jaworowska et al. 2004; Sánchez-Villagra 2013; Williamson et al. 2014; Wilson et al. 2016). Yet, surprisingly few studies have quantitatively investigated the paleoecologies implied by that diversity (Clemens 1966; Luo 2007; Wilson 2013; Grossnickle and Polly 2013; Wilson et al. 2016; Grossnickle and Newham 2016). In general, because of the preservational bias toward teeth in the mammalian fossil record, studies of the paleoecology of Mesozoic mammals have primarily focused on reconstructions of diets based on dental shape and functional morphology (e.g., Crompton and Kielan-Jaworowska 1978; Jernvall et al. 1996; Wilson et al. 2012). Analysis of the dentary can also be used in functional morphological studies to infer feeding behaviors in both extant and extinct mammals (Biknevicius and Ruff 1992a, b; Grossnickle and Polly 2013; Gill et al. 2014; Grossnickle 2017). For example, cross-sectional properties of the dentary, including cortical bone structure, reflect the biomechanical bending strength of the dentary and can help constrain dietary inferences (e.g., Therrien 2005; Binder et al. 2016; Wilson et al. 2016).

In this study, we quantify biomechanical properties of the dentary in the metatherian clade Stagodontidae, which includes some of the largest bodied mammals known from the Cretaceous of North America (body mass estimate of *Didelphodon vorax* UWBM 94084 = 5.2 kg; Wilson et al. 2016). The genera *Eodelphis* and *Didelphodon* are included in this clade, in addition to the recently described genera *Fumodelphodon* and *Hoodootherium* from the Straight Cliffs Formation of Utah (Cohen 2017); a fifth genus, *Pariadens*, has also been considered a basal stagodontid (Cifelli and Eaton 1987; Rougier et al. 2004, 2015; Wilson et al. 2016; Cohen

2017; but see Fox and Naylor 2006; Williamson et al. 2012, 2014). Furthermore, the Eocene genus *Eobrasilia* of South America most recently has been proposed as a sister taxon to *Didelphodon* (Carneiro and Oliveira 2017). In addition to larger body size, stagodontids are characterized by several dental characters, including: (1) upper molars with a robust metacone, a small paracone, well-developed conules near the paracone and metacone, but without a metacingulum; (2) lower molars with mesiodistally compressed trigonids, a cristid obliqua that meets the trigonid buccal to the protocristid notch, a reduced metaconid, an enlarged paraconid, a carnassial notch, and paraconids and protoconids that are subequal in height; (3) as a result of those modifications, prevallum/postvallid shearing is reduced and the postvallum/prevallid shearing is emphasized; (4) enlarged upper and lower third premolars; and (5) three or fewer lower incisors (Fox and Naylor 2006; Scott and Fox 2015).

Specifically, we describe two dentary fossils of the genus *Eodelphis*, and we incorporate them and 20 other metatherian specimens into a biomechanical analysis based on beam theory (Therrien 2005). We use the resulting bending strength profiles to test whether *Eodelphis cutleri* and *Eodelphis browni*, like *D. vorax*, were capable of hard-object feeding (durophagy). We aim to improve our understanding of the evolutionary steps toward durophagy within the Stagodontidae and, more broadly, the diversification of feeding strategies within Metatheria during the Late Cretaceous.

3.3.1 Background

The genus *Eodelphis* is represented in the fossil record by isolated teeth, dentary fragments with teeth, and cranial fragments from localities in the Western Interior of North

America, most of them in Montana and Alberta (Fig. 3.1; Fox 1971; Sahni 1972; Rigby and Wolberg 1987; Eaton and Cifelli 1988; Fiorillo 1989; Montellano 1992; Peng and Russell 2001; DeMar and Breithaupt 2006; Scott and Fox 2015). These localities sample the Aquilan, Judithian, and possibly "Edmontonian" North American land mammal "ages" (NALMAs), which together correspond to a temporal range of ca. 84–70 million years ago (Ma) or late Santonian to early Maastrichtian of the Late Cretaceous (Cifelli et al. 2004; Wilson et al. 2010). Although the oldest specimen of this genus, referred to *Eodelphis* sp., was recovered from the Aquilan-age Deadhorse Coulee Member of the Milk River Formation in southern Alberta (Drees and Mhyr 1981; Fox and Naylor 2006), most specimens have been found at localities assigned a Judithian age (ca. 80–74 Ma; Wilson et al. 2010). Additionally, two very fragmentary dentaries that were recovered from Lane's Little Jaw Site Quarry in the Hell Creek Formation of southeastern Montana were tentatively assigned to *Eodelphis* (Kelly 2014). There is some uncertainty in the taxonomic identifications of the specimens and the age of the locality; it might be Lancian (latest Cretaceous), Puercan (earliest Paleocene), or mixed in age (Kelly 2014). Regardless, if the specimens are correctly assigned, the temporal range of *Eodelphis* would be extended at least ca. 4–5 Ma into the Lancian (Kelly 2014).

The two species of *Eodelphis* (*E. browni* and *E. cutleri*) were once proposed as sexual dimorphs of a single species by Montellano (1992), but Fox and Naylor (2006) convincingly argued that the qualitative differences in their dentition and inferred dietary preferences exceed what would be expected within a single species. Compared to *E. browni*, *E. cutleri* is larger, has a more robust dentary, more inflated teeth, and larger third premolars (Fox 1981; Scott and Fox 2015). Williamson et al. (2012, 2014) also treated *E. browni* and *E. cutleri* as separate species

and recovered them as sister taxa within the Stagodontidae in their cladistic analyses of Late Cretaceous and Paleogene metatherians.

The genus *Didelphodon* is known from the Judithian through Lancian (early Campanian–late Maastrichtian; ca. 80–66 Ma) in the northern Western Interior of North America (Alberta, Saskatchewan, Montana, North Dakota, South Dakota, and Wyoming). The Lancian species, *D. vorax*, is known from across this geographic range from many specimens, including dentulous dentary fragments and partial crania (Wilson et al. 2016); a second Lancian species, *D. padanicus*, is restricted to only those specimens from South Dakota (Clemens 1966); and a third species, *D. coyi*, is known from only a few specimens from the "Edmontonian" and Lancian of Alberta (Fox and Naylor 1986, 2006). Several other poorly preserved specimens of *Didelphodon* from the Judithian Dinosaur Park Formation and the "Edmontonian" St. Mary River Formation, both in Alberta, have not been assigned to species (Sloan and Russell 1974; Fox and Naylor 1986; Scott and Fox 2015).

Both *Eodelphis* and *Didelphodon* have carnivorous dental adaptations, including the reduction of prevallum/postvallid shearing and emphasis of postvallum/prevallid shearing, but *Didelphodon* has more robust dental and dentary morphology, leading to the interpretation that it was more durophagous relative to *Eodelphis* and a powerful predator/scavenger (Clemens 1966, 1968; Scott and Fox 2015; Wilson et al. 2016). Furthermore, on the basis of size, premolar morphology, and stratigraphic occurrence, the conventional hypothesis is that *Didelphodon* arose from an *E. cutleri*-like ancestor (Clemens 1966; Fox and Naylor 1986, 2006; Scott and Fox 2015; but see Fox 1981; Fox and Naylor 1986 for comments on using morphological comparisons of premolars instead of molars). In contrast, Cohen (2017) hypothesized that the newly described Turonian stagodontid *Fumodelphodon* is more closely related to *Didelphodon*

than *Eodelphis* is to *Didelphodon*, on the basis of similarities in premolar morphology and the results of his phylogenetic analysis. This would imply a ghost lineage that pre-dates the evolutionary split proposed by the conventional hypothesis. Additionally, the phylogenetic analysis results of Carneiro and Oliveira (2017) concluded that *Fumodelphodon* is most closely related to *Hoodootherium*; this clade (*Fumodelphodon* + *Hoodootherium*) is proposed as sister to a clade including (*Eodelphis* + [*Didelphodon* + *Eobrasilia*]). Nevertheless, we defer acceptance of the phylogenetic hypotheses of both Cohen (2017) and Carneiro and Oliveira (2017) until further evidence can be brought to bear on the association of the isolated premolars and molars referred to *Fumodelphodon*—presently, it is made primarily on the basis of size (Cohen 2017)—and on the proposed phylogenetic relationships between *Didelphodon* and *Fumodelphodon* and between *Didelphodon* and *Eobrasilia*. Because a detailed phylogenetic analysis of the Stagodontidae is beyond the scope of this paper, we proceed with the working hypothesis that *Didelphodon* arose from an *E. cutleri*-like ancestor (Clemens 1966; Fox and Naylor 1986, 2006; Scott and Fox 2015).

Accordingly, it might be expected that *E. cutleri* possessed morphology reflecting a trend toward durophagy, whereas *E. browni* would lack or have fewer of these adaptations. Indeed, the premolars of *E. cutleri*, like those of *Didelphodon*, are more robust than those of *E. browni* (Scott and Fox 2015). *Eodelphis cutleri* has thus been interpreted as having had a more scavenging or hard-object feeding habit, whereas *E. browni* has been interpreted as insectivorous or possibly carnivorous (Scott and Fox 2015). It follows that the feeding capabilities of these species should also be evident in the morphology of their dentaries; however, until now this hypothesis has not yet been quantitatively tested.

3.4 INSTITUTIONAL ABBREVIATIONS

AMNH, American Museum of Natural History, New York, New York, USA.; **MOR**, Museum of the Rockies, Bozeman, Montana, USA; **NHMUK**, Natural History Museum, United Kingdom, London, UK; **OMNH**, Oklahoma Museum of Natural History, Norman, Oklahoma, USA; **RSMP**, Palaeontological Collections of the of the Royal Saskatchewan Museum, Regina, Saskatchewan, Canada; **TMDC**, Two Medicine Dinosaur Center, Bynum, Montana, USA; **TMP**, Royal Tyrrell Museum of Palaeontology, Drumheller, Alberta, Canada; **UALVP**, University of Alberta Laboratory for Vertebrate Paleontology, Edmonton, Alberta, Canada; **UCMP**, University of California Museum of Paleontology, Berkeley, California, USA; **UWBM**, University of Washington Burke Museum, Seattle, Washington, USA.

3.5 SYSTEMATIC PALEONTOLOGY

MAMMALIA Linnaeus, 1758

THERIA Parker and Haswell, 1897

METATHERIA Huxley, 1880

MARSUPIALIFORMES Vullo et al., 2009

STAGODONTIDAE Marsh, 1889

EODELPHIS Matthew, 1916

EODELPHIS cf. *E. BROWNI* Matthew, 1916 (Fig. 3.2a–f)

3.5.1 Holotype

AMNH 14169: parts of the left squamosal and left jugal, anterior region of right dentary, and an incomplete left dentary with i1–3, p1–3, m2–4, and m1 roots present (Matthew 1916).

The holotype was found in the Dinosaur Park Formation (Judithian; Late Cretaceous in age) in southeastern Alberta, Canada.

3.5.2 Referred Specimens

MOR 739, an incomplete right dentary with m2–4 and the alveoli of p2, p3, and m1 (Fig. 3.2a–c); TMDC TA2008.3.2, an incomplete right dentary with m1–4, fragments of p2–3, alveoli for p1, and an incomplete alveolus for the canine (Fig. 3.2d–f).

3.5.3 Locality Data

MOR 739 was found at MOR locality JR-120 "Long Time Waiting" in the Judith River Formation of Watson Coulee in Hill County, Montana. For more information regarding this locality, qualified researchers should contact the Museum of the Rockies. TMDC 2008.3.2 was found in the Judith River Formation of Kennedy Coulee in Hill County, Montana. For more information regarding this locality, qualified researchers should contact the Two Medicine Dinosaur Center.

3.5.4 Description

MOR 739 is a moderately well-preserved; right dentary; it includes most of the horizontal ramus, the anteroventral margin of the coronoid process, and the anterior part of the masseteric fossa, as well as m2–4 and the alveoli for p2, p3, and m1 (Fig. 3.2a–c). Most of the symphysis and the alveoli for the lower incisors, canine, and p1 are not preserved.

The horizontal ramus is long and gracile relative to that of *Didelphodon*. It is dorsoventrally deepest ventral to the m4 (10.55 mm) and tapers anteriorly (Fig. 3.2a, b). A slight bony projection on the ventral margin below the p2–p3 embrasure and fracturing along the lateral margins suggest that the specimen might have experienced mediolateral compressive deformation. An ovoid mental foramen occurs ventral to the level of the p3 alveoli; a second one is not present, but this absence may be due to the lack of preservation of the dentary ventral to the p1 posterior alveolus (Fig. 3.2a). The anterior edge of the coronoid process has a vertical orientation posterior to m4, as described for other dentaries of *E. browni* (Fox 1981). The preserved parts of the masseteric fossa are deep. Its anterior border does not extend onto the horizontal ramus of the dentary, but it does extend near to the ventral margin of the dentary, where there is a prominent masseteric line (Fig. 3.2a).

Alveoli for the p1 are not present, but a diastema anterior to the p2 alveoli provides some information about spacing of p1 relative to more posterior premolars (Fig. 3.2c). The p2 alveoli are subequal in size and laterally compressed (although some compression may be due to post-mortem deformation). The p3 alveoli are directly posterior to the p2 posterior alveolus; they are also larger than those of p2 and less laterally compressed (Table 3.1). The m1 alveoli are partly obscured by sediment infilling, but they are directly posterior to the p3 posterior alveolus; this differs from *Didelphodon* in which the anterior alveolus of m1 is buccal to the posterior alveolus of p3 (Clemens 1966).

The molar row of MOR 739 is slightly oblique to the long axis of the horizontal ramus (Fig. 3.2c). The molar crowns are well preserved, although some cusp apices, particularly those of the protoconids, are chipped or slightly worn. The m2 trigonid is narrower than the talonid and mesiodistally shorter than it. The trigonid angle is acute. The paraconid is taller than the

protoconid, although the latter has a broken apex (and was probably taller than the paraconid before breakage), and the metaconid is by far the smallest trigonid cusp, as is characteristic of stagodontids (Clemens 1966; Fox 1981; Scott and Fox 2015). The paracristid, which shows some wear, steeply descends from the apex of the paraconid forming a notch at the lingual base of the protoconid; additionally, a ridge juts out from the mesial aspect of the apex of the paraconid, and extends ventrally toward the base of the cusp. The precingulid extends buccoventrally from just below the middle of the paracristid to the base of the protoconid. In distal view, the protocristid is broad and V-shaped, rather than sharply notched; the lingual face of the trigonid is slightly convex; and the buccal and distal faces are nearly vertical. In occlusal view, the distal face is transverse, rather than oblique, to the mesiodistal axis of the crown. The talonid basin is broad and deepest mesiolingually. The entoconid and hypoconulid are "twinned" and taller than the hypoconid, although the hypoconid has a larger base. The entocristid, which shows some wear buccally, extends mesioventrally at a steep angle to make contact with the distal face of the trigonid at a sharp angle. The cristid obliqua extends from the hypoconid to contact the distal face of the trigonid buccal to the protocristid notch. Distally, the hypoconulid is braced between the precingulid and the mesial ridge of the paraconid of the m3, as seen in other specimens of *Eodelphis* and *Didelphodon* (e.g., Fox 1981).

The m3 and m4 differ only slightly in morphology from the m2 (Fig. 3.2c). The m3 is larger than the m2 (Table 3.2), and the trigonid and talonid are subequal in length and width. The morphology and arrangement of the m3 trigonid cusps differ from those of the m2 in that the trigonid angle is more acute and the paraconid shows greater apical wear. The m3 talonid also differs from that of m2 in that the basin is deeper and the entoconid and hypoconulid show less wear. On m4, the trigonid is wider than the talonid. The entoconid and hypoconulid are of

subequal height and almost as tall as the metaconid. All dental measurements are provided in Table 3.2.

TMDC TA2008.3.2 is a right dentary that preserves m1–4, fragments of p2 and p3, and alveoli for the p1 and canine (Fig. 3.2d–f). Overall, the dentary is like MOR 739, in having a gracile appearance compared to previously described specimens of *Didelphodon* and *E. cutleri*. It is deepest ventral to m4 (8.62 mm), and gently tapers in depth towards the canine. The anterior margin of the masseteric fossa is present, but the angular process, condyloid process, and most of the coronoid process are missing (Fig. 3.2e, f). The small portion of the anterior edge of the coronoid process that is preserved appears to steeply rise behind m4, as in MOR 739. At the anterior end, part of the symphysis is preserved, forming a roughened, raised, and oval surface (Fig. 3.2f). When the symphyseal region is oriented vertically, the anterior region of the dentary, the canine, and the premolars lean buccally—a condition that has also been observed in *Didelphodon* (Fig. 3.2d; Fox and Naylor 2006). There is an ovoid mental foramen ventral to m1, and another below the posterior alveolus of p1; this condition differs from that in MOR 739 in both the position and number of foramina, which may be due to individual variation (although see above for comments on non-preservation of the dentary ventral to the p1 posterior alveolus; Fig. 3.2e).

The posterior half of a large canine alveolus is preserved. The p1 alveoli are ovoid, with the anterior one smaller and positioned slightly more buccally than the posterior one, as in the holotype of *E. browni* (Scott and Fox 2015). A slight diastema separates the posterior alveolus of p1 from the anterior alveolus of p2, as in MOR 739 (Fig. 3.2d).

The mesial root of p2 is preserved, but most of the crown and distal root are missing. The posterior alveolus of p2 is circular and is slightly larger than the anterior alveolus. The p3 alveoli are subequal in size and slightly larger than those of p2. The distal root of p3 and a fragment of the base of the crown are present, but the latter does not provide any coronal details. The mesial root of m1 is directly posterior to the distal root of p3, as in MOR 739 and other described specimens of *Eodelphis* (Fig. 3.2d; Clemens 1966).

The occlusal surfaces of m1–3 show substantial horizontal wear and exposed dentine, which prevent detailed description of the coronal morphology (Fig. 3.2d). The m4, in contrast, shows only slight apical wear on the trigonid cusps and along the paracristid and protocristid. The m4 protoconid is slightly taller than the paraconid, and the metaconid is the shortest and smallest of the trigonid cusps. These cusps form a more acute trigonid angle than what can be ascertained from the other molars. Some wear or damage on the talonid has made the individual cusps difficult to discern, although twinning of the entoconid and hypoconulid is evident (Fig. 3.2d). Overall, the minimal wear on m4 implies that this tooth erupted only shortly before death and the individual was a young adult. In contrast, the heavy wear on the m1–3 implies that this individual had a highly abrasive diet (Fox 1981) even before reaching dental maturity (eruption of m4). See Table 3.2 for dental measurements.

3.5.5 Remarks

The molar morphology (e.g., the small metaconid) of m2–m4 of MOR 739 and the m4 of TMDC TA2008.3.2, as well as the size of the molars and overall dentary morphology, support the referral of these specimens to the genus *Eodelphis*. Whereas molar morphology does not typically permit species-level identification of specimens of *Eodelphis*, premolar morphology,

especially that of p3, is more diagnostic (Scott and Fox 2015). Specifically, (i) the p3 crown is generally larger, more inflated, and less sectorial in *E. cutleri* than in *E. browni* (Fox 1981; Scott and Fox 2015); (ii) the roots of p2 and p3 are parallel and vertically oriented in *E. cutleri*, but ventrally divergent in *E. browni* (Clemens 1966); and (iii) the premolars are aligned and relatively uncrowded in *E. browni*, but crowded in *E. cutleri* (Clemens 1966; Clemens, pers. comm. 2017). Computed tomography (CT) scans reveal that TMDC TA2008.3.2 and MOR 739 have p2 and p3 alveoli or roots that are vertical and parallel—the condition ascribed to both *E. cutleri* and *Didelphodon* (3.13: Appendix 1; Clemens 1966). Both specimens described here have a small diastema between p1 and p2 (uncrowded), instead of having alveoli of successive premolars tightly packed (crowded) as seen in *E. cutleri* specimens (Clemens 1966: figure 36); additionally, the p1 and p2 alveoli of TMDC TA2008.3.2 are mainly anteroposteriorly aligned with the horizontal ramus, not strongly oblique to it as in the holotype of *E. cutleri* (Clemens 1966; Scott and Fox 2015). Following a thorough cleaning of the holotype of *E. browni* (AMNH 14169), Scott and Fox (2015) noted that the p1 anterior alveolus of this taxon is also oriented obliquely across the dentary, in-line with the trajectory of the tooth row (contra Clemens 1966). Further study of the intra- and interspecific variation of these premolar characters in *Eodelphis* is required to confirm their reliability in taxonomic diagnoses. The morphology of p3 remains as the most consistent way to discriminate between the species of *Eodelphis*. However, because the p3 is not preserved in our specimens, we rely on premolar alignment, tooth measurements, and robustness of the dentary to tentatively refer them to *E. browni*.

The morphological differences between TMDC TA2008.3.2 and MOR 739 are likely due to some combination of intraspecific variation, ontogenetic stage, sexual dimorphism, and differences in feeding behavior of the individuals represented. Both specimens represent dentally

mature individuals (fully erupted m4); however, the dentary and the teeth of MOR 739 are larger than those of TMDC TA2008.3.2 (Fig. 3.2; Tables 3.1 and 3.2), possibly reflecting sexual dimorphism, age, intraspecific variation, or some combination of those factors. Intriguingly, the molar wear pattern of MOR 739 runs counter to the interpretation that the larger individual is older. The m1–4 of MOR 739, the larger specimen, shows only minor apical wear and very little horizontal wear, in contrast to the pattern in TMDC TA2008.3.2, the smaller specimen. Extensive wear to m1–3 of TMDC TA2008.3.2 has formed a broad horizontal platform. The m4 is relatively unworn, suggesting that this tooth erupted only shortly before the individual died. This would imply that the individual was a young adult and that the extensive wear on m1–3 formed mostly during earlier ontogenetic stages. The m4 of MOR 739, the larger specimen, is relatively unworn as well, but no more so than its m1–3; thus, it probably represents an individual at a similar ontogenetic stage relative to TMDC TA2008.3.2. In their observations of dentulous dentary fragments of *Eodelphis*, Fox and Naylor (1995, 2006) inferred that juveniles of *Eodelphis* primarily employed molar shearing, and individuals shifted toward more crushing as wear leveled the cusps into broad platforms; this functional shift also implies a shift in diet. The molar wear patterns in our specimens imply that timing of this transition varies across individuals, such that some juveniles might have begun to emphasize crushing and hard-object feeding before dental maturity.

MOR 739 was found in deposits that include three stratigraphically distinct nesting horizons of the lambeosaurine dinosaur *Hypacrosaurus stebingeri* (Horner 1999). MOR 739 was found in the middle horizon of this stratigraphic sequence. Nest predation has been hypothesized as a factor in the extinction of non-avian dinosaurs (Benton 1990), and mammals have been proposed as possible predators of dinosaur eggs and hatchlings (e.g.,Wilson et al. 2016; Bois and

Mullin 2017). Bois and Mullin (2017) also suggested that Late Cretaceous mammals, including *Didelphodon vorax* (5.2 kg; Wilson et al. 2016), *Bubodens magnus* (5.25 kg; Wilson 1987), and *Vintana sertichi* (9 kg; Krause et al. 2014), were all large enough to prey upon dinosaur eggs and hatchlings (also see Wilson et al. 2016 for discussion of dinosaur predation by *D. vorax*). We speculate that *Eodelphis* also might have preyed upon or scavenged the hatchlings and eggs of *H. stebingeri*, given the carnivorous adaptations of its molars, in general, and the juxtaposition of MOR 739 and the lambeosaurine nests. Certainly, *Eodelphis* would have been capable of cracking eggs open with its jaws and teeth or possibly by other egg-breaking strategies employed by extant egg predators (see Bois and Mullin 2017).

3.6 BENDING FORCE ANALYSIS OF METATHERIAN DENTARIES

3.6.1 Methods

To further constrain the feeding behavior of stagodontids and other metatherians, we quantified the biomechanical properties of the dentary in a sample of taxa. Following the methods of Therrien (2005), we modeled the horizontal ramus of the dentary as an elliptical, solid beam (i.e., modeled as a cantilever in which the articular condyle is the fulcrum), and estimated the resistance of that beam to bending forces in the mediolateral and dorsoventral axes. A hollow beam model was not used because developing this model would require quantification of the cortical bone distribution in the horizontal ramus via CT scans of all specimens, and we did not have access to such data (Biknevicius and Ruff 1992a; Therrien et al. 2016). Although hollow beam models are more accurate in determining the exact values of bending strength along the dentary, Therrien et al. (2016) demonstrated that solid beam and hollow beam models are generally consistent in their depiction of relative patterns of change in bending force along the

dentary. Because we are interested in the relative patterns of bending force among taxa, the use of solid beam models is appropriate. The second moment of area, I, is a measure of the distribution of bone around a given axis (i.e., Ix = distribution of bone about the mediolateral axis; Iy = distribution of bone about the dorsoventral axis) and is used to calculate the bending force of the dentary about each axis (i.e., Zx = bending force about the mediolateral axis; Zy = bending force about the dorsoventral axis; see Therrien 2005 for a review). The maximum force that the horizontal ramus of the dentary can withstand at any point is calculated as a ratio of the bending force (Z) over the distance separating the point of interest from the articular condyle (L; the fulcrum). Relative bending force is calculated as a ratio of the bending force about the mediolateral axis (Zx) over the bending force about the dorsoventral axis (Zy) and reflects the overall shape of the horizontal ramus (Therrien 2005; Therrien et al. 2016).

We also assumed that the material properties of the dentary bone do not vary among these taxa and individuals (Biknevicius and Ruff 1992a; Therrien 2005; Therrien et al. 2016) and that the dentary is principally loaded in bending (Hylander 1979, 1981, 1984, 1985). We ignored other loading types at the symphyseal region because this region is more complex than the rest of the dentary, undergoes various types of stresses during the chewing cycle (Hylander 1981, 1984, 1985; Hylander et al. 1998; Ravosa and Hogue 2004), and is not preserved in most fossil specimens in our sample. As such, a dorsoventrally deep horizontal ramus is interpreted as better able to withstand forces in the dorsoventral axis, which largely result from bite forces exerted on food (Hylander 1979; Therrien 2005). A mediolaterally wide horizontal ramus is interpreted as better able to withstand forces in the mediolateral axis, which are associated with transverse or torsional stresses produced by struggling prey or feeding on hard-object foods (Hylander 1979; Therrien 2005). The ratio of the bending force in the dorsoventral direction to the bending force

in the mediolateral direction is a product of the cross-sectional shape of the dentary, and in large part reflects adaptation to load directions related to feeding habits (Biknevicius and Ruff 1992a; Therrien 2005; Therrien et al. 2016). Additionally, bending force of the dentary tends to scale with body size, such that larger bodied animals can generally withstand higher bending forces than smaller bodied animals can (Therrien 2005).

To construct force profiles of the dentaries, we took digital images of specimens using a Canon 5DS camera (Canon 100 mm Macro EF IS USM Lens), mounted on a high precision P-51 Cam-Lift system (Dun, Inc.), in standardized dorsal and lateral views with the same scale bar. We took measurements on those images and on published figures of specimens using ImageJ (Rasband 1997–2016). We measured dorsoventral depth and mediolateral width at six positions along the horizontal ramus, following the interdental gap scheme of Wilson et al. (2016; Fig. 3.3); this scheme was adapted from Therrien (2005) for use on metatherians, which in most cases have a different dental formula than eutherians. To gauge the effect of our approach versus direct measurement of the specimen, we compared measurements taken on a digital image of a cast (*D. coyi* TMP 84.64.1, cataloged as UCMP 152395) to those taken directly on the cast with digital calipers. The difference in measurements was minimal and did not affect the bending strength estimates for this specimen. To minimize error that could be introduced into our measurements by using published figures, we verified the orientation of specimens in the figures; if the orientation was oblique to the dorsal or lateral view, we did not include the image in our dataset. For stereopair images (seven included specimens), we selected a dorsal view image, if one had little to no lateral rotation. The resulting dataset is based on 22 specimens representing at least four extinct families (stagodontids, alphadontids, pediomyids, deltatheriids), two extant families (didelphids, dasyurids), eight genera, and at least 11 species of metatherians, including the

measurements of *D. vorax*, *Didelphis virginiana*, and *Sarcophilus harrisii* from Wilson et al. (2016; measurements in that study were taken on actual specimens using digital calipers). See 3.13: Appendix 2 for details of the dataset (Fox 1979, 1981; Montellano 1988; Cifelli 1993; Fox and Naylor 2006; Fox et al. 2007; Scott and Fox 2015; Wilson et al. 2016) and 3.13: Appendix 3 for bending strength calculations.

Whereas relative bending forces (dorsoventral vs. mediolateral) can be assessed without a known distance of the interdental gap position to the articular condyle (Therrien 2005), estimates of the bending forces in a specific axis (dorsoventral or mediolateral) require that measurement. Because of the incomplete nature of the fossil record, a relatively complete dentary with the condyle is rarely preserved. Among specimens of *Eodelphis* used in this study, only the holotype of *E. browni* (AMNH 14169) preserves the articular condyle. Thus, for many specimens we were only able to estimate relative bending forces. To provide provisional estimates of the dorsoventral and mediolateral bending forces of the dentary of *E. cutleri* (a taxon critical to this study), we modeled the condyle position of the most complete *E. cutleri* specimen in this study (NHMUK M11532), first using a specimen of *E. browni* with an articular condyle as the model and second using a specimen of *D. vorax* with a condyle. The modeled condyle position of *E. cutleri* was calculated as follows:

$$L_{E.cutleri,i} = \frac{tooth\ row\ length_{E.cutleri} * L_{E.browni \text{ or } D.vorax}}{tooth\ row\ length_{E.browni \text{ or } D.vorax}},$$

where $L_{E.\ cutleri}$ is the modeled distance of the articular condyle to each interdental gap for *E. cutleri*, *i* represents the interdental gap position, $L_{E.\ browni \text{ or } D.\ vorax}$ is the actual distance of the articular condyle to that interdental gap in *E. browni* or *D. vorax*, and tooth row length is length from the posterior part of the canine alveolus to the distal end of the m4. The resulting distances

from both models were then used in calculations, which constrain the dorsoventral and mediolateral bending forces for *E. cutleri*.

3.6.2 Data Availability Statement

All data generated or analyzed during this study are included in this published article [and its supplementary information files].

3.6.3 Results

The dorsoventral force profiles (Zx/L; Fig. 3.4a, d) of the metatherian dentaries studied here are characterized as either: (1) a relatively steep, positive slope posteriorly (*E. browni* and *E. cutleri*), in which bending force is low at the canine and increases toward the molars; (2) a positive slope posteriorly (*D. vorax* and *Didelphis virginiana*), in which bending force is not as low at the canine and gently increases toward the molars; or (3) an initially negative slope at the anterior region of the dentary that becomes positive posteriorly towards a maximum value behind m4 (*D. coyi* and *Sarcophilus harrisii*). These results are mostly consistent with the predictions that the dentary typically encounters the greatest forces, in either the dorsoventral or mediolateral directions, at the posteriormost position (post m4) due to the mechanical advantage of short output levers (i.e., the distance to the fulcrum, which is the articular condyle), and that larger bodied taxa can generate and withstand higher dorsoventral bending forces (i.e., bite forces) than smaller bodied taxa can (Fig. 3.4a, d). For example, dorsoventral bending force values increase with body size from *Alphadon halleyi* to *E. browni* to *Sarcophilus harrisii*.

The mediolateral force profiles (Zy/L; Fig. 3.4b, e) of the studied metatherian dentaries are characterized as either: (1) a relatively steep, positive slope posteriorly (*E. browni*), in which bending force of the dentary is low at the canine and increases toward the molars; (2) an initially negative slope at the anterior region of the dentary that becomes positive posteriorly toward a maximum value behind m4 (*D. coyi* and *E. cutleri*); or (3) a relatively flat profile (*D. vorax* and *Didelphis virginiana*) or a broad U-shaped curve (*Sarcophilus harrisii*), in which bending force of the dentary at the canine is subequal or greater than values at the molars. The relatively high Zy/L values anteriorly on the dentary of *E. cutleri* indicate that it was better able to withstand mediolateral forces at the canine (i.e., from torsional stresses or hard-object feeding) than the dentary of *E. browni* was (Fig. 3.4b).

The relative bending force (Zx/Zy) profiles (Figs. 3.4c, f and 3.5; 3.13: Appendix 4) are characterized as either: (1) a relatively steep, positive slope posteriorly, in which relative bending force at the molars is more than double the values at the anterior region of the dentary (*Turgidodon praesagus*, *Nanocuris improvida*, and *Didelphis virginiana*); a pattern that implies a sharp increase posteriorly in the capability of these dentaries to withstand dorsoventral loading (as reflected by horizontal ramus depth) relative to mediolateral loading (as reflected by horizontal ramus width); (2) a broad inverted U-shaped curve, in which relative bending force at the canine is subequal to 1.00, considerably less than values at the molars (*Kokopellia juddi*, *D. vorax*, *D. coyi*, *Sarcophilus harrisii*, and *E. cutleri*); a pattern that indicates the capability of some of these dentaries to withstand greater dorsoventral loading anteriorly (e.g., at the level of the crushing premolars and anterior molars) than would be expected by lever mechanics alone; or (3) a relatively flat line in which relative bending force at anterior region of the dentary is subequal to the values posteriorly at the molars (E. browni); a pattern that implies a consistent

ratio of dorsoventral to mediolateral force along the horizontal ramus length, with the advantage in the dorsoventral direction. Note that the profiles of one specimen of *D. coyi* (Fig. 3.4c) and one specimen of *D. vorax* (3.13: Appendix 4) differ from that of all other specimens of *Didelphodon* (Fig. 3.5b and 3.13: Appendix 4); the relative bending force of the dentary at the canine for these specimens is greater than 1.00, rather than less than 1.00. This discrepancy implies that these individuals were not as well adapted for resisting mediolateral loads anteriorly (e.g., hard-object feeding) as other individuals of *Didelphodon* that we sampled—a result that might reflect ontogenetic variation in feeding behavior (Peng et al. 2017).

?*Protolambda clemensi* and *Alphadon halleyi* are represented by incomplete dentaries from which relative bending force at the canine could not be calculated. *Alphadon halleyi* has a broad, inverted U-shaped profile from the premolars to the molars, like that of *Didelphodon* (Fig. 3.4c, f). ?*Protolambda clemensi* is unique in our sample in having a gentle negative slope posteriorly (i.e., Zx/Zy of the premolars > Zx/Zy of the molars), implying that the dentary becomes relatively wider posteriorly. Nevertheless, because both *Alphadon halleyi* and ?*Protolambda clemensi* have relative bending force values greater than 1.00, each had a greater capacity to withstand dorsoventral loads, rather than mediolateral loads, along the dentary (Fig. 3.5a).

As for the specimens of *Eodelphis* described in this paper, the relative force profile of MOR 739 (*Eodelphis* cf. *E. browni*, see above in Systematic Paleontology) differs from all other specimens of *Eodelphis* and other metatherian taxa included in this study (Fig. 3.5b). It forms a broad U-shaped curve, in which the relative bending force value at the p2–p3 position is high (i.e., the dentary is over 2.5 times deeper than it is wide at this point in the dentary). The relative bending force values along the entire horizontal ramus are between 2.00 and 2.50—greater than

the relative bending force values of other *Eodelphis* specimens (< 2.00). We interpret these anomalously high relative bending force values as being skewed toward dorsoventral loadings as a result of the post-mortem lateral compression experienced by MOR 739 (see Systematic Paleontology). For TMDC TA2008.3.2, despite gross morphological similarity to *E. browni*, it has a relative force profile of the dentary that is better aligned with that of *E. cutleri* (Figs. 3.4c and 3.5b). It forms a broad inverted U-shaped curve, in which relative bending force at the anterior region of the dentary is less than 1.00 (considerably lower than at the molars), as in *Didelphodon* and *E. cutleri*. Thus, anteriorly the dentary was better adapted to withstand forces in the mediolateral direction than in the dorsoventral direction. This profile could reflect intraspecific or ontogenetic variation, possibly resulting from a morphogenetic response to a more abrasive diet (recall the heavily worn m1–3; see Systematic Paleontology: Remarks).

3.7 THE EVOLUTION OF DUROPHAGY IN THE STAGODONTIDAE

In this study, we examined dentary shape with the goal of inferring function and feeding behavior in extinct metatherians, particularly stagodontids. Whereas considerable research has shown how tooth shape correlates with function and diet in extant mammals (e.g., see review by Evans 2013), the link between dentary shape, function, and diet has not been as well established. In fact, Ross and Iriarte-Diaz (2014) remarked that most studies have not shown a clear relationship between dentary morphology and diet (e.g., Brown 1997; Daeling and Grine 2006; Wright et al. 2009); notably, those studies were mainly focused on primates, a group in which the form-function relationship might be complicated by the transverse movement permitted at the jaw joint. In contrast, carnivorans, which have little to no transverse movement at their jaw joint, have a stronger correlation between dentary morphology and feeding behavior (Therrien 2005;

Therrien et al. 2016). The extant marsupials in our study, as well as the Cretaceous metatherians that are known by more complete fossils (e.g., *Didelphodon* and *Eodelphis*), have a jaw articulation that similarly did not permit much transverse movement (spool-shaped articular condyle that fits within a trough-like glenoid fossa). As such, we argue that inferring function and feeding behavior from the dentary morphology of these taxa should be tenable. Indeed, the bending force profiles of the two extant taxa in our sample, *Sarcophilus* and *Didelphis*, are consistent with their known feeding ecologies. Thus, we used the results of our bending force analysis to interpret functional and paleoecological changes within stagodontids and across Cretaceous metatherians.

3.7.1 Mediolateral Buttressing of the Dentary

The mediolateral force profile of *E. cutleri* is intermediate between that of *E. browni* and *D. vorax*. The mediolateral force values of the dentary of *E. browni* indicate that it was not able to withstand large torsional loads at the canine (Fig. 3.4b), such as those induced by struggling prey or by cracking hard objects; instead, it was better suited for dorsoventral loads, such as those incurred from large bite forces (Fig. 3.4c). Thus, *E. browni* likely preyed on insects and small vertebrates and was not capable of hard-object feeding (e.g., molluscs and bone). In contrast, the anterior region of the dentary of *E. cutleri* is mediolaterally buttressed (Fig. 3.4b). Although the associated mediolateral bending force values are less than those of *D. vorax*, they are subequal to those of *D. coyi* at both the canine and p2–p3 positions (the profiles then diverge from each other posteriorly). It follows that the dentary of *E. cutleri* could have withstood relatively large torsional loads anteriorly, but critically it lacked the mediolateral buttressing more posteriorly to withstand similar loads at the p3 crushing locus and the molars. In contrast,

both species of *Didelphodon* possessed this mediolateral buttressing posteriorly, suggesting a greater capacity for durophagous diets as compared to *E. cutleri*.

3.7.2 Dorsoventral Buttressing of the Dentary

The dorsoventral bending force values of the four stagodontid taxa included in this study are similar posteriorly (post m4 position) but differ anteriorly (Fig. 3.4a). In *E. browni*, which serves as a baseline, values are low anteriorly and steadily increase posteriorly as bite forces increase with decreasing distance to the fulcrum (i.e., the out lever becomes shorter). In comparison, the dorsoventral force profiles of *E. cutleri*, *D. coyi*, and *D. vorax* are increasingly shallower (in that order), reflecting increasingly greater bending force values at the anterior region of the dentary. This dorsoventral buttressing in the dentary of *E. cutleri* extends from the canine to the p2–p3 position; in *D. coyi*, it extends from the canine to the p3–m1 position; and in *D. vorax*, it extends the length of the dentary (canine to post m4 position) and the values are greater than in all other taxa. This pattern of dorsoventral buttressing implies that *E. cutleri* could have generated and withstood greater bite forces in the anterior region of the dentary than what *E. browni* could have, but less than what either species of *Didelphodon* could have. In *D. coyi*, the sharp uptick in dorsoventral bending force values at the p3–m1 position (and continuing more posteriorly in *D. vorax*) represents buttressing around the crushing locus, a feature that appears to be critical in hard-object feeding (Biknevicius and Ruff 1992a; Therrien 2005: figures. 6 and 7). Eodelphis cutleri lacks this degree of dorsoventral buttressing, despite having a p3 that appears well suited for crushing (i.e., large, bulbous).

Thus, the results of our bending strength analysis support the hypothesis that *E. cutleri* was better suited for durophagy than *E. browni*, but less so than either species of *Didelphodon*

(Fig. 3.4a–c). In *Didelphodon*, the dentary was buttressed anteriorly and at the crushing locus to withstand the high torsional stresses and the high bite forces involved in hard-object feeding. Hyaenids and *Sarcophilus harrisii* similarly exhibit both dorsoventral and mediolateral buttressing, suggesting that buttressing both axes might be required for mammals that consume a high percentage of hard-object foods (Therrien 2005: figure 7). In turn, the lack of buttressing at the crushing locus (and posteriorly) of *E. cutleri* implies that its capacity for durophagy was less than that of *Didelphodon*, an interpretation that is consistent with other morphological differences between these taxa; for example, the cross-sectional shape of the canine of *E. cutleri* is not as round as that of *Didelphodon*, indicating that it would not have been as resistant to torsional stresses incurred when deep bites contacted bone or when adjacent premolars crushed hard objects (Wilson et al. 2016; Fig. 3.6).

3.7.3 Vertical Position of the Articular Condyle of the Dentary

The relative vertical position (i.e., elevation) of the articular condyle differs between *Eodelphis* and *Didelphodon*, and likely affected their relative durophagous capabilities. The articular condyle of *Eodelphis* is only preserved in anatomical position in the holotype of *E. browni* (AMNH 14169), where the vertical position of the articular condyle is dorsal to the level of the tooth row. In *Didelphodon*, it is more ventral, closer to the level of the tooth row. Such a difference in condyle position could impact the mechanical advantage of dentary rotation around a mediolaterally oriented axis (i.e., the pitch; Grossnickle 2017; Grossnickle pers. comm. 2017, 2018). Specifically, if we assume that (i) the axis of pitch rotation of the dentary passed through or near the articular condyles, (ii) the typical bite point (i.e., out-lever distance) does not differ significantly, and (iii) the relative coronoid height did not change substantially between these

taxa, then the relatively lower articular condyle of *Didelphodon* would have moved the axis of rotation farther from the force vector of the temporalis muscle—most likely the largest and most powerful masticatory muscle of these mammals (Turnbull 1970)—and would have thus increased the length of the moment arm of the temporalis muscle and enabled the temporalis to generate more force during pitch (Maynard Smith and Savage 1959). Such mechanical advantage would have been beneficial for crushing hard objects, especially at more anterior regions of the dentary.

The vertical position of the articular condyle also modifies the effect of gape angle on bite force. Large gape angles increase the stretch of jaw muscles, and thereby decrease bite forces generated (Herring and Herring 1974; Lindauer et al. 1993; Turkawski and van Eijden 2001; Dumont and Herrel 2003; Santana 2016). However, a more ventral position of the articular condyle of the dentary would effectively result in a lower vertical position of the zygomatic arch and the pterygoid of the cranium, where the superficial masseter and the medial pterygoid muscles originate, respectively. It follows that those muscles, which insert on the angular process of the dentary, would experience less stretch during wide gapes, and, thus, associated bite forces would be less diminished (as long as the position of the angular process is unchanged; Herring and Herring 1974). Indeed, extant carnivores, which often require a wide gape for consumption of large prey, tend to have a vertically lower articular condyle and small angular process (Maynard Smith and Savage 1959; Grossnickle and Polly 2013). Accordingly, we infer that the more ventral position of the articular condyle of *Didelphodon* would have permitted it to maintain higher bite forces at wide gape angles to consume bigger, harder food items than *Eodelphis* could have.

3.7.4 Evolutionary Scenarios

Taken together, we propose two possible scenarios for the evolution o durophagy within the Stagodontidae (Fig. 3.6). If the sister-taxon relationship of *Didelphodon* and *Eodelphis* is valid (Scenario I), then our results would imply that a suite of morphological changes associated with durophagy evolved twice within stagodontids, once in *E. cutleri* and once in the most recent common ancestor of *D. coyi* and *D. vorax* (we exclude *D. padanicus* from the discussion because it was not included in our analyses). These changes would have included (1) development of an enlarged, inflated ultimate premolar (p3) for crushing; (2) the relative reduction of horizontal ramus length (manifest as crowded premolars; Clemens 1966), which resulted in increased mechanical advantage via shorter out levers; (3) mediolateral buttressing of the anterior region of the dentary to withstand greater torsional stresses; and (4) dorsoventral buttressing of the anterior region of the dentary to withstand greater bite forces anteriorly. Subsequently, the most recent common ancestor of *D. coyi* and *D. vorax* would have also evolved features 1–4 as well as three other features related to durophagy: (5) dorsoventral buttressing of the dentary posterior to premolars to withstand greater bite forces associated with the crushing locus (Clemens 1966; Therrien 2005; Wilson et al. 2016); (6) rounded cross-sectional shape of the canines for resisting stresses incurred from deep bites that contact bone or from adjacent premolars crushing objects (Wilson et al. 2016); and (7) a lower vertical position of the articular condyle to generate greater force during pitch rotation of the dentary. Scenario II is a more parsimonious alternative. Under this scenario, features 1–4 would have evolved only once in the most recent common ancestor of *E. cutleri* and *Didelphodon*; however, it would also imply that *Eodelphis* is paraphyletic, a topology that has not previously been supported by species-level cladistic analyses (Williamson et al. 2012, 2014). Features 5–7 would have then evolved in the most recent common ancestor of

D. coyi and *D. vorax*, as in Scenario I. Additional morphological data are needed to resolve the phylogenetic relationships among species of *Eodelphis* and *Didelphodon* (as well as *Fumodelphodon* and *Hoodootherium*) and to further test these scenarios for the evolution of durophagy within the Stagodontidae.

3.8 CONCLUSIONS

In this study, we described two new dentary specimens of *Eodelphis*, and applied beam theory to a sample of 22 metatherian dentaries, an oft-neglected source of morphological data. The resulting bending strength profiles of the dentaries enabled us to investigate variation in the biomechanical capabilities of stagodontids and other metatherians. Our results point to two possible scenarios for the evolution of durophagy in stagodontids, one which requires considerable parallel evolutionary change within *Eodelphis* and *Didelphodon*, and the other which requires fewer evolutionary changes but a reconsideration of the monophyly of *Eodelphis*. Additional data and analyses will be required to discriminate between these two scenarios.

More broadly, our study highlights bending strength analysis of dentaries as a tool for constraining dietary inferences of extinct mammals independent of dental shape analyses (e.g., Evans 2013). Results from its novel application to a broad sample of fossil metatherians echo previous studies that have shown Mesozoic mammals were more ecomorphologically diverse than previously thought (e.g., Luo 2007; Wilson et al. 2012; Grossnickle and Polly 2013; Chen and Wilson 2015; Grossnickle and Newham 2016; Wilson et al. 2016). By way of example, the relative force profile of the mid-Cretaceous basal metatherian Kokopellia juddi is unexpectedly similar to those of taxa with durophagous capabilities (*Didelphodon*, *E*, *cutleri*, and *Sarcophilus harrisii*; Fig. 3.5a; Wilson et al. 2016). The relative force profile of the Campanian pediomyid

?*Protolambda clemensi*, in contrast, is unlike all other metatherian taxa included in this study—suggesting that posterior region of the dentary, rather than the anterior region, is better suited to withstand mediolateral loads. Furthermore, the relative force profile of the Lancian deltatheridiid *Nanocuris improvida* implies that this taxon was able to withstand high torsional stresses at the symphysis—such as those induced by struggling prey—corroborating previous interpretations of its carnivorous lifestyle (Fox et al. 2007; Wilson and Riedel 2010). In sum, this study has shed light on a broad range of morphologies of the dentary among Cretaceous metatherians that at minimum hint at a correspondingly broad range of biomechanical capabilities and feeding ecologies among these taxa, and that further study is merited.

3.9 ACKNOWLEDGEMENTS

We thank the Museum of the Rockies (MOR), especially Dr. John Scannella, the University of California Museum of Paleontology (UCMP), especially Drs. Patricia Holroyd and William A. Clemens, and the Two Medicine Dinosaur Center Museum, especially Stacia Martineau and Cory Coverdell for access to specimens. We thank Dr. Sharlene Santana for access and use of the Santana Lab micro CT scanner, and Brody Hovatter for completing scans of these specimens. Funding for this research was provided by the National Science Foundation (NSF EAR SGP 1325674). We are grateful to members of the Wilson Lab (Dr. Stephanie Smith, Dr. Jonathan Calede, Dr. David DeMar, Jr., Lucas Weaver, and Brody Hovatter) for helpful comments and discussion concerning this manuscript. We also express our gratitude to Dr. David M. Grossnickle and one anonymous reviewer for their insightful comments and suggestions.

3.10 REFERENCES CITED

Benton MJ (1990) Scientific methodologies in collision: the history of the study of the extinction of the dinosaurs. Evol Biol 24:371–400

Biknevicius AR, Ruff CB (1992a) The structure of the mandibular corpus and its relationship to feeding behaviours in extant carnivorans. J Zool 228(3):479–507

Biknevicius AR, Ruff CB (1992b) Use of biplanar radiographs for estimating cross-sectional geometric properties of mandibles. Anat Rec 232(1):157–163

Binder WJ, Cervantes KS, Meachen JA (2016) Measures of relative dentary strength in Rancho La Brea *Smilodon fatalis* over time. PLoS One. https://doi.org/10.1371/journal.pone.0162270

Bois J, Mullin SJ (2017) Dinosaur nest ecology and predation during the Late Cretaceous: was there a relationship between Upper Cretaceous extinction and nesting behavior? Hist Biol. https://doi.org/10.1080/08912963.2016.1277423

Brown B (1997) Miocene hominoid mandibles: functional and phylogenetic perspectives. In: Begun DR, Ward CV, Rose MD (eds) Function, Phylogeny and Fossils: Miocene Hominoid Evolution and Adaptation. Plenum, New York, pp 153–171

Carneiro LM, Oliveira ÉV (2017) Systematic affinities of the extinct metatherian *Eobrasilia coutoi* Simpson, 1947, a South American early Eocene Stagodontidae: implications for "Eobrasiliinae." Rev Brasil Paleontol 20(3):355–372

Chen M, Wilson GP (2015) A multivariate approach to infer locomotor modes in Mesozoic mammals. Paleobiology 41(2):280–312

Cifelli RL (1993) Early Cretaceous mammals from North America and the evolution of marsupial dental characters. Proc Natl Acad Sci USA 90:9413–9316

Cifelli RL, Eaton JG (1987) Marsupial from the earliest Late Cretaceous of the western U.S. Nature 325:520–522

Cifelli RL, Eberle JJ, Lofgren DL, Lillegraven JA, Clemens WA (2004) Mammalian biochronology of the latest Cretaceous. In: Woodburne MO (ed) Late Cretaceous and Cenozoic Mammals of North America: Biostratigraphy and Geochronology. Columbia University Press, New York, pp 21–42

Clemens WA (1966) Fossil mammals of the type Lance Formation, Wyoming. Part II. Marsupialia. Univ Calif Publ Geol Sci 62:1–122

Clemens WA (1968) A mandible of Didelphodon vorax (Marsupialia, Mammalia). Los Angeles County Mus Nat Hist Contrib Sci 133: 1–11

Cohen JE (2017) Earliest divergence of stagodontid (Mammalia: Marsupialiformes) feeding strategies from the Late Cretaceous (Turonian) of North America. J Mammal Evol. https://doi.org/10.1007/s10914-017-9382-0

Crompton AW, Kielan-Jaworowska Z (1978) Molar structure and occlusion in Cretaceous therian mammals. In: Butler PM, Joysey KA (eds) Studies on the Development, Structure, and Function of Teeth. Academic Press, New York, pp 249–287

Daeling DJ, Grine FE (2006) Mandibular biomechanics and the paleontological evidence for the evolution of human diet. In: Ungar PS (ed) Evolution of the Human Diet: The Known, the Unknown, and the Unknowable. Oxford University Press, Cary, pp 77–105

DeMar DG Jr, Breithaupt BH (2006) The nonmammalian vertebrate microfossil assemblages of the Mesaverde Formation (Upper Cretaceous, Campanian) of the Wind River and Bighorn basins, Wyoming. Bull New Mex Mus Nat Hist Sci 35:33–53

Drees NM, Mhyr DW (1981) The Upper Cretaceous Milk River and Lea Park formations in southeastern Alberta. Bull Canadian Petroleum Geol 29(1):42–74

Dumont ER, Herrel A (2003) The effects of gape angle and bite point on bite force in bats. J Exp Biol 206:2117–2123

Eaton JG, Cifelli RL (1988) Preliminary report on Late Cretaceous mammals of the Kaiparowits Plateau, southern Utah. Contrib Geol Univ Wyo 26(2):45–55

Evans AR (2013) Shape descriptors as ecometrics in dental ecology. Hystrix, Ital J Mammal. https://doi.org/10.4404/hystrix-24.1-6363

Fiorillo AR (1989) The vertebrate fauna from the Judith River Formation (Late Cretaceous) of Wheatland and Golden Valley counties, Montana. Mosasaur 4:127–142

Fox RC (1971) Marsupial mammals from the early Campanian Milk River Formation, Alberta, Canada. In: Kermack DM, Kermack KA (eds) Early Mammals. Suppl. No. 1, Zool J Linn Soc 50:145–164

Fox RC (1979) Mammals from the Upper Cretaceous Oldman Formation, Alberta. Can J Earth Sci 16:91–102

Fox RC (1981) Mammals form the Upper Cretaceous Oldman Formation. V. *Eodelphis* Matthew, and the evolution of Stagodontidae (Marsupialia). Can J Earth Sci 18:350–365

Fox RC, Naylor BG (1986) A new species of *Didelphodon* Marsh (Marsupialia) from the Upper Cretaceous of Alberta, Canada: paleobiology and phylogeny. Neues Jahrbuch für Geologie und Paläontologie Abhandlungen 172:357–380

Fox RC, Naylor BG (1995) The relationships of the Stagodontidae, primitive North American Late Cretaceous mammals. In: Sun A, Wang Y (eds) Sixth Symposium on Mesozoic Terrestrial Ecosystems and Biota. China Ocean Press, Beijing, pp 247–250

Fox RC, Naylor BG (2006) Stagodontid marsupials from the Late Cretaceous of Canada and their systematic and functional implications. Acta Palaeontol Pol 51(1):13–36

Fox RC, Scott C, Bryant HN (2007) A new, unusual therian mammal form the Upper Cretaceous of Saskatchewan, Canada. Cret Res 28: 821–829

Gill PG, Purnell MA, Crumpton N, Robson Brown K, Gostling NJ, Stampanoni M, Rayfield EM (2014) Dietary specializations and diversity in feeding ecology of the earliest stem mammals. Nature. https://doi.org/10.1038/nature13622

Grossnickle DM (2017) The evolutionary origin of jaw yaw in mammals. Sci Reports. https://doi.org/10.1038/srep45094

Grossnickle DM, Polly PD (2013) Mammal disparity decreases during the Cretaceous angiosperm radiation. Proc R Soc B 280:20132110. https://doi.org/10.1098/rspb.2013.2110

Grossnickle DM, Newham E (2016) Therian mammals experience an ecomorphological radiation during the Late Cretaceous and selective extinction at the K–Pg boundary. Proc R Soc B 283:20160256. https://doi.org/10.1098/rspb.2016.0256

Herring SW, Herring SE (1974) The superficial masseter and gape in mammals. Am Nat 108(962):561–576

Horner J (1999) Egg clutches and embryos of two hadrosaurian dinosaurs. J Vertebr Paleontol 19(4):607–611

Hylander WL (1979) The functional significance of primate mandibular form. J Morphol 160:223–240

Hylander WL (1981) Patterns of stress and strain in the macaque mandible. In: Carlson DS (ed) Craniofacial Biology, Monograph 10, Craniofacial Growth Series: Center for Human Growth and Development. University of Michigan, Ann Arbor, pp 1–35

Hylander WL (1984) Stress and strain in the mandibular symphysis of primates: a test of competing hypotheses. Am J Phys Anthropol 64: 1–46

Hylander WL (1985) Mandibular function and biomechanical stress and scaling. Am Zool 25:315–330

Hylander WL, Ravosa MJ, Ross CF, Johnson KR (1998) Mandibular corpus strain in primates: further evidence for a functional link between symphyseal fusion and jaw-adductor muscle force. Am J Phys Anthropol 107:257–271

Jernvall J, Hunter JP, Fortelius M (1996) Molar tooth diversity, disparity, and ecology in Cenozoic ungulate radiations. Science 274(5292): 1489–1492

Kelly TS (2014) Preliminary report on the mammals from Lane's Little Jaw Site Quarry: a latest Cretaceous (earliest Puercan?) local fauna, Hell Creek Formation, southeastern Montana. Paludicola 10(1):50–91

Kielan-Jaworowska Z-X, Cifelli RL, Luo ZX (2004) Mammals from the Age of Dinosaurs: Origins, Evolution, and Structure. Columbia University Press, New York

Krause DW, Hoffmann S, Wible JR, Kirk EC, Schultz JR, von Koenigswald W, Groenke JR, Rossie JB, O'Connor PM, Seiffert ER, Dumont ER, Holloway WL, Rogers RR, Rahantarisoa LJ, Kemp AD, Andriamialison H (2014) First cranial remains of a gondwanatherian mammal reveal remarkable mosaicism. Nature 515:512–517

Lindauer SJ, Gay T, Rendell J (1993) Effect of jaw opening on masticatory muscle EMG-force characteristics. J Dental Res 72:51–55

Luo Z-X (2007) Transformation and diversification in early mammal evolution. Nature 50:1011–1019

Matthew WD (1916) A marsupial from the Belly River Cretaceous. With critical observations upon the affinities of the Cretaceous mammals. Bull Am Mus Nat Hist 35:477–500

Maynard Smith J, Savage RJG (1959) The mechanics of mammalian jaws. School Sci Rev 40:289–301

Montellano M (1988) *Alphadon halleyi* (Didelphidae, Marsupialia) from the Two Medicine Formation (Late Cretaceous, Judithian) of Montana. J Vertebr Paleontol 8(4):378–382

Montellano M (1992) Mammalian fauna of the Judith River Formation (Late Cretaceous, Judithian), northcentral Montana. Univ Calif Publ Geol Sci 136:1–115

Peng A, Toews N, Wilson GP (2017) An ontogenetic investigation of a Cretaceous North American mammal, *Didelphodon vorax* (Metatheria: Marsupialiformes: Stagodontidae), through quantitative and descriptive analysis of the dentary. Geol Soc Am Annual Meeting Abstracts with Programs 49(6). https://doi.org/10.1130/abs/2017AM-300648

Peng J, Russell AP (2001) Vertebrate microsite assemblages (exclusive of mammals) from the Foremost and Oldman formations of the Judith River Group (Campanian) of southeastern Alberta: an illustrated guide. Provincial Museum of Alberta, Nat Hist Occas Pap 25:1–54

Rasband WS (1997–2016) ImageJ, U. S. National Institutes of Health, Bethesda, Maryland, https://imagej.nih.gov/ij/

Ravosa MJ, Hogue AS (2004) Function and fusion of the mandibular symphysis in mammals: a comparative and experimental perspective. In: Ross CF, Kay RF (eds) Anthropoid Origins: New Visions. Spinger Science+Business Media, LLC, New York, pp 413–462

Rigby JK, Wolberg DL (1987) The therian mammalian fauna (Campanian) of Quarry 1, Fossil Forest study area, San Juan Basin, New Mexico. Geol Soc Am Spec Pap 209:51–79

Ross CF, Iriarte-Diaz J (2014) What does feeding system morphology tell us about feeding? Evol Anthropol 23:105–120

Rougier GW, Davis BM, Novacek MJ (2015) A deltatheroidan mammal from the Upper Cretaceous Baynshiree Formation, eastern Mongolia. Cret Res 52:167–177

Rougier GW, Wible JR, Novacek MJ (1998) Implications of Deltatheridium specimens for early marsupial history. Nature 396: 459–463

Rougier GW, Wible JR, Novacek MJ (2004) New specimen of *Deltatheroides cretacicus* (Metatheria, Deltatheroida) from the Late Cretaceous of Mongolia. Bull Carnegie Mus Nat Hist 36: 245–266

Sahni A (1972) The vertebrate fauna of the Judith River Formation, Montana. Bull Am Mus Nat Hist 147:321–412

Sánchez-Villagra MR (2013) Why are there fewer marsupials than placentals? On the relevance of geography and physiology to evolutionary patterns of mammalian diversity and disparity. J Mammal Evol 20:279–290

Santana SE (2016) Quantifying the effect of gape and morphology on bite force: biomechanical modelling and in vivo measurements in bats. Funct Ecol 30:557–565

Scott CS, Fox RC (2015) Review of Stagodontidae (Mammalia, Marsupialia) from the Judithian (Late Cretaceous) Belly River Group of southeastern Alberta, Canada. Can J Earth Sci 52:682–695

Sloan RE, Russell LS (1974) Mammals from the St. Mary River Formation (Cretaceous) of southwestern Alberta. Life Sci Contrib R Ont Mus 95:1–21

Therrien F (2005) Mandibular force profiles of extant carnivorans and implications for the feeding behavior of extinct predators. J Zool 267:249–270

Therrien F, Quinney A, Tanaka K, Zelenitsky DA (2016) Accuracy of mandibular force profiles for bite force estimation and feeding behavior reconstruction in extant and extinct carnivorans. J Exp Biol 291:3738–3749

Turkawski SJJ, van Eijden T (2001) Mechanical properties of single motor units in the rabbit masseter muscle as a function of jaw position. Exp Brain Res 138:153–162

Turnbull WD (1970) Mammalian masticatory apparatus. Fieldiana: Geol 18:149–156

Williamson TE, Brusatte SL, Carr TD,Weil A, Standhardt BR (2012) The phylogeny and evolution of Cretaceous-Paleogene metatherians: cladistic analysis and description of new early Palaeocene specimens form the Nacimiento Formation, New Mexico. J Sys Palaeontol 10(4):635–651

Williamson TE, Brusatte SL, Wilson GP (2014) The origin and early evolution of metatherian mammals: the Cretaceous record. ZooKeys 465:1–76

Wilson GP (2013) Mammals across the K/Pg boundary in northeastern Montana, U.S.A.: dental morphology and body-size patterns reveal extinction selectivity and immigrant-fueled ecospace filling. Paleobiology 39(3):429–469

Wilson GP, Dechesne M, Anderson IR (2010) New latest Cretaceous mammals from northeastern Colorado with biochronologic and biogeographic implications. J Vertebr Paleontol 30(2):499–520

Wilson GP, Ekdale EG, Hoganson JW, Calede JJ, Vander Linden A (2016) A large carnivorous mammal from the Late Cretaceous and the North American origin of marsupials. Nat Comm. https://doi.org/10.1038/ncomms13734

Wilson GP, Evans AR, Corfe IJ, Smits PD, Fortelius M, Jernvall, J (2012) Adaptive radiation of multituberculate mammals before the extinction of dinosaurs. Nature 483:457–460

Wilson GP, Riedel JA (2010) New specimen reveals deltatheroidan affinities of the North American Late Cretaceous mammal *Nanocuris*. J Vertebr Paleontol 30(3):872–884

Wilson RW (1987) Late Cretaceous (Fox Hills) multituberculates from the Red Owl local fauna of western South Dakota. Dakoterra 3:118–122

Wright BW, Wright KA, Chalk J, Verderane MP, Fragaszy D, Visalberghi E, Izar P, Ottoni EB, Constantino P, Vinyard C (2009) Fallback foraging as a way of life: using dietary toughness to compare the fallback signal among capuchins and implications for interpreting morphological variation. Am J Phys Anthropol 140:687–699

3.11 FIGURES

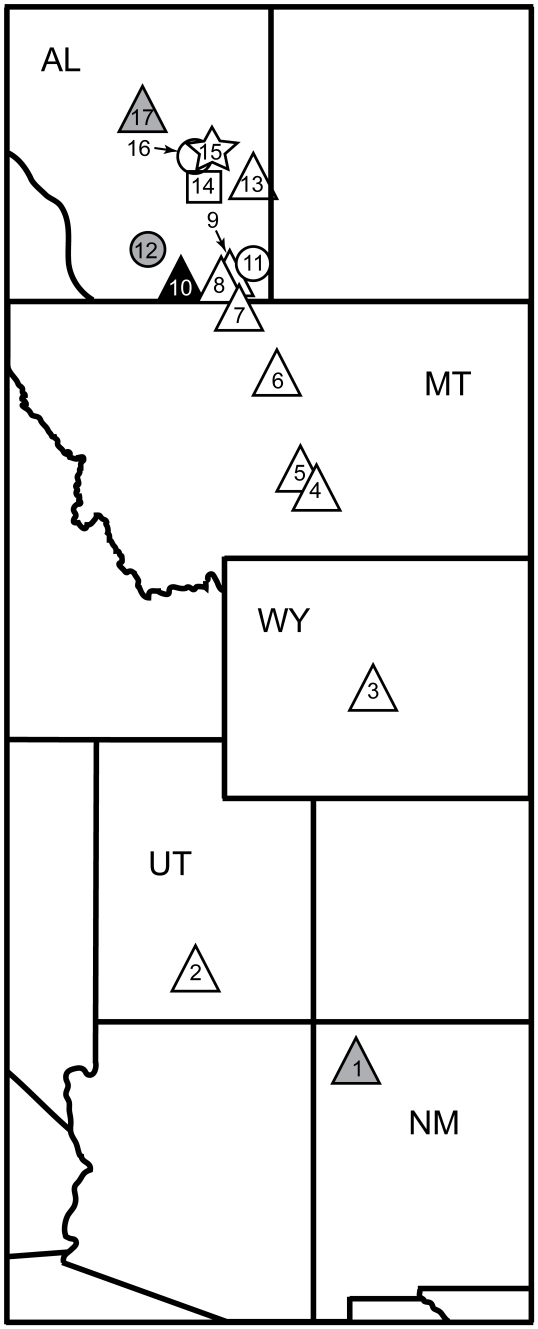

Figure 3.1 Map of *Eodelphis* fossil localities in western United States and Canada. Circles for *E. cutleri*, squares for *E. browni*, the star for both *E. cutleri* and *E. browni*, and triangles for

Eodelphis sp. 1 = Fossil Forest Quarry 1, Kirtland Fm., New Mexico; 2 = OMNH V5, Kaiparowits Fm., Utah; 3 = Fales Rocks/Barwin Quarry, Mesaverde Fm., Wyoming; 4 = Top Cat Quarry, Judith River Fm., Montana; 5 = Hidden Valley Quarry, Judith River Fm., Montana; 6 = Clambank Hollow Quarry, Judith River Fm., Montana; 7 = Coke's Microsite (UCMP V-82165), Makela's French 1 (UCMP V-77083), Put's Plunder (UCMP V-81234), and Makela's French 2 (UCMP V-77084), Judith River Fm., Montana; 8 = Hoodoo Site (RTMP L1126), Oldman Fm., Alberta; 9 = Pinhorn Range #1 (RTMP L1125), Foremost Fm., Alberta; 10 = Verdigris Coulee (UAMR-6 and UA-MR-8), Milk River Fm., Alberta; 11 = Manyberries, Oldman Fm., Alberta; 12 = Scabby Butte Site 3, St. Mary Fm., Alberta; 13 = Dinosaur Provincial Park, Oldman Fm., Alberta; 14 = Sand Creek (middle fork, AMNH), Dinosaur Park Fm., Alberta; 15 = 6.4 m below mouth of Berry Creek (Little Sand Creek), Oldman Fm., Alberta; 16 = Onetree Creek, Oldman Fm., Alberta; 17 = 7 miles northwest of Rumsey, Edmonton Group, Alberta. Locality marker colors correspond to NALMA: black = Aquilan, white = Judithian, and gray = "Edmontonian" (Fox 1971; Sahni 1972; Rigby and Wolberg 1987; Eaton and Cifelli 1988; Fiorillo 1989; Montellano 1992; Peng and Russell 2001; DeMar and Breithaupt 2006; Scott and Fox 2015)

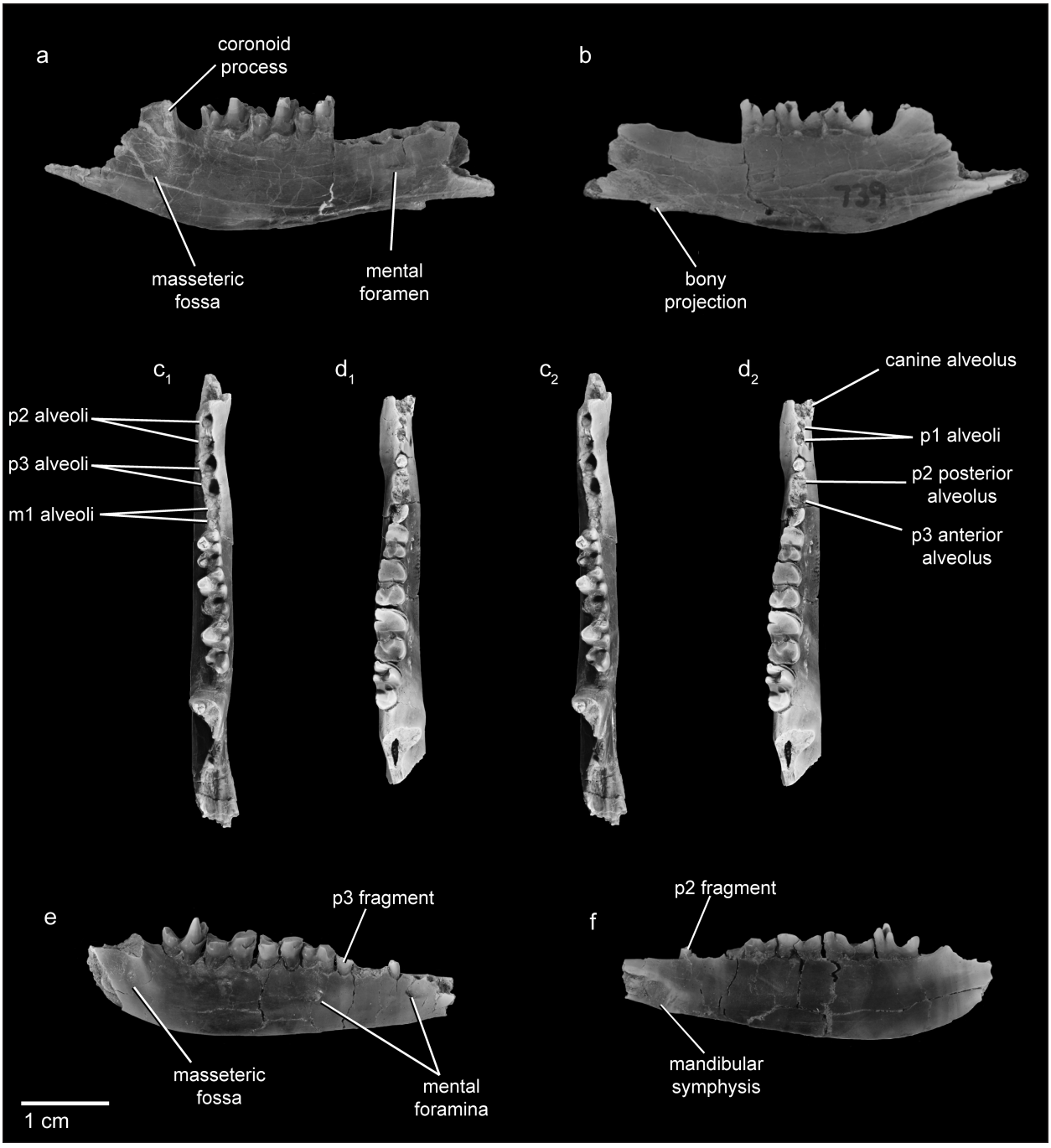

Figure 3.2 MOR 739, an incomplete right dentary of *Eodelphis* cf. *E. browni* (**a–c$_{1–2}$**) TMDC TA2008.3.2, an incomplete right dentary of *Eodelphis* cf. *E. browni*, specimen (**d$_{1–2–f}$**). **a**, **e** buccal views; **b**, **f** lingual views; **c$_{1–2}$**, **d$_{1–2}$** stereo occlusal views

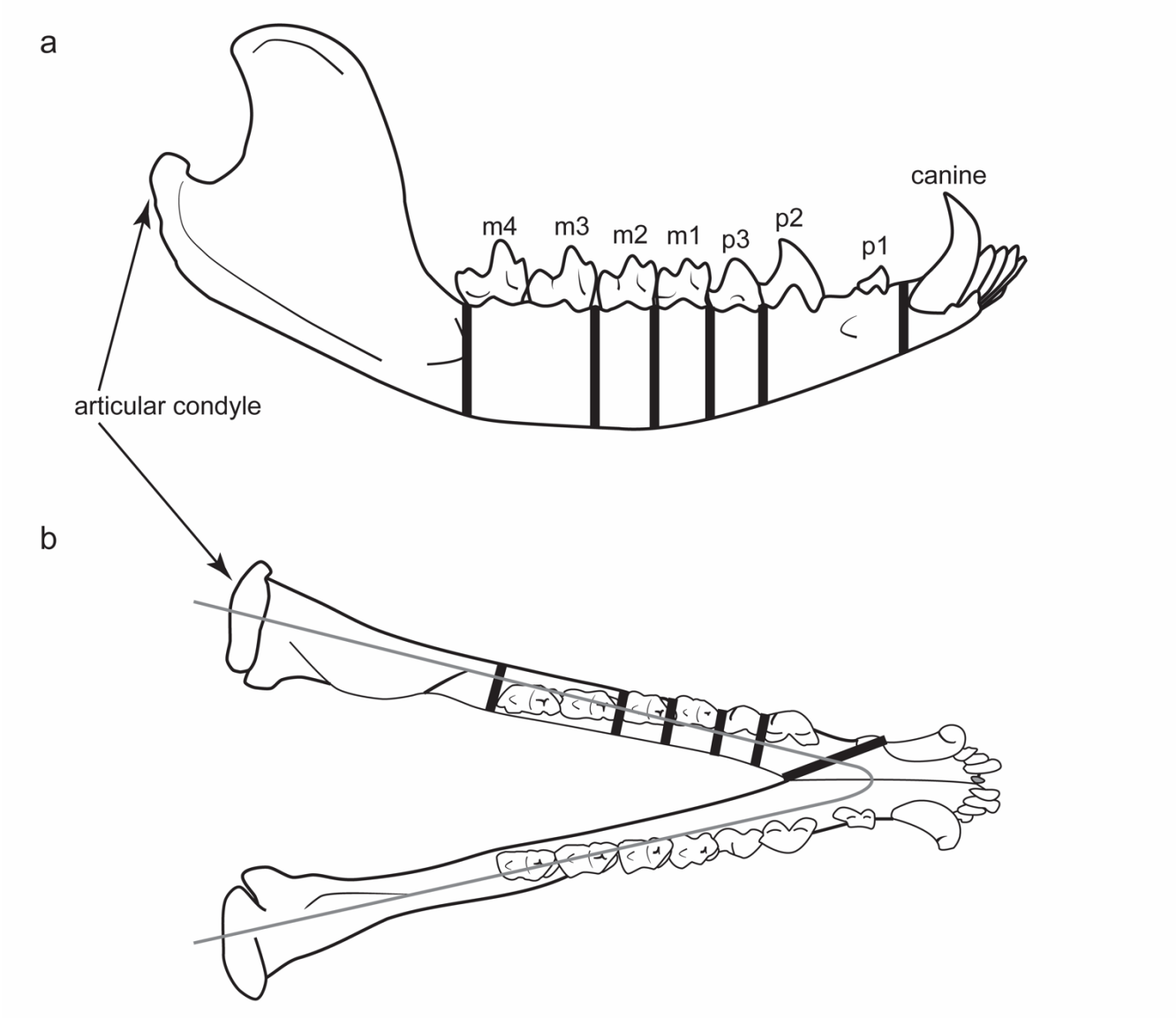

Figure 3.3 Dorsoventral (**a**) and mediolateral (**b**) measurement scheme for bending strength analysis of metatherians dentaries following Therrien (2005) and Wilson et al. (2016). Measurements (thick lines) were taken at interdental gaps (canine, p2-p3, p3-m1, m1-m2, m2-m3, post m4) and perpendicular to the central axis of the dentary (gray line), except for the

canine. The measurement at the canine was taken from the posterolingual aspect of the symphysis to the posterobuccal margin of the canine alveolus (Therrien 2005; Therrien et al. 2016). Specimen figured is UWBM 6640 (*Didelphis virginiana*)

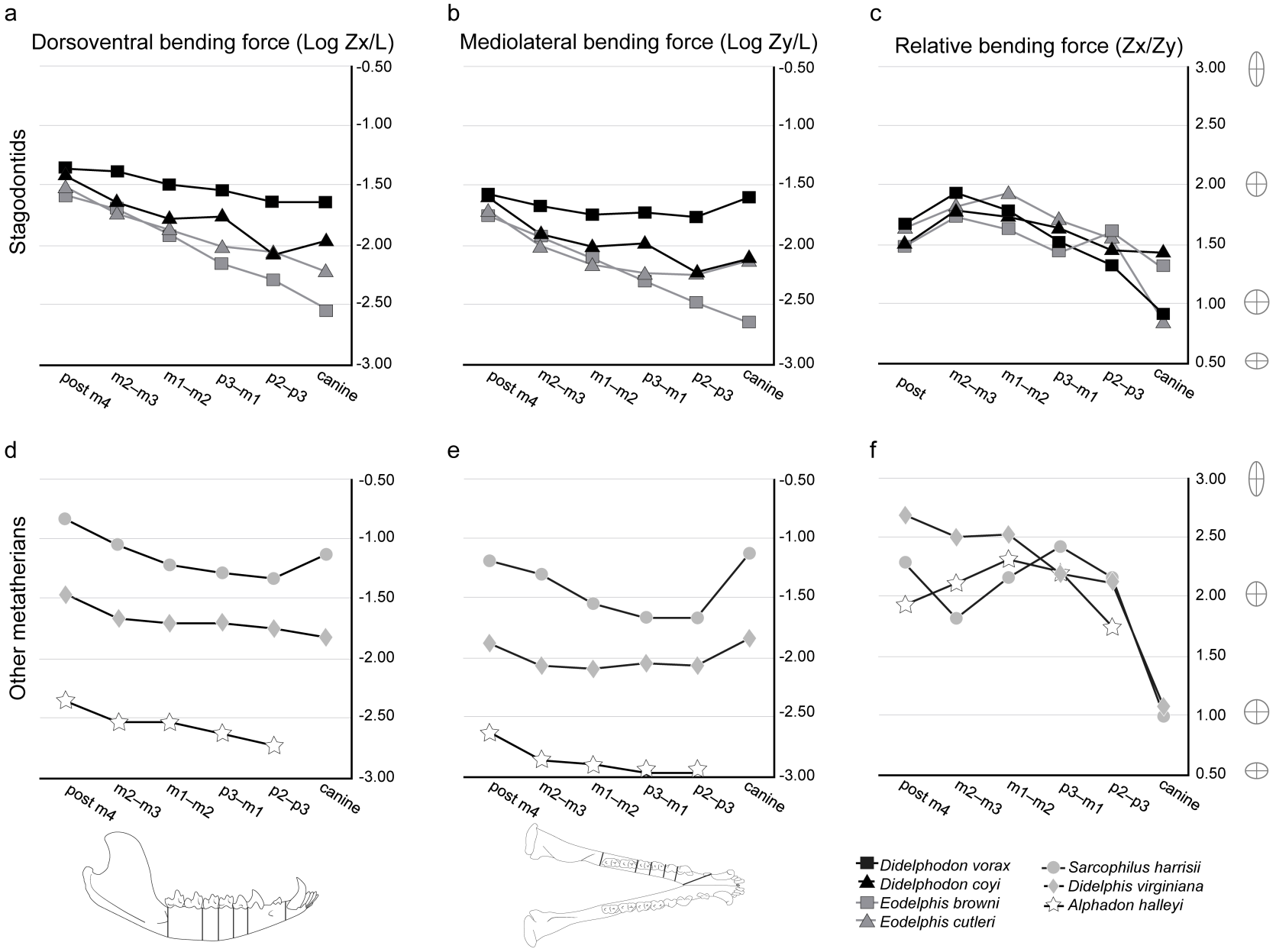
a
Dorsoventral bending force (Log Zx/L)
Stagodontids
b
Mediolateral bending force (Log Zy/L)
c
Relative bending force (Zx/Zy)
d
Other metatherians
e
f
post m4
post
m2–m3
m1–m2
p3–m1
p2–p3
canine
-0.50
-1.00
-1.50
-2.00
-2.50
-3.00
3.00
2.50
2.00
1.50
1.00
0.50
Didelphodon vorax
Didelphodon coyi
Eodelphis browni
Eodelphis cutleri
Sarcophilus harrisii
Didelphis virginiana
Alphadon halleyi

Figure 3.4 Dorsoventral (**a**, **d**), mediolateral (**b**, e), and relative (**c**, **f**) bending force profiles of metatherian dentaries. Dentary cross-sections that correspond with relative bending force values are plotted in c and **f** (gray ovals with dorsoventral and mediolateral axes). **a–c**, stagodontid force profiles (black squares = *Didelphodon vorax* UWBM 102139; black triangles = *Didelphodon coyi* TMP 84.64.1; dark gray squares = *Eodelphis browni* AMNH14169; dark gray triangles = *Eodelphis cutleri* NHMUK M11532 in **c**). In **a** and **b**, plotted values for *E. cutleri* are based on the *E. browni* model (see Methods section; the *D. vorax* model resulted in a similar profile). **d–f**, other metatherian force profiles (light gray circles = extant *Sarcophilus harrisii* UWBM 20671; light gray diamonds = extant *Didelphis virginiana* UWBM 12555; white stars = *Alphadon halleyi* MOR 250). Zx = section modulus or bending strength about the mediolateral axis; Zy = section modulus or bending strength about the dorsoventral axis; L = distance from the articular condyle (fulcrum of the cantilever) to each studied interdental gap (Therrien 2005)

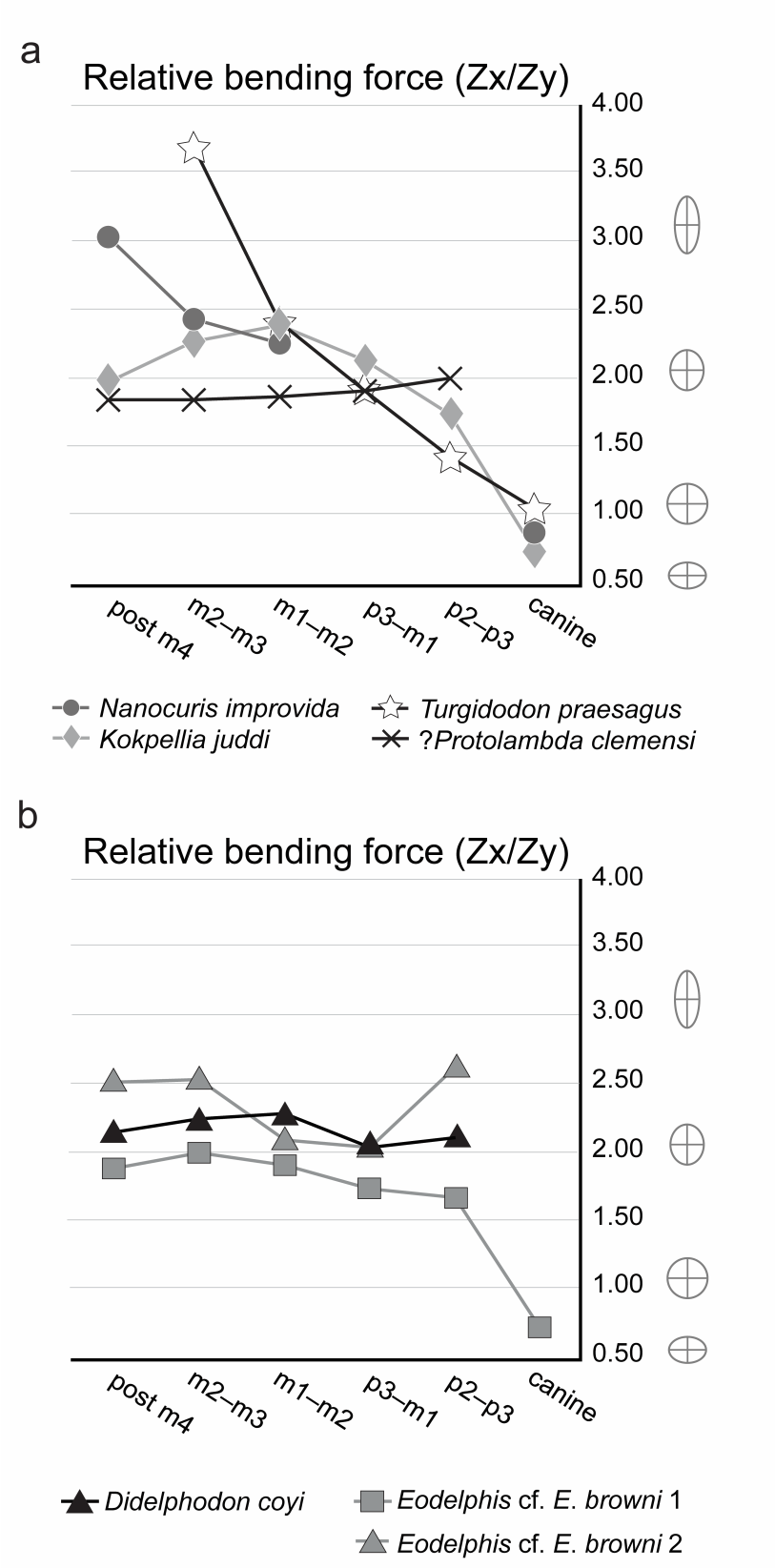
a
Relative bending force (Zx/Zy)
4.00
3.50
3.00
2.50
2.00
1.50
1.00
0.50
post m4
m2–m3
m1–m2
p3–m1
p2–p3
canine
Nanocuris improvida
Turgidodon praesagus
Kokpellia juddi
?Protolambda clemensi
b
Relative bending force (Zx/Zy)
4.00
3.50
3.00
2.50
2.00
1.50
1.00
0.50
post m4
m2–m3
m1–m2
p3–m1
p2–p3
canine
Didelphodon coyi
Eodelphis cf. E. browni 1
Eodelphis cf. E. browni 2

Figure 3.5 Relative bending force profiles of additional metatherian dentaries. **a** non-stagodontid metatherians (gray circles = *Nanocuris improvida* RSM P2523.260; light gray diamonds = *Kokopellia juddi* OMNH 26361; white stars = *Turgidodon praesagus* UALVP 670; black Xs =?*Protolambda clemensi* UALVP 14810) and **b** stagodontids (black triangles = *Didelphodon coyi* TMP90.12.29; gray squares = *Eodelphis* cf. *E. browni* TMDC TA2008.3.2; gray triangles = *Eodelphis* cf. *E. browni* MOR 739). Dentary cross-sections that correspond with relative bending force values are plotted in **a** and **b** (gray ovals with dorsoventral and mediolateral axes)

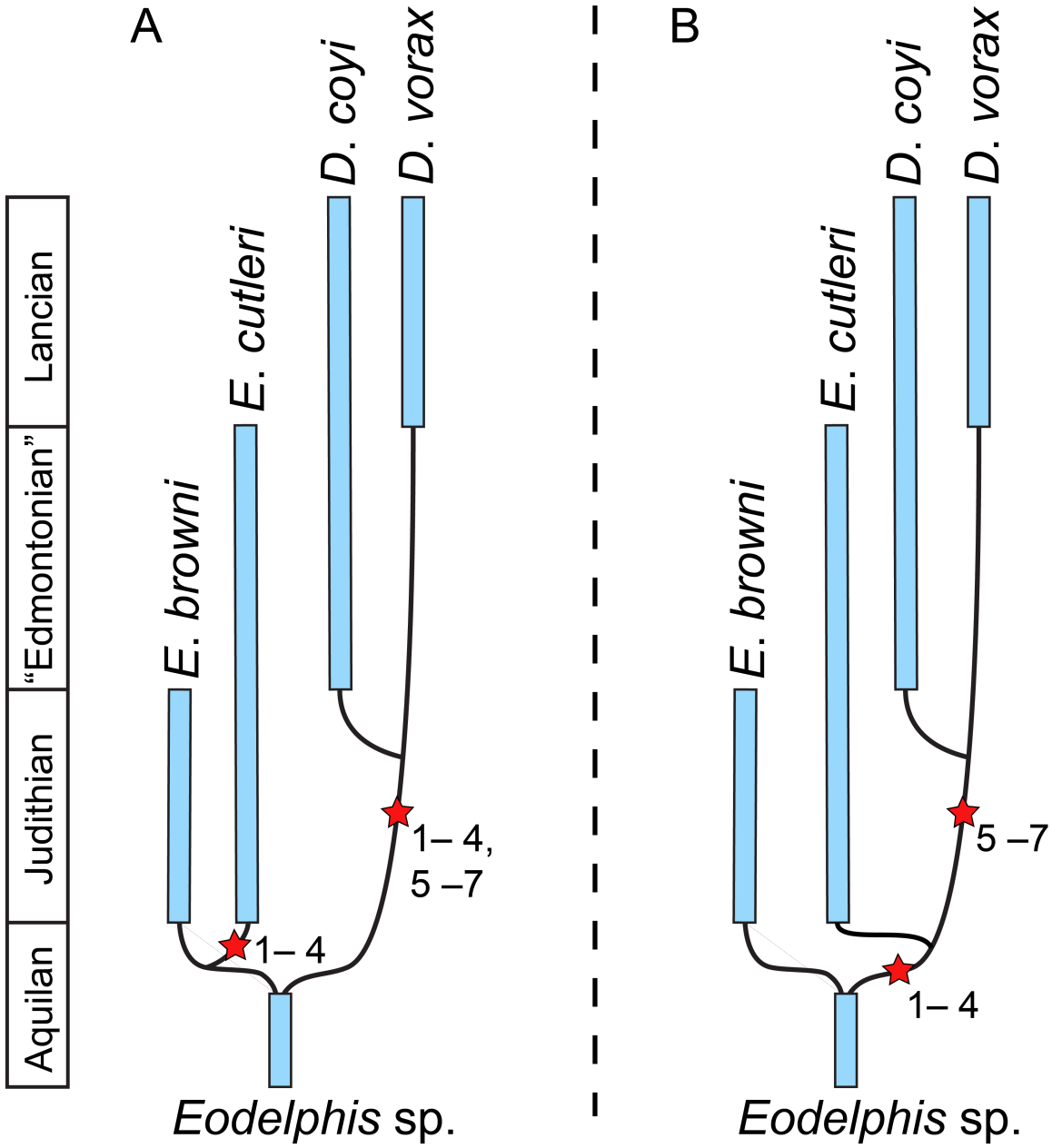

Figure 3.6 Possible scenarios for the evolution of durophagy in the Stagodontidae. In Scenario I, the evolution of durophagy traits is mapped, using parsimony, on the accepted tree of stagodontids (Clemens 1966; Fox and Naylor 1986, 2006; Scott and Fox 2015). In Scenario II, the evolution of durophagy traits is mapped on a tree that was constructed to minimize independent the evolution of these traits in stagodontids. The morphological traits are: 1 = an

enlarged, convex ultimate premolar (p3) for crushing; 2 = reduced length of the horizontal ramus (manifest as crowded premolars), resulting in increased mechanical advantage via shorter out levers; 3 =mediolateral buttressing of the anterior region of the dentary capable of withstanding greater torsional stresses; 4 = dorsoventral buttressing of the anterior region of the dentary capable of withstanding greater bite forces anteriorly; 5 = dorsoventral buttressing of the dentary posterior to premolars capable of withstanding greater bite forces associated with the crushing locus; 6 = rounded cross-sectional shape of the canines capable of withstanding stresses incurred from deep bites that contact hard objects such as bone or from adjacent premolars crushing objects; and 7 = lower position of the articular condyle relative to the tooth row. Gray bars represent the temporal range of fossil occurrences for each taxon. Black stars represent the evolution of the numbered morphological traits

3.12 TABLES

Table 3.1 Measurements of lower premolar alveoli of *Eodelphis* cf. *E. browni*. Abbreviations: ant = anterior alveolus; L = length; post = posterior alveolus; W = width. All measurements in millimeters (mm)

	p1 alveoli		p2 alveoli		p3 alveoli	
	ant.	post.	ant.	post.	ant.	post.
MOR 739						
L	-	-	1.47	1.54	1.95	2.09
W	-	-	1.23	1.25	1.69	1.61
TMDC TA2008.3.2						
L	0.96	0.97	1.57	1.63	1.55	1.71
W	0.79	0.70	1.35	1.44	1.76	2.04

Table 3.2 Measurements of lower molars of *Eodelphis* cf. *E. browni*. Abbreviations: DW = distal width; L = length; MW = mesial width. All measurements in millimeters (mm)

	m1	m2	m3	m4
MOR 739				
L	-	4.21	5.22	6.27
MW	-	2.72	3.06	3.25
DW	-	2.80	3.00	2.68
TMDC TA2008.3.2				
L	3.90	5.00	5.64	5.10
MW	2.60	2.95	3.20	2.93
DW	2.52	3.17	3.43	2.33

3.13 APPENDICES

Appendix 1: Computed Tomography of *Eodelphis* Specimens

Computed tomography slices of *Eodelphis* cf. *E. browni* specimens (a) MOR 739 and (b) TMDC TA2008.3.2. The red lines outline the alveoli shape of p2 and p3 in both specimens.

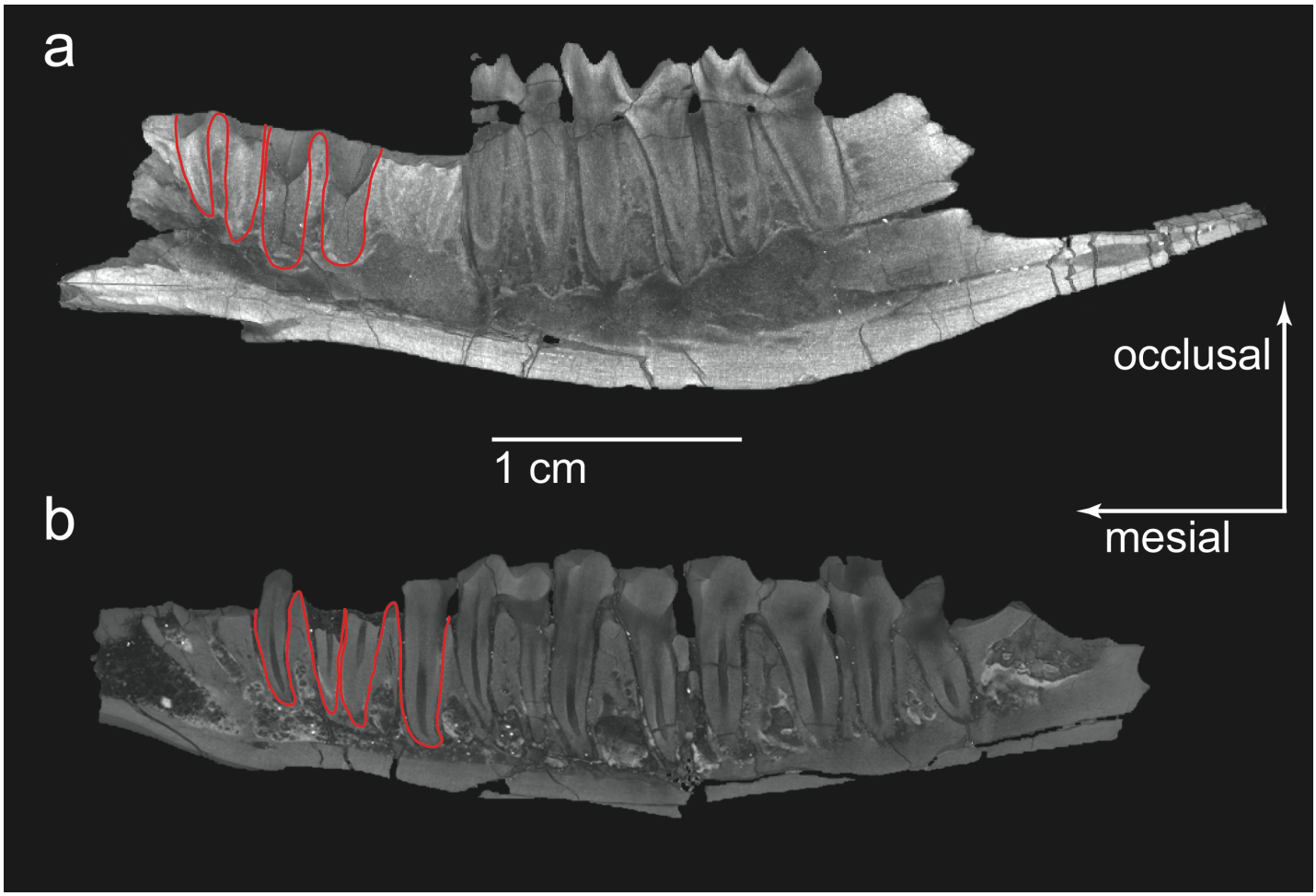

Appendix 2: Dataset for Bending Strength Analysis

List of publications, with corresponding specimens and specimen numbers, from which published photographs or figures were used to take measurements for bending force calculations of metatherian dentaries. Measurements used for mandibular bending force calculations were taken directly from Wilson et al. 2016. Daggers denoted extinct species.

Species	Family	Specimen Number	Publication
Eodelphis browni†	Stagodontidae	AMNH 14169	Scott and Fox 2015
Eodelphis browni†	Stagodontidae	ROM 11715	Fox 1981
Eodelphis cf. *E.browni*†	Stagodontidae	UALVP 7011	Scott and Fox 2015
Eodelphis cutleri†	Stagodontidae	ROM 701	Fox 1981
Eodelphis cutleri†	Stagodontidae	NHMUK M11532	Scott and Fox 2015
Eodelphis cutleri†	Stagodontidae	UALVP 671	Fox 1981
Eodelphis cf. *E. cutleri*†	Stagodontidae	TMP 2002.012.0007	Scott and Fox 2015
Didelphodon vorax†	Stagodontidae	UWBM 102139	Wilson et al. 2016
Didelphodon vorax†	Stagodontidae	UCMP 159909	Wilson et al. 2016
Didelphodon coyi†	Stagodontidae	TMP 91.161.1	Fox and Naylor 2006
Didelphodon coyi†	Stagodontidae	TMP 90.12.29	Fox and Naylor 2006
?*Protolambda clemensi*†	Pediomyidae	UALVP 14810	Fox 1979
Kokopellia juddi†	*incertae sedis*	OMNH 26361	Cifelli 1993
Nanocuris improvida†	Deltatheridiidae	RSM P2523.260	Fox et al. 2007
Alphadon halleyi†	Alphadontidae	MOR 250	Montellano 1988
Turgidodon praesagus†	Alphadontidae	UALVP 670	Fox 1979
Sarcophilus harrisii	Dasyuridae	UWBM 20671	Wilson et al. 2016
Didelphis virginiana	Didelphidae	UWBM 12555	Wilson et al. 2016

Appendix 3: Bending Strength Calculations

Relative bending force calculations of the dentaries of *Eodelphis* and other taxa based on the equations of Therrien (2005). DV = dorsoventral, Ix = distribution of bone about the labiolingual axis (cm^4), Iy = distribution of bone about the dorsoventral axis (cm^4), ML = mediolateral, Zx = bending strength in the dorsoventral plane (or about the labiolingual axis, in cm^3), and Zy = bending strength in the labiolingual plane (or about the dorsoventral axis, in cm^3). All measurements are reported in cm.

Species	Tooth position	Distance to condyle (L)	DV radius (a)	ML radius (b)	Ix	Zx	DV bending force (Zx/L)	Iy	Zy	ML bending force (Zy/L)	Relative force (Zx/Zy)
Nanocuris improvida†	canine	–	0.20	0.22	0.00	0.01	–	0.00	0.01	–	0.88
RSM P2523.260	p2-p3	–	–	–	–	–	–	–	–	–	–
	p3-m1	–	–	–	–	–	–	–	–	–	–
	m1-m2	–	0.37	0.16	0.01	0.02	–	0.00	0.01	–	2.26
	m2-m3	–	0.42	0.17	0.01	0.02	–	0.00	0.01	–	2.42
	post m4	–	0.47	0.16	0.01	0.03	–	0.00	0.01	–	3.04
Kokopellia juddi†	canine	–	0.10	0.13	0.00	0.00	–	0.00	0.00	–	0.74
OMNH 26361	p2-p3	–	0.15	0.08	0.00	0.00	–	0.00	0.00	–	1.73
	p3-m1	–	0.16	0.08	0.00	0.00	–	0.00	0.00	–	2.12
	m1-m2	–	0.18	0.07	0.00	0.00	–	0.00	0.00	–	2.40
	m2-m3	–	0.19	0.08	0.00	0.00	–	0.00	0.00	–	2.29
	post m4	–	0.18	0.09	0.00	0.00	–	0.00	0.00	–	1.96
?*Protolambda clemensi*†	canine	–	–	–	–	–	–	–	–	–	–
UALVP 14810	p2-p3	–	0.13	0.06	0.00	0.00	–	0.00	0.00	–	2.00

	p3-m1	–	0.13	0.07	0.00	0.00	–	0.00	0.00	–	1.93
	m1-m2	–	0.14	0.07	0.00	0.00	–	0.00	0.00	–	1.86
	m2-m3	–	0.14	0.07	0.00	0.00	–	0.00	0.00	–	1.86
	post m4	–	0.14	0.07	0.00	0.00	–	0.00	0.00	–	1.86
Alphadon halleyi†	canine	–	–	–	–	–	–	–	–	–	–
MOR 250	p2-p3	2.68	0.22	0.13	0.00	0.00	-2.73	0.00	0.00	-2.97	1.73
	p3-m1	2.45	0.25	0.12	0.00	0.01	-2.62	0.00	0.00	-2.97	2.21
	m1-m2	2.25	0.27	0.12	0.00	0.01	-2.54	0.00	0.00	-2.90	2.32
	m2-m3	2.02	0.25	0.12	0.00	0.01	-2.54	0.00	0.00	-2.87	2.11
	post m4	1.58	0.26	0.13	0.00	0.01	-2.35	0.00	0.00	-2.64	1.93
Turgidodon praesagus†	canine	–	0.13	0.12	0.00	0.00	–	0.00	0.00	–	1.04
UALVP 670	p2-p3	–	0.16	0.11	0.00	0.00	–	0.00	0.00	–	1.43
	p3-m1	–	0.19	0.10	0.00	0.00	–	0.00	0.00	–	1.90
	m1-m2	–	0.23	0.10	0.00	0.00	–	0.00	0.00	–	2.39
	m2-m3	–	0.31	0.09	0.00	0.01	–	0.00	0.00	–	3.69
	post m4	–	–	–	–	–	–	–	–	–	–
Eodelphis browni†	canine	5.17	0.29	0.22	0.00	0.01	-2.54	0.00	0.01	-2.65	1.30
AMNH 14169	p2-p3	4.67	0.36	0.23	0.01	0.02	-2.29	0.00	0.02	-2.49	1.59
	p3-m1	4.04	0.38	0.26	0.01	0.03	-2.15	0.01	0.02	-2.31	1.44
	m1-m2	3.75	0.46	0.28	0.02	0.05	-1.91	0.01	0.03	-2.12	1.63
	m2-m3	3.38	0.53	0.31	0.04	0.07	-1.70	0.01	0.04	-1.93	1.73
	post m4	2.42	0.49	0.33	0.03	0.06	-1.58	0.01	0.04	-1.75	1.47
Eodelphis browni†	canine	–	–	–	–	–	–	–	–	–	–
ROM 11715	p2-p3	–	0.30	0.23	0.01	0.02	–	0.00	0.01	–	1.32
	p3-m1	–	0.34	0.22	0.01	0.02	–	0.00	0.01	–	1.54
	m1-m2	–	0.38	0.21	0.01	0.02	–	0.00	0.01	–	1.82

	m2-m3	–	0.39	0.22	0.01	0.03	–	0.00	0.01	–	1.78
	post m4	–	0.42	0.25	0.01	0.03	–	0.01	0.02	–	1.64
Eodelphis cf. *E. browni*†	canine	–	–	–	–	–	–	–	–	–	–
UALVP 7011	p2-p3	–	–	–	–	–	–	–	–	–	–
	p3-m1	–	0.37	0.17	0.01	0.02	–	0.00	0.01	–	2.11
	m1-m2	–	0.40	0.18	0.01	0.02	–	0.00	0.01	–	2.25
	m2-m3	–	0.47	0.20	0.02	0.03	–	0.00	0.01	–	2.33
	post m4	–	0.42	0.25	0.01	0.03	–	0.01	0.02	–	1.68
Eodelphis cf. *E. browni*†	canine	–	–	–	–	–	–	–	–	–	–
MOR 739	p2-p3	–	0.42	0.16	0.01	0.02	–	0.00	0.01	–	2.61
	p3-m1	–	0.40	0.20	0.01	0.03	–	0.00	0.01	–	2.03
	m1-m2	–	0.45	0.21	0.01	0.03	–	0.00	0.02	–	2.09
	m2-m3	–	0.54	0.21	0.03	0.05	–	0.00	0.02	–	2.53
	post m4	–	0.57	0.23	0.03	0.06	–	0.01	0.02	–	2.50
Eodelphis cf. *E. browni*†	canine	–	0.23	0.32	0.00	0.01	–	0.01	0.02	–	0.73
TMDC TA2008.3.2	p2-p3	–	0.32	0.19	0.00	0.01	–	0.00	0.01	–	1.68
	p3-m1	–	0.34	0.20	0.01	0.02	–	0.00	0.01	–	1.73
	m1-m2	–	0.39	0.20	0.01	0.02	–	0.00	0.01	–	1.90
	m2-m3	–	0.41	0.20	0.01	0.03	–	0.00	0.01	–	2.01
	post m4	–	0.45	0.24	0.02	0.04	–	0.00	0.02	–	1.90
Eodelphis cutleri†	canine	–	–	–	–	–	–	–	–	–	–
UALVP 671	p2-p3	–	–	–	–	–	–	–	–	–	–
	p3-m1	–	0.33	0.20	0.01	0.02	–	0.00	0.01	–	1.63
	m1-m2	–	0.37	0.18	0.01	0.02	–	0.00	0.01	–	2.01
	m2-m3	–	0.40	0.16	0.01	0.02	–	0.00	0.01	–	2.44

	post m4	–	0.35	0.22	0.01	0.02	–	0.00	0.01	–	1.60
Eodelphis cutleri†	canine	–	–	–	–	–	–	–	–	–	–
ROM 701	p2-p3	–	–	–	–	–	–	–	–	–	–
	p3-m1	–	0.46	0.28	0.02	0.05	–	0.01	0.03	–	1.63
	m1-m2	–	0.52	0.28	0.03	0.06	–	0.01	0.03	–	1.88
	m2-m3	–	0.58	0.32	0.05	0.09	–	0.02	0.05	–	1.80
	post m4	–	0.60	0.37	0.06	0.11	–	0.02	0.07	–	1.61
Eodelphis cutleri†	canine	–	0.34	0.40	0.01	0.04	–	0.02	0.04	–	0.84
NHMUK M11532	p2-p3	–	0.45	0.29	0.02	0.05	–	0.01	0.03	–	1.56
	p3-m1	–	0.46	0.27	0.02	0.04	–	0.01	0.03	–	1.69
	m1-m2	–	0.52	0.27	0.03	0.06	–	0.01	0.03	–	1.93
	m2-m3	–	0.55	0.30	0.04	0.07	–	0.01	0.04	–	1.83
	post m4	–	0.56	0.34	0.05	0.08	–	0.02	0.05	–	1.62
Eodelphis cutleri†	canine	5.84	0.34	0.40	0.01	0.04	-2.22	0.02	0.04	-2.14	0.84
E. browni model	p2-p3	5.28	0.45	0.29	0.02	0.05	-2.05	0.01	0.03	-2.25	1.56
NHMUK M11532	p3-m1	4.57	0.46	0.27	0.02	0.04	-2.01	0.01	0.03	-2.24	1.69
	m1-m2	4.24	0.52	0.27	0.03	0.06	-1.88	0.01	0.03	-2.16	1.93
	m2-m3	3.82	0.55	0.30	0.04	0.07	-1.74	0.01	0.04	-2.00	1.83
	post m4	2.73	0.56	0.34	0.05	0.08	-1.51	0.02	0.05	-1.72	1.62
Eodelphis cutleri†	canine	7.38	0.34	0.40	0.01	0.04	-2.32	0.02	0.04	-2.24	0.84
D. vorax model	p2-p3	6.92	0.45	0.29	0.02	0.05	-2.17	0.01	0.03	-2.36	1.56
NHMUK M11532	p3-m1	6.39	0.46	0.27	0.02	0.04	-2.15	0.01	0.03	-2.38	1.69
	m1-m2	5.94	0.52	0.27	0.03	0.06	-2.02	0.01	0.03	-2.31	1.93
	m2-m3	5.48	0.55	0.30	0.04	0.07	-1.90	0.01	0.04	-2.16	1.83
	post m4	4.27	0.56	0.34	0.05	0.08	-1.70	0.02	0.05	-1.92	1.62

Eodelphis cf. *E. cutleri*†	canine	–	–	–	–	–	–	–	–	–	–
TMP 2002.012.0007	p2-p3	–	0.42	0.28	0.02	0.04	–	0.01	0.02	–	1.52
	p3-m1	–	0.44	0.25	0.02	0.04	–	0.01	0.02	–	1.78
	m1-m2	–	0.50	0.25	0.02	0.05	–	0.01	0.02	–	1.97
	m2-m3	–	0.50	0.24	0.02	0.05	–	0.01	0.02	–	2.12
	post m4	–	0.53	0.28	0.03	0.06	–	0.01	0.03	–	1.87
Didelphodon vorax†	canine	–	0.42	0.55	0.03	0.07	–	0.05	0.10	–	0.76
TCMI 2002.113.1	p2-p3	–	0.45	0.35	0.03	0.06	–	0.01	0.04	–	1.31
	p3-m1	–	0.45	0.35	0.03	0.06	–	0.02	0.04	–	1.28
	m1-m2	–	0.49	0.29	0.03	0.06	–	0.01	0.03	–	1.71
	m2-m3	–	0.51	0.33	0.03	0.07	–	0.01	0.04	–	1.56
	post m4	–	0.53	0.41	0.05	0.09	–	0.03	0.07	–	1.30
Didelphodon vorax†	canine	8.08	0.60	0.66	0.11	0.18	-1.64	0.13	0.20	-1.60	0.91
UWBM 102139	p2-p3	7.58	0.66	0.50	0.12	0.17	-1.64	0.07	0.13	-1.76	1.32
	p3-m1	7.00	0.73	0.48	0.15	0.20	-1.54	0.06	0.13	-1.72	1.52
	m1-m2	6.51	0.78	0.44	0.16	0.21	-1.50	0.05	0.12	-1.75	1.78
	m2-m3	6.00	0.84	0.44	0.21	0.25	-1.39	0.06	0.13	-1.67	1.93
	post m4	4.68	0.76	0.45	0.15	0.20	-1.36	0.06	0.12	-1.58	1.67
Didelphodon vorax†	canine	–	0.82	0.59	0.26	0.31	–	0.13	0.22	–	1.39
UCMP 159909	p2-p3	–	0.87	0.56	0.29	0.33	–	0.12	0.21	–	1.56
	p3-m1	–	0.89	0.55	0.30	0.34	–	0.11	0.21	–	1.63
	m1-m2	–	0.88	0.47	0.25	0.28	–	0.07	0.15	–	1.87
	m2-m3	–	0.91	0.45	0.27	0.29	–	0.07	0.15	–	2.00
	post m4	–	–	–	–	–	–	–	–	–	–

Didelphodon coyi†	canine	6.21	0.50	0.35	0.03	0.07	-1.96	0.02	0.05	-2.12	1.44
TMP 84.64.1	p2-p3	5.87	0.45	0.31	0.02	0.05	-2.08	0.01	0.03	-2.24	1.45
	p3-m1	5.10	0.57	0.35	0.05	0.09	-1.77	0.02	0.05	-1.98	1.63
	m1-m2	4.85	0.56	0.33	0.05	0.08	-1.78	0.02	0.05	-2.01	1.72
	m2-m3	4.41	0.61	0.34	0.06	0.10	-1.65	0.02	0.05	-1.91	1.80
	post m4	3.48	0.63	0.42	0.08	0.13	-1.43	0.04	0.09	-1.60	1.49
Didelphodon coyi†	canine	–	0.31	0.58	0.01	0.04	–	0.05	0.08	–	0.54
TMP 91.161.1	p2-p3	–	0.52	0.34	0.04	0.07	–	0.02	0.05	–	1.52
	p3-m1	–	0.52	0.34	0.04	0.07	–	0.02	0.05	–	1.55
	m1-m2	–	0.57	0.32	0.05	0.08	–	0.01	0.05	–	1.80
	m2-m3	–	0.58	0.32	0.05	0.08	–	0.01	0.05	–	1.81
	post m4	–	0.58	0.37	0.05	0.09	–	0.02	0.06	–	1.58
Didelphodon coyi†	canine	–	–	–	–	–	–	–	–	–	–
TMP 90.12.29	p2-p3	–	0.55	0.34	0.04	0.08	–	0.02	0.05	–	1.59
	p3-m1	–	0.58	0.38	0.06	0.10	–	0.03	0.07	–	1.53
	m1-m2	–	0.63	0.35	0.07	0.11	–	0.02	0.06	–	1.77
	m2-m3	–	0.62	0.36	0.07	0.11	–	0.02	0.06	–	1.72
	post m4	–	0.66	0.41	0.09	0.14	–	0.04	0.09	–	1.62
Sarcophilus harrisii	canine	9.51	0.96	0.97	0.67	0.70	-1.13	0.68	0.70	-1.13	0.99
UWBM 20671	p2-p3	8.42	1.02	0.47	0.40	0.39	-1.33	0.09	0.18	-1.67	2.16
	p3-m1	7.57	1.06	0.44	0.41	0.39	-1.29	0.07	0.16	-1.67	2.42
	m1-m2	6.57	1.03	0.48	0.41	0.40	-1.22	0.09	0.18	-1.56	2.17
	m2-m3	5.48	1.03	0.57	0.50	0.48	-1.06	0.15	0.27	-1.31	1.80
	post m4	4.13	1.20	0.53	0.72	0.60	-0.84	0.14	0.26	-1.19	2.28
Didelphis virginiana	canine	9.27	0.57	0.54	0.08	0.14	-1.82	0.07	0.13	-1.85	1.06

UWBM 12555	p2-p3	7.83	0.72	0.34	0.10	0.14	-1.75	0.02	0.07	-2.08	2.13
	p3-m1	7.04	0.73	0.33	0.10	0.14	-1.71	0.02	0.06	-2.05	2.19
	m1-m2	6.55	0.75	0.30	0.10	0.13	-1.71	0.02	0.05	-2.11	2.52
	m2-m3	5.95	0.74	0.30	0.09	0.13	-1.67	0.01	0.05	-2.07	2.50
	post m4	4.60	0.82	0.31	0.13	0.16	-1.45	0.02	0.06	-1.88	2.68

Appendix 4: Bending Strength Profiles of other *Eodelphis* and *Didelphodon* Specimens

Relative bending force profiles of other (**a**) *Eodelphis* and (**b**) *Didelphodon* specimens not included in Figures 4 or 5. Squares and gray connecting lines represent *Didelphodon* specimens, circles and black connecting lines represent *E. cutleri* specimens, and triangles and black connecting lines represent *E. browni* specimens. Specimen numbers are listed in the legend. Gray circles next to the y-axis of relative bending force profiles represent cross-sections of a hypothetical mandibles and dorsoventral and mediolateral planes (represented by the gray lines inside the circles) to demonstrate how mandibular cross-sectional shapes changes with the values on the y-axis; as values increase, mandibles become taller (dorsoventral plane) than they are wide (mediolateral plane)

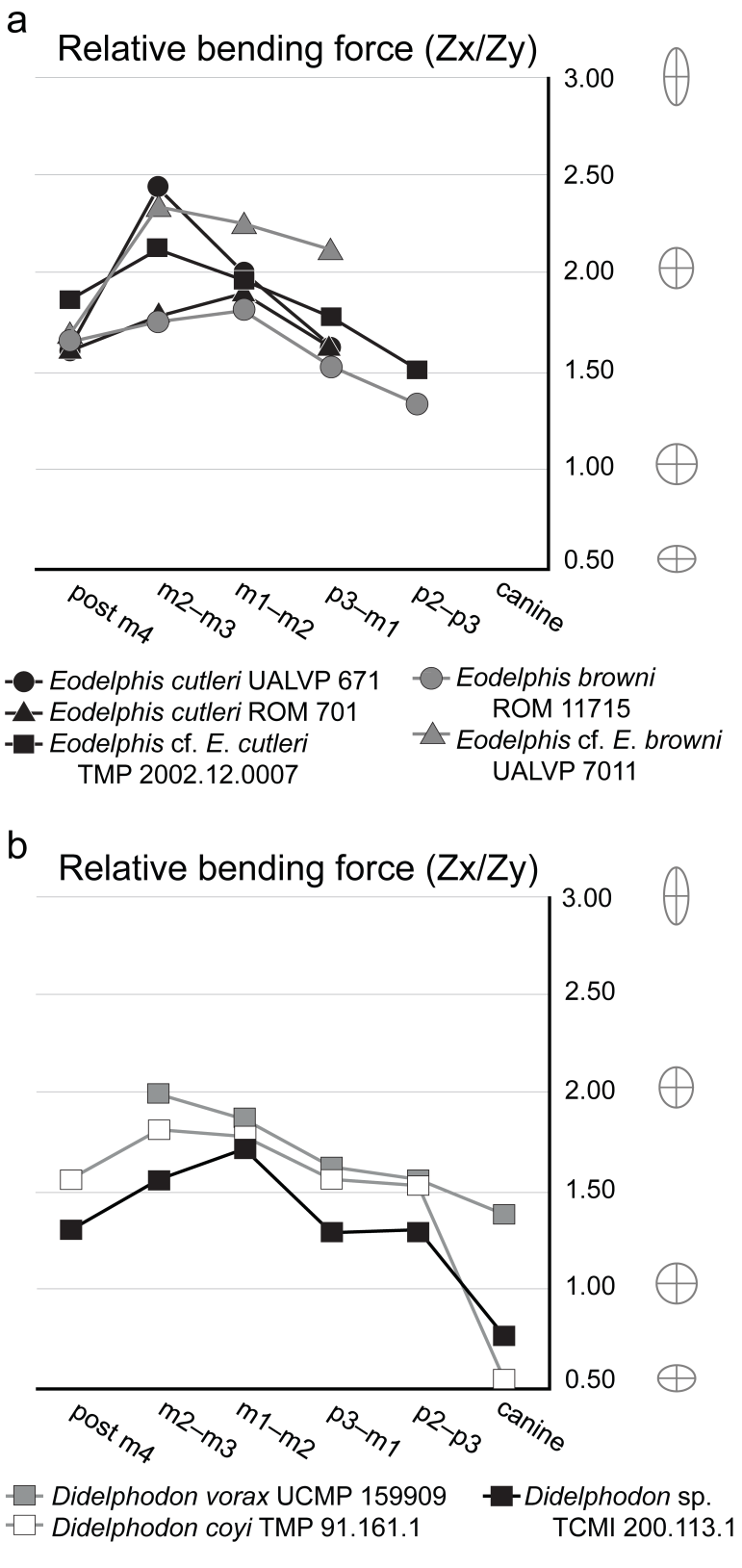
a
Relative bending force (Zx/Zy)
3.00
2.50
2.00
1.50
1.00
0.50
post m4
m2–m3
m1–m2
p3–m1
p2–p3
canine
Eodelphis cutleri UALVP 671
Eodelphis cutleri ROM 701
Eodelphis cf. E. cutleri TMP 2002.12.0007
Eodelphis browni ROM 11715
Eodelphis cf. E. browni UALVP 7011
b
Relative bending force (Zx/Zy)
3.00
2.50
2.00
1.50
1.00
0.50
post m4
m2–m3
m1–m2
p3–m1
p2–p3
canine
Didelphodon vorax UCMP 159909
Didelphodon coyi TMP 91.161.1
Didelphodon sp. TCMI 200.113.1

CHAPTER 4: DENTAL ECOMORPHOLOGY AND MACROEVOLUTIONARY PATTERNS OF LATE CRETACEOUS NORTH AMERICAN METATHERIANS

At the time of submission of this dissertation, this manuscript was submitted for publication to Palaeontologica Electronica under the following author list: Alexandria L. Brannick, Henry Z. Fulghum, David M. Grossnickle, and Gregory P. Wilson Mantilla.

4.1 AUTHOR CONTRIBUTIONS

ALB and GPWM conceived of the project. ALB collected and curated data, conducted formal analyses, and wrote and prepared the original draft of this manuscript. HZF collected data and reviewed and edited writing. DMG assisted with analyses and reviewed, edited, and contributed to writing. GPWM supervised this project and reviewed, edited, and contributed to writing.

4.2 ABSTRACT

Metatherian mammals were taxonomically rich and abundant in Late Cretaceous faunas of North America. Although much attention has been paid to metatherian taxonomy, a comprehensive, quantitative study on the ecomorphology of this clade is lacking. Here, we utilize three-dimensional dental topographic analysis to predict the diets of a large sample of metatherians to try to understand macroevolutionary patterns in dental morphology and dietary diversity. Contrary to their taxonomic diversity, our results show that dental disparity and dietary diversity did not significantly change throughout the Late Cretaceous and that most metatherians were

insectivorous. Nevertheless, we also found that metatherians occupied a wide range of dietary niches and were arguably the most dietarily diverse of any mammalian clade of the Late Cretaceous. Regarding the timing of metatherian ecomorphological diversification, our results indicate that this ecological diversification began prior to the ecological diversification of angiosperms and was more correlated in time with the Cretaceous Terrestrial Revolution and the mid-Cretaceous taxonomic diversification of angiosperms.

4.3 PLAIN LANGUAGE SUMMARY

Metatherian mammals (the group of mammals that includes living marsupials and their closest relatives) were species rich and evolutionarily successful during the Late Cretaceous (ca. 100–66 million years ago). Theoretical models and empirical data indicate taxonomic radiation is often accompanied by diversification in ecology and anatomy, but this has not been explicitly demonstrated for metatherian mammals of the Late Cretaceous. Previous studies have noted that Late Cretaceous metatherians were more ecologically diverse than previously recognized, but studies using three-dimensional anatomical data within a broad phylogenetic context are lacking. We examined the three-dimensional tooth morphology of Late Cretaceous metatherians to infer diet in these fossil taxa, quantify dental morphological diversity and disparity of these metatherians, and evaluate the resulting patterns of ecomorphological diversity and disparity through time relative to corresponding patterns of taxonomic richness. We found that dental disparity and dietary diversity did not significantly change throughout the Late Cretaceous and that most metatherians were insectivorous. Nevertheless, we also found that metatherians occupied a wide range of diets and had greater dietary diversity than contemporaneous mammal groups. Our results also indicate that this ecological diversification of metatherians began prior

to the ecological diversification of angiosperms (flowering plants) (ca. 85–80 million years ago) and was more correlated in time with the Cretaceous Terrestrial Revolution (ca. 125–80 million years ago) and the mid-Cretaceous taxonomic diversification of angiosperms.

4.4. INTRODUCTION

Metatherian mammals (the stem-based clade of extant marsupials and their closest relatives; e.g., Rougier et al., 1998) were evolutionarily successful during the Late Cretaceous (ca. 100–66 million years ago [Ma]). They were geographically widespread, occupying all northern landmasses and possibly some southern ones (Rougier et al., 1998; Krause, 2001; Kielan-Jaworowska et al., 2004; Martin et al., 2005; Vullo et al., 2009; Averianov et al., 2010; Williamson et al., 2014; Goin et al., 2016). Late Cretaceous metatherians were also numerically abundant, making up as much as 45% of all mammalian fossil individuals within local faunas (e.g., Cifelli, 2004; Wilson, 2014), and were taxonomically rich (Bennett et al., 2018) — at least 68 species are known worldwide from the Late Cretaceous (Williamson et al., 2014). It has been hypothesized that during the early Late Cretaceous (Albian-Cenomanian–late Santonian; 100–85 Ma), metatherians underwent a taxonomic radiation that led to at least five major lineages (Glasbiidae, Pediomyidae, Alphadontidae, Stagodontidae, and Marsupialia; Clemens, 1966; Davis, 2007; Johanson, 1996; Wilson et al., 2016; see Benson et al., 2013; Newham et al., 2014; Grossnickle and Newham, 2016; and Bennett et al., 2018 for discussion on the possible effect of fossil sampling on mammalian taxonomic diversity patterns in the Late Cretaceous). Despite theoretical models and empirical data that indicate taxonomic radiation is often accompanied by ecomorphological diversification (e.g., Rabosky and Adams, 2012; Ramírez-Barahona et al., 2016), this pattern has never been explicitly demonstrated for Late Cretaceous metatherians.

Several studies, mostly qualitative in nature and focused on individual taxa, have highlighted ecomorphological diversity among Late Cretaceous metatherians. The postcranial fossil record of these taxa is sparse, so few studies have measured their locomotor diversity and substrate use (Szalay, 1994; Szalay and Trofimov, 1996; Szalay and Sargis, 2006; DeBey and

Wilson, 2017); instead, most studies have used the abundant craniodental fossil record to reconstruct feeding ecology. For example, the highly distinctive, broad-basined, bunodont molars of *Glasbius* have prompted interpretations that it was frugivorous (e.g., Clemens, 1966, 1979); the large, bulbous premolars of *Didelphodon* and its broad-basined molars with enhanced shearing facets and robust skull morphology have led to inferences of carnivory, omnivory, and durophagy (Clemens, 1966, 1968, 1979; Fox and Naylor, 1986, 2006); and the elongated, buccolingually compressed molars of *Nanocuris* with their exaggerated postvallum-prevallid shearing crest and a reduced talonid indicate adaptation to carnivory (Fox et al., 2007; Wilson and Riedel, 2010).

Other studies have taken more quantitative approaches to investigating metatherian dental ecomorphology. Gordon (2003) used three-dimensional (3D) geometric morphometrics and shearing-crest measurements to examine dietary morphospace of 10 fossil mammal species (five metatherian species) in relation to a sample of extant mammals; she found that most metatherians and eutherians from the Lancian North American land mammal 'age' (NALMA; ca. 69–66 Ma; Woodburne, 2004) largely overlapped in morphospace with extant insectivores. Using 2D geometric morphometrics, Wilson (2013) quantified the morphological disparity of mammalian (including metatherian) teeth immediately before and after the Cretaceous-Paleogene (K-Pg) boundary. He found that metatherians exploited a wide range of body sizes and feeding ecologies in the Lancian, but that local extinction contributed to a loss in ecological endmembers within the Hell Creek mammalian fauna. Grossnickle and Newham (2016) took a more synoptic approach by investigating dental morphological disparity through time on a global scale and found that metatherian disparity increased throughout the Late Cretaceous. Nonetheless, studies

utilizing 3D morphological data in concert with broader taxonomic sampling of Metatheria within a phylogenetic context are lacking.

Here, we quantify the ecomorphological diversity of metatherians through the Late Cretaceous, using North America's densely sampled dental fossil record (Cifelli et al., 2004; Williamson et al., 2014). We (i) apply dental topographic analyses (e.g., Boyer, 2008; Pampush et al., 2016; López- Torres et al., 2017) to upper molars of 42 species of Late Cretaceous metatherians; (ii) map and quantify the resulting dental morphological diversity and disparity of these metatherians by time bin and taxonomic family; (iii) infer diet in these fossil taxa, by comparing their dental topographic values to those of 30 extant mammalian species with known diets; and (iv) evaluate the resulting patterns of ecomorphological diversity and disparity through time relative to corresponding patterns of taxonomic richness and to possible evolutionary drivers, such as the Cretaceous Terrestrial Revolution (KTR; Lloyd et al., 2008), the ecological rise of angiosperms (e.g., Wing and Boucher, 1998), and the Cretaceous-Paleogene mass extinction (e.g., Simpson, 1937).

4.5 BACKGROUND

Two hypotheses provide a framework to discuss the timing of metatherian taxonomic and ecomorphological diversification (see Grossnickle et al., 2019 for review). "The Early Rise Hypothesis," coined by Grossnickle et al. (2019), is related to the ecological radiation of crown-group angiosperms (flowering plants), which began after the KTR (ca. 85–80 Ma). Angiosperms experienced a taxonomic radiation during the KTR (125–80 Ma; Wing and Boucher, 1998; Anderson et al., 2005; Magallón et al., 2013; Magallón et al., 2015), but the Early Rise Hypothesis is more closely linked to the post-KTR ecological (not taxonomic) rise of

angiosperms (beginning by ca. 85–80 Ma), which may have been a more critical driver of increases in mammalian diversity (Meredith et al., 2011; Eriksson, 2016), as evidenced by mammals (Grossnickle and Polly, 2013; Grossnickle and Newham, 2016; Chen et al., 2019), such as multituberculates (Wilson et al., 2012), which increased both their taxonomic and ecomorphological diversity during the late Late Cretaceous (ca. 83–66 Ma; see Grossnickle et al., 2019 for review). Specifically, this radiation likely spurred co-evolution and diversification of insects (Grimaldi, 1999) and provided novel food sources—such as new fruits and social insects—for mammals. Angiosperms also evolved to provide a complex canopy structure by the Late Cretaceous or early Paleogene (Wing and Boucher, 1998; Crifò et al., 2014), allowing for more arboreal lifestyles among mammals (Chen et al., 2019). Thus, under the Early Rise Hypothesis, we predict that beginning in the late Late Cretaceous metatherians increased both the disparity (magnitude of morphological differences) of their dental morphologies and the diversity of their diets (number of dietary categories).

Alternatively, the downstream effects of the KTR might have manifested among non-therian mammals only (e.g., multituberculates; Wilson et al., 2012), and despite the increasing diversity of food resources and novel evolutionary adaptations of tribosphenic molars (e.g., increased grinding capabilities), therians were ecomorphologically constrained until the extinction of non-avian dinosaurs (e.g., Simpson, 1937; Van Valen and Sloan, 1977; Archibald, 1983, 2011; Stucky, 1990; Alroy, 1999; Grossnickle et al., 2019). This hypothesis, called “the Suppression Hypothesis” (Grossnickle and Newham, 2016), is supported by evidence of sharp increases in origination rates (Alroy, 1999), body size (Alroy, 1999; Smith et al. 2010), and morphological disparity (Halliday and Goswami, 2016) in early Cenozoic mammalian faunas.

For this hypothesis, we predict that throughout the Late Cretaceous the disparity of dental morphologies and the diversity of dietary categories remained low and stable for metatherians.

4.6 METHODS

4.6.1 Previous methodological approaches

Diet is a critical component of an animal's ecology and informs trophic relationships within ecosystems (e.g., Pineda-Munoz et al., 2016). Tooth shape correlates with diet (e.g., Kay, 1975; Boyer, 2008; Bunn and Ungar, 2009; Ungar, 2010; Evans, 2013), and a variety of methods have been developed to investigate this relationship. Here, we use dental topographic analysis (DTA; López-Torres et al., 2017) to quantify the shape of three-dimensional models of entire tooth crown surfaces. Our application of DTA encompasses three metrics—relief index (RFI; Ungar and M'Kirera, 2003; Boyer, 2008), Dirichlet normal energy (DNE; Bunn et al., 2011; Winchester, 2016), and orientation patch count rotated (OPCR; Evans et al., 2007; Evans and Jernvall, 2009), all of which have been shown to correlate with diet in extant mammals. Much of the research that has applied these dental topographic measures has focused on placental mammals, mainly Primates (e.g., Boyer, 2008; Boyer et al., 2010; Bunn et al., 2011; Winchester et al., 2014; Pampush et al., 2016; López- Torres et al., 2017), but also carnivorans (Evans et al., 2007; Evans and Jernvall, 2009), bats (Santana et al., 2011), rodents (Evans et al., 2007; Evans and Jernvall, 2009; Prufrock et al., 2016; Spradley, 2017), and other euarchontans (Boyer, 2008; Selig et al., 2019). Dietary interpretations of some fossil taxa, including multituberculates (Wilson et al., 2012) and meridiolestidans (Harper et al., 2018), have also been proposed using DTA. Metatherians (including marsupials) have been undersampled and understudied in DTA studies (but see Smits and Evans, 2012; Spradley, 2017; Smith, 2017); nevertheless, studies have

shown that dental topographic metrics also correlate with diet in metatherians in a way that is consistent with the patterns seen in primates and other placentals (e.g., frugivores have lower DNE values than folivores and insectivores do; Smith, 2017; Spradley, 2017).

4.6.2 Extant sampling

To provide a modern analog, we collected dental surface data for 56 upper molar specimens (and a few upper fourth premolars) representing eight taxonomic orders, 27 genera and 30 species of extant marsupials and placentals (Table 4.1; Figure 4.1). The species in our dataset were selected in order to provide diverse representation of dental morphology, diet, and phylogeny. We sampled only adult specimens and, whenever possible, both male and female specimens from each species. We tried to avoid specimens of captive individuals, but due to availability of specimens, this was unavoidable for some taxa. Any effects of captive diets on tooth morphology should be minimal because we selected teeth with little to no wear (see below). Because we are interested in the dental morphology and diet of Late Cretaceous metatherians with tribosphenic molars, extant mammals with derived dental morphology or dental formulae were not considered for our extant sample (i.e., homodont dentitions, enamel-less teeth) as we assumed these morphologies would not be informative for our fossil sample. We primarily sampled small-bodied extant mammals (all but six species are ≤ 5 kg) because most fossil metatherians in our sample were also relatively small (≤ 5 kg), thus minimizing potential biases related to differences in body sizes. Likewise, we chose not to include folivores in our extant sample because small-bodied folivorous mammals typically have extremely derived teeth (e.g., *Phloeomys*, the giant cloud rat) and there tends to be a lower body-size limit on folivory and almost all of the fossil metatherian taxa sampled here have been predicted to have

body sizes below this threshold (Kay, 1975, 1984). Although our study focuses on metatherian mammals, we included placental mammals in our sample to increase both the sample size and range of diets (Smith, 2017). By including placentals, we form an extant phylogenetic bracket (Witmer, 1995) around our sample of fossil metatherians. Although placentals and marsupials possess dental morphological differences, the metrics used in our DTA are homology-free and based on overall crown shape (e.g., Evans et al., 2007; Boyer, 2008; Bunn et al., 2011; Evans, 2013; Berthaume et al., 2019), so including placental mammals in our extant sample should not negatively impact our interpretations.

4.6.3 Tooth position

Some DTA studies have assessed complete post-canine tooth rows (e.g., Evans et al., 2007; Wilson et al., 2012; Pineda-Munoz et al., 2016). That approach treats the post-canine tooth row as a functional unit and captures morphological differences along it that may help to more accurately determine feeding ecology (e.g., bone-cracking premolar morphology versus reduced upper molar morphology of hyenas; Figueirido et al., 2013). Nevertheless, obtaining a complete cheek tooth row for fossil taxa can be challenging—the fossil record for many extinct species included in this study does not include teeth from all post-canine tooth positions. To maximize our taxonomic sample, we chose to sample one tooth position, but we acknowledge that this choice might impact the resolution and potentially the accuracy of our results; we note this issue for individual cases where it might be relevant. Whereas most DTAs have focused on lower molars, specifically the lower second molar (m2) or penultimate lower molar (e.g., Boyer, 2008; Selig et al., 2019), we focus on the penultimate upper molar (most commonly M3 in metatherians and M2 in eutherians; Tables 4.1–4.2). We chose this tooth position because it is

heavily involved in mechanical food processing and tends to be more representative of the general molar morphology of a taxon than are the first or last molars (Wilson, 2013). As the penultimate molar position, the M2 of eutherians and the M3 of metatherians occupy functionally analogous positions in the jaw (Janis, 1990; Wilson, 2013). Moreover, the M2 of eutherians (the stem-based clade of living placentals and their closest relatives; Wible et al., 2007) may be homologous to the M3 of metatherians (McKenna, 1975; Luckett, 1993; O'Leary et al., 2013), despite the predominant dental-formula convention. There were two special instances in our tooth-position sampling in which the M2 of eutherians was not sampled: those species with a specialized carnassial pair and those species with a reduced dental formula. For those with a specialized carnassial pair, the ultimate premolar (part of the carnassial pair) was sampled because it is heavily involved in food processing (Van Valkenburg, 2007); in both instances of species with a carnassial pair (*Crocuta crocuta* and *Lynx rufus*), the ultimate premolar is also the penultimate tooth. For those species with a reduced dental formula, either the penultimate tooth (e.g., *Procyon lotor*) or the only molar (e.g., *Spilogale putorius*) was sampled—in both cases the M1 was sampled (Table 4.1).

For both extant and fossil taxa, we selected upper molars with as little wear as possible to avoid artifacts or possible confounding signals in dietary interpretations caused by dental wear (Selig et al., 2019). Although some extant mammal species have teeth in which dental wear is important for food processing function (e.g., ungulates; Fortelius, 1985)—and it has been hypothesized that some fossil species changed dietary habits as excessive amounts of dental wear accumulated (e.g., stagodontid metatherians; Fox and Naylor, 1995, 2006)—we assumed that unworn teeth would most accurately reflect the average lifetime dietary ecologies of both the extant and fossil taxa sampled here. We did not include in our sample any extant mammal

species with teeth that have, to our knowledge, secondary wear-induced functionality. Specimens with cusps missing due to breakage were also excluded.

4.6.4 Dietary categories

Each extant species in our dataset was classified into one of six dietary categories: carnivory (carn), animal-dominated omnivory (ado), plant-dominated omnivory (pdo), frugivory (frug), insectivory (ins), or soft-insect specialists (sis) (Table 4.1). We chose to include six dietary categories because it avoids the oversimplification and loss of information that studies are subjected to when using the classic three-diet classification of carnivory, omnivory, and herbivory (Pineda-Munoz and Alroy, 2014). Following Pineda-Munoz and Alroy (2014), we classified diets of each species, with emphasis on its primary food resource. A species was classified as a specialist (i.e., non-omnivore) if one food resource makes up 50% or more of its total diet. We used online archives of diet information (e.g., EltonTraits [Wilman et al., 2014] and Mammal DIET [Kissling et al., 2014]) supplemented by the primary literature and natural history compendia (Nowak, 1999) when species-level information was extrapolated from genus-level information in the online archives (see Kissling et al., 2014; Table 4.1).

We acknowledge that our decision to use six dietary categories rather than the classic 'carnivore-omnivore-herbivore' trophic classification could lead to greater overlap of categories in the morphospace and less power to predict diet. Also, note that we classified the feeding behavior of some extant taxa in our sample differently than previous studies have. For example, *Nasua narica* (white-nosed coati) is known to eat insects, but it is strictly frugivorous when fruit is available (e.g., Nowak, 1999). Although some studies classified its diet as plant-dominated omnivory (Smith, 2017), we followed EltonTraits, which records its diet as 70% fruit, and

considered this taxon a frugivore. We recognize that in this and any large-scale study of mammalian feeding behaviors, decisions that are made to distill the complexities of dietary data into discrete categories have an impact on the results.

4.6.5 Fossil sampling

We sampled 71 isolated upper molars of 42 species (22 genera; six major clades) of North American Late Cretaceous (NALK) metatherians from the Western Interior region (Table 4.2). Our sample includes two stagodontids, one deltatheriid, two glasbiids, eight pediomyids, six taxa classified as *incertae sedis*, four herpetotheriids, and 19 alphadontids. To increase our taxonomic sampling of Cretaceous metatherians, we substituted the M2 (which tends to be morphologically very similar to the M3) for some species that did not have an available M3, and we used upper molar specimens of uncertain position (i.e., "Mx") for some species that did not have definitive M2 or M3 specimens available (see Table 4.2 for details). Our sample includes 62% of the known species of NALK metatherians (42 of 68 known species; Case et al., 2005; Williamson et al., 2014; Cohen, 2018; Cohen et al., 2020). Some species were omitted from our sample for the lack of either a well-preserved upper molar in the fossil record or the availability of an appropriate specimen for loan; in particular, our sampling of deltatheriids and stagodontids is limited. We estimate that the absence of some of these taxa in our analyses artificially reduced the morphological disparity values and the occupied regions of the morphospace (e.g., *Nanocuris* has been interpreted as a specialized carnivore), especially during the pre-Aquilan and Lancian time bins (see below); whereas the absence of other taxa likely had a negligible effect on the results because their morphologies are approximated by other sampled taxa (e.g., the absence of

the pediomyid genus *Aquiladelphis* is likely accounted for by the pediomyid genera in our sample).

We assigned each fossil species in our sample to one (or more) of our four time bins depending on the known temporal range of each species (Williamson et al., 2014), using a range-through approach. Three of our bins are Cretaceous NALMAs (Woodburne, 2004): Aquilan (ca. 86–79 Ma), Judithian (79–69 Ma), and Lancian (69–66 Ma). We binned the eight specimens from geologic units that pre-date the Aquilan NALMA, into a "pre-Aquilan" time bin (ca.126–86 Ma). Most taxa that we assigned to the pre-Aquilan time bin are from 100–86 Ma, but we also include *Atokatheridium*, which has a range of ca. 126–100 Ma. Because the "Edmontonian" NALMA is poorly characterized and not well sampled (Cifelli et al., 2004), we lumped the "Edmontonian" taxa into the Judithian bin. We recognize that these time bins are uneven in duration and that the longer duration bins could artificially inflate measures of disparity and diversity; however, we were unable to more finely and precisely bin our data due to uneven sample sizes across time bins and the lack of high-precision ages for certain geologic units.

4.6.6 3D data collection

Three-dimensional digital models of the sampled teeth were created using micro-computed tomography (μCT) scan data. We scanned original specimens of teeth, molds of teeth, and epoxy casts of teeth (Tables 4.1–4.2). López-Torres et al. (2017) found that OPCR values of epoxy casts tend to be higher than those from their original specimens, due to potential for artificially rougher surfaces on the casts (both DNE and RFI are more robust to this effect). Thus, we interpret OPCR results for the relatively few casts in our sample (15 of 71 specimens) with caution. Specimens were scanned using either a Bruker Skyscan 1172, Skyscan 1173, or NSI

X5000 scanner—all of which are housed on the University of Washington campuses. We also downloaded image stacks (TIFF format) of scan data for eight extant specimens (Table 4.1) from MorphoSource (morphosource.org) to bolster our modern comparative dataset (4.14: Appendix 1). For detailed information regarding scanner types and scan settings, see 4.14: Appendix 2. Molds of extant teeth were made using Coltene President Plus polyvinylsiloxane (type 2, medium consistency), and epoxy casts were collected from the UWBM, University of California Museum of Paleontology, and Sam Noble Oklahoma Museum of Natural History collections. For specimens scanned with Bruker Skyscan scanners, scan data were reconstructed using NRecon (Bruker microCT, Belgium); scans completed using the NSI X5000 were reconstructed using efX Reconstruction (North Star Imaging, Inc.). We segmented raw scan data using Avizo Lite 9.2.0 (Thermo Fisher Scientific). We then removed artifacts ("cleaning"), cropped, and oriented tooth models using GeoMagic Studio (3DS Systems). Specimen models were cropped to include the entire enamel cap (EEC cropping method; see Berthaume et al., 2019 for details) and oriented such that the occlusal plane is perpendicular to the Z-axis. We exported the cleaned and oriented 3D tooth models from GeoMagic Studio as PLY files. These PLY files were imported back into Avizo Lite 9.2.0, and the 3D tooth models were simplified to 20,000 faces using the Simplification Editor tool. We then used the "Remesh Surface" function to downsample the tooth models to ~10,000 faces. The remesh function was used because it reduces the chance that surfaces with extremely disparate polygon mesh face-sizes are produced during simplification (Spradley, personal comm., 2018). We then used the "Smooth Surface" function with 25 iterations and lambda = 0.6 (Spradley et al., 2017; Spradley, personal comm., 2018). Because the consistency of model creation and processing is extremely important for producing comparable DTA results (Spradley et al., 2017; Berthamue et al., 2019), we used the same workflow for the

creation of all models in this study. The resulting smoothed tooth models were saved as PLY files and used in our DTA analyses.

4.6.7 Dental topographic analyses (DTA)

We computed RFI, DNE, and OPCR for all 3D tooth models using the molaR_Batch function from the package molaR, version 4.2 (Pampush et al., 2016), in R version 3.3.3 (R Core Team, 2017). RFI is the ratio between the 3D surface area of a tooth crown and the 2D "footprint" area of a tooth (Ungar and M'Kirera, 2003). We use a modified version of this ratio in which the entire tooth crown is more accurately taken into account (Boyer, 2008). The modified RFI calculation is: $RFI = \ln(\frac{\sqrt{A3D}}{\sqrt{A2D}})$ (A3D = 3D embedded surface area of the tooth crown, A2D = 2D tooth crown footprint area in occlusal view; Boyer, 2008; López- Torres et al., 2017). DNE represents the curvature of the tooth crown by calculating the sum energy values across the entire occlusal surface (Bunn et al., 2011; Winchester et al., 2014; Winchester, 2016). OPCR measures tooth crown complexity by calculating the total number of patches, or "tools", on the crown of a tooth. A patch is a contiguous group of pixels that face the same cardinal direction on the tooth model (Evans et al., 2007; Evans and Jernvall, 2009; Wilson et al., 2012). Parameters for each metric were set as follows: RFI—alpha = 0.15; DNE—boundary discard = "Vertex"; and OPCR—step size = 8 and minimum patch size = 3 pixels (Evans et al., 2007; Pampush et al., 2016; Smith, 2017; Spradley, 2017). We ran a second DTA with the OPCR minimum patch size = 5 pixels to minimize any "noise" that might artificially inflate values for our extant and fossil samples, which include molds and casts, respectively (Winchester, 2016; López- Torres et al., 2017).

We log-transformed our DTA data to reduce skew. We generated scatter biplots of all possible combinations of the dental metrics to visualize morphospace occupation of extant dietary groups. We then plotted our fossil metatherian DTA values within the same morphospace of the extant dataset to examine both how fossil morphospace occupation compared to extant mammal morphospace occupation and how fossil morphospace occupation changed through time. We also tested for correlation between our DTA metrics by calculating Spearman's rho and using least-squares linear regressions.

4.6.8 Dietary inference

To quantitatively infer diet in our sample of fossil metatherians, we conducted a discriminant function analysis (DFA) using the function lda() from the package MASS (Venables and Ripley, 2002). We first used the extant comparative dataset and a leave-one-out cross validation to assess the accuracy of discriminant functions in predicting diet (see MASS package documentation for more information). We then applied this DFA to the fossil metatherian DTA data (with fossils treated as having unknown diets). In a second permutation, we conducted a DFA on the extant comparative dataset using both the DTA data and mean body mass (compiled from the primary literature) to see if we could significantly improve the discriminatory power of our model (Winchester et al., 2014). Because the resulting accuracy did not significantly improve discrimination, we only report the results from the first permutation. For fossil species that had more than one sampled specimen, we summed the posterior probabilities of each dietary category across all specimens and assigned the taxon to the dietary category with the highest sum value.

4.6.9 Dental disparity

We calculated morphological disparity in our sample of fossil metatherians as: i) intra-family disparity and ii) total disparity per time bin. We did not calculate the intra-family disparity per time bin because sample sizes were too small. All disparity calculations used mean species values of each standardized, log-transformed DTA metric. We measured disparity as both the variance of each DTA metric and the sum of variances (Ciampaglio et al., 2001) using the morphol.disparity function in the geomorph package in R (Adams et al., 2020), which calculates a simulation-based *p*-value for statistical comparison between groups (i.e., between families or between time bins). We generated 95% confidence intervals using a custom bootstrapping function in R with 1,000 replicates.

4.6.10 Phylogenetic signal

We tested for phylogenetic signal in the DTA results of our extant comparative dataset using a phylogenetic tree that we generated from timetree.org (Kumar et al., 2017). We calculated Blomberg's K (Blomberg et al., 2003) and Pagel's lambda (Pagel, 1992) using the phylosig function in the package phytools in R (Revell, 2012). We did not test for phylogenetic signal in the DTA results of our fossil taxa because the most recent species-level phylogeny that includes all of the fossil taxa in our sample (Williamson et al., 2014) is highly unresolved with a large polytomy.

4.7 RESULTS

4.7.1 Phylogenetic signal

Only OPCR shows a significant phylogenetic signal (Table 4.3); both DNE and RFI have a moderate but insignificant phylogenetic signal ($p > 0.05$ for Blomberg's K and Pagel's lambda for both). The detected phylogenetic signal is likely due to the inclusion in our extant dataset of many species of Didelphimorphia, which have molars of similar gross tooth morphology despite differing in dietary ecologies. Spradley (2017) also noted this gross morphological similarity among didelphimorphians molars but still found them to be informative extant analogs for inferring dietary habits of fossil taxa.

4.7.2 Dental topographic analyses

In our extant dataset, DNE values are positively correlated with both RFI and OPCR values (Table 4.4), which is consistent with the results of Spradley (2017). The dietary patterns for raw DNE data and the raw RFI data are more similar to each other than they are for the raw OPCR data (Figure 4.2; 4.14: Appendix 3). In both DNE and RFI, mean values are highest in insectivores and soft-insect specialists, which seems to be driving the correlation between these dental metrics. The other dietary categories have overlapping DNE ranges, with the exception of carnivores that have the lowest mean DNE values (Figure 4.2).

The RFI values are only correlated with the DNE values. Mean RFI is lowest in frugivores and highest in soft-insect specialists. Mean RFI generally increases with the percentage of animal material in the diet; however, we did not include folivores in our sample which are known to also have high RFI values (e.g., Boyer, 2008; Winchester, 2014).

Insectivores and soft-insect specialists have the highest mean RFI values, which is consistent with the tall, pointy cusps on their crowns (Figure 4.2).

The pattern of OPCR values is not as clear as those of the two other DTA metrics, and the ranges of values for most dietary categories overlap. Mean OPCR is lowest in carnivores, as in other studies (Figure 4.2; Evans et al., 2007; Spradley, 2017) and highest in insectivores (Bunn et al., 2011), which contrasts with most studies in which frugivores typically have the highest OPCR (e.g., Santana et al., 2010; Pineda-Munoz et al., 2017). It appears that OPCR is most useful in distinguishing carnivory from other dietary categories.

In our fossil dataset, the most densely sampled clades (alphadontids, pediomyids, and herpetotheriids) have similar mean values and ranges for all three metrics. Mean DNE values of the fossil clades are similar to soft-insect specialists, but their DNE ranges overlap with insectivores as well (Figure 4.2; 4.14: Appendix 4). Fossil clade RFI ranges are not as large as DNE or OPCR ranges, and they overlap mostly with insectivore and soft-insect specialists. However, fossil clade RFI values also slightly overlap with extant carnivores. The OPCR ranges of the fossil clades overlap with ranges of almost all of the dietary categories, except carnivores.

4.7.3 Morphospace occupation

In the bivariate scatterplots and the 3D scatterplot of the log-transformed DTA values of our extant sample, there is moderate separation between some dietary categories (Figure 4.3). Carnivores, with a combination of low DNE and OPCR values and wide range of RFI values, form a loose cluster that is mostly segregated from other groups, although some specimens overlap with plant-dominated omnivores and frugivores. Plant-dominated omnivores and animal-dominated omnivores largely overlap with each other, with intermediate values of all three dental

topography metrics—we explore the effects of this overlap among the omnivore categories on our DFA (see below). Insectivores and soft-insect specialists, with high DNE and RFI values and mid-range OPCR values, occupy similar regions of the morphospace. Frugivores largely overlap with the two omnivore categories but segregate on the basis of generally lower RFI values and some higher OPCR values. Consistent with other DTA studies (e.g., Smith, 2017), some areas of the morphospace are unoccupied, including the region with low DNE, high OPCR, and high RFI values and the region with high DNE, low OPCR, and low RFI values.

The NALK metatherians occupy a more restricted region of the morphospace than the extant sample does (Figure 4.4). Most NALK metatherian taxa have mid to high OPCR values, mid to high RFI values, and high DNE values and accordingly overlap with extant insectivores and soft-insect specialists in the morphospace. A smaller proportion plot in the morphospace occupied by plant-dominated and animal-dominated omnivores. The specimens of *Glasbius* have mid-range DNE, OPCR, and RFI values and thus fall among plant-dominated omnivores and frugivores. The two specimens of *Didelphodon vorax* plot in regions occupied by the extant animal-dominated omnivores and insectivores. *Iugomortiferum thoringtoni* and *Dakotadens morrowi* plot away from the main cluster of NALK metatherians near the edge of the omnivore-carnivore region of the morphospace.

4.7.4 Discriminant function analysis (DFA)

The DFA correctly classified the diets of 58.9% (33 of 56) of the extant specimens (Table 4.5). Animal-dominated omnivores were most frequently misclassified (11 of 23 misclassifications; 48%) as either frugivores, insectivores, or plant-dominated omnivores (Table 4.5). Frugivores and carnivores were misclassified at the next highest rates (40% and 33.3%,

respectively). For many of the incorrectly classified specimens (14 of 23), their DFA-predicted diet had a low posterior probability (< 0.50) that was often only slightly higher than the posterior probability for their true diet (Table 4.6).

Our DFA predicted the diets of the fossil taxa with about the same certainty as extant taxa, with 35.2% of fossil specimens classified with posterior probabilities > 0.60 for their predicted diet (Table 4.7; 33.9% of extant specimens had posterior probabilities of > 0.60, of which three specimens were misclassified). Almost all of the fossil specimens classified with posterior probabilities > 0.60 were classified as insectivores. Of the 41 fossil species sampled here, 20 species had more than one specimen sampled; ten species with more than one specimen sampled were classified with two different diets by the DFA. Classifications for these species mostly overlap between insectivores, soft-insect specialists, and plant-dominated omnivores (Table 4.7). Of the total 71 fossil specimens sampled, 46.5% were classified as insectivores, 28.2% were classified as soft-insect specialists, and 22.5% were classified as plant-dominated omnivores. One specimen of *Didelphodon vorax* was classified as an animal-dominated omnivore. *Iugomortiferum thoringtoni* was identified as the sole carnivore in the sample (although we urge caution about this assignment, see discussion below), and no frugivores were identified. The only deltatheriid, a specimen of *Atokatheridium boreni*, was identified as a soft-insect specialist, and all four glasbiid specimens sampled were identified as plant-dominated omnivores. The DFA that used the OPCR data with a minimum patch count = 5 (rather than 3) (4.14: Appendix 5; Winchester, 2016; López- Torres et al., 2017) was slightly less accurate than our original DFA (OPCR minimum patch count = 3). The second DFA correctly classified 57.1% of the extant specimens whereas the original DFA correctly classified 58.9% of the extant specimens. We compared the diet predictions between the two DFAs for both extant and fossil

taxa and found minimal differences (Tables 4.6–4.7; 4.14: Appendix 5). Hereafter, we focus only on the results of the analyses of the first DFA (OPCR minimum patch count = 3).

4.7.5 NALK metatherian dental disparity and diet diversity through time

Metatherian dental disparity, as calculated by the variance of each DTA metric and the sum of variances, does not significantly change throughout the Late Cretaceous (Figure 4.5; Table 4.8). The lnDNE, lnOPCR, and sum of variance values decrease from the Aquilan to Lancian bins, but in most cases these changes were not significant (Table 4.8). The dental disparity values of alphadontids are greater than the corresponding values of pediomyids, but again the differences are not statistically significant, except for lnDNE.

Our DFA results suggest that the diversity of diets among NALK metatherians differs through the Late Cretaceous. Insectivores, soft-insect specialists, and plant-dominated omnivores occur in all four Cretaceous time bins but in variable proportions (Table 4.9). The patterns of dietary category count and relative abundance are generally congruent before and after interpretation adjustments, but we focus here on the raw values and relative abundances of diet categories after taking previous interpretations and other posterior probabilities into account (Table 4.9; see discussion of dietary interpretations below). The raw number of plant-dominated omnivore species does not vary much across time bins (from one to three), but their relative abundance is high in the pre-Aquilan and low from the Aquilan through Lancian. The number of insectivore species is high in the Aquilan and younger Late Cretaceous time bins; likewise, their relative abundance (75%) is very high in the Aquilan but slightly lower thereafter. The number of soft-insect specialists is low until the Judithian time bin, and their relative abundance follows

a similar pattern. The only animal-dominated omnivore, *Didelphodon vorax*, occurs in the Lancian time bin and has the lowest relative abundance of all diet categories.

4.8 DISCUSSION

North American metatherians reached substantial taxonomic diversity during the Late Cretaceous (Williamson et al., 2014; Bennet et al., 2018). However, there is uncertainty surrounding the dietary diversity and ecomorphological patterns of NALK metatherians. It has been hypothesized that the novel food sources and habitats that arose with the angiosperm ecological diversification in the late Late Cretaceous (starting ca. 85–80 Ma) catalyzed an ecomorphological diversification (e.g., Grossnickle et al., 2019) and possibly a taxonomic diversification (Williamson et al., 2014; Wilson et al., 2016) of metatherians and additional mammal groups (e.g., Wilson et al., 2012; Grossnickle and Newham, 2016). Others contend that most mammalian clades, including metatherians, remained ecomorphologically constrained until the extinction of non-avian dinosaurs at the K-Pg boundary (e.g., Alroy, 1999). Below, we discuss the results of our dental topographic analyses (DTA) and how they and associated disparity measures, ecomorphospace plots, and dietary inferences shed light on those differing viewpoints of the evolutionary ecology of NALK metatherians.

4.8.1 Extant mammal DTA metrics and DFA performance

Dental topographic analyses are still relatively new, having only been applied for the last 15 years, and few DTA studies have utilized upper molars (Santana et al., 2011; Smits and Evans, 2012; Pineda-Munoz et al., 2017). Our study provides a test of the validity and utility of applying those DTA methods to isolated upper molars and a predominantly marsupial sample,

and our results are mostly congruent with previous studies on lower molars. Both types of insectivores in our extant sample (i.e., 'insectivores' and 'soft-insect specialists') show characteristically high RFI and high DNE values (Figure 4.2; Boyer, 2008; Bunn et al., 2011; Winchester et al., 2014; López-Torres et al., 2017; Smith, 2017; Spradley, 2017), reflecting the tall, sharp cusps and high shearing-crest-lengths used to puncture insect carapaces and shear soft-bodied insects (Strait, 1993, 1997). Omnivores plot in the middle of the morphospace with low to mid-range values for DNE and mid-range values for RFI and OPCR, which is consistent with lower DTA values of lower molars in Boyer (2008), Bunn et al. (2001), Winchester et al. (2014), López-Torres et al. (2017), and Smith (2017). The intermediate values of omnivores reflect a morphology that is adapted to process a wide variety of food materials through a balance of shearing, crushing, and grinding (Ungar, 2010). The general congruence of our results from upper molars and others' results from lower molars and the separation of diets via the DTA metrics lend support to the use of upper molars in ecomorphological analyses on fossils of unknown diets.

Some of our DTA results differ from those of previous studies. Although the low OPCR values and low to mid-range RFI values of our extant carnivore sample are consistent with other studies (Figure 4.2; Evans et al., 2007; Evans and Jernvall, 2009; Pineda-Munoz et al., 2016; Smith, 2017), the relatively low DNE values of our carnivores are more similar to the values of hard-object feeders in other studies (Bunn et al., 2011; Winchester et al., 2014; Smith, 2017). Although this discrepancy could reflect different DTA patterns in upper and lower molars, we believe that this discrepancy is likely due to the idiosyncrasies of our carnivore sample. Two of the six carnivore taxa (*Crocuta crocuta*, the spotted hyena and *Sarcophilus harrisii*, the Tasmanian devil) are known for their bone-cracking/durophagous habits (e.g., Werdelin, 1989;

Wroe et al., 2005), and another taxon (*Eira barbara*, the tayra) supplements its carnivorous diet with fruit and honey (Bisbal, 1986), which may be skewing our carnivore results. Increasing the sampling of hypercarnivorous taxa may add clarity to DTA patterns for carnivores and subsequent DFA carnivore classifications. Additionally, the DNE and OPCR values of our frugivore sample differ from those of previous studies: they are slightly higher and more variable (Bunn et al., 2011; Winchester et al., 2014). This discrepancy also likely reflects differences in taxon sampling. Whereas previous studies heavily sample primate frugivores, our sample includes one primate and four other taxa from Chiroptera, Carnivora, and Cetartiodactyla. Most of these other taxa incorporate small amounts of foods besides fruit into their diet (e.g., *Pecari tajacu*, the collared peccary, incorporates roots, insects, and small vertebrates in addition to fruit [Nowak, 1999; Desbiez et al., 2009]). The higher DNE and OPCR values in our frugivore sample may reflect dental adaptations, such as rugosities, for processing these other food materials (Santana et al., 2011; Smith, 2017), or other specialized features for processing poorly documented fallback foods (food consumed less often but are critical for survival during times of environmental stress)—an example of Liem's paradox (e.g., Ungar, 2010).

Among the diet categories, our DFA had the highest success rate in correctly classifying insectivores and soft-insect specialists in our extant sample (Table 4.5). All misclassified insectivore specimens were classified as soft-insect specialists and vice versa. In contrast, our DFA did not as reliably predict animal-dominated omnivores, which included specimens misclassified as frugivores, plant-dominated omnivores, and one as an insectivore. Frugivores had two specimens classified as plant-dominated omnivores, one specimen misclassified as a carnivore, and one specimen misclassified as an animal-dominated omnivore, whereas plant-dominated omnivores had one specimen misclassified as an animal-dominated omnivore and one

specimen misclassified as a frugivore. Often the true diet had the second highest posterior probability. These misclassifications likely stem in part from the overlap in DTA ranges and, in turn, morphospace occupation among these dietary categories (Figures 4.2–4.3), which perhaps reflects similar dental adaptations among the animals in our extant sample, the incomplete dietary data available, or the imperfect nature of the diet categorizations.

We also note that there were nine instances in which two specimens of the same species were classified into different dietary categories by the DFA, and multiple fossil species also have specimens that were classified differently (Tables 4.6–4.7). In most of these cases (seven out of nine), there were very slight differences in wear among the specimens, which may have led to the different dietary assignments. In the other two cases, there were no apparent differences in the amount of wear between the specimens of the same species. However, in both of those cases, one specimen was classified as an insectivore and the other as a soft-insect specialist. The degree of overlap in morphospace between these two insect-eating diets illustrates the difficulty in distinguishing them (Figure 4.3). This intraspecific variation in diet assignment implies that studies should, whenever possible, attempt to account for this variation by sampling more than one specimen per species and by controlling for wear across taxa; it also highlights the need for further standardization and ground truthing DTA methods.

4.8.2 Dietary inferences and dietary diversity of NALK metatherians

Although most Mesozoic mammals have conventionally been portrayed as small-bodied, terrestrial insectivores (e.g., Van Valen and Sloan, 1977; Kielan-Jaworowska et al., 2004), recent fossil discoveries and ecomorphological analyses have provided counterexamples, both among non-therians and therians, implying a much broader range of ecologies (e.g., Luo, 2007; Wilson

et al., 2012; Grossnickle and Polly, 2013; Chen et al., 2019). Our quantitative study of dental ecomorphology in part reinforces the conventional view by reconstructing most NALK metatherians (81%, 34 of 42 species) as either insectivores or soft-insect specialists (Tables 4.7, 4.9; Figure 4.6). These results are consistent with previous inferences from other studies (Gordon, 2003; Wilson, 2013; Williamson et al., 2014; Grossnickle and Newham, 2016) and with the observation that the most taxonomically rich families of Cretaceous metatherians (e.g., alphadontids and pediomyids) have conservative tribosphenic molar morphologies. Nevertheless, our DFA diet reconstructions predicted that a few NALK metatherians had diets beyond insectivory, indicating that NALK metatherians as a whole achieved greater dietary diversity than is conventionally portrayed. For example, our DFA reconstructed *Glasbius* as a plant-dominated omnivore, a prediction that is in line with previous interpretations that this taxon was either herbivorous or frugivorous (Clemens, 1966, 1979; Gordon, 2003; Kielan-Jaworowska et al., 2004; Wilson, 2013; Williamson et al., 2014). Overall, we see evidence of the following diets in NALK metatherians: insectivory, carnivory, animal- and plant-dominated omnivory (including durophagy), and likely frugivory.

We also found that the dietary predictions for several taxa in our study conflicted with diet inferences from previous studies. To provisionally resolve each discrepancy until additional analyses can be undertaken, we considered the diet classification with the second highest posterior probability in our DFA. When that diet category agreed with the interpretations from primary literature, we revised our initial dietary inferences. Below we explain our decisions on these taxa and these decisions are summarized here: (i) *Iugomortiferum thoringtoni* as a plant-dominated omnivore, (ii) *Apistodon exiguus* as an insectivore, (iii) *Alphadon halleyi*, *Alphadon*

wilsoni, and *Protalphadon foxi* as soft-insect specialists; and (iv) *Didelphodon vorax* as an animal-dominated omnivore.

Seven taxa (*Pariadens kirklandi*, *Eoalphadon lillegraveni*, *Apistodon exiguus*, *Alphadon halleyi*, *Alphadon wilsoni*, *Turgidodon lillegraveni*, *Protalphadon foxi*) were reconstructed as plant-dominated omnivores. Qualitatively, most of these taxa lack most of the morphological features (e.g., large talonid basin, large protocone, bunodont cusps) characteristic of the crushing and grinding function necessary for most plant-based diets. Instead, most of these taxa have the conservative tribosphenic molar morphology (e.g., sharp shearing crests and unexpanded protocones) that is typically found among insectivores (e.g., Cifelli, 1990; Johanson, 1996; Davis, 2007; Williamson et al., 2014; Cohen, 2018). Such discrepancies between our diet reconstruction and those from previous studies are expected, considering the difficulty that the DFA model had in correctly predicting animal-dominated omnivory, and to a lesser extent, plant-dominated omnivory, frugivory, and carnivory. We provisionally accept the plant-dominated omnivore interpretation for *Pariadens kirklandi*, *Eoalphadon lillegraveni*, and *Turgidodon lillegraveni*. The second highest posterior probabilities for these taxa were for the animal-dominated omnivore category, and posterior probabilities of other dietary categories were much lower (Table 4.7). Conversely, we modify the DFA diet reconstructions for *Apistodon exiguus*, *Alphadon halleyi*, *Alphadon wilsoni*, and *Protalphadon foxi*. We interpret *Apistodon exiguus* as an insectivore, which is consistent with its very small size, previous interpretations of its gross dental morphology (Williamson et al., 2014), and with insectivory having the second highest posterior probability for this taxon in our DFA. We interpret both *Alphadon halleyi* and *Alphadon wilsoni* as soft-insect specialists, in line with analyses of the jaw morphology (Grossnickle and Polly, 2013; Brannick and Wilson, 2020; Morales-García et al., 2021), gross

dental morphology (Gordon, 2003; Wilson, 2013; Grossnickle and Newham, 2016), and that this dietary category had the second highest posterior probability for both of these species in our DFA. Finally, we re-classify *P. foxi* as a soft-insect specialist, which is its dietary classification in a similar DTA study on lower molars (Smith, 2017) and the diet with the second highest posterior probability (within 0.10 of the highest posterior probability) in our DFA.

Our DFA reconstructed the relatively large-bodied *Didelphodon* as an insectivore overall (based on the total posterior probabilities of the two *D. vorax* specimens); however, this conflicts with previous interpretations that it was a predator-scavenger with durophagous capabilities (Clemens, 1966, 1968, 1979; Fox and Naylor, 1986, 2006; Wilson et al., 2016; Brannick and Wilson, 2020) or an omnivore as indicated by dental microwear (Wilson et al., 2016). One possible explanation for this discrepancy is that we used relatively unworn teeth (earlier ontogenetic wear stage) of *Didelphodon* in our analysis. It has been hypothesized that *Didelphodon* and other stagodontids experienced an ontogenetic shift in diet that tracks body size (Fox and Naylor, 1995, 2006; Peng et al., 2017). Younger individuals show more faunivorous adaptations (e.g., molars with enhanced postvallum/prevallid shear and dentary shapes more capable of withstanding dorsoventral bending forces), whereas older individuals show more indications of omnivory/durophagy (e.g., horizontally worn grinding platforms and dentary shapes more capable of withstanding mediolateral forces; Fox and Naylor, 1995, 2006; Peng et al., 2017; Brannick and Wilson, 2020). Moreover, having analyzed only molar morphology, we have in some cases overlooked critical dietary data from other tooth positions (Wilson, 2013; Smith, 2017). *Didelphodon* has highly distinctive bulbous premolars that are well suited for crushing hard objects, like bone and shells (Clemens, 1966; Fox and Naylor, 1995, 2006; Wilson et al., 2016; Cohen, 2018). Additionally, it is important to note that one of the two specimens of

Didelphodon analyzed here was individually reconstructed as an animal-dominated omnivore by our DTA (Table 4.7). Taking all of these points and previous interpretations into account in conjunction with the second highest posterior probability in our DFA for *Didelphodon* overall, we re-classify *D. vorax* as an animal-dominated omnivore. We also suggest that future studies more deeply explore potential biases by comparing dietary inferences from DTA on a single tooth position to those from larger functional units like cheek tooth rows (Evans et al., 2007; Wilson et al., 2012). Another productive line of inquiry for other taxa would be to compare dietary inferences from DTA to those from other quantitative methods that are independent of gross morphology of teeth (e.g., microwear, isotopic analyses, mandibular bending strength), as has been done for *Didelphodon* (Wilson et al., 2016; Brannick and Wilson, 2020).

Although our DFA classified *Iugomortiferum thoringtoni* as a carnivore, this taxon has low-crowned molar morphology with inflated cusps and weakly developed conules (Cifelli, 1990), all of which is inconsistent with interpretation of carnivory (de Muizon and Lange-Badré, 1997). The DNE value of *I. thoringtoni* is within the range of extant carnivores, plant-dominated omnivores, and frugivores, whereas its RFI value is within the range of extant carnivores, plant-dominated omnivores, and insectivores. In contrast, its low OPCR value is within the range of extant carnivores and insectivores and is likely driving its DFA classification as a carnivore. The OPCR value of *I. thoringtoni* may be underestimated because we used an epoxy cast of the specimen (OMNH 20936) and the small size of the specimen might have amplified any infidelities of the cast (although see discussion of cast fidelity and OPCR values in López-Torres et al., 2017). Taking qualitative observations and previous interpretations into account, we use the second highest posterior probability from the DFA to classify *I. thoringtoni* as a plant-dominated omnivore.

4.8.3 Metatherian ecomorphology through the Late Cretaceous

By the beginning of the Late Cretaceous (ca. 100 Ma) metatherians in North America had diversified into at least four clades (Deltatheriidae, Stagodontidae, Aquiladelphidae, Alphadontidae, and possibly Glasbiidae, Pediomyidae, and Marsupialia were also present, see Wilson et al., 2016). This higher-level taxonomic diversification was associated with moderate dietary diversity—three of the six dietary categories that we recognize here (plant-dominated omnivory, insectivory, and soft-insect specialists; Figure 4.6; Tables 4.7, 4.9). Raw species richness peaked in the Judithian (32 recognized species) and stayed relatively high in the Lancian leading up to the K-Pg mass extinction (22 species), although this peak might shift earlier in time or flatten if we account for differential sampling intensity through the Late Cretaceous (e.g., Grossnickle and Newham, 2016; Cohen, 2018; Bennet et al., 2018; Cohen et al., 2020). Nevertheless, according to our results, dental morphological disparity did not significantly change throughout the Late Cretaceous and only in the Lancian did ecological diversity (number of diet categories) increase slightly to include animal-dominated omnivory (Figures 4.5–4.6). Indeed, over 80% of the taxa sampled (34 of 42) were either insectivores or soft-insect specialists (Table 4.9; Figure 4.6). A literal reading of our results would thus suggest that ecomorphological diversity and disparity did not track increases in taxonomic richness of NALK metatherians. This decoupled pattern may be a common phenomenon because it has also been found in other taxonomic groups, such as anomodont therapsids (Ruta et al., 2013), graptoloids (Bapst et al., 2012), and angiosperms (e.g., Wing and Boucher, 1998; Lupia et al., 1999). That said, we caution that additional sampling might change this pattern. We were unable to sample several important stagodontids, including the middle Turonian (pre-Aquilan) *Hoodootherium*, and

Fumodelphodon, the Aquilan through possibly "Edmontonian" *Eodelphis*, and Judithian and "Edmontonian" members of *Didelphodon*. These taxa, which have previously been interpretated as carnivores and animal-dominated omnivores (e.g., Scott and Fox, 2015; Cohen, 2018; Brannick and Wilson, 2020), would have likely pushed back the appearance of those diet categories and increased disparity values earlier in the Late Cretaceous. The Lancian deltatheriid *Nanocuris*, which has also been considered carnivorous on the basis of its distinctive, sectorial molars with carnassial notches (Fox et al., 2007; Wilson and Riedel, 2010), would have further added to the range of Lancian ecomorphologies and likely increased disparity values. We also did not sample the middle Turonian *Scalaridelphys* and Aquilan *Aquiladelphis*, respectively, both pediomyoids which have both been interpreted as plant-dominated omnivores (Cohen et al., 2020). Thus, we underscore that our results should be taken as minimum estimates both for the magnitude of dietary diversity and dental morphological disparity achieved by NALK metatherians and for when they achieved it.

The oldest known dental fossils of metatherians, which date ca. 110 Ma (Davis et al., 2008; Davis and Cifelli, 2011 and see Williamson et al., 2014; Bi et al., 2018 for discussion regarding *Sinodelphys szalayi* and the earliest eutherians), strongly suggest that insectivory was plesiomorphic for the clade (e.g., Williamson et al., 2014; Grossnickle and Newham, 2016). Our dietary inferences and published interpretations of taxa that we were not able to sample indicate that by the early Late Cretaceous (ca. 100 Ma) metatherians were exploiting other food sources beyond insects (Cohen, 2018; Cohen et al., 2020). Notably, the dietary shifts toward omnivory (plant-dominated and animal-dominated omnivory) and carnivory largely occurred in metatherian subclades other than the most taxonomically prolific clades (the Alphadontidae and Pediomyidae) (Figure 4.6). Plant-dominated omnivory first appeared by the late Cenomanian (ca.

96 Ma) in the Stagodontidae (*Pariadens kirklandi*) and possibly Aquiladelphidae (*Dakotadens morrowi*, see discussion of phylogenetic relationships in Cohen et al., 2020). Later in the middle Turonian, stagodontids began their more thorough exploration of the carnivore and animal-dominated omnivore regions of ecomorphospace, culminating in the Lancian with the relatively large-bodied, durophagous predator-scavenger *Didelphodon vorax*. Glasbiidae is another group that shows up in the fossil record only at the very end of the Cretaceous (last 300–500 ky; Wilson, 2005); this sister taxon to Pediomyidae has only two species (*Glasbius twitchelli* and *Glasbius intricatus*), but they are the most morphologically distinctive examples of plant-dominated omnivory-frugivory among NALK metatherians. Finally, deltatheroidans were likely the most carnivorous among the NALK metatherians—although some Albian–Aptian members had relatively larger talonids and less reduction of the metaconid, which are indicative of diets other than strict carnivory (Rougier et al., 2015)—and culminated in the highly specialized carnivore *Nanocuris* in the Lancian (Fox et al., 2007; Wilson and Riedel, 2010).

In contrast, the two most taxonomically rich clades of NALK metatherians, the Alphadontidae and Pediomyidae, show relatively little dietary diversity (Figure 4.6). Alphadontids originated by at least the Cenomanian (but probably earlier; Wilson et al., 2016) and peaked in taxonomic richness in the Judithian (15 species, including alphadontids not sampled here). The oldest known pediomyids are from the Santonian, but like alphadontids, probably originated earlier and reached their highest taxonomic richness in the Judithian (5 species, including pediomyids not sampled here) and sustained that level through the Lancian. Many of these alphadontid and pediomyid species were sympatric; for example, *Protalphadon lulli*, *Alphadon marshi*, *Alphadon wilsoni*, *Turgidodon rhaister*, *Pediomys elegans*, *Leptalestes cooki*, *Leptalestes krejcii*, *Protolambda florencae*, and *Protolambda hatcheri* are all found in the

Lance Formation (see Williamson et al., 2014 a tabulation of species occurrences per locality). Although previous studies have hypothesized that pediomyids had greater crushing and grinding capacity relative to other metatherian groups and, in turn, likely incorporated more plant material into their diets (Wilson, 2013; Cohen et al., 2020), our DFA shows that both pediomyids and alphadontids mainly fed on insects. Diet partitioning within the insectivore adaptive zone may help explain how alphadontids and pediomyids were able to maintain their tremendous taxonomic richness (e.g., eight species in the Hell Creek fauna) (Hardin, 1960). As more pediomyid taxa appear in the Judithian, alphadontids appear to experience a dietary shift from insectivory to soft-insect specialization, whereas pediomyids were mostly insectivores (Table 4.9; Figure 4.6). It is possible that further dietary differences, such as specialization for particular species of insects, drove the niche partitioning, but that level of diet specificity cannot be detected by the methods utilized here. Other potential explanations of niche or resource partitioning include spatial separation (using different habitats), temporal avoidance, or separation along an ecological axis different from diet, such locomotor mode or body size (e.g., Schoener, 1975; Keddy, 1989). For example, the two pediomyid species *Protolambda florencae* and *Pediomys elegans* are contemporaneous (Lance and Hell Creek faunas) and were both reconstructed by our DFA as insectivores. Resource partitioning may have occurred along the axis of body size (i.e., *P. florencae* is larger and so probably consumed larger insect than *Pediomys elegans*), which might have enabled these pediomyids to co-exist. However, these other potential ecological axes on which partitioning might have occurred are difficult to discern in this fossil record.

During the Late Cretaceous in North America, metatherians shared the ecospace with other mammalian groups, including eutriconodontans, multituberculates, spalacotherioids, and

their sister taxon eutherians. Among those groups, metatherians were arguably the most dietarily diverse, having occupied up to five categories: insectivory, carnivory, animal- and plant-dominated omnivory, and likely frugivory. It has been suggested that the non-tribosphenic dentitions of most non-therian mammals were more morphologically constrained than tribosphenic dentitions, and, consequently, non-therians attained less dietary diversity than therians did (Chen et al., 2019; but see Harper et al., 2019 on dryolestoids). For instance, spalacotherioids and eutriconodonts were likely restricted to insectivory and faunivory, respectively (Hu et al., 2005; Grossnickle and Polly, 2013; Chen et al., 2019; Morales-García et al., 2021).

Multituberculates were the most dietarily diverse non-therian mammal group. Their diets ranged from insectivory to animal- and plant-dominated omnivory, and by the late Late Cretaceous (ca. 84 Ma) even herbivory (Wilson et al., 2012; Grossnickle and Polly, 2013; Weaver et al., 2019). Still, metatherians probably had a broader dietary range than multituberculates and attained that diversity earlier in the Cretaceous. However, unlike multituberculates, metatherians did not continue to diversify in North America after the K-Pg mass extinction (Wilson, 2014; Williamson et al., 2014). The early eutherians, which include many lineages that retain the plesiomorphic tribosphenic molar morphology, were mostly insectivorous during the Late Cretaceous, although some of the larger-bodied taxa, such as *Altacreodus magnus* (formerly *Cimolestes magnus*), were likely faunivorous (e.g., Wilson, 2013; Grossnickle and Newham, 2016; Chen et al., 2019). Additionally, zhelestid (Harper, 2012; Gheerbrant and Astibia, 2012; Harper et al., 2019) and gypsonictopid eutherians (Crompton and Kielan-Jaworowska, 1978), which both first appear in North America in the Campanian, and the Lancian taeniodont *Schowalteria* (Fox and Naylor, 2003), are inferred to have included plant

material in their diets based on their tooth morphology. Archaic ungulates, which appear in the very latest Cretaceous but very rarely, and plesiadapiform primates, which have lineages that are believed to extend back into the Late Cretaceous, have both been interpreted as animal- and plant-dominated omnivores (e.g., Archibald et al., 2011; Fox and Scott, 2011; Wilson Mantilla et al., 2021). Whereas Late Cretaceous eutherians ranged from insectivory, faunivory, and animal- and plant-dominated omnivory, they were less dietarily diverse compared to contemporaneous metatherians and did not expand beyond insectivory until the Campanian (at least in North America; Harper, 2012; Harper et al., 2019), well after metatherians had.

Thus, our study does not exclusively support either the Suppression Hypothesis or the Early Rise Hypothesis. The Suppression Hypothesis predicts that the ecomorphological diversity (number of diets) and disparity (magnitude of morphological difference) in metatherians was low and stable throughout the Late Cretaceous. Whereas our quantitative results of dental disparity and ecomorphological diversity are consistent with this hypothesis— that is, dental disparity does not significantly change through the Late Cretaceous and most metatherians were insectivores and soft-insect specialists (Figure 4.6); we posit that inclusion of, for example, the middle Turonian stagodontids (*Fumodelphodon* and *Hoodootherium*) and aquiladelphids (*Scalaridelphys*) and the Lancian *Nanocuris* would likely increase dental disparity and diversity of dietary categories recorded for at least those intervals. Moreover, the ecomorphological diversity and disparity values are likely greater than those of other contemporary mammalian clades, which exhibit a smaller range of diets and dental morphologies.

The Early Rise Hypothesis predicts that rapid increases in ecomorphological diversity and disparity of metatherians began in the late Late Cretaceous. Although our DFA shows that metatherians were mostly insectivores and soft-insect specialists, it also shows that by the pre-

Aquilan—prior to the ecological radiation of angiosperms—they had begun to exploit other diets as well, including plant-dominated omnivory (Figures 4.6–4.7). Whereas dietary diversity and disparity were both stable throughout the Late Cretaceous, they were elevated relative to contemporary mammalian groups; we hypothesize that the diversification that produced this relatively high dietary diversity and dental disparity arose during the late Early Cretaceous. As such, we would suggest that the ecomorphological expansion of NA metatherians was not temporally correlated with the ecological rise of angiosperms but perhaps with their earlier taxonomic diversification (Cohen et al., 2020), which occurred during the Cretaceous Terrestrial Revolution (ca. 125–80 Ma). As new species of angiosperms appeared during their taxonomic diversification, they may have provided new food resources for metatherians to exploit, thus catalyzing the ecomorphological expansion of metatherians. Or perhaps other possible co-occurring factors during the Cretaceous Terrestrial Revolution, such as the extinction of eutriconodontans and spalacotherioids (Grossnickle and Polly, 2013; Cohen et al., 2020), allowed metatherians to expand into newly vacated niches. Future studies should test this hypothesis by applying DTA to samples of Early Cretaceous metatherians; however, to achieve this additional field work should be undertaken to bolster the sparse fossil record from this interval.

4.9 SUMMARY

Our study is the most comprehensive study to date to apply dental topographic analysis to a large sample of metatherian molars from the Late Cretaceous of North America. Our aim was to provide a more detailed, quantitative understanding of the macroevolutionary patterns of dental morphology and diet during the early history of this important clade. Although dietary

inferences from our DTA suggest that many NALK metatherians were insectivorous, the analyses also indicate that early metatherians exhibited a broad range of diets, including insectivory, soft-insect specialists, carnivory, animal- and plant-dominated omnivory, and likely frugivory. Our morphological disparity results show that dental disparity did not significantly increase in the Late Cretaceous. However, our results do not meet predictions of the Suppression Hypothesis (i.e., that mammalian ecological diversity was suppressed until the K-Pg mass extinction event), as our diet reconstructions and those from previous studies of taxa not sampled in our study show that NALK metatherians diversified into a wider range of dietary niches—more so than any other contemporary mammalian clade. We argue that relative to other mammalian clades, both dental disparity and dietary diversity of metatherians were moderately high and stable throughout the Late Cretaceous. Our results indicate a pre-K-Pg ecological diversification that is distinct from that predicted by the Early Rise Hypothesis because it began prior to the diversification of angiosperms and was more correlated in time with the Cretaceous Terrestrial Revolution and the mid-Cretaceous taxonomic diversification of angiosperms.

4.10 ACKNOWLEDGEMENTS

Special thanks to S. Smith and J. Spradley for guidance in implementing DTA methodology and J. Cohen and J. Case for helpful advice and communications regarding specimens. We also thank J. Calede, M. Chen, J. Claytor, and A. Magee for coding support. We thank L. Weaver, P. Wilson, J. Claytor, B. Hovatter, and M. Whitney for helpful feedback on the manuscript and B. Hovatter for scanning support. For access to specimens and help with specimen loans, we are grateful to S. Santana (UWBM), J. Bradley (UWBM), P. Holroyd (UCMP), W.A. Clemens (UCMP), R.L. Cifelli (OMNH), J. Larsen (OMNH), M. Caldwell (UALVP), H. Gibbins (UALVP), J. Gillette (MNA), D. Gillette (MNA), A. King (MNA), R. Irmis (UMNH), C. Levitt-Bussian (UMNH), E. Sargis (YPM), C. Norris (YPM), D. Brinkman (YPM), and M. Fox (YPM). We are grateful to S. Santana and A. Summers for access to μCT scanners on the UW campuses and K. Cohen, J. Huie, and K. Hall for scanner training and support. We also thank A. Kinahan for help with CT scan segmentation of extant specimens and MorphoSource.org, G.S. Yapuncich, D.M. Boyer, P. Whitmer, E. Delson, and J. Shi for allowing access to μCT scans of some of the extant mammal specimens used here. We are also grateful to the Paleontological Society N. Gary Lane Award and the UW Biology Department Walter and Margaret Sargent award for funding this research.

4.11 REFERENCES CITED

Adams, D.C., Collyer, M.L., and Kaliontzopoulou, A. 2020. Geomorph: software for geometric morphometric analyses. R package version 3.2.1.

Agosta, S.J. and Morton, D. 2003. Diet of the big brown bat, *Eptesicus fuscus*, from Pennsylvania and western Maryland. Northeastern Naturalist, 10(1):89-104

Alroy, J. 1999. The fossil record of North American mammals: evidence for a Paleocene evolutionary radiation. Systematic Biology, 48(1):107-118

Andersen, G.E., Johnson, C.N., Barmuta, L.A., and Jones, M.E. 2017. Dietary partitioning of Australia's two marsupial hypercarnivores, the Tasmanian devil and the spotted-tailed quoll, across their shared distributional range. PLoS ONE, 12(11): e0188529. https://doi.org/10.1371/journal. pone.0188529

Anderson, C.L., Bremer, K., and Friis, E.M. 2005. Dating phylogenetically basal eudicots using *rbcL* sequences and multiple fossil reference points. American Journal of Botany, 92(10):1737-1748

Archibald, D. 1983. Structure of the K-T mammal radiation in North America: speculations on turnover rates and tropic structure. Acta Palaeontologica Polonica, 28(1-2):7-17

Archibald, D. 2011. Extinction and Radiation: How the Fall of Dinosaurs Led to the Rise of Mammals. The Johns Hopkins University Press, Baltimore, Maryland

Archibald, J.D., Zhang, Y., Harper, T., and Cifelli, R.L. 2011. *Protungulatum*, confirmed Cretaceous occurrence of an otherwise Paleocene eutherian (placental?) mammal. Journal of Mammalian Evolution, 18:153-161

Atramentowicz, M. 1988. La frugivorie opportuniste de trios marsupiaux didelphidé de Guyane. Revue d'Écologie, 43:47-57

Averianov, A.O., Archibald, D., and Ekdale, E.G. 2010. New material of the Late Cretaceous Deltatheroidan mammal *Sulestes* from Uzbekistan and phylogenetic reassessment of the metatherian-eutherian dichotomy. Journal of Systematic Paleontology, 8(3):301-330. https://doi.org/10.1080/14772011003603499

Baker, R.H. and Baker, M.W. 1975. Montane habitat used by the spotted skunk (*Spilogale putorius*) in Mexico. Journal of Mammalogy, 56(3):671-673

Bapst, D.E., Bullock, P.C., Melchin, M.J., Sheets, H.D., and Mitchell, C.E. 2012. Graptoloid diversity and disparity became decoupled during the Ordovician mass extinction. PNAS, 109(9):3428-3433

Bartoszewicz, M., Okarma, H., Zalewski, A., and Szczęsna, J. 2008. Ecology of the raccoon (*Procyon lotor*) from western Poland. Annales Zoologici Fennici, 45:291-298

Belcher, C.A., Nelson, J.L., and Darrant, J.P. 2007. Diet of the tiger quoll (*Dasyurus maculatus*) in south-eastern Australia. Australian Journal of Zoology, 55:117-122

Bennet, C.V., Upchurch, P., Goin, F.J., and Goswami, A. 2018. Deep time diversity of metatherian mammals: implications for evolutionary history and fossil-record quality. Paleobiology, 44(2):171-198. https://doi.org/10.1017/pab.2017.34

Benson, R.B.J., Mannion, P.D., Butler, R.J., Upchurch, P., Goswami, A., and Evans, S.E. 2013. Cretaceous tetrapod fossil record sampling and faunal turnover: implications for biogeography and the rise of modern clades. Palaeogeography, Palaeoclimatology, Palaeoecology, 372:88-107. http://dx.doi.org/10.1016/j.palaeo.2012.10.028

Berthaume, M.A., Winchester, J., and Kupczik, K. 2019. Effects of cropping, smoothing, triangle count, and mesh resolution on 6 dental topographic metrics. PLoS ONE, 14(5):e0216229. https://doi.org/10.1371/journal.pone.0216229

Bi, S., Jin, X., Li, S., and Du, T. 2015. A new Cretaceous metatherian mammal from Henan, China. PeerJ, 3:e896. https://doi.org/10.7717/peerj.896

Bisbal, E J. 1986. Food habits of some Neotropical carnivores in Venezuela (Mammalia, Carnivora). Mammalia, 50:329-339

Blomberg, S.P., Garland Jr, T., and Ives, A.R. 2003. Testing for phylogenetic signal in comparative data: behavioral traits are more labile. Evolution, 57:717-745

Boyer, D.M. 2008. Relief index of second mandibular molars is a correlate of diet among prosimian primates and other euarchontan mammals. Journal of Human Evolution, 55:1118-1137. http://doi.org/10.1016/j.jhevol.2008.08.002

Boyer, D.M., Evans, A.R., and Jernvall, J. 2010. Evidence of dietary differentiation among Late Paleocene–Early Eocene plesiadapids (Mammalia, Primates). American Journal of Physical Anthropology, 142:194-210. https://doi.org/10.1002/ajpa.21211

Brannick, A.L. and Wilson, G.P. 2020. New specimens of the Late Cretaceous metatherian *Eodelphis* and the evolution of hard-object feeding in the Stagodontidae. Journal of Mammalian Evolution, 27:1-16. https://doi.org/10.1007/s10914-018-9451-z

Bunn, J.M. and Ungar, P.S. 2009. Dental topography and diets of four Old World monkey species. American Journal of Primatology, 71:466-477. https://doi.org/10.1002/ajp.20676

Bunn, J.M., Boyer, D.M., Lipman, Y., St. Clair, E.M., Jernvall, J., and Daubechies, I. 2011. Comparing Dirichlet normal surface energy of tooth crowns, a new technique of molar shape quantification for dietary inference, with previous methods in isolation and in

combination. American Journal of Physical Anthropology, 145:247-261. https://doi.org/10.1002/ajpa.21489

Cáceres, N.C. 2002. Food habits and seed dispersal by the white-eared opossum *Didelphis albiventris* in southern Brazil. Studies on Neotropical Fauna and Environment, *37*(2):97-104

Cantor, M., Ferreira, L.A., Silva, W.R., and Setz, E. Z.F. 2010. Potential seed dispersal by *Didelphis albiventris* (Marsupialia, Didelphidae) in highly disturbed environment. Biota Neotropica, 10(2):45-51

Carey, A.B., Colgan III, W., Trappe, J.M., and Molina, R. 2002. Effects of forest management on truffle abundance and squirrel diets. Northwest Science, 76(2):148-157

Case, J.A., Goin, F.J., and Woodburne, M.O. 2005. "South American" marsupials from the Late Cretaceous of North America and the origin of marsupial cohorts. Journal of Mammalian Evolution, 12(3-4):461-494. https://doi.org/10.1007/s10914-005-7329-3

Casella, J. and Cáceres, N.C. 2006. Diet of four small mammal species from Atlantic forest patches in South Brazil. Neotropical Biology and Conservation, 1(1):5-11

Charles-Dominique, P., Atramentowicz, M., Charles-Dominique, M., Gérard, H., Hladik, A., Hladik, C.M., and Prévost, M.F. 1981. Les mammiféres frugivorés arboricolés d'une foret Guyanaise: inter-relations plantes–animaux. Revue d'Écologie, 35:342-435

Chen, M., Strömberg, C.A.E., and Wilson, G.P. 2019. Assembly of modern mammal community structure driven by Late Cretaceous dental evolution, rise of flowering plants, and dinosaur demise. PNAS, 116(20):9931-9940. https://doi.org/10.1073/pnas.1820863116

Ciampaglio, C.N., Kemp, M., and McShea, D.W. 2001. Detecting changes in morphospace occupation patterns in the fossil record: characterization and analysis of measures of disparity. Paleobiology, 27(4):695-715

Cifelli, R.L. 2004. Marsupial mammals form the Albian–Cenomanian (Early–Late Cretaceous) boundary, Utah. Bulletin of the American Museum of Natural History, 285:62-79. http://dx.doi.org/10.1206/0003-0090(2004)285<0062:C>2.0.CO;2

Cifelli, R.L., Eberle, J.J., Lofgren, D.L., Lillegraven, J.A., and Clemens, W.A. 2004. Mammalian biochronology of the Late Cretaceous, p. 21-42. In Woodburne, M.O. (ed.), Late Cretaceous and Cenozoic Mammals of North America: Biostratigraphy and Geochronology. Columbia University Press, New York

Clemens, W.A. 1966. Fossil mammals of the type Lance Formation Wyoming. Part II. Marsupialia. University of California Publications in Geological Sciences, 62:1-122

Clemens, W.A. 1968. A mandible of *Didelphodon vorax* (Marsupialia, Mammalia). Los Angeles County Museum Contributions in Science, 133:1-11

Clemens, W.A. 1979. Marsupialia, p. 192-220. In Lillegraven, J.A., Kielan-Jaworowska, Z. and Clemens, W.A. (eds.), Mesozoic mammals: the First Two-Thirds of Mammalian History. University of California Press, Berkeley, California

Clotheir, R.R. 1955. Contribution to the life history of *Sorex vagrans* in Montana. Journal of Mammalogy, 36(2):214-221

Cohen, J.E. 2018. Earliest divergence of stagodontid (Mammalia: Marsupialiformes) feeding strategies from the Late Cretaceous (Turonian) of North America. Journal of Mammalian Evolution. https://doi.org/10.1007/s10914-017-9382-0

Cohen, J.E., Davis, B.M., and Cifelli, R.L. 2020. Geologically oldest Pediomyoidea (Mammalia, Marsupialiformes) from the Late Cretaceous of North America, with implications for taxonomy and diet of earliest Late Cretaceous mammals. Journal of Vertebrate Paleontology. https://doi.org/10.1080/02724634.2020.1835935

Cooper, S.M., Holekamp, K.E., and Smale, L. 1999. A seasonal feast: long-term analysis of feeding behaviour in the spotted hyaena (*Crocuta crocuta*). African Journal of Ecology, 37:149-160

Crabb, W.D. 1941. Food habits of the prairie spotted skunk in southeastern Iowa. Journal of Mammalogy, 22(4):349-364

Crifó, C., Currano, E.D., Baresch, A., and Jaramillo, C. 2014. Variations in angiosperm leaf vein density have implications for interpreting life form in the fossil record. Geology, 42(10):919-922

Crompton, A. W. and Kielan-Jaworowska, Z. 1978. Molar structure and occlusion in Cretaceous therian mammals, p.249-287. In Butler, P.M. and Joysey, K.A. (eds.), Studies in the Development, Function and Evolution of Teeth, Academic Press, New York

Davis, B.M. 2007. A revision of "pediomyid" marsupials from the Late Cretaceous of North America. Acta Palaeontologica Polonica, 52(2):217-256

Debelica, A., Matthews, A.K., and Ammerman, L.K. 2006. Dietary study of big free-tailed bats (*Nyctinomops macrotis*) in Big Bend National Park, Texas. The Southwestern Naturalist, 51(3):414-418

DeBey L.B. and Wilson, G.P. 2017. Mammalian distal humerus fossils from eastern Montana, USA with implications for the Cretaceous-Paleogene mass extinction and the adaptive

radiation of placentals. Palaeontologia Electronica 20.3.49A:1-92. https://doi.org/10.26879/694

De Carvalho, R.F., Passos, D.C., and Lessa, L.G. 2019. Diet variations in short-tailed opossum *Monodelphis domestica* (Didelphimorphia, Didelphidae) due to seasonal and intersexual factors. Mastozoología Neotropical, 26(2):340-348

Easterla, D.A. and Whitaker, Jr, J.O. 1972. Food habits of some bats from Big Bend National Park, Texas. Journal of Mammalogy, 53:887-890

Eriksson, O. 2016. Evolution of angiosperm seed disperser mutualisms: the timing of origins and their consequences for coevolutionary interactions between angiosperms and frugivores. Biological Reviews, 91:168-186. https://doi.org/10.1111/brv.12164

Evans, A.R. 2013. Shape descriptors as ecometrics in dental ecology. Hystrix, the Italian Journal of Mammalogy, 24(1):133-140. https://doi.org/10.4404/hystrix-24.1-6363

Evans, A.R., Wilson, G.P., Fortelius, M., and Jernvall, J. 2007. High-level similarity of dentitions in carnivorans and rodents. Nature, 445:78-81. https://doi.org/10.1038/nature05433

Evans, A.R. and Jernvall, J. 2009. Patterns and constraints in carnivoran and rodent dental complexity and tooth size. Journal of Vertebrate Paleontology, 29:24A

Figueirido, B., Tseng, Z.J., and Martín-Serra, A. 2013. Skull shape evolution in durophagous carnivorans. Evolution, 67(7):1975-1993. https://doi.org/10.1111/evo.12059

Fortelius, M. 1985. Ungulate cheek teeth: developmental, functional, and evolutionary interrelations. Acta Zoologica Fennica, 185:1-76

Fox, B.J. 1984. The diets of *Sminthopsis murina* and *Antechinus stuartii* (Marsupialia: Dasyuridae) in sympatry. Australian Wildlife Research, 11:235-248

Fox, R.C. and Naylor, B.G. 1995. The relationships of the Stagodontidae, primitive North American Late Cretaceous mammals, p. 247-250. In Sun, A. and Wang, Y. (eds.), Sixth Symposium on Mesozoic Terrestrial Ecosystems and Biota. China Ocean Press, Beijing

Fox, R.C. and Naylor, B.G. 1986. A new species of *Didelphodon* Marsh (Marsupialia) from the Upper Cretaceous of Alberta, Canada: paleobiology and phylogeny. Neues Jahrbuch für Geologie und Paläontologie Abhandlungen, 172(3):357-380

Fox, R.C. and Naylor, B.G. 2003. A Late Cretaceous taeniodont (Eutheria, Mammalia) from Alberta, Canada. Neues Jahrbuch für Geologie und Paläontologie Abhandlungen, 229:393–420

Fox, R.C. and Naylor, B.G. 2006. Stagodontid marsupials from the Late Cretaceous of Canada and their systematic and functional implications. Acta Palaeontologica Polonica, 51(1):13-26

Fox, R.C. and Scott, C.S. 2011. A new, early Puercan (earliest Paleocene) species of *Purgatorius* (Plesiadapiformes, Primates) from Saskatchewan Canada. Journal of Paleontology, 85(3):537-548

Fox, R.C., Scott, C.S., and Bryant, H.N. 2007. A new, unusual therian mammal from the Upper Cretaceous of Saskatchewan, Canada. Cretaceous Research, 28:821-829.

Fritts, S.H. and Sealander, J.A. 1978. Diets of bobcats in Arkansas with special reference to age and sex differences. The Journal of Wildlife Management, 42(3):533-539

Gheerbrant, E. and Astibia, H. 2012. Addition to the Late Cretaceous Laño mammal faunule (Spain) and to the knowledge of European “Zhelestidae” (Lainodontinae nov.). Bulletin de la Société géologique de France, 183(6):537-546

Glendenning, R. 1959. Biology and control of the coast mole, *Scapanus orarius orarius* True, in British Columbia. Canadian Journal of Animal Science, 39:34-44

Goin, F.J., Woodburne, M.O., Zimicz, A.N., Martin, G.M., and Chornogubsky, L. 2016. A Brief History of South American Metatherians: Evolutionary Contexts and Intercontinental Dispersals. Springer, Dordrecht Heidelberg New York London

Gompper, M.E. 1996. Sociality and asociality in white-nosed coatis (*Nasua narica*): foraging costs and benefits. Behavioral Ecology, 7(3):254-263

Gordon, C.L. 2003. Functional morphology and diet of Late Cretaceous mammals of North America. Unpublished PhD Thesis, University of Oklahoma, Norman, Oklahoma, USA

Grimaldi, D. 1999. The co-radiations of pollinating insects and angiosperms in the Cretaceous. Annals of the Missouri Botanical Garden, 86:373-406

Grossnickle, D.M. and Polly, P.D. 2013. Mammal disparity decreases during the Cretaceous angiosperm radiation. Proceedings of the Royal Society B, 280:20132110. http://dx.doi.org/10.1098/rspb.2013.2110

Grossnickle, D.M. and Newham, E. 2016. Therian mammals experience an ecomorphological radiation during the Late Cretaceous and selective extinction at the K–Pg boundary. Proceedings of the Royal Society B, 283:20160256. http://dx.doi.org/10.1098/rspb.2016.0256

Grossnickle, D.M., Smith, S.M., and Wilson, G.P. 2019. Untangling the multiple ecological radiations of early mammals. Trends in Ecology and Evolution, 34(10):936-949. https://doi.org/10.1016/j.tree.2019.05.008

Hall, E.R. and Dalquest, W.W. 1963. The mammals of Veracruz. University of Kansas Publications Museum of Natural History, 14:165-362

Halliday, T.J.D. and Goswami, A. 2016. Eutherian morphological disparity across the end Cretaceous mass extinction. Biological Journal of the Linnean Society, 118:152-168

Hardin, G. 1960. The competitive exclusion principle. Science, 131(3409):1292-1297

Harper, A.M. 2012. Three dimensional analysis of large scale dental wear in Late Cretaceous eutherians, Dzharakuduk region, Uzbekistan. Unpublished Masters Thesis, San Diego State University, San Diego, California

Harper, T., Parras, A., and Rougier, G.W. 2019. *Reigitherium* (Meridiolestida, Mesungulatoidea) an enigmatic Late Cretaceous mammal from Patagonia, Argentina: morphology, affinities, and dental evolution. Journal of Mammalian Evolution, 26:447-478. https://doi.org/10.1007/s10914-018-9437-x

Hopkins, D.D. and Forbes, R.B. 1980. Dietary patterns of the Virginia opossum in an urban environment. The Murrelet, 61(1)20-30

Hu, Y., Meng, J., Wang, Y., and Li, C. 2005. Large Mesozoic mammals fed on young dinosaurs. Nature, 433:149-152

Janis, C. M. 1990. Correlation of cranial and dental variables with body size in ungulates and macropodoids, p. 255-300. In Damuth, J. and MacFadden, B.J. (eds.), Body Size in Mammalian Paleobiology: Estimation and Biological Implications. Cambridge University Press, New York

Johanson, Z. 1996. Revision of the Late Cretaceous North American marsupial genus *Alphadon*. Palaeontographica Abteilung A: Palaeozoologie-Stratigraphie, 242(4-6):127-184

Jones, M.E. and Barmuta, L.A. 1998. Diet overlap and relative abundance of sympatric dasyurid carnivores: a hypothesis of competition.

Joshi, A.R., David Smith, J.L., and Cuthbert, F.J. 1995. Influence of food distribution and predation pressure on spacing behavior in palm civets. Journal of Mammalogy, 76(4):1205-1212

Julien-Laferrière, D. and Atramentowicz, M. 1990. Feeding and reproduction of three didelphid marsupials in two neotropical forests (French Guiana). Biotropica, 22(4):404-415

Kay, R.F. 1975. The functional adaptations of primate molar teeth. American Journal of Physical Anthropology, 43:195-216

Kay, R.F. 1984. On the use of anatomical features to infer foraging behavior in extinct primates, p. 21-53. In: Rodman, P.S., and Cant, J.G.H.(eds.), Adaptations for Foraging in Nonhuman Primates: Contributions to an Organismal Biology of Prosimians, Monkeys, and Apes. Columbia University Press, New York

Keddy, P.A. 1989. Competition. Chapman and Hall, New York

Kielan-Jaworoska, Z., Cifelli, R.L., and Luo, Z. 2004. Mammals from the Age of Dinosaurs: Origins, Evolution, and Structure. Columbia University Press, New York

Kissling, W.D., Dalby, L., Fløjgaard, C., Lenoir, J., Sandel, B., Sandom, C., Trøjelsgaard, K., and Svenning, J. 2014. Establishing macroecological trait datasets: digitization, extrapolation, and validation of diet preferences in terrestrial mammals worldwide. Ecology and Evolution, 4(14):1913-2930. https://doi.org/10.1002/ece3.1136

Krause, D. W. 2001. Fossil molar from a Madagascan marsupial. Nature, 412:497-498. https://doi.org/10.1038/35087649

Kruuk, H. 1972. The Spotted Hyena: a Study of Predation and Social Behavior. University of Chicago Press, Chicago

Kumar, S., Stecher, G., Suleski, M., and Hedges, S.B. 2017. TimeTree: a resource for timelines, timetrees, and divergence times. Molecular Biology and Evolution, 34:1812-1819

Lessa, L.G. and Geise, L. 2014. Food habits of *Metachirus nudicaudatus* (Didelphimorphia, Didelphidae) in a Brazilian Cerrado: diet composition and dietary seasonality. Studies on Neotropical Fauna and Environment, 49(2):75-78

Linley, G.D., Rypalski, A., Story, G., and Ritchie, E.G. 2020. Run rabbit run: spotted-tailed quoll diet reveals invasive prey is top of the menu. Australian Mammalogy, 43:221-225

Lloyd, G.T., Davis, K.E., Pisani, D., Tarver, J.E., Ruta, M., Sakamoto, M., Hone, D.W.E., Jennings, R., and Benton, M.J. 2008. Dinosaurs and the Cretaceous Revolution. Proceedings of the Royal Society B, 275:2483-2490. https://doi.org/10.1098/rspb.2008.0715

López- Torres, S., Selig, K.R., Prufrock, K.A., Lin, D., and Silcox, M.T. 2017. Dental topographic analysis of paromomyid (Plesiadapiformes, Primates) cheek teeth: more than 15 million years of changing surfaces and shifting ecologies. Historical Biology, 30(1-2):76-88. http://dx.doi.org/10.1080/08912963.2017.1289378

Luckett, W. P. 1993. An ontogenetic assessment of dental homologies in therian mammals, p.182-204. In Szalay, F.S., Novacek, M.J. and McKenna, M.C. (eds.), Mammal Phylogeny: Mesozoic Differentiation, Multituberculates, Monotremes, Early Therians, and Marsupials. Springer, New York

Luo, Z. 2007. Transformation and diversification in early mammal evolution. Nature Reviews, 450: https://doi.org/10.1038/nature06277

Lupia, R., Lidgard, S., and Crane, P.R. 1999. Comparing palynological abundance and diversity: implications for biotic replacement during the Cretaceous angiosperm radiation. Paleobiology, 25(3):305-340

Magallón, S., Hilu, K.W., and Quandt, D. 2013. Land plant evolutionary timeline: gene effects are secondary to fossil constraints in relaxed clock estimation of age and substitution rates. American Journal of Botany, 100(3):556-573

Magallón, S., Gómez-Acevedo, S., Sánchez-Reyes, L.L., and Hernández- Hernández, T. 2015. A metacalibrated time-tree documents the early rise of flowering plant phylogenetic diversity. New Phytologist, 207:437-453

Martin, J.E., Case, J.A., Jagt, J.W.M., Schulp, A.S., and Mulder, E.W.A. 2005. Journal of Mammalian Evolution, 12:495-511. https://doi.org/10.1007/s10914-005-7330-x

McCracken, K.E. 1990. Microhabitat and dietary partitioning in three species of shrews at Yellow Bay Montana. Unpublished Masters Thesis, University of Montana, Missoula, Montana, USA

McKenna, M. C. 1975. Toward a phylogenetic classification of the Mammalia, p. 21-46. In Luckett, W.P. and Szalay, F.S. (eds.), Phylogeny of the Primates. Plenum, New York

Medellin, R.A. 1994. Seed dispersal of *Cecropia obtusifolia* by two species of opossums in the Selva Lacandona, Chiapas, Mexico. Biotropica, 26(4):400-407

Meredith, R.W, Janečka, J.E., Gatesy, J., Ryder, O.A., Fisher, C.A., Teeling, E.C., Goodbla, A., Eizirik, E., Simão, T.L.L., Stadler, T., Rabosky, D.L., Honeycutt, R.L., Flynn, J.J., Ingram, C.M., Steiner, C., Williams, T.L., Robinson, T.J., Burk-Herrick, A., Westerman, M., Ayoub, N.A., Springer, M.S., and Murphy, W.J. 2011. Impacts of the Cretaceous

Terrestrial Revolution and KPg extinction on mammal diversification. Science, 334:521-524

Meserve, P.L. 1981. Trophic relationships among small mammals in a Chilean semiarid thorn scrub community. Journal of Mammalogy, 62(2):304-314

Mondolfi, E. and Padilla,G. M. 1958. Contribución al conocimiento del "perrito de agua" (*Chironectes minimus* Zimmermann). Memoria de la Sociedad de Ciencias Naturales La Salle, 17:41-155

Moore, A.W. 1933. Food habits of Townsend and coast moles. Journal of Mammalogy, 14:36-40

Morales-García, N.M., Gill, P.G., Janis, C.M., and Rayfield, E.J. 2021. Jaw shape and mechanical advantage are indicative of diet in Mesozoic mammals. Communications Biology, 4(242). https://doi.org/10.1038/s42003-021-01757-3

Nakashima, Y., Inoue, E., Inoue-Murayama, M., and Abd. Sukor, J. 2010. High potential of a disturbance-tolerant frugivore, the common palm civet *Paradoxurus hermaphroditus* (Viverridae), as a seed disperser for large-seeded plants. Mammal Study, 35(3):209-215

Newham, E., Benson, R., Upchurch, P., and Goswami, A. 2014. Mesozoic mammaliaform diversity: the effect of sampling corrections on reconstructions of evolutionary dynamics. Palaeogeography, Palaeoclimatology, and Palaeoecology, 412:32-44. https://doi.org/10.1016/j.palaeo.2014.07.017

Nowak, R.M. 1999. Walker's Mammals of the World, Sixth Edition. The Johns Hopkins University Press, Baltimore, Maryland

O'Leary, M.A., Bloch, J.I., Flynn, J.J., Gaudin, T.J., Giallombardo, A., Giannini, N.P., Goldberg, S.L., Kraatz, B.P., Luo, Z., Meng, J., Ni, X., Novacek, M.J., Perini, F.A., Randall, Z.S., Rougier, G.W., Sargis, E.J., Silcox, M.T., Simmons, N.B., Spaulding, M., Velazco, P.M.,

Weksler, M., Wible, J.R., and Cirranello, A.L. 2013. The Placental mammal ancestor and the post–K-Pg radiation of placentals. Science, 339:662-667

Pagel, M.D. 1992. A method for the analysis of comparative data. Journal of Theoretical Biology, 156:431-442

Pampush, J.D., Winchester, J.M., Morse, P.E., Vining, A.Q., Boyer, D.M., and Kay, R.F. 2016. Introducing molaR: a new R package for quantitative topographic analysis of teeth (and other topographic surfaces). Journal of Mammalian Evolution, 23:397-412. https://doi.org/10.1007/s10914-016-9326-0

Parolin, L.C., Bianconi, G.V., and Mikich, S.B. 2016. Consistency in fruit preferences across the geographical range of the frugivorous bats *Artibeus*, *Carollia* and *Sturnira* (Chiroptera). Iheringia, Série Zoologia, 106: e2016010. https://doi.org/10.1590/1678-4766e2016010

Pemberton, D., Gales, S., Bauer, B., Gales, R., Lazenby, B., and Medlock, K. 2008. The diet of the Tasmanian Devil, *Sarcophilus harrisii*, as determined from analysis of scat and stomach contents. Papers and Proceedings of the Royal Society of Tasmania, 142(2):13-22

Peng, A., Toews, N., and Wilson, G.P. 2017. An ontogenetic investigation of a Cretaceous North American mammal, *Didelphodon vorax* (Metatheria: Marsupialiformes: Stagodontidae), through quantitative and descriptive analysis of the dentary. Geological Society of America Annual Meeting Abstracts with Programs, 49(6). https://doi.org/10.1130/abs/2017AM-300648

Pineda-Munoz, S. and Alroy, J. 2014. Dietary characterization of terrestrial mammals. Proceedings of the Royal Society B, 281:20141173. http://dx.doi.org/10.1098/rspb.2014.1173

Pineda-Munoz, S., Lazagabaster, I.A., Alroy, J., and Evans, A.R. 2016. Inferring diet from dental morphology in terrestrial mammals. Methods in Ecology and Evolution, 8:481-491. https://doi.org/10.1111/2041-210X.12691

Prufrock, K.A., López- Torres, S., Silcox, M.T., and Boyer, D.M. 2016. Surfaces and spaces: troubleshooting the study of dietary niche space overlap between North American stem primates and rodents. Surface Topography: Metrology and Properties, 4:024005. http://dx.doi.org/10.1088/2051-672X/4/2/024005

Rabosky, D.L. and Adams, D.C. 2012. Rate of morphological evolution are correlated with species richness in salamanders. Evolution, 66(6):1807-1818. https://doi.org/10.1111/j.1558-5646.2011.01557.x

Ramírez-Barahona, S., Barrera-Redondo, J., and Eguiarte, L.E. 2016. Rates of ecological divergence and body size evolution are correlated with species diversification in scaly tree ferns. Proceedings of the Royal Society B, 283:20161098. http://dx.doi.org/10.1098/rspb.2016.1098

Revell, L.J. 2012. phytools: an R package for phylogenetic comparative biology (and other things). Methods in Ecology and Evolution, 3:217-223

Robinson, J.G. and Redford, K.H. 1986. Body size, diet, and population density of neotropical forest mammals. The American Naturalist, 128(5):665-680

Rose, C. and Prange, S. 2015. Diet of the recovering Ohio bobcat (*Lynx rufus*) with a consideration of two subpopulations. The American Midland Naturalist, 173(2):305-317

Rostovskaya, M.S., Zhukova, D.V., Illarionova, A.E., Ustyugovia, S.V., Borissenko, A.V., and Sviridoz, A.V. 2000. Insect prey of the long-eared bat *Plecotus auritus* (L.) (Chiroptera: Vespertilionidae). Russian Entomological Journal, 9:185-189

Rougier, G.W., Wible, J.R., and Novacek, M. J. 1998. Implications of Deltatheridium specimens for early marsupial history. Nature, 396:459-463. https://doi.org/10.1038/24856

Rulison, E.L., Luiselli, L., and Burke, R.L. 2012. Relative impacts of habitat and geography on raccoon diets. The American Midland Naturalist, 168(2):231-246

Ruta M., Angielczyk K.D., Fröbisch J., and Benton M.J. 2013 Decoupling of morphological disparity and taxic diversity during the adaptive radiation of anomodont therapsids. Proceedings of the Royal Society B, 280: 20131071. http://dx.doi.org/10.1098/rspb.2013.1071

Sánchez-González, R., Hernández-Saint Martin, A.D., Rosas-Rosas, O.C., and García-Chávez, J. 2018. Diet and abundance of bobcat (*Lynx rufus*) in the Potosino-Zacatecano Plateau, Mexico. Therya, 9(2):107-112

Sánchez-Villagra, M.R. 2013. Why are there fewer marsupials than placentals? On the relevance of geography and physiology to evolutionary patterns of mammalian diversity and disparity. Journal of Mammal Evolution, 20:279-290. https://doi.org/10.1007/s10914-012-9220-3

Sandidge, L.L. 1953. Food and dens of the opossum (*Didelphis virginiana*) in northeastern Kansas. Transactions of the Kansas Academy of Science, 56(1):97-106

Santana, S.E., Strait, S., and Dumont, E.R. 2011. The better to eat you with: functional correlates of tooth structure in bats. Functional Ecology, 25:839-847. https://doi.org/10.1111/j.1365-2435.2011.01832.x

Santori, R.T., Astúa de Moraes, D., and Cerqueira, R. 1995. Diet composition of *Metachirus nudicaudatus* and *Didelphis aurita* (Marsupialia, Didelphoidea) in Southeastern Brazil. Mammalia, 59:511-516

Schoener, T.W. 1974. Resource partitioning in ecological communities. Science, 185(4145):27-39

Schoonover, L.T. and Marshall, W.H. 1951. Food Habits of the Raccoon (*Procyon lotor hirtus*) in North-Central Minnesota. Journal of Mammalogy, 32(4):422-428

Scott, C.S. and Fox, R.C. 2015. Review of Stagodontidae (Mammalia, Marsupialia) from the Judithian (Late Cretaceous) Belly River Groups of southeastern Alberta, Canada. Canadian Journal of Earth Sciences, 52:682-695. https://doi.org/10.1139/cjes-2014-0170

Scott, L.K., Hume, I.D., and Dickman, C.R. 1999. Ecology and population biology of long-nosed bandicoots (*Perameles nasuta*) at North Head, Sydney Harbour National Park. Wildlife Research, 26(6):805-821

Selig, K.R., Sargis, E.J., and Silcox, M.T. 2019. The frugivorous insectivores? Functional morphological analysis of molar topography for inferring diet in extant treeshrews (Scandentia). Journal of Mammalogy, 100(6):1901-1917. https://doi.org/10.1093/jmammal/gyz151

Simpson, G.G. 1937. The beginning of the age of mammals. Biological Reviews, 12(1):1-46. https://doi.org/10.1111/j.1469-185X.1937.tb01220.x

Smith, F.A., Boyer, A.G., Brown, J.H., Costa, D.P., Dayan, T., Ernest, S.K.M., Evans, A.R., Fortelius, M., Gittleman, J.L., Hamilton, M.J., Harding, L.E., Lintulaakso, K., Lyons, S.K., McCain, C., Okie, J.G., Saarinen, J.J., Sibly, R.M., Stephens, P.R., Theodor, J., and Uhen, M.D. 2010. The evolution of maximum body size of terrestrial mammals. Science, 330:1216-1219

Smith, S.M. 2017. Mammalian faunal recovery following the Cretaceous-Paleogene mass extinction: a multifaceted investigation. Unpublished PhD Thesis, University of

Washington, Seattle, Washington, USA

Smits, P.D. and Evans, A.R. 2012. Functional constraints on tooth morphology in carnivorous mammals. BMC Evolutionary Biology, 12:146. https://doi.org/10.1186/1471-2148-12-146

Spradley, J.P. 2017. Dental ecometrics as a proxy of paleoenvironment reconstruction in the Miocene of South America. Unpublished PhD Thesis, Duke University, Durham, North Carolina, USA

Spradley, J.P., Pampush, J.D., Morse, P.E., and Kay, R.F. 2017. Smooth operator: The effects of different 3D mesh retriangulation protocols on the computation of Dirichlet normal energy. American Journal of Physical Anthropology. https://doi.org/10.1002/ajpa.23188

Streilein, K. E. 1982. Behavior, ecology, and distribution of South American marsupials. Special Publication of the Pymatuning Laboratory of Ecology, 6:231-250

Steiner, K.E. 1981. Nectarivory and potential pollination by a neotropical marsupial. Annals of the Missouri Botanical Garden, 68(4):505-513

Strait, S.G. 1993. Molar morphology and food texture among small-bodied insectivorous mammals. Journal of Mammalogy, 74(2):391-402

Strait, S.G. 1997. Tooth use and the physical properties of food. Evolutionary Anthropology, (5):199-211

Stucky, R.K. 1990. Evolution of land mammal diversity in North America during the Cenozoic. Current mammalogy, 2:375-432

Szalay, F.S. 1994. Evolutionary History of the Marsupials and an Analysis of Osteological Characters. Cambridge University Press, New York

Szalay, F.S. and Trofimov, B.A. 1996. The Mongolian Late Cretaceous *Asiatherium*, and the

early phylogeny and paleobiology of Metatheria. Journal of Vertebrate Paleontology, 16(3):474-509

Szalay, F.S. and Sargis, E.J. 2006. Cretaceous therian tarsals and the metatherian-eutherian dichotomy. Journal of Mammalian Evolution, 13:171-210

Thums, M., Klaassen, M., and Hume, I.D. 2005. Seasonal changes in diet of the long-nosed bandicoot (*Perameles nasuta*) assessed by analysis of faecal scats and of stable isotopes in blood. Australian Journal of Zoology, 53:87-93

Tiffney, B.H. and Mazer, S.J. 1995. Angiosperms growth habit, dispersal and diversification Reconsidered. Evolutionary Ecology, 9:93-117

Trombulak, S.C. 1985. The influence of interspecific competition on home range size in chipmunks (*Eutamias*). Journal of Mammalogy, 66(2):329-337

Ungar, P.S. 2010. Mammal Teeth: Origin, Evolution, and Diversity. The Johns Hopkins University Press, Baltimore, Maryland, USA

Ungar, P.S. and M'Kirera, F. 2003. A solution to the worn tooth conundrum in primate functional anatomy. PNAS, 100(7):3874-3877. https://doi.org/10.1073/pnas.0637016100

Van Valen, L. and Sloan, R.E. 1997. Contemporaneity of late Cretaceous extinctions. Nature, 270:193

Van Valkenburg, B. 2007. Déjà vu: the evolution of feeding morphologies in the Carnivora. Integrative and Comparative Biology, 47(1):147-163

Venables, W.N. and Ripley, B.D. 2013. Modern applied statistics with S-PLUS. Springer Science and Business Media, Berlin, Germany

Vullo, R., Gheerbrant, E., de Muizon, C., and Néraudeau, D. 2009. The oldest modern therian mammal from Europe and its bearing on stem marsupial paleobiology. Proceedings of the

National Academy of Sciences, 106(47):19910-19915. https://doi.org/10.1073/pnas.0902940106

Weaver, L.N. and Wilson, G.P. 2020. Shape disparity in the blade-like premolars of multituberculate mammals: functional constraints and the evolution of herbivory. Journal of Mammalogy, gyaa029. https://doi.org/10.1093/jmammal/gyaa029

Weaver, L.N., Wilson, G.P., Krumenacker, L.J., McLaughlin, K., Moore, J.R., and Varricchio, D.J. 2019. New multituberculate mammals from the mid-Cretaceous (Lower Cenomanian) Wayan Formation of southeastern Idaho and implications for the early evolution of Cimolodonta. Journal of Vertebrate Paleontology, 39(2):e1604532

Weaver, L.N., Fulghum, H.Z., Grossnickle, D.M., Brightly, W.H., Kulik, Z.T., Wilson Mantilla, G.P. and Whitney, M.R. in review. Multituberculate mammals show evidence of a life history similar to that of placentals, no marsupials.

Werdelin, L. 1989. Constraint and adaptation in the bone-cracking canid *Osteoborus* (Mammalia: Canidae). Paleobiology, 15(4):387-401

Whitaker, Jr. J.O. 1995. Food of the big brown bat *Eptesicus fuscus* from maternity colonies in Indiana and Illinois. The American Midland Naturalist, 134 (2):346-360

Whitaker, J.O. and Karataş, A. 2009. Food and feeding habits of some bats from Turkey. Acta Chiropterologica, 11(1):393-403

Wible, J.R., Rougier, G.W., Novacek, M.J, and Sher, R.J. 2007. Cretaceous eutherians and Laurasian origin for placental mammals near the K/T boundary. Nature, 447. https://doi.org/10.1038/nature05854

Williamson, T.E., Brusatte, S.L., and Wilson, G.P. 2014. The origin and early evolution of metatherian mammals: The Cretaceous record. ZooKeys, 76(465):1-76.

https://doi.org/10.3897/zookeys.465.8178

Wilman, H., Belmaker, J., Simpson, J., De La Rosa, C., Rivadeneira, M.M., and Jetz, W. 2014. EltonTraits 1.0: species-level foraging attributes of the world's birds and mammals. Ecology, 95(7):2027. https://doi.org/10.1890/13-1917.1

Wilson, G.P. 2005. Mammalian faunal dynamics during the last 1.8 million years of the Cretaceous in Garfield County, Montana. Journal of Mammalian Evolution, 12(1/2):53-76

Wilson, G.P. 2013. Mammals across the K/Pg boundary in northeastern Montana, U.S.A.: dental morphology and body-size patterns reveal extinction selectivity and immigrant-fueled ecospace filling. Paleobiology, 39(3):429-469

Wilson, G.P., 2014. Mammalian extinction, survival, and recovery dynamics across the Cretaceous-Paleogene boundary in northeastern Montana, USA, p. 1-28. In Wilson, G.P., Clemens, W.A., Horner, J.R., and Hartman, J.H. (eds.), Through the End of the Cretaceous in the Type Locality of the Hell Creek Formation in Montana and Adjacent Areas. https://doi.org/10.1130/2014.2503(15)

Wilson, G.P., and Riedel, J.A. 2010. New specimen reveals deltatheroidan affinities of the North American Late Cretaceous mammal *Nanocuris*. Journal of Vertebrate Paleontology, 30(3):872-884

Wilson, G.P., Evans, A.R., Corfe, I.J., Smits, P.D., Fortelius, M., and Jernvall, J. 2012. Adaptive radiation of multituberculate mammals before the extinction of dinosaurs. Nature, 483:457-460. https://doi.org/10.1038/nature10880

Wilson, G.P., Ekdale, E.G., Hoganson, J.W., Calede, J.J., and Vander Linden, A. 2016. A large carnivorous mammal from the Late Cretaceous and the North American origin of

marsupials. Nature Communications, 7:13734. https://doi.org/10.1038/ncomms13734

Wilson Mantilla, G.P. et al. 2021. Earliest Paleocene purgatoriids and the initial radiation of stem primates. Royal Society Open Science, 8:210050. https://doi.org/10.1098/rsos.210050

Winchester, J.M. 2016. MorphoTester: an open source application for morphological topographic analysis. PLoS ONE, 11(2):e0147649. https://doi.org/10.1371/journal.pone.0147649

Winchester, J.M., Boyer, D.M., St. Clair, E.M., Gosselin-Ildari, A.D., Cooke, S.B., and Ledogar, J.A. 2014. Dental topography of platyrrhines and prosimians: convergence and contrasts. American Journal of Physical Anthropology, 153:29-44. https://doi.org/10.1002/ajpa.22398

Wing, S.L., and Boucher, L.D. 1998. Ecological aspects of the Cretaceous flowering plant radiation. Annual Review of Earth and Planetary Sciences, 26:379-421.

Witmer, L.M. 1995. The extant phylogenetic bracket and the importance of reconstructing soft tissues in fossils, p.19-33. In Thomason, J. (ed.), Functional morphology in Vertebrate Paleontology. Cambridge University Press, New York

Woodburne, M.O. 2004. Definitions, p. xi–xvi, In Woodburne, M. O. (ed.), Late Cretaceous and Cenozoic Mammals of North America: Biostratigraphy and Geochronology. Columbia University Press, New York

Wroe, S., McHenry, C., and Thomason, J. 2005. Bite club: comparative bite force in big biting mammals and the prediction of predatory behaviour in fossil taxa. Proceedings of the Royal Society B, 272:691-625

Zortéa, M. and Mendes, S.L. 1993. Folivory in the big fruit-eating bat, *Artibeus lituratus* (Chiroptera: Phyllostomidae) in eastern Brazil. Journal of Tropical Ecology, 9(1):117-120

4.12 FIGURES

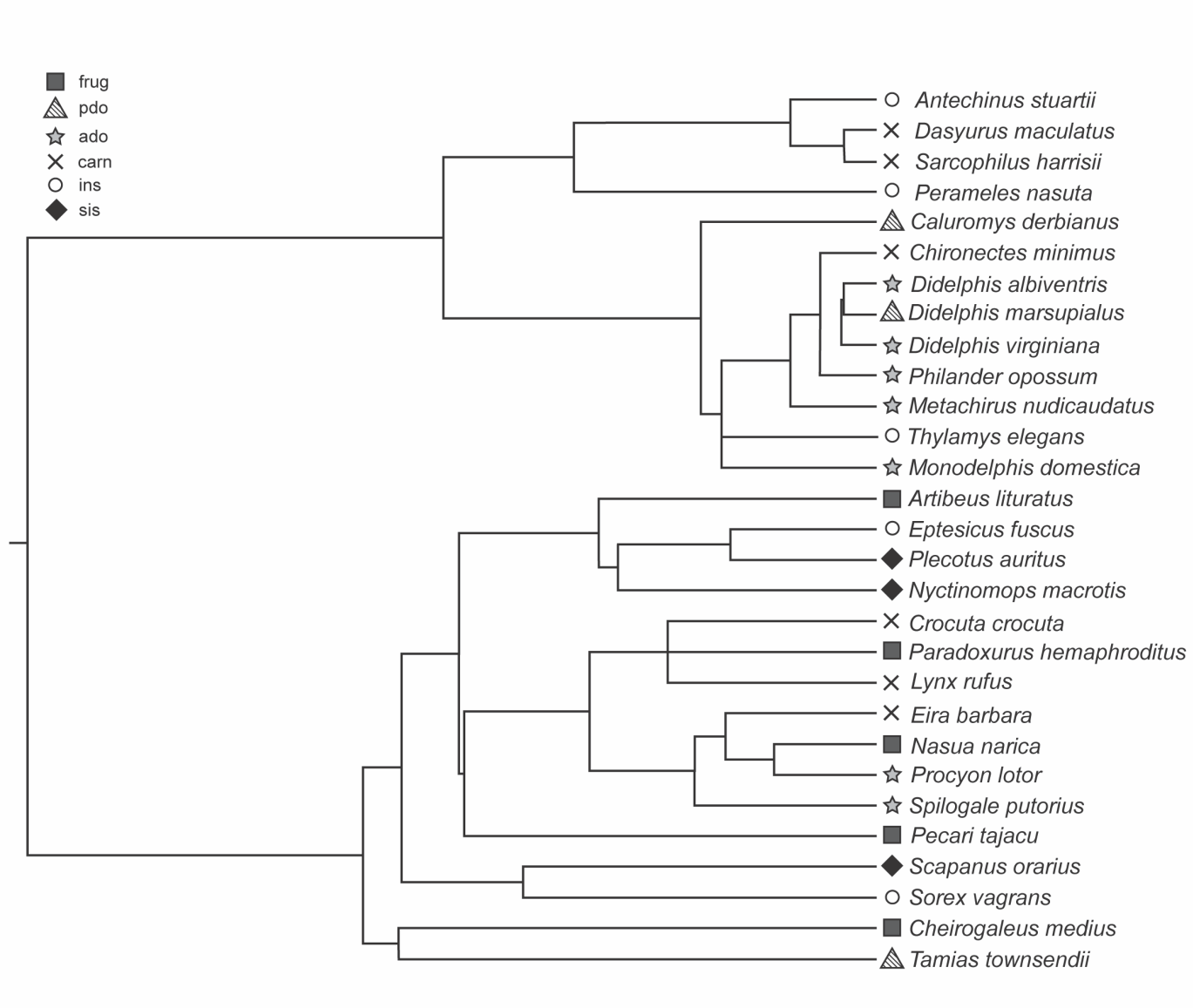
frug
pdo
ado
carn
ins
sis
Antechinus stuartii
Dasyurus maculatus
Sarcophilus harrisii
Perameles nasuta
Caluromys derbianus
Chironectes minimus
Didelphis albiventris
Didelphis marsupialus
Didelphis virginiana
Philander opossum
Metachirus nudicaudatus
Thylamys elegans
Monodelphis domestica
Artibeus lituratus
Eptesicus fuscus
Plecotus auritus
Nyctinomops macrotis
Crocuta crocuta
Paradoxurus hemaphroditus
Lynx rufus
Eira barbara
Nasua narica
Procyon lotor
Spilogale putorius
Pecari tajacu
Scapanus orarius
Sorex vagrans
Cheirogaleus medius
Tamias townsendii

Figure 4.1. Phylogenetic tree of our extant comparative sample generated using timetree.org. Abbreviations for diet categories: ado = animal-dominated omnivore; carn = carnivore; frug = frugivore; ins = insectivore; pdo = plant-dominated omnivore; sis = soft-insect specialist.

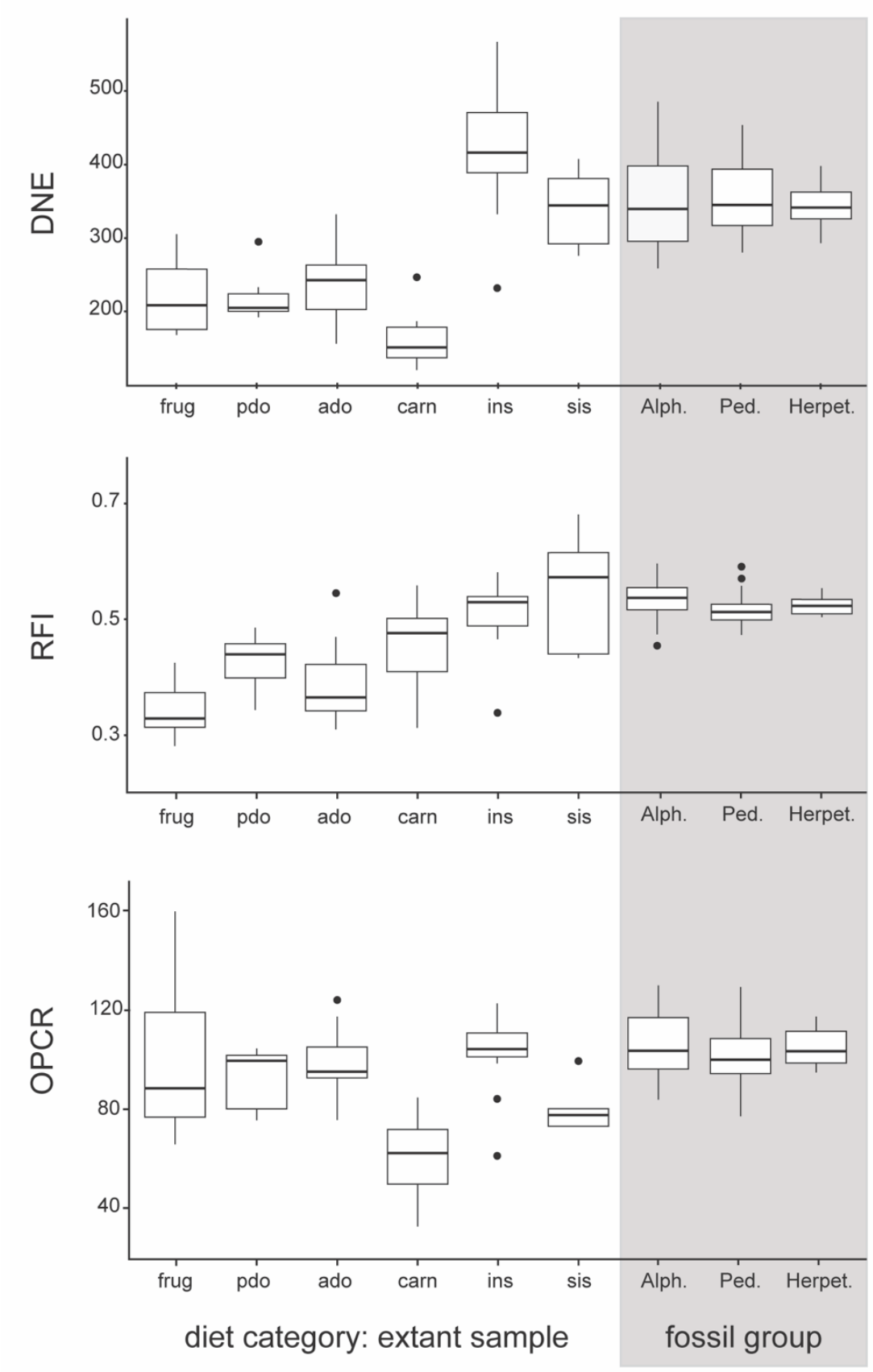
DNE
500
400
300
200
frug
pdo
ado
carn
ins
sis
Alph.
Ped.
Herpet.
RFI
0.7
0.5
0.3
OPCR
160
120
80
40
diet category: extant sample
fossil group

Figure 4.2. Boxplots of Dirichlet normal energy (DNE), relief index (RFI), and orientation patch count rotated (OPCR) across extant mammals classified by diet and a subset of fossil groups. Abbreviations for diet categories: ado = animal-dominated omnivore; carn = carnivore; frug = frugivore; ins = insectivore; pdo = plant-dominated omnivore; sis = soft-insect specialist. Abbreviations for fossil groups: Alph. = Alphadontidae; Herpet. = Herpetotheriidae; Ped. = Pediomyidae.

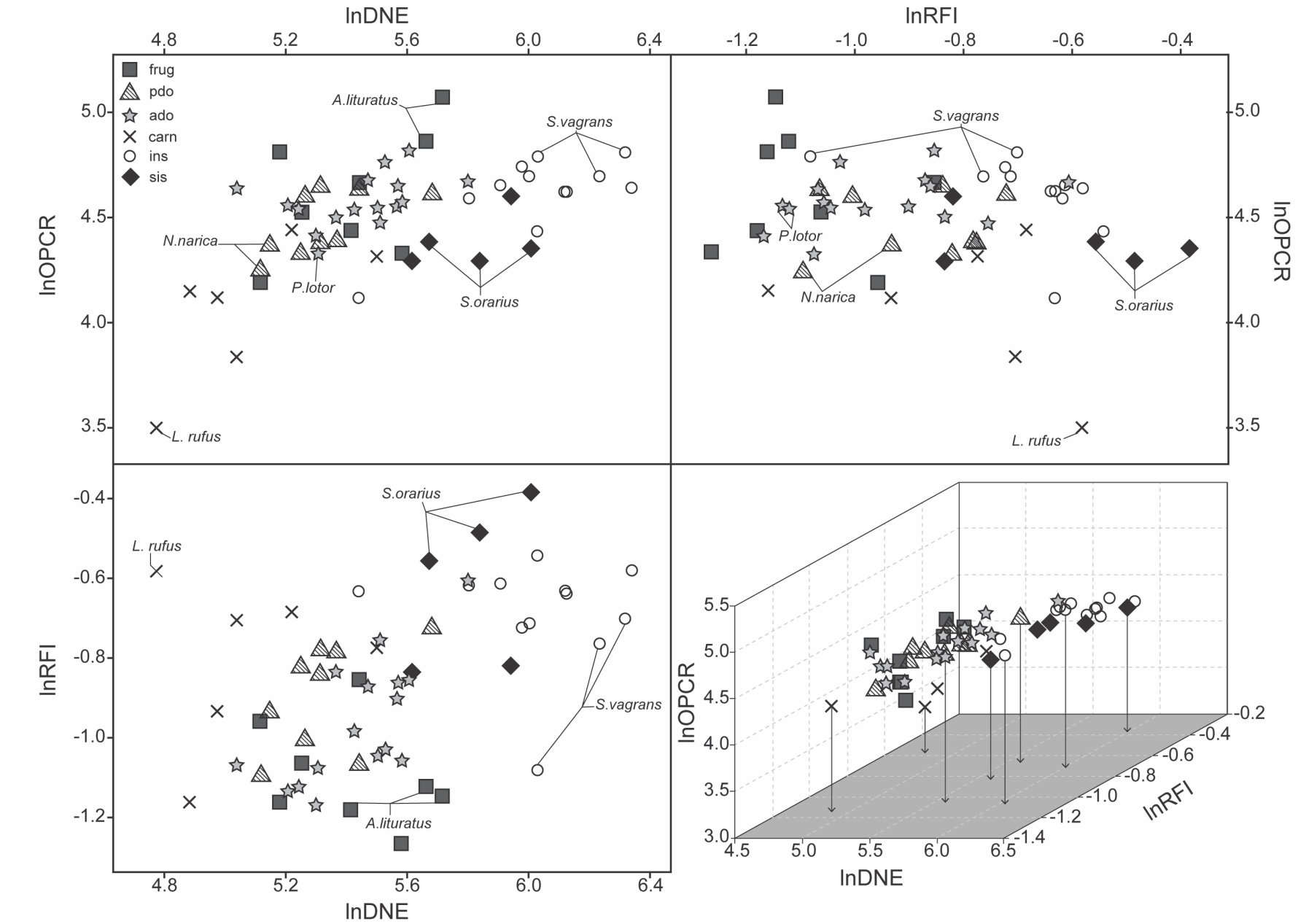
lnDNE
lnRFI
lnOPCR
frug
pdo
ado
carn
ins
sis
A.lituratus
S.vagrans
N.narica
P.lotor
S.orarius
L. rufus

Figure 4.3. Bivariate scatter plots of log-transformed Dirichlet normal energy (lnDNE), relief index (lnRFI), and orientation patch count rotated (lnOPCR) values, and a 3D scatterplot of all three DTA metrics (bottom right) for our extant comparative sample. Shapes correspond to our true diet categorizations. See Table 4.1 for taxonomic names. Abbreviations for diet categories: ado = animal-dominated omnivore; carn = carnivore; frug = frugivore; ins = insectivore; pdo = plant-dominated omnivore; sis = soft-insect specialist.

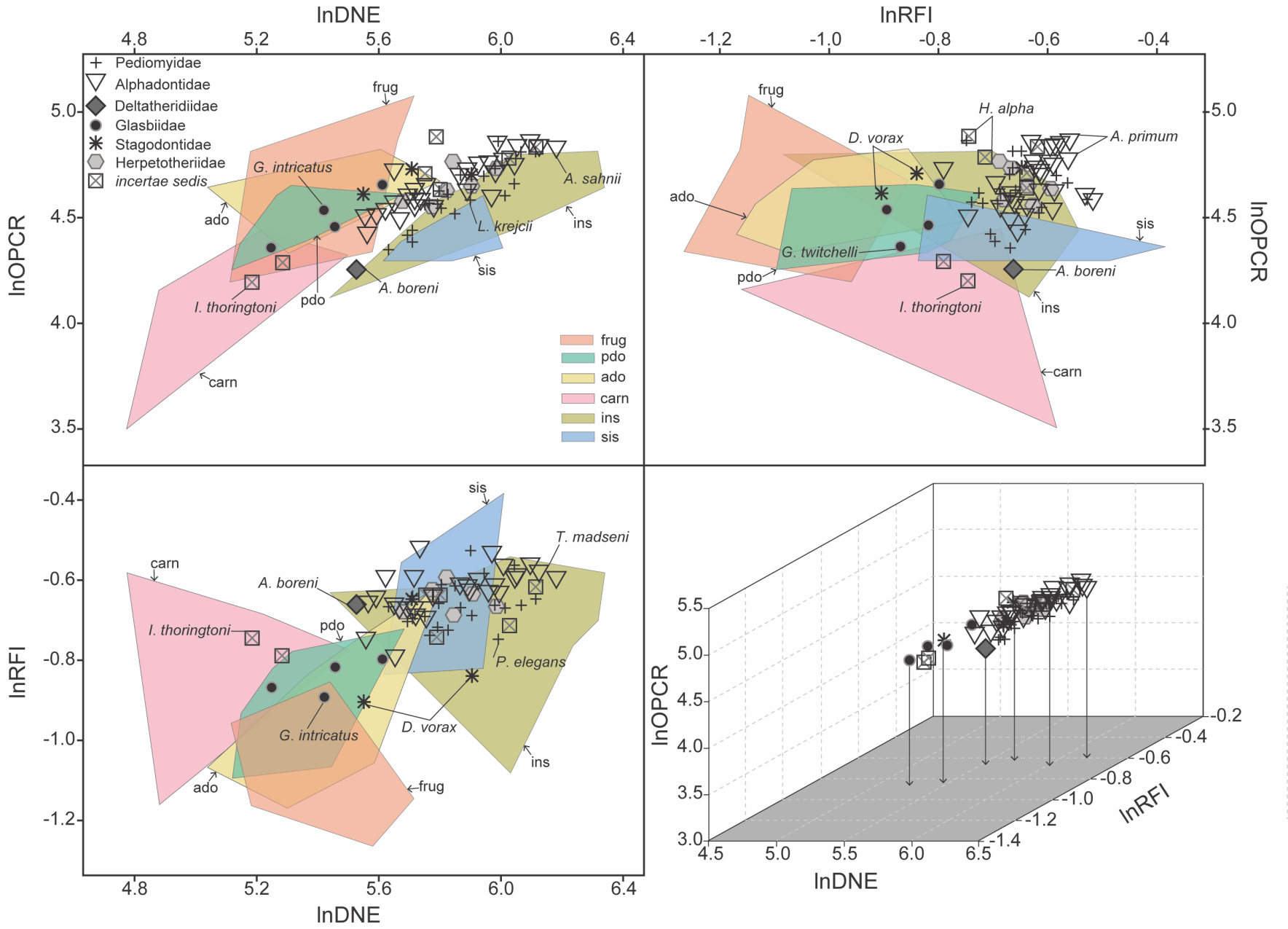
lnDNE
lnRFI
lnOPCR
Pediomyidae
Alphadontidae
Deltatheridiidae
Glasbiidae
Stagodontidae
Herpetotheriidae
incertae sedis
frug
pdo
ado
carn
ins
sis
G. intricatus
A. sahnii
L. krejcli
A. boreni
I. thoringtoni
H. alpha
D. vorax
A. primum
G. twitchelli
T. madseni
P. elegans

Figure 4.4. Bivariate scatter plots of log-transformed Dirichlet normal energy (lnDNE), relief index (lnRFI), and orientation patch count rotated (lnOPCR) values, and a 3D scatterplot of all three DTA metrics (bottom right) for our fossil sample. Colored polygons are regions of the morphospace occupied by extant mammals in our dietary categories. Shapes correspond to fossil groups. See Table 4.2 for taxonomic names. Abbreviations for diet categories: ado = animal-dominated omnivore; carn = carnivore; frug = frugivore; ins = insectivore; pdo = plant-dominated omnivore; sis = soft-insect specialist.

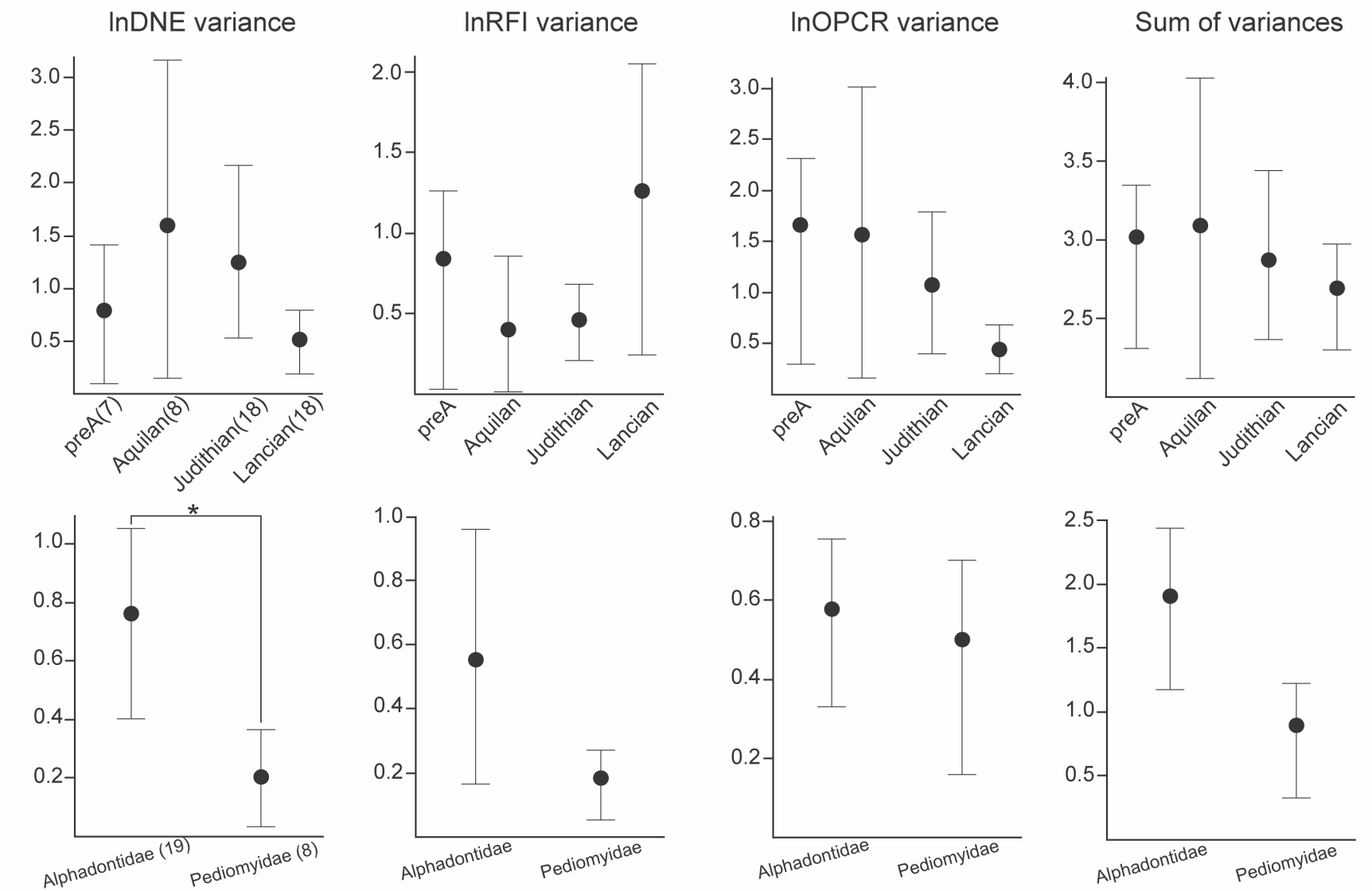
lnDNE variance
lnRFI variance
lnOPCR variance
Sum of variances
preA(7)
Aquilan(8)
Judithian(18)
Lancian(18)
preA
Aquilan
Judithian
Lancian
*
Alphadontidae (19)
Pediomyidae (8)
Alphadontidae
Pediomyidae

Figure 4.5. Morphological disparity of NALK metatherians, calculated as the variance of each DTA metric and the sum of variances. The 95% confidence intervals were generated using a custom bootstrapping function with 1,000 replicates. Top row: all-metatherian disparity for each time bin. Sample size for each time bin is shown in parentheses at the bottom of the far-left plot: pre-Aquilan (preA) = 7; Aquilan = 8; Judithian = 18; Lancian = 18. Bottom row: disparity of alphadontids vs. disparity of pediomyids. Sample size for each taxon is shown in parentheses at the bottom of the far-left plot: Alphadontidae = 19 and Pediomyidae = 8. See Table 4.8 for *p*-values.

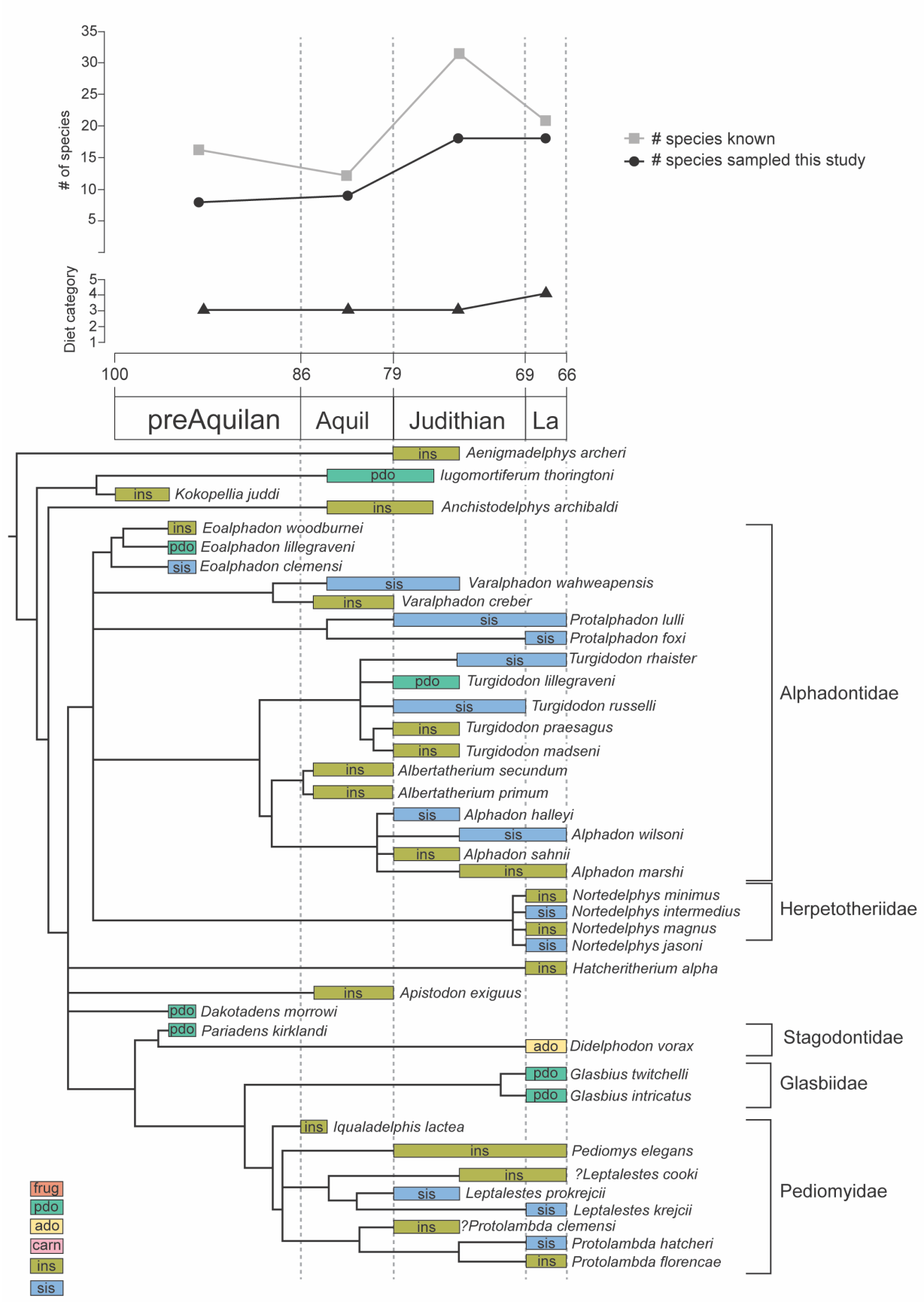
# of species
35
30
25
20
15
10
5
species known
species sampled this study
Diet category
5
4
3
2
1
100
86
79
69
66
preAquilan
Aquil
Judithian
La
ins Aenigmadelphys archeri
pdo Iugomortiferum thoringtoni
ins Kokopellia juddi
ins Anchistodelphys archibaldi
ins Eoalphadon woodburnei
pdo Eoalphadon lillegraveni
sis Eoalphadon clemensi
sis Varalphadon wahweapensis
ins Varalphadon creber
sis Protalphadon lulli
sis Protalphadon foxi
sis Turgidodon rhaister
pdo Turgidodon lillegraveni
sis Turgidodon russelli
ins Turgidodon praesagus
ins Turgidodon madseni
ins Albertatherium secundum
ins Albertatherium primum
sis Alphadon halleyi
sis Alphadon wilsoni
ins Alphadon sahnii
ins Alphadon marshi
ins Nortedelphys minimus
sis Nortedelphys intermedius
ins Nortedelphys magnus
sis Nortedelphys jasoni
ins Hatcheritherium alpha
ins Apistodon exiguus
pdo Dakotadens morrowi
pdo Pariadens kirklandi
ado Didelphodon vorax
pdo Glasbius twitchelli
pdo Glasbius intricatus
ins Iqualadelphis lactea
ins Pediomys elegans
ins ?Leptalestes cooki
sis Leptalestes prokrejcii
sis Leptalestes krejcii
ins ?Protolambda clemensi
sis Protolambda hatcheri
ins Protolambda florencae
Alphadontidae
Herpetotheriidae
Stagodontidae
Glasbiidae
Pediomyidae
frug
pdo
ado
carn
ins
sis

Figure 4.6. Patterns of taxonomic diversity and dietary diversity of NALK metatherians. Top: Known taxonomic diversity (gray squares and line) of NALK metatherians versus the metatherian diversity sampled in this study (black circles and line). Middle: Dietary diversity of NALK metatherians through time (out of six dietary categories). Bottom: Hypothesized phylogenetic relationships of NALK metatherians sampled in this study (the deltatheriid *Atokatheridium boreni* was removed). Thick horizontal bars represent the known temporal range of each species. Bar colors represent the dietary categories assigned to each taxon in this study. Abbreviations for diet categories: ado = animal-dominated omnivore; carn = carnivore; frug = frugivore; ins = insectivore; pdo = plant-dominated omnivore; sis = soft-insect specialist. Abbreviations for NALMAs: Aquil = Aquilan; La = Lancian. Hypothesized phylogeny modified from Williamson et al. (2014), Wilson et al. (2016), and Cohen et al. (2020).

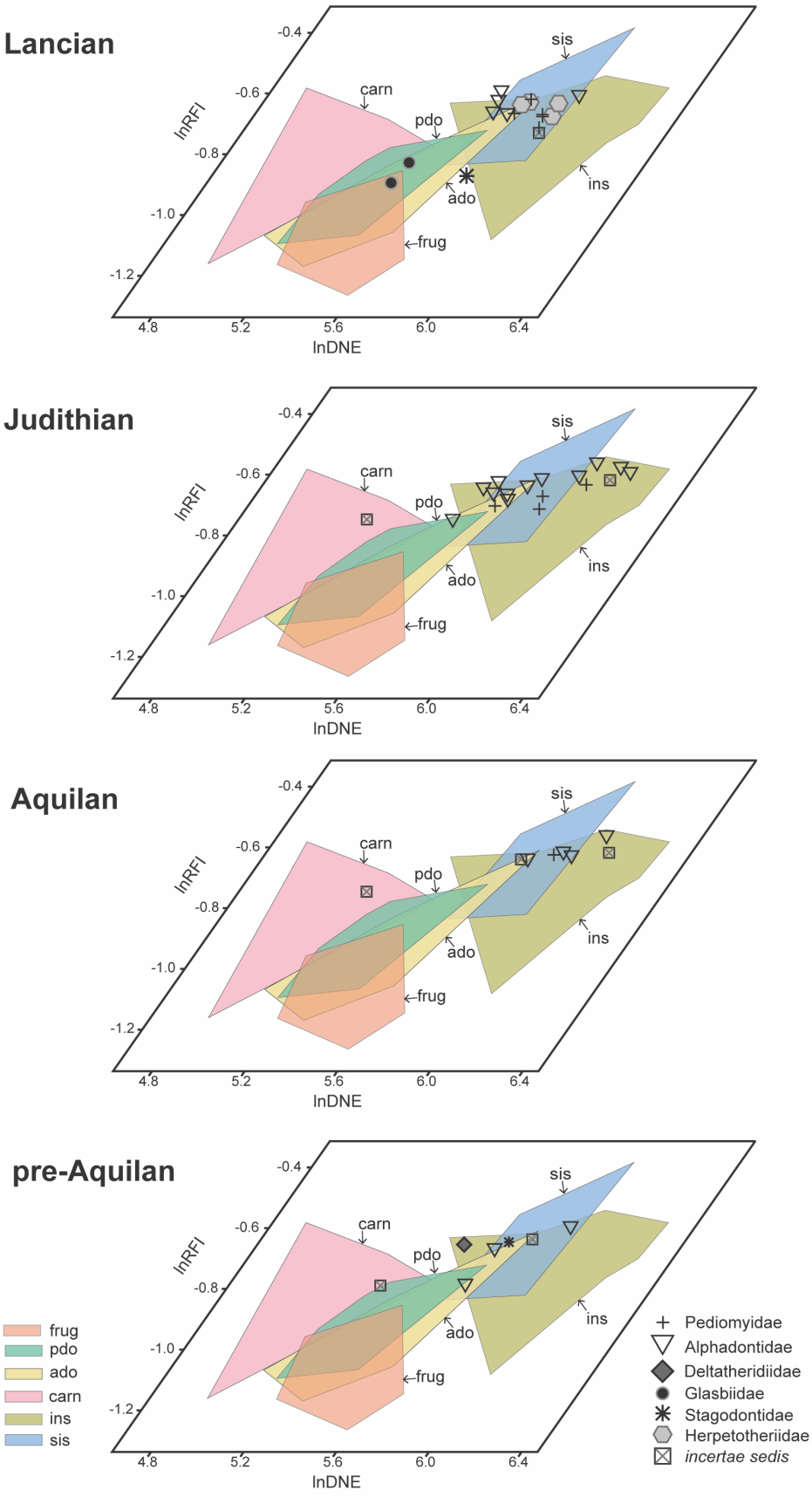
Lancian
Judithian
Aquilan
pre-Aquilan
lnRFI
lnDNE
-0.4
-0.6
-0.8
-1.0
-1.2
4.8
5.2
5.6
6.0
6.4
carn
pdo
ado
frug
ins
sis
frug
pdo
ado
carn
ins
sis
Pediomyidae
Alphadontidae
Deltatheridiidae
Glasbiidae
Stagodontidae
Herpetotheriidae
incertae sedis

Figure 4.7. Scatterplots of lnDNE versus lnRFI of NALK metatherians through time. Points represent species averages for each DTA metric. Time proceeds upward with the oldest time bin (pre-Aquilan) at the bottom and the youngest time bin (Lancian) at the top. Colored polygons are regions of the morphospace occupied by extant mammals in our dietary categories. Markers correspond to fossil groups. Abbreviations for diet categories: ado = animal-dominated omnivore; carn = carnivore; frug = frugivore; ins = insectivore; pdo = plant-dominated omnivore; sis = soft-insect specialist.

4.13 TABLES

Table 4.1. Extant mammalian comparative dataset. The online archives EltonTraits (Wilman et al., 2014) and Mammal DIET (Kissling et al., 2014) and a natural history compendium (Nowak, 1999) were used as the main source for determining diets, but we supplemented this data with information from the primary literature. Abbreviations for diet categories: ado = animal-dominated omnivore; carn = carnivore; frug = frugivore; ins = insectivore; pdo = plant-dominated omnivore; sis = soft-insect specialist.

Species	Order	N	Tooth position	Diet	Supplemental diet source(s)
Antechinus stuartii	Dasyuromorphia	3	M3	ins	Fox and Archer 1984
Artibeus lituratus	Chiroptera	3	M2	frug	Zortéa and Mendes, 1993; Parolin et al., 2016
Caluromys sp.	Didelphimorphia	1	M3	pdo	Robinson and Redford, 1986; Casella and Cáceres, 2006
Caluromys derbianus	Didelphimorphia	1	M3	pdo	Steiner, 1981; Robinson and Redford, 1986
Cheirogaleus medius	Primates	3	M2	frug	Fietz and Ganzhorn, 1999
Chironectes minimus	Didelphimorphia	1	M3	carn	Monodolfi and Padilla, 1958
Crocuta crocuta	Carnivora	1	P4	carn	Kruuk, H. 1972; Cooper et al., 1999
Dasyurus maculatus	Dasyuromorphia	1	M3	carn	Belcher et al., 2007; Andersen et al., 2017; Linley et al., 2020
Didelphis albiventris	Didelphimorphia	1	M3	ado	Cáceres, 2002; Cantor et al., 2010
Didelphis marsupialis	Didelphimorphia	2	M3	pdo	Robinson and Redford, 1986; Julien-Laferriere and Atramentowicz, 1990; Medellin, 1994

Didelphis virginiana	Didelphimorphia	3	M3	ado	Sandidge, 1953; Hopkins and Forbes, 1980
Eira barbara	Carnivora	1	M1	carn	Bisbal 1986
Eptesicus fuscus	Chiroptera	3	M2	ins	Whitaker 1995; Agosta and Morton 2003
Lynx rufus	Carnivora	1	P4	carn	Fritts and Sealander 1978; Rose and Prange 2015; Sánchez-González et al. 2018
Metachirus nudicaudatus	Didelphimorphia	3	M3	ado	Santori et al., 1995; Lessa and Geise, 2014
Monodelphis domestica	Didelphimorphia	1	M3	ado	Streilein, 1982; de Carvalho et al., 2019
Nasua narica	Carnivora	2	M2	frug	Gompper, 1996
Nyctinomops macrotis	Chiroptera	1	M2	sis	Easterla and Whitaker, 1972; Debelica et al., 2006
Paradoxurus hermaphroditus	Carnivora	1	M1	frug	Joshi et al., 1995; Nakashima et al., 2010
Pecari tajacu	Cetartiodactyla	1	M2	frug	Desbiez et al., 2009
Perameles nasuta	Peramelemorphia	1	M3	ins	Scott et al., 1999; Thums et al., 2005
Philander opossum	Didelphimorphia	3	M3	ado	Hall and Dalquest, 1963; Charles-Dominique et al., 1981; Atramentowicz, 1988
Plecotus auritus	Chiroptera	1	M2	sis	Rostovskaya et al., 2000; Whitaker and Karatas, 2009
Procyon lotor	Carnivora	3	M1	ado	Schoonover and Marshall, 1951; Bartoszewicz et al. 2008; Rulison et al., 2012
Sarcophilus harrisii	Dasyuromorphia	1	M3	carn	Jones and Barmuta, 1998; Pemberton et al., 2008; Andersen et al., 2017

Scapanus orarius	Soricomorpha	3	M2	sis	Moore, 1933; Glendenning, 1959
Sorex vagrans	Soricomorpha	3	M2	ins	Clothier 1955; McCracken, 1990
Spilogale putorius	Carnivora	2	M1	ado	Crabb, 1941; Baker and Baker, 1975
Tamias townsendii	Rodentia	3	M2	pdo	Trombulak, 1985; Carey et al., 2002
Thylamys elegans	Didelphimorphia	2	M3	ins	Meserve, 1981

Table 4.2. Fossil metatherian dataset. Specimen type refers to whether the original fossil specimen or a cast of the fossil specimen was μCT scanned and subsequent tooth model was used in our analyses.

Species	Specimen number	Tooth position	Clade	NALMA	Specimen type
Aenigmadelphys archeri	OMNH 20160	M2	Alphadontidae	Judithian	cast
Aenigmadelphys archeri	OMNH 23328	M3	Alphadontidae	Judithian	cast
Albertatherium primum	UALVP 29611	M3	Alphadontidae	Aquilan	fossil
Albertatherium primum	UALVP 29612	M3	Alphadontidae	Aquilan	fossil
Albertatherium secundum	UALVP 29534	M3	Alphadontidae	Aquilan	fossil
Alphadon halleyi	UCMP 130501	M3	Alphadontidae	Judithian	fossil
Alphadon marshi	UCMP 52450	M3	Alphadontidae	Lancian	fossil
Alphadon marshi	UCMP 53097	M3	Alphadontidae	Lancian	fossil
Alphadon sahnii	OMNH 20114	M2 or M3	Alphadontidae	Judithian	cast
Alphadon wilsoni	UALVP 3532	M3	Alphadontidae	Lancian	fossil
Eoalphadon clemensi	MNA.V.5387	M2	Alphadontidae	pre-Aquilan	fossil
Eoalphadon lillegraveni	MNA.V.5835	M2	Alphadontidae	pre-Aquilan	cast
Eoalphadon woodburnei	UMNH VP 12842	M3	Alphadontidae	pre-Aquilan	fossil
Protalphadon foxi	UCMP 109031	M3	Alphadontidae	Lancian	fossil
Protalphadon lulli	UCMP 47446	M3	Alphadontidae	Lancian	fossil
Protalphadon lulli	UCMP 47475	M3	Alphadontidae	Lancian	fossil
Turgidodon lillegraveni	OMNH 20117	M2(?)	Alphadontidae	Judithian	cast
Turgidodon madseni	OMNH 20538	M3	Alphadontidae	Judithian	cast
Turgidodon praesagus	UALVP 55849	M3	Alphadontidae	Judithian	fossil
Turgidodon praesagus	UCMP 122168	M3	Alphadontidae	Judithian	fossil
Turgidodon praesagus	UCMP 131345	M2	Alphadontidae	Judithian	fossil

Turgidodon rhaister	UCMP 47366	M2	Alphadontidae	Lancian	fossil
Turgidodon russelli	UALVP 55852	M3	Alphadontidae	Judithian	fossil
Turgidodon russelli	UALVP 6983	M3	Alphadontidae	Judithian	fossil
Varalphadon creber	UALVP 29525	M3	Alphadontidae	Aquilan	fossil
Varalphadon creber	UALVP 29527	M3	Alphadontidae	Aquilan	fossil
Varalphadon creber	UALVP 5529	M3	Alphadontidae	Aquilan	fossil
Varalphadon wahweapensis	UALVP 5544	M3	Alphadontidae	Aquilan	fossil
Atokatheridium boreni	OMNH 61623	M2	Deltatheridiidae	pre-Aquilan	cast
Glasbius intricatus	UCMP 102111	M3	Glasbiidae	Lancian	fossil
Glasbius twitchelli	UCMP 153679	M3	Glasbiidae	Lancian	fossil
Glasbius twitchelli	UCMP 156143	M3	Glasbiidae	Lancian	fossil
Glasbius twitchelli	UCMP 224090	M3	Glasbiidae	Lancian	fossil
Nortedelphys intermedius	UCMP 134776	M3	Herpetotheriidae	Lancian	fossil
Nortedelphys jasoni	UCMP 174506	M3	Herpetotheriidae	Lancian	fossil
Nortedelphys jasoni	UCMP 177838	M3	Herpetotheriidae	Lancian	fossil
Nortedelphys magnus	UA 2846	M3	Herpetotheriidae	Lancian	cast
Nortedelphys minimus	UCMP 52715	M2	Herpetotheriidae	Lancian	fossil
Nortedelphys minimus	UCMP 72211	M3	Herpetotheriidae	Lancian	fossil
Anchistodelphys archibaldi	OMNH 21033	M3	*incertae sedis*	Aquilan	cast
Apistodon exiguus	UALVP 29693	M3	*incertae sedis*	Aquilan	fossil
Dakotadens morrowi	OMNH 49450	Mx	*incertae sedis*	pre-Aquilan	cast
Hatcheritherium alpha	YPM.VP.014911	M3	*incertae sedis*	Lancian	fossil
Hatcheritherium alpha	YPM.VP.014912	M1(?)	*incertae sedis*	Lancian	fossil
Iugomortiferum thoringtoni	OMNH 20936	M1(?)	*incertae sedis*	Aquilan	cast
Kokopellia juddi	OMMH 33248	M3	*incertae sedis*	pre-Aquilan	cast

Iqualadelphis lactea	UALVP 22827	M3	Pediomyidae	Aquilan	fossil
Iqualadelphis lactea	UALVP 29676	M3	Pediomyidae	Aquilan	fossil
Leptalestes cooki	UCMP 46306	M3	Pediomyidae	Lancian	fossil
Leptalestes cooki	UCMP 48351	M3	Pediomyidae	Lancian	fossil
Leptalestes cooki	UCMP 51344	M3	Pediomyidae	Lancian	fossil
Leptalestes krejcii	UCMP 47061	M3	Pediomyidae	Lancian	fossil
Leptalestes krejcii	UCMP 47552	M3	Pediomyidae	Lancian	fossil
Leptalestes krejcii	UCMP 52761	M3	Pediomyidae	Lancian	fossil
Leptalestes prokrejcii	UCMP 131341	M1	Pediomyidae	Judithian	fossil
Pediomys elegans	UCMP 168701	M3	Pediomyidae	Lancian	cast
Pediomys elegans	UCMP 47558	M3	Pediomyidae	Lancian	fossil
Pediomys elegans	UCMP 51335	M3	Pediomyidae	Lancian	fossil
Protolambda clemensi	UALVP 55855	M3	Pediomyidae	Judithian	fossil
Protolambda clemensi	UCMP 122179	M3	Pediomyidae	Judithian	fossil
Protolambda clemensi	UCMP 131340	M3	Pediomyidae	Judithian	cast
Protolambda florencae	UCMP 186770	M3	Pediomyidae	Lancian	fossil
Protolambda florencae	UCMP 48331	M3	Pediomyidae	Lancian	fossil
Protolambda florencae	UCMP 51389	M2	Pediomyidae	Lancian	fossil
Protolambda florencae	UCMP 52323	M3	Pediomyidae	Lancian	fossil
Protolambda hatcheri	UCMP 46232	M3	Pediomyidae	Lancian	fossil
Protolambda hatcheri	UCMP 47262	M3	Pediomyidae	Lancian	fossil
Protolambda hatcheri	UCMP 52404	M3	Pediomyidae	Lancian	fossil
Didelphodon vorax	UCMP 187607	M3	Stagodontidae	Lancian	fossil
Didelphodon vorax	UCMP 47304	M3(?)	Stagodontidae	Lancian	cast
Pariadens kirklandi	MNA.V.5843	M3(?)	Stagodontidae	pre-Aquilan	fossil

Table 4.3. Phylogenetic correlation in our log-transformed DTA data for our extant comparative dataset. We report Blomberg's K and Pagel's lambda. *P*-values associated with each measurement are also reported here.

	Blomberg's K	K, *p*-value	Pagel's λ	λ, *p*-value
lnDNE	0.36	0.068	0.57	1
lnRFI	0.35	0.071	0.02	0.900
lnOPCR	0.48	0.02	0.91	0.060

Table 4.4. Correlations among DTA metrics in our extant comparative dataset. DTA metric data are log-transformed. Linear regression R^2 values are reported in the upper right cells of this table, with associated *p*-values in parentheses. Significant *p*-values are in bold ($p < 0.05$). Spearman's rho values are reported in the lower left cells of the table, with associated *p*-values in parentheses. Significant *p*-values are in bold ($p < 0.05$).

	lnDNE	lnRFI	lnOPCR
lnDNE	–	0.22 (**2.51e-04**)	0.29 (**1.49e-05**)
lnRFI	0.47 (**2.27e-04**)	–	0.04 (0.15)
lnOPCR	0.51 (**5.75e-05**)	0.09 (0.48)	–

Table 4.5. Contingency table visualization of extant mammal dietary classifications by our DFA. Rows represent the true diet classification, whereas the columns represent the classifications made by our DFA. Correctly classifications are highlighted in dark gray along the diagonal. Incorrect classifications are highlighted in light gray. Note the number of incorrect classifications of animal-dominated omnivores and other diets as plant-dominated omnivores. Abbreviations for diet categories: ado = animal-dominated omnivore; carn = carnivore; frug = frugivore; ins = insectivore; pdo = plant-dominated omnivore; sis = soft-insect specialist.

	ado	carn	frug	ins	pdo	sis	% correctly classified
ado	5	0	7	1	3	0	31.3
carn	0	4	0	0	2	0	66.7
frug	1	1	6	0	2	0	60.0
ins	0	0	0	9	0	3	75.0
pdo	1	0	1	0	5	0	71.4
sis	0	0	0	1	0	4	80.0

Table 4.6. Posterior probabilities of dietary categories resulting from discriminant function analysis (DFA) of our extant mammal dataset. The highest posterior probability representing the diet identified by DFA is in bold. Posterior probabilities < 0.001 are not reported. Other posterior probabilities that are within 0.10 to the highest posterior probability are marked with an asterisk. Abbreviations for diet categories: ado = animal-dominated omnivore; carn = carnivore; frug = frugivore; ins = insectivore; pdo = plant-dominated omnivore; sis = soft-insect specialist.

Species	Specimen	diet	frug	pdo	ado	carn	ins	sis
Antechinus stuartii	UWBM 68899	ins	0.009	0.049	0.060	-	**0.642**	0.240
Antechinus stuartii	UWBM 68915	ins	0.001	0.006	0.009	-	**0.727**	0.256
Antechinus stuartii	UWBM 68916	ins	-	-	-	-	0.455*	**0.545**
Artibeus lituratus	UWBM 62023	frug	**0.470**	0.098	0.428*	-	0.003	0.001
Artibeus lituratus	UWBM 62030	frug	0.440*	0.096	**0.463**	-	0.001	-
Artibeus lituratus	UWBM 62034	frug	**0.673**	0.059	0.254	0.011	0.001	0.001
Caluromys derbianus	UWBM 32255	pdo	0.047	**0.344**	0.251*	0.008	0.156	0.194
Caluromys sp.	EA 181	pdo	0.111	**0.576**	0.298	0.015	-	-
Cheirogaleus medius	DLC 1607	frug	**0.443**	0.216	0.321	0.020	-	-
Cheirogaleus medius	DLC 1636	frug	**0.512**	0.182	0.305	0.001	-	-
Cheirogaleus medius	DLC 3640	frug	0.173	0.174	0.138	**0.514**	-	0.001
Chironectes minimus	MVZ 173550	carn	0.032	**0.671**	0.147	0.148	-	0.002
Crocuta crocuta	UWBM 33257	carn	0.001	0.010	0.002	**0.985**	-	0.002
Dasyurus maculatus	UWBM 68901	carn	0.074	**0.266**	0.199	0.140	0.056	0.265*
Didelphis albiventris	UWBM 38710	ado	0.081	**0.469**	0.293	0.051	0.027	0.079
Didelphis marsupialis	UWBM 39942	pdo	**0.443**	0.169	0.382*	0.004	0.001	0.001

Didelphis marsupialis	UWBM 44459	pdo	0.320	0.320	**0.346**	0.014	-	-
Didelphis virginiana	UWBM 39628	ado	0.129	0.427*	**0.434**	0.001	0.006	0.003
Didelphis virginiana	UWBM 76104	ado	0.159	0.386*	**0.420**	0.007	0.014	0.014
Didelphis virginiana	UWBM 76135	ado	0.156	**0.444**	0.390*	0.007	0.002	0.002
Eira barbara	UWBM 39436	carn	0.383*	0.076	0.096	**0.444**	-	-
Eptesicus fuscus	UWBM 66977	ins	-	-	-	-	**0.723**	0.276
Eptesicus fuscus	UWBM 66980	ins	-	-	-	-	**0.827**	0.173
Eptesicus fuscus	UWBM 79331	ins	-	-	-	-	**0.730**	0.269
Lynx rufus	OUVC 9576	carn	-	-	-	**1.000**	-	-
Metachirus nudicaudatus	UWBM 35439	ado	**0.541**	0.152	0.294	0.013	-	-
Metachirus nudicaudatus	UWBM 35440	ado	0.347*	0.210	**0.439**	0.001	0.001	0.001
Metachirus nudicaudatus	UWBM 35438	ado	**0.372**	0.335	0.279*	0.014	-	-
Monodelphis domestica	AMNH 261241	ado	0.007	0.149	0.078	0.002	**0.384**	0.380*
Nasua narica	UWBM 41687	frug	0.215	**0.363**	0.243	0.179	-	-
Nasua narica	UWBM 41688	frug	**0.462**	0.127	0.195	0.216	-	-
Nyctinomops macrotis	UMMZ 113271	sis	0.005	0.008	0.018	-	**0.682**	0.287
Paradoxurus hermaphroditus	UWBM 14711	frug	**0.770**	0.017	0.176	0.007	0.017	0.014
Pecari tajacu	UWBM 20670	frug	0.137	**0.484**	0.366	0.009	0.001	0.002
Perameles nasuta	UWBM 82259	ins	0.007	0.081	0.030	0.317	0.033	**0.532**
Philander opossum	UWBM 44451	ado	0.331*	0.258	**0.390**	0.017	0.002	0.003
Philander opossum	UWBM 44452	ado	0.133	**0.497**	0.315	0.050	0.001	0.004
Philander opossum	UWBM 44469	ado	0.218	0.295	**0.417**	0.014	0.025	0.031
Plecotus auritus	UMMZ 111012	sis	0.049	0.071	0.097	0.041	0.189	**0.554**
Procyon lotor	UWBM 32812	ado	**0.450**	0.125	0.398*	0.005	0.013	0.009

Procyon lotor	UWBM 32814	ado	**0.437**	0.156	0.389*	0.009	0.004	0.004
Procyon lotor	UWBM 32819	ado	**0.505**	0.133	0.278	0.081	0.001	0.002
Sarcophilus harrisii	UWBM 20671	carn	0.070	0.107	0.056	**0.767**	-	-
Scapanus orarius	UWBM 64808	sis	0.002	0.057	0.021	0.012	0.176	**0.732**
Scapanus orarius	UWBM 64811	sis	-	-	-	-	0.278	**0.722**
Scapanus orarius	UWBM 64820	sis	-	0.001	-	-	0.200	**0.798**
Sorex vagrans	UWBM 58640	ins	-	-	-	-	**0.915**	0.085
Sorex vagrans	UWBM 58646	ins	-	-	-	-	**0.874**	0.126
Sorex vagrans	UWBM 60640	ins	0.069	0.009	0.080	-	**0.779**	0.063
Spilogale putorius	UWBM 20192	ado	**0.654**	0.079	0.245	0.021	-	-
Spilogale putorius	UWBM 76080	ado	**0.552**	0.153	0.284	0.011	-	-
Tamias townsendii	UWBM 20077	pdo	0.095	**0.476**	0.255	0.149	0.004	0.021
Tamias townsendii	UWBM 43787	pdo	0.085	**0.502**	0.231	0.171	0.001	0.010
Tamias townsendii	UWBM 44335	pdo	0.105	**0.412**	0.209	0.269	0.001	0.005
Thylamys elegans	UWBM 49007	ins	0.002	0.022	0.016	-	**0.555**	0.405
Thylamys elegans	UWBM 49057	ins	0.004	0.068	0.041	0.002	0.400	**0.485**

Table 4.7. Posterior probabilities of dietary categories resulting from the discriminant function analysis (DFA) of our fossil metatherian sample. The highest posterior probability representing the diet identified by DFA is in bold. Posterior probabilities < 0.001 are not reported. Other posterior probabilities that are within 0.10 to the highest posterior probability are marked with an asterisk. Abbreviations for diet categories: ado = animal-dominated omnivore; carn = carnivore; frug = frugivore; ins = insectivore; pdo = plant-dominated omnivore; sis = soft-insect specialist.

Species	Specimen	pred. diet	frug	pdo	ado	carn	ins	sis
Aenigmadelphys archeri	OMNH 20160	ins	-	0.004	0.002	-	**0.529**	0.466
Aenigmadelphys archeri	OMNH 23328	ins	-	0.005	0.004	-	**0.725**	0.266
Albertatherium primum	UALVP 29611	ins	-	0.006	0.004	-	**0.799**	0.191
Albertatherium primum	UALVP 29612	ins	-	0.012	0.008	-	**0.692**	0.288
Albertatherium secundum	UALVP 29534	ins	0.002	0.026	0.021	-	**0.671**	0.280
Alphadon halleyi	UCMP 130501	pdo	0.027	**0.435**	0.185	0.029	0.086	0.239
Alphadon marshi	UCMP 52450	ins	0.001	0.010	0.008	-	**0.770**	0.211
Alphadon marshi	UCMP 53097	ins	0.004	0.060	0.042	-	**0.564**	0.330
Alphadon sahnii	OMNH 20114	ins	-	0.001	0.001	-	**0.846**	0.153
Alphadon wilsoni	UALVP 3532	pdo	0.028	**0.375**	0.195	0.013	0.137	0.251
Eoalphadon clemensi	MNA.V.5387	sis	0.019	0.192	0.115	0.014	0.211	**0.450**
Eoalphadon lillegraveni	MNA.V.5835	pdo	0.093	**0.442**	0.394*	0.003	0.038	0.029
Eoalphadon woodburnei	UMNH VP 12842	ins	0.002	0.044	0.029	-	**0.611**	0.314
Protalphadon foxi	UCMP 109031	pdo	0.015	**0.403**	0.141	0.020	0.113	0.307*
Protalphadon lulli	UCMP 47446	sis	0.011	0.292*	0.121	0.005	0.225	**0.346**
Protalphadon lulli	UCMP 47475	pdo	0.027	**0.349**	0.156	0.055	0.086	0.328*

Turgidodon lillegraveni	OMNH 20117	pdo	0.073	**0.444**	0.291	0.033	0.048	0.112
Turgidodon madseni	OMNH 20538	ins	-	0.003	0.002	-	**0.815**	0.180
Turgidodon praesagus	UALVP 55849	sis	0.020	0.171	0.120	0.006	0.282	**0.401**
Turgidodon praesagus	UCMP 122168	ins	0.002	0.037	0.031	-	**0.724**	0.205
Turgidodon praesagus	UCMP 131345	sis	0.003	0.159	0.049	0.004	0.259	**0.526**
Turgidodon rhaister	UCMP 47366	sis	0.021	0.236	0.145	0.006	0.249*	**0.343**
Turgidodon russelli	UALVP 55852	ins	0.026	0.227*	0.169	0.003	**0.298**	0.277*
Turgidodon russelli	UALVP 6983	pdo	0.026	**0.312**	0.181	0.008	0.196	0.278*
Varalphadon creber	UALVP 29525	ins	0.001	0.011	0.009	-	**0.669**	0.311
Varalphadon creber	UALVP 29527	ins	0.002	0.022	0.016	-	**0.530**	0.430
Varalphadon creber	UALVP 5529	ins	0.004	0.070	0.044	0.001	**0.515**	0.367
Varalphadon wahweapensis	UALVP 5544	sis	0.006	0.068	0.044	0.002	0.370	**0.510**
Atokatheridium boreni	OMNH 61623	sis	0.013	0.128	0.061	0.118	0.082	**0.597**
Glasbius intricatus	UCMP 102111	pdo	0.203	**0.388**	0.375*	0.027	0.002	0.005
Glasbius twitchelli	UCMP 153679	pdo	0.156	**0.397**	0.251	0.193	-	0.003
Glasbius twitchelli	UCMP 156143	pdo	0.103	**0.436**	0.383*	0.007	0.034	0.037
Glasbius twitchelli	UCMP 224090	pdo	0.131	**0.435**	0.331*	0.060	0.011	0.032
Nortedelphys intermedius	UCMP 134776	sis	0.005	0.073	0.044	0.003	0.358	**0.518**
Nortedelphys jasoni	UCMP 174506	pdo	0.030	**0.312**	0.189	0.010	0.180	0.279*
Nortedelphys jasoni	UCMP 177838	sis	0.004	0.073	0.039	0.001	0.423*	**0.460**
Nortedelphys magnus	UA 2846	ins	0.002	0.021	0.017	-	**0.567**	0.393
Nortedelphys minimus	UCMP 52715	ins	0.017	0.170	0.141	0.001	**0.446**	0.226
Nortedelphys minimus	UCMP 72211	ins	0.001	0.013	0.013	-	**0.706**	0.267
Anchistodelphys archibaldi	OMNH 21033	ins	-	0.003	0.003	-	**0.820**	0.174
Apistodon exiguus	UALVP 29693	pdo	0.019	**0.331**	0.177	0.003	0.242*	0.228

Dakotadens morrowi	OMNH 49450	pdo	0.082	**0.374**	0.183	0.346*	0.001	0.014
Hatcheritherium alpha	YPM.VP.014911	pdo	0.054	**0.414**	0.366*	0.001	0.122	0.044
Hatcheritherium alpha	YPM.VP.014912	ins	0.002	0.009	0.014	-	**0.783**	0.192
Iugomortiferum thoringtoni	OMNH 20936	carn	0.033	0.247	0.080	**0.632**	-	0.007
Kokopellia juddi	OMMH 33248	ins	0.008	0.109	0.070	0.002	**0.407**	0.405*
Iqualadelphis lactea	UALVP 22827	ins	-	0.002	0.001	-	**0.651**	0.345
Iqualadelphis lactea	UALVP 29676	sis	0.027	0.253*	0.171	0.006	0.245*	**0.299**
Leptalestes cooki	UCMP 46306	ins	0.001	0.006	0.007	-	**0.801**	0.185
Leptalestes cooki	UCMP 48351	sis	0.015	0.117	0.090	0.004	0.343*	**0.432**
Leptalestes cooki	UCMP 51344	ins	0.010	0.107	0.076	0.002	**0.408**	0.398*
Leptalestes krejcii	UCMP 47061	sis	0.006	0.064	0.038	0.007	0.259	**0.626**
Leptalestes krejcii	UCMP 47552	sis	-	0.010	0.005	-	0.451*	**0.533**
Leptalestes krejcii	UCMP 52761	sis	0.006	0.037	0.030	0.008	0.267	**0.651**
Leptalestes prokrejcii	UCMP 131341	sis	0.012	0.069	0.055	0.010	0.261	**0.592**
Pediomys elegans	UCMP 168701	ins	0.008	0.038	0.058	-	**0.749**	0.147
Pediomys elegans	UCMP 47558	ins	0.007	0.071	0.060	0.001	**0.538**	0.323
Pediomys elegans	UCMP 51335	ins	0.012	0.059	0.063	0.001	**0.489**	0.376*
Protolambda clemensi	UALVP 55855	ins	-	0.002	0.003	-	**0.824**	0.171
Protolambda clemensi	UCMP 122179	ins	0.001	0.017	0.011	-	**0.602**	0.369
Protolambda clemensi	UCMP 131340	ins	-	0.002	0.002	-	**0.659**	0.336
Protolambda florencae	UCMP 48331	ins	0.003	0.019	0.021	-	**0.590**	0.367
Protolambda florencae	UCMP 51389	sis	0.001	0.014	0.010	0.001	0.422	**0.553**
Protolambda florencae	UCMP 186770	ins	0.002	0.013	0.014	-	**0.700**	0.271
Protolambda florencae	UCMP 52323	sis	0.022	0.103	0.104	0.003	0.380*	**0.388**
Protolambda hatcheri	UCMP 46232	sis	0.012	0.066	0.064	0.002	0.427*	**0.430**

Protolambda hatcheri	UCMP 47262	sis	0.003	0.040	0.024	0.001	0.386	**0.546**
Protolambda hatcheri	UCMP 52404	sis	0.010	0.085	0.051	0.026	0.173	**0.655**
Didelphodon vorax	UCMP 187607	ado	0.214	0.323*	**0.429**	0.009	0.012	0.013
Didelphodon vorax	UCMP 47304	ins	0.024	0.040	0.085	-	**0.644**	0.207
Pariadens kirklandi	MNA.V.5843	pdo	0.027	**0.493**	0.243	0.003	0.118	0.116

Table 4.8. Simulation-based *p*-values using the morphol.disparity function in the geomorph package in R (Adams et al., 2020) for calculations of dental disparity for each DTA metric and the sum of variances.

	lnDNE	**lnRFI**	**lnOPCR**	**Sum of variances**
Intraclade disparity				
Alphadontidae v. Pediomyidae	0.043	0.318	0.664	0.097
Disparity through time				
pre-Aquilan v. Aquilan	0.410	0.525	0.911	0.92
pre-Aquian v. Judithian	0.578	0.556	0.469	0.822
pre-Aquilan v. Lancian	0.735	0.502	0.105	0.553
Aquilan v. Judithian	0.702	0.923	0.523	0.669
Aquilan v. Lancian	0.137	0.112	0.114	0.436
Judithian v. Lancian	0.241	0.056	0.31	0.676

Table 4.9. Dietary categories present in each time bin as determined by the DFA. At the top of each column, the number of species sampled in each time bin is in parentheses. Table cells include the number of taxa assigned to each diet category and the corresponding percentage rounded to the nearest tenth (in parentheses) for that time bin. Adjusted columns include the number of taxa assigned to each diet category and corresponding percentage after adjusting for interpretations from the primary literature and the second highest posterior probability (see Discussion). Abbreviations for diet categories: ado = animal-dominated omnivore; carn = carnivore; frug = frugivore; ins = insectivore; pdo = plant-dominated omnivore; sis = soft-insect specialist.

Diet	pre-Aquilan (7)	pre-Aquilan adjusted	Aquilan (8)	Aquilan adjusted	Judithian (18)	Judithian adjusted	Lancian (18)	Lancian adjusted
frug	-	-	-	-	-	-	-	-
pdo	3 (42.9)	3 (42.8)	1 (12.5)	1 (12.5)	3 (16.7)	2 (11.1)	4 (22.2)	2 (11.1)
ado	-	-	-	-	-	-	-	1 (5.6)
carn	-	-	1 (12.5)	-	1 (5.6)	-	-	-
ins	2 (28.6)	2 (28.6)	5 (62.5)	6 (75.0)	9 (50.0)	9 (50.0)	8 (44.4)	7 (38.9)
sis	2 (28.6)	2 (28.6)	1 (12.5)	1 (12.5)	5 (27.8)	7 (38.9)	6 (33.3)	8 (44.4)

4.14 APPENDICES

Appendix 1: Specimens included in this study that were downloaded from MorphoSource.org

Genus	species	Specimen number	Tooth	MorphoSource media number	DOI	Citation
Caluromys	sp.	DU:EA181	M3	000028492	https://doi.org/10.17602/M2/M28492	Duke University, MorphoSource.org
Cheirogaleus	*medius*	DLC 1607	M2	000014380	https://doi.org/10.17602/M2/M14380	The Duke Lemur Center provided access to these data, originally appearing in Yapuncich et al. (2019), the collection of which was funded by NSF BCS 1540421 to Gabriel S. Yapuncich and Doug M. Boyer.
Cheirogaleus	*medius*	DLC 1636	M2	000014389	https://doi.org/10.17602/M2/M14389	The Duke Lemur Center provided access to these data, originally appearing in Yapuncich et al. (2019), the collection of which was funded by NSF BCS 1540421 to Gabriel S. Yapuncich and Doug M. Boyer.
Cheirogaleus	*medius*	DLC 3640	M2	000015246	https://doi.org/10.17602/M2/M15246	The Duke Lemur Center provided access to these data, originally appearing in Yapuncich et al. (2019), the collection of which was funded by NSF BCS 1540421 to Gabriel S. Yapuncich and Doug M. Boyer.

Lynx	*rufus*	OUVC 9576	P4	000067438	no DOI available	WitmerLab at Ohio University provided access to these data originally appearing on the Visible Interactive Bobcat website, the collection of which was funded by NSF.
Monodelphis	*domestica*	AMNH 261241	M3	000023879	no DOI available	Eric Delson and the AMNH Department of Mammalogy provided access to these data originally appearing in the collection of which was funded by AMNH and NYCEP.
Nyctinomops	*macrotis*	UMMZ 113271	M2	000035462	no DOI available	Shi et al. 2018 and the University of Michigan
Plecotus	*auritus*	UMMZ 111012	M2	000035566	no DOI available	Shi et al. 2018 and the University of Michigan

Appendix 2: Scanner information and settings for all specimens (extant and fossil) used in this study. Specimens with an asterisk (*) were downloaded from MorphoSouce—please contact MorphoSource for more information regarding scanner information and scanner settings

Genus	Species	Specimen number	Scanner	Voltage (kV)	Current (uA)	Image pixel size (um)	Filter	Exposure (ms)	Rotation Step	Frame Averaging	Random Movement
Antechinus	*stuartii*	UWBM 68899	SkyScan 1172	48	208	6.66	Al 0.5mm	680	0.25	5	20
Antechinus	*stuartii*	UWBM 68916	SkyScan 1172	48	208	6.65	Al 0.5mm	680	0.25	5	20
Antechinus	*stuartii*	UWBM 68915	SkyScan 1172	48	208	7.56	Al 0.5mm	680	0.25	5	20
Artibeus	*lituratus*	UWBM 62023	Skyscan 1173	65	123	13.49	Al 1.0mm	1150	0.3	4	10
Artibeus	*lituratus*	UWBM 62030	Skyscan 1173	65	123	13.49	Al 1.0mm	1150	0.3	4	10
Artibeus	*lituratus*	UWBM 62034	SkyScan 1173	65	123	14.2	Al 1.0mm	1175	0.3	4	10

Caluromys	*derbianus*	UWBM 32255_B	SkyScan 1172	48	208	12.0	Al 0.5mm	1170	0.25	5	20
Caluromys	*sp.**	EA 181	Nikon XTH 225 ST (Duke)	153	103	45.34					
Cheirogaleus	*medius**	DLC 1607	Nikon XTH 225 ST (Duke)	140	115	29.46				1	
Cheirogaleus	*medius**	DLC 1636	Nikon XTH 225 ST (Duke)	150	100	30.69				1	
Cheirogaleus	*medius**	DLC 3640	Nikon XTH 225 ST (Duke)	150	146	23.77				1	
Chironectes	*minimus*	MVZ 173550	NSI X5000	104	500	42.5	none				
Crocuta	*crocuta*	UWBM 33257	SkyScan 1173	65	123	19.8	Al 1.0mm	1175	0.3	4	10
Dasyurus	*maculatus*	UWBM 68901	SkyScan 1173	55	135	15.9	Al 1.0mm	1175	0.3	4	10

Didelphis	*albiventris*	UWBM 38710	Skyscan 1173	65	123	13.49	Al 1.0mm	1150	0.3	4	10
Didelphis	*marsupialis*	UWBM 44459	SkyScan 1173	65	123	16.3	Al 1.0mm	1175	0.3	4	10
Didelphis	*marsupialis*	UWBM 39942	Skyscan 1173	65	123	13.49	Al 1.0mm	1150	0.3	4	10
Didelphis	*virginiana*	UWBM 39628	Skyscan 1173	65	123	15.2	Al 1.0mm	1150	0.3	4	10
Didelphis	*virginiana*	UWBM 76104	Skyscan 1173	65	123	13.49	Al 1.0mm	1150	0.3	4	10
Didelphis	*virginiana*	UWBM 76135	Skyscan 1173	65	123	15.2	Al 1.0mm	1150	0.3	4	10
Eira	*barbara*	UWBM 39436	SkyScan 1173	65	123	16.3	Al 1.0mm	1175	0.3	4	10
Eptesicus	*fuscus*	UWBM 66977	SkyScan 1172	49	200	6.0	Al 0.5mm	735	0.25	3	20
Eptesicus	*fuscus*	UWBM 66980	SkyScan 1172	48	208	8.22	Al 0.5mm	735	0.25	5	20
Eptesicus	*fuscus*	UWBM 79331	SkyScan 1172	49	200	6.0	Al 0.5mm	735	0.25	3	20

Lynx	*rufus**	OUVC 9576	TriFoil Imaging eXplore CT 120	80	450	90				7	
Metachirus	*nudicaudatus*	UWBM 35438	SkyScan 1173	65	123	14.2	Al 1.0mm	1175	0.3	4	10
Metachirus	*nudicaudatus*	UWBM 35439	SkyScan 1173	65	123	13.4	Al 1.0mm	1170	0.3	4	10
Metachirus	*nudicaudatus*	UWBM 35440	Skyscan 1173	65	123	14.2	Al 1.0mm	1150	0.3	4	10
Monodelphis	*domestica**	AMNH 261241	General Electric phoenix v|tome|x			24.34					
Nasua	*narica*	UWBM 41687	SkyScan 1173	65	123	13.4	Al 1.0mm	1170	0.3	4	10
Nasua	*narica*	UWBM 41688	SkyScan 1173	58	125	16.3	Al 1.0mm	1175	0.3	4	10
Nyctinomops	*macrotis**	UMMZ 113271	Nikon XT H 225ST (Duke)	70	114	20	Al 0.5mm		0.25		

Paradoxurus	*hermaphroditus*	UWBM 14711	SkyScan 1173	58	125	15.2	Al 1.0mm	1175	0.3	4	10
Pecari	*tajacu*	UWBM 20670	SkyScan 1173	58	123	15.6	Al 1.0mm	1175	0.3	4	10
Perameles	*nasuta*	UWBM 82259	SkyScan 1173	65	123	16.3	Al 1.0mm	1175	0.3	4	10
Philander	*opossum*	UWBM 44469	SkyScan 1173	58	123	15.6	Al 1.0mm	1175	0.3	4	10
Philander	*opossum*	UWBM 44451	SkyScan 1173	65	123	13.4	Al 1.0mm	1170	0.3	4	10
Philander	*opossum*	UWBM 44452	Skyscan 1173	65	123	14.2	Al 1.0mm	1150	0.3	4	10
Plecotus	*auritus**	UMMZ 111012	Scanco Medical µCT 100	70	114	20	Al 0.5mm		0.25		
Procyon	*lotor*	UWBM 32812	SkyScan 1173	65	123	16.3	Al 1.0mm	1175	0.3	4	10
Procyon	*lotor*	UWBM 32814	Skyscan 1173	65	123	14.2	Al 1.0mm	1150	0.3	4	10
Procyon	*lotor*	UWBM 39819	Skyscan 1173	65	123	13.49	Al 1.0mm	1150	0.3	4	10

Sarcophilus	*harrisii*	UWBM 20671_B	SkyScan 1173	65	123	12.07	Al 1.0mm	1175	0.3	4	10
Scapanus	*orarius*	UWBM 64808	SkyScan 1172	48	208	12.65	Al 0.5mm	1500	0.25	5	20
Scapanus	*orarius*	UWBM 64811	SkyScan 1172	48	208	12.65	Al 0.5mm	1500	0.25	5	20
Scapanus	*orarius*	UWBM 64820	SkyScan 1172	48	208	9.0	Al 0.5mm	735	0.25	5	20
Sorex	*vagrans*	UWBM 58640	SkyScan 1172	48	208	11.21	Al 0.5mm	1170	0.25	5	20
Sorex	*vagrans*	UWBM 58646	SkyScan 1172	48	208	6.78	Al 0.5mm	735	0.25	5	20
Sorex	*vagrans*	UWBM 60640	SkyScan 1172	48	208	11.21	Al 0.5mm	1170	0.25	5	20
Spilogale	*putorius*	UWBM 20192	SkyScan 1173	58	125	15.2	Al 1.0mm	1175	0.3	4	10
Spilogale	*putorius*	UWBM 76080	Skyscan 1173	65	123	13.49	Al 1.0mm	1150	0.3	4	10
Tamias	*townsendii*	UWBM 20077	NSI X5000	70	800	24.1	none				

Tamias	*townsendii*	UWBM 43787	NSI X5000	70	800	24.1	none				
Tamias	*townsendii*	UWBM 44335	NSI X5000	70	800	26.2	none				
Thylamys	*elegans*	UWBM 49057	NSI X5000	70	800	22.7	none				
Thylamys	*elegans*	UWBM 49007	SkyScan 1172	48	208	11.47	Al 0.5mm	1170	0.25	5	20
Aenigmadelphys	*archeri*	OMNH 20160	Skyscan 1172	48	208	3.78	none	200	0.25	5	20
Aenigmadelphys	*archeri*	OMNH 23328	Skyscan 1172	48	208	3.26	none	200	0.25	5	20
Albertatherium	*primum*	UALVP 29611	Skyscan 1172	48	208	8.2	Al 0.5mm	705	0.25	5	20
Albertatherium	*primum*	UALVP 29612	Skyscan 1172	48	208	8.2	Al 0.5mm	705	0.25	5	20
Albertatherium	*secundum*	UALVP 29534	Skyscan 1172	48	208	8.2	Al 0.5mm	705	0.25	5	20
Alphadon	*halleyi*	UCMP 130501	Skyscan 1172	48	208	10.84	Al 0.5mm	1300	0.25	5	20

Alphadon	*marshi*	UCMP 52450	Skyscan 1172	48	208	12.78	Al 0.5mm	1755	0.25	5	20
Alphadon	*marshi*	UCMP 53097	Skyscan 1172	48	208	10.95	Al 0.5mm	1170	0.25	5	20
Alphadon	*sahnii*	OMNH 20114	Skyscan 1172	48	208	3.78	none	200	0.25	5	20
Alphadon	*wilsoni*	UALVP 3532	Skyscan 1172	48	208	7.4	Al 0.5mm	700	0.25	5	20
Anchistodelphys	*archibaldi*	OMNH 21033	Skyscan 1172	48	208	3.78	none	200	0.25	5	20
Apistodon	*exiguus*	UALVP 29693	Skyscan 1172	48	208	7.4	Al 0.5mm	700	0.25	5	20
Atokatheridium	*boreni*	OMNH 61623	Skyscan 1172	48	208	3.52	none	200	0.25	5	20
Dakotadens	*morrowi*	OMNH 49450	Skyscan 1173	40	160	6.04	none	1500	0.2	3	10
Didelphodon	*vorax*	UCMP 187607	Skyscan 1172	48	208	8.59	Al 0.5mm	750	0.25	5	20
Didelphodon	*vorax*	UCMP 47304	Skyscan 1172	48	208	7.69	none	200	0.25	5	20

Eoalphadon	*clemensi*	MNA.V.5387	Skyscan 1172	48	208	8.07	Al 0.5mm	750	0.25	5	20
Eoalphadon	*lillegraveni*	MNA.V.5835	Skyscan 1172	48	208	3.65	none	200	0.25	5	20
Eoalphadon	*woodburnei*	UMNH VP 12842	Skyscan 1172	48	208	6.39	Al 0.5mm	650	0.25	5	20
Glasbius	*intricatus*	UCMP 102111	Skyscan 1172	48	208	12.78	Al 0.5mm	1755	0.25	5	20
Glasbius	*twitchelli*	UCMP 153679	Skyscan 1172	48	208	8.59	Al 0.5mm	750	0.25	5	20
Glasbius	*twitchelli*	UCMP 156143	Skyscan 1172	48	208	8.59	Al 0.5mm	750	0.25	5	20
Glasbius	*twitchelli*	UCMP 224090	Skyscan 1172	48	208	8.59	Al 0.5mm	750	0.25	5	20
Hatcheritherium	*alpha*	YPM.VP.014911	Skyscan 1172	48	208	8.07	Al 0.5mm	750	0.25	5	20
Hatcheritherium	*alpha*	YPM.VP.014912	Skyscan 1172	48	208	8.07	Al 0.5mm	750	0.25	5	20
Iqualadelphis	*lactea*	UALVP 22827	Skyscan 1172	48	208	8.2	Al 0.5mm	705	0.25	5	20

Iqualadelphis	*lactea*	UALVP 29676	Skyscan 1172	48	208	7.14	Al 0.5mm	700	0.25	5	20
Iugomortiferum	*thoringtoni*	OMNH 20936	Skyscan 1172	48	208	3.78	none	200	0.25	5	20
Kokopellia	*juddi*	OMNH 33248	Skyscan 1173	40	160	6.04	none	1500	0.2	3	10
Leptalestes	*cooki*	UCMP 48351	Skyscan 1172	48	208	10.84	Al 0.5mm	1300	0.25	5	20
Leptalestes	*cooki*	UCMP 51344	Skyscan 1172	48	208	8.08	Al 0.5mm	680	0.25	5	20
Leptalestes	*cooki*	UCMP 46306	Skyscan 1172	48	208	12.78	Al 0.5mm	1755	0.25	5	20
Leptalestes	*krejcii*	UCMP 47061	Skyscan 1172	48	208	13.04	Al 0.5mm	1500	0.25	5	20
Leptalestes	*krejcii*	UCMP 47552	Skyscan 1172	48	208	13.04	Al 0.5mm	1500	0.25	5	20
Leptalestes	*krejcii*	UCMP 52761	Skyscan 1173	48	208	12.00	Al 0.5mm	1170	0.25	5	20
Leptalestes	*prokrejcii*	UCMP 131341	Skyscan 1173	48	208	12.00	Al 0.5mm	1170	0.25	5	20

Nortedelphys	*intermedius*	UCMP 134776	Skyscan 1172	48	208	10.95	Al 0.5mm	1170	0.25	5	20
Nortedelphys	*jasoni*	UCMP 174506	Skyscan 1172	48	208	10.84	Al 0.5mm	1300	0.25	5	20
Nortedelphys	*jasoni*	UCMP 177838	Skyscan 1172	48	208	8.59	Al 0.5mm	750	0.25	5	20
Nortedelphys	*magnus*	UALVP 2846	Skyscan 1173	40	160	8.16	none	1500	0.2	3	10
Nortedelphys	*minimus*	UCMP 52715	Skyscan 1172	48	208	10.95	Al 0.5mm	1170	0.25	5	20
Nortedelphys	*minimus*	UCMP 72211	Skyscan 1172	48	208	10.95	Al 0.5mm	1170	0.25	5	20
Pariadens	*kirklandi*	MNA.V.5843	Skyscan 1172	48	208	8.07	Al 0.5mm	750	0.25	5	20
Pediomys	*elegans*	UCMP 47558	Skyscan 1173	48	208	12.00	Al 0.5mm	1170	0.25	5	20
Pediomys	*elegans*	UCMP 51335	Skyscan 1172	48	208	8.08	Al 0.5mm	680	0.25	5	20
Pediomys	*elegans*	UCMP 168701	Skyscan 1172	47	200	11.90	none	200	0.25	5	20

Protalphadon	*foxi*	UCMP 109031	Skyscan 1172	48	208	10.95	Al 0.5mm	1170	0.25	5	20
Protalphadon	*lulli*	UCMP 47446	Skyscan 1172	48	208	12.78	Al 0.5mm	1755	0.25	5	20
Protalphadon	*lulli*	UCMP 47475	Skyscan 1172	48	208	10.95	Al 0.5mm	1170	0.25	5	20
Protolambda	*clemensi*	UALVP 55855	Skyscan 1172	48	208	8.07	Al 0.5mm	700	0.25	5	20
Protolambda	*clemensi*	UCMP 122179	Skyscan 1172	48	208	8.08	Al 0.5mm	680	0.25	5	20
Protolambda	*clemensi*	UCMP 131340	Skyscan 1172	48	208	3.26	Al 0.5mm	200	0.25	5	20
Protolambda	*florencae*	UCMP 186770	Skyscan 1172	48	208	10.84	Al 0.5mm	1300	0.25	5	20
Protolambda	*florencae*	UCMP 48331	Skyscan 1172	48	208	12.78	Al 0.5mm	1755	0.25	5	20
Protolambda	*florencae*	UCMP 51389	Skyscan 1172	48	208	8.08	Al 0.5mm	680	0.25	5	20
Protolambda	*florencae*	UCMP 52323	Skyscan 1173	48	208	12.00	Al 0.5mm	1170	0.25	5	20

Protolambda	*hatcheri*	UCMP 46232	Skyscan 1172	48	208	13.04	Al 0.5mm	1500	0.25	5	20
Protolambda	*hatcheri*	UCMP 47262	Skyscan 1172	48	208	13.04	Al 0.5mm	1500	0.25	5	20
Protolambda	*hatcheri*	UCMP 52404	Skyscan 1172	48	208	13.04	Al 0.5mm	1500	0.25	5	20
Turgidodon	*lillegraveni*	OMNH 20117	Skyscan 1172	48	208	3.78	none	200	0.25	5	20
Turgidodon	*madseni*	OMNH 20538	Skyscan 1172	48	208	6.78	none	200	0.25	5	20
Turgidodon	*praesagus*	UALVP 55849	Skyscan 1172	48	208	7.4	Al 0.5mm	700	0.25	5	20
Turgidodon	*praesagus*	UCMP 122168	Skyscan 1172	48	208	8.08	Al 0.5mm	680	0.25	5	20
Turgidodon	*praesagus*	UCMP 131345	Skyscan 1172	48	208	13.04	Al 0.5mm	1500	0.25	5	20
Turgidodon	*rhaister*	UCMP 47366	Skyscan 1173	48	208	12	Al 0.5mm	1170	0.25	5	20
Turgidodon	*russelli*	UALVP 55852	Skyscan 1172	48	208	8.07	Al 0.5mm	700	0.25	5	20

Turgidodon	*russelli*	UALVP 6983	Skyscan 1172	48	208	8.07	Al 0.5mm	700	0.25	5	20
Varalphadon	*creber*	UALVP 29525	Skyscan 1172	48	208	7.14	Al 0.5mm	700	0.25	5	20
Varalphadon	*creber*	UALVP 29527	Skyscan 1172	48	208	7.14	Al 0.5mm	700	0.25	5	20
Varalphadon	*creber*	UALVP 5529	Skyscan 1172	48	208	7.4	Al 0.5mm	700	0.25	5	20
Varalphadon	*wahweapensis*	UALVP 5544	Skyscan 1172	48	208	7.14	Al 0.5mm	700	0.25	5	20

Appendix 3: Dental topographic analysis (DTA) values for sample of extant mammals

Species	Specimen number	Sex	Specimen type	DNE	RFI	OPCR
Antechinus stuartii	UWBM 68899	m	original	371.95	0.48	115.75
Antechinus stuartii	UWBM 68915	m	original	404.43	0.49	109.38
Antechinus stuartii	UWBM 68916	f	original	414.91	0.58	84.25
Artibeus lituratus	UWBM 62023	m	mold	287.69	0.33	129.38
Artibeus lituratus	UWBM 62030	f	mold	303.45	0.32	159.62
Artibeus lituratus	UWBM 62034	m	mold	224.44	0.31	84.62
Caluromys derbianus	UWBM 32255	?	original	293.24	0.49	100.50
Caluromys sp.	EA 181	?	MorphoSource	203.07	0.43	104.62
Cheirogaleus medius	DLC 1607	m	MorphoSource	191.07	0.35	92.50
Cheirogaleus medius	DLC 1636	m	MorphoSource	177.66	0.31	123.12
Cheirogaleus medius	DLC 3640	f	MorphoSource	166.49	0.38	66.12
Chironectes minimus	MVZ 173550	m	original	184.84	0.50	84.88
Crocuta crocuta	UWBM 33257	?	mold	154.21	0.49	46.38
Dasyurus maculatus	UWBM 68901	m	mold	244.61	0.46	74.88
Didelphis albiventris	UWBM 38710	m	mold	247.47	0.47	87.88
Didelphis marsupialis	UWBM 39942	f	mold	231.12	0.34	103.00
Didelphis marsupialis	UWBM 44459	f	mold	193.54	0.37	99.75
Didelphis virginiana	UWBM 39628	m	mold	272.11	0.43	124.00
Didelphis virginiana	UWBM 76104	m	mold	262.56	0.42	104.75
Didelphis virginiana	UWBM 76135	f	mold	237.79	0.42	107.75
Eira barbara	UWBM 39436	?	mold	131.75	0.31	63.75
Eptesicus fuscus	UWBM 66977	?	original	454.92	0.53	101.88

Eptesicus fuscus	UWBM 66980	?	original	566.38	0.56	103.50
Eptesicus fuscus	UWBM 79331	?	original	456.88	0.53	101.88
Lynx rufus	OUVC 9576	?	MorphoSource	118.42	0.56	33.13
Metachirus nudicaudatus	UWBM 35439	f	mold	189.21	0.33	93.88
Metachirus nudicaudatus	UWBM 35440	m	mold	251.67	0.36	117.38
Metachirus nudicaudatus	UWBM 35438	f	mold	154.26	0.34	103.50
Monodelphis domestica	AMNH 261241	m	MorphoSource	330.53	0.55	106.88
Nasua narica	UWBM 41687	?	mold	171.78	0.39	79.12
Nasua narica	UWBM 41688	f	mold	167.05	0.33	70.00
Nyctinomops macrotis	UMMZ 113271	f	MorphoSource	380.24	0.44	99.50
Paradoxurus hermaphroditus	UWBM 14711	?	mold	264.76	0.28	76.25
Pecari tajacu	UWBM 20670	f	mold	230.91	0.43	106.50
Perameles nasuta	UWBM 82259	m	original	230.42	0.53	61.38
Philander opossum	UWBM 44451	f	mold	227.24	0.37	93.62
Philander opossum	UWBM 44452	m	mold	213.91	0.43	90.38
Philander opossum	UWBM 44469	m	mold	261.51	0.41	95.12
Plecotus auritus	UMMZ 111012	m	MorphoSource	274.67	0.43	73.12
Procyon lotor	UWBM 32812	f	mold	266.00	0.35	97.00
Procyon lotor	UWBM 32814	f	mold	245.53	0.35	94.50
Procyon lotor	UWBM 32819	m	mold	201.61	0.34	75.88
Sarcophilus harrisii	UWBM 20671	m	mold	144.66	0.39	61.50
Scapanus orarius	UWBM 64808	m	original	290.77	0.57	80.25
Scapanus orarius	UWBM 64811	m	original	406.62	0.68	77.75
Scapanus orarius	UWBM 64820	f	original	343.35	0.62	73.25
Sorex vagrans	UWBM 58640	m	original	554.22	0.50	122.75

Sorex vagrans	UWBM 58646	m	original	509.66	0.47	109.50
Sorex vagrans	UWBM 60640	f	original	415.48	0.34	120.38
Spilogale putorius	UWBM 20192	m	mold	200.23	0.31	82.62
Spilogale putorius	UWBM 76080	m	mold	182.53	0.32	95.38
Tamias townsendii	UWBM 20077	m	original	214.20	0.46	80.38
Tamias townsendii	UWBM 43787	m	original	203.30	0.46	80.25
Tamias townsendii	UWBM 44335	f	original	190.31	0.44	75.75
Thylamys elegans	UWBM 49007	f	original	367.46	0.54	105.00
Thylamys elegans	UWBM 49057	f	original	331.34	0.54	98.62

Appendix 4: Dental topographic metrics (DTA) values for sample of NALK metatherians

Species	Specimen	Specimen type	DNE	RFI	OPCR
Aenigmadelphys archeri	OMNH 20160	cast	392.30	0.59	99.62
Aenigmadelphys archeri	OMNH 23328	cast	422.14	0.55	115.88
Albertatherium primum	UALVP 29611	fossil	444.77	0.57	129.88
Albertatherium primum	UALVP 29612	fossil	407.47	0.57	118.50
Albertatherium secundum	UALVP 29534	fossil	388.22	0.53	117.25
Alphadon halleyi	UCMP 130501	fossil	268.97	0.53	91.38
Alphadon marshi	UCMP 52450	fossil	425.40	0.55	126.75
Alphadon marshi	UCMP 53097	fossil	362.59	0.54	113.25
Alphadon sahnii	OMNH 20114	cast	484.49	0.55	125.88
Alphadon wilsoni	UALVP 3532	fossil	285.11	0.52	96.75
Eoalphadon clemensi	MNA.V.5387	cast	290.47	0.51	89.62
Eoalphadon lillegraveni	MNA.V.5835	fossil	285.35	0.45	113.25
Eoalphadon woodburnei	UMNH VP 12842	fossil	375.32	0.55	116.75
Protalphadon foxi	UCMP 109031	fossil	277.24	0.55	93.62
Protalphadon lulli	UCMP 47446	fossil	304.42	0.55	102.25
Protalphadon lulli	UCMP 47475	cast	261.10	0.52	84.00
Turgidodon lillegraveni	OMNH 20117	cast	259.44	0.47	90.75
Turgidodon madseni	OMNH 20538	fossil	458.15	0.56	127.12
Turgidodon praesagus	UALVP 55849	fossil	305.44	0.50	95.38
Turgidodon praesagus	UCMP 122168	fossil	399.86	0.53	128.50
Turgidodon praesagus	UCMP 131345	fossil	310.35	0.60	98.12
Turgidodon rhaister	UCMP 47366	fossil	303.98	0.51	98.88

Turgidodon russelli	UALVP 55852	fossil	316.17	0.50	105.00
Turgidodon russelli	UALVP 6983	fossil	297.67	0.51	100.00
Varalphadon creber	UALVP 29525	fossil	397.10	0.54	111.88
Varalphadon creber	UALVP 29527	fossil	362.53	0.54	102.50
Varalphadon creber	UALVP 5529	fossil	353.74	0.54	110.25
Varalphadon wahweapensis	UALVP 5544	cast	324.02	0.53	95.00
Atokatheridium boreni	OMNH 61623	fossil	251.57	0.52	70.38
Glasbius intricatus	UCMP 102111	fossil	226.32	0.41	93.25
Glasbius twitchelli	UCMP 153679	fossil	190.53	0.42	78.12
Glasbius twitchelli	UCMP 156143	fossil	273.98	0.45	105.12
Glasbius twitchelli	UCMP 224090	fossil	234.74	0.44	86.38
Nortedelphys intermedius	UCMP 134776	fossil	322.45	0.53	95.00
Nortedelphys jasoni	UCMP 174506	fossil	292.72	0.51	97.50
Nortedelphys jasoni	UCMP 177838	fossil	337.70	0.55	102.62
Nortedelphys magnus	UA 2846	cast	367.75	0.53	104.38
Nortedelphys minimus	UCMP 52715	fossil	345.55	0.50	117.38
Nortedelphys minimus	UCMP 72211	fossil	397.74	0.51	113.88
Anchistodelphys archibaldi	OMNH 21033	cast	452.47	0.54	125.62
Apistodon exiguus	UALVP 29693	fossil	315.13	0.53	110.62
Dakotadens morrowi	OMNH 49450	cast	197.22	0.45	72.75
Hatcheritherium alpha	YPM.VP.014911	fossil	326.99	0.48	131.88
Hatcheritherium alpha	YPM.VP.014912	fossil	415.27	0.49	119.50
Iugomortiferum thoringtoni	OMNH 20936	cast	178.56	0.47	66.38
Kokopellia juddi	OMMH 33248	cast	330.91	0.53	103.25
Iqualadelphis lactea	UALVP 22827	fossil	422.06	0.57	105.75

Iqualadelphis lactea	UALVP 29676	fossil	304.89	0.50	100.50
Leptalestes cooki	UCMP 46306	fossil	431.69	0.52	123.00
Leptalestes cooki	UCMP 48351	fossil	315.06	0.50	95.75
Leptalestes cooki	UCMP 51344	fossil	329.62	0.52	102.25
Leptalestes krejcii	UCMP 47061	fossil	302.44	0.53	84.88
Leptalestes krejcii	UCMP 47552	fossil	365.78	0.59	97.88
Leptalestes krejcii	UCMP 52761	fossil	302.57	0.50	80.25
Leptalestes prokrejcii	UCMP 131341	fossil	297.55	0.49	82.88
Pediomys elegans	UCMP 168701	cast	400.49	0.47	129.38
Pediomys elegans	UCMP 47558	fossil	353.77	0.51	110.25
Pediomys elegans	UCMP 51335	fossil	339.73	0.48	100.62
Protolambda clemensi	UALVP 55855	fossil	452.89	0.52	123.00
Protolambda clemensi	UCMP 122179	fossil	382.09	0.56	109.62
Protolambda clemensi	UCMP 131340	cast	409.48	0.51	99.75
Protolambda florencae	UCMP 48331	fossil	367.11	0.50	102.88
Protolambda florencae	UCMP 51389	fossil	347.66	0.54	91.75
Protolambda florencae	UCMP 186770	fossil	396.09	0.52	113.75
Protolambda florencae	UCMP 52323	fossil	319.62	0.48	96.50
Protolambda hatcheri	UCMP 46232	fossil	328.43	0.49	96.12
Protolambda hatcheri	UCMP 47262	fossil	332.33	0.54	94.12
Protolambda hatcheri	UCMP 52404	fossil	279.61	0.51	77.62
Didelphodon vorax	UCMP 187607	fossil	257.68	0.40	100.75
Didelphodon vorax	UCMP 47304	cast	367.07	0.43	110.50
Pariadens kirklandi	MNA.V.5843	fossil	301.52	0.52	113.50

Appendix 5: Posterior probabilities of dietary categories resulting from discriminant function analysis (DFA) for our extant mammal dataset and NALK metatherian dataset using the OPCR parameter minimum patch count = 5.

The highest posterior probability representing the diet identified by DFA is in bold. Posterior probabilities < 0.001 are not reported. Other posterior probabilities that are within 0.10 to the highest posterior probability are marked with an asterisk. Fossil specimens are listed directly after the extant sample. Abbreviations for diet categories: ado = animal-dominated omnivore; carn = carnivore; frug = frugivore; ins = insectivore; pdo = plant-dominated omnivore; sis = soft-insect specialist.

Species	Specimen	diet	frug	pdo	ado	carn	ins	sis
Antechinus stuartii	UWBM 68899	ins	0.006	0.031	0.034	-	**0.629**	0.300
Antechinus stuartii	UWBM 68915	ins	0.001	0.006	0.007	-	**0.709**	0.276
Antechinus stuartii	UWBM 68916	ins	-	0.001	-	-	0.496*	**0.503**
Artibeus lituratus	UWBM 62023	frug	0.441*	0.093	**0.461**	-	0.004	0.001
Artibeus lituratus	UWBM 62030	frug	0.371	0.077	**0.551**	-	0.002	-
Artibeus lituratus	UWBM 62034	frug	**0.708**	0.071	0.210	0.010	0.001	0.001
Caluromys derbianus	UWBM 32255	pdo	0.037	0.258*	0.172	0.010	0.199	**0.325**
Caluromys sp.	EA 181	pdo	0.104	**0.512**	0.364	0.018	-	0.001
Cheirogaleus medius	DLC 1607	frug	**0.471**	0.201	0.280	0.048	-	-
Cheirogaleus medius	DLC 1636	frug	**0.475**	0.143	0.380	0.002	-	-
Cheirogaleus medius	DLC 3640	frug	0.173	0.187	0.108	**0.530**	-	0.001
Chironectes minimus	MVZ 173550	carn	0.031	**0.641**	0.170	0.156	-	0.002
Crocuta crocuta	UWBM 33257	carn	0.002	0.017	0.002	**0.977**	-	0.002
Dasyurus maculatus	UWBM 68901	carn	0.088	**0.387**	0.211	0.099	0.041	0.175
Didelphis albiventris	UWBM 38710	ado	0.078	**0.505**	0.294	0.037	0.022	0.064

Didelphis marsupialis	UWBM 39942	pdo	**0.430**	0.171	0.393*	0.004	0.001	0.001
Didelphis marsupialis	UWBM 44459	pdo	0.305*	0.297*	**0.382**	0.016	-	-
Didelphis virginiana	UWBM 39628	ado	0.124	0.370	**0.484**	0.002	0.011	0.009
Didelphis virginiana	UWBM 76104	ado	0.150	0.377*	**0.435**	0.007	0.015	0.017
Didelphis virginiana	UWBM 76135	ado	0.147	0.409*	**0.431**	0.008	0.002	0.003
Eira barbara	UWBM 39436	carn	0.408*	0.090	0.088	**0.414**	-	-
Eptesicus fuscus	UWBM 66977	ins	-	-	-	-	**0.704**	0.295
Eptesicus fuscus	UWBM 66980	ins	-	-	-	-	**0.804**	0.196
Eptesicus fuscus	UWBM 79331	ins	-	-	-	-	**0.713**	0.286
Lynx rufus	OUVC 9576	carn	-	-	-	**0.999**	-	-
Metachirus nudicaudatus	UWBM 35439	ado	**0.501**	0.158	0.333	0.008	-	-
Metachirus nudicaudatus	UWBM 35440	ado	0.327	0.195	**0.474**	0.002	0.002	0.001
Metachirus nudicaudatus	UWBM 35438	ado	**0.355**	0.278*	0.343*	0.023	-	-
Monodelphis domestica	AMNH 261241	ado	0.007	0.149	0.082	0.001	0.373*	**0.388**
Nasua narica	UWBM 41687	frug	0.206	**0.336**	0.210	0.248	-	0.001
Nasua narica	UWBM 41688	frug	**0.474**	0.140	0.155	0.230	-	-
Nyctinomops macrotis	UMMZ 113271	sis	0.007	0.012	0.020	-	**0.679**	0.282
Paradoxurus hermaphroditus	UWBM 14711	frug	**0.840**	0.022	0.111	0.006	0.012	0.010
Pecari tajacu	UWBM 20670	frug	0.120	**0.442**	0.429*	0.007	0.001	0.002
Perameles nasuta	UWBM 82259	ins	0.016	0.268*	0.064	0.273	0.029	**0.350**
Philander opossum	UWBM 44451	ado	0.328*	0.270	**0.380**	0.017	0.002	0.003
Philander opossum	UWBM 44452	ado	0.131	**0.487**	0.315	0.059	0.002	0.007
Philander opossum	UWBM 44469	ado	0.213	0.321*	**0.409**	0.011	0.021	0.026
Plecotus auritus	UMMZ 111012	sis	0.060	0.103	0.080	0.041	0.176	**0.538**
Procyon lotor	UWBM 32812	ado	**0.458**	0.145	0.375*	0.004	0.011	0.008

Procyon lotor	UWBM 32814	ado	**0.424**	0.177	0.388*	0.005	0.003	0.003
Procyon lotor	UWBM 32819	ado	**0.525**	0.166	0.252	0.054	-	0.001
Sarcophilus harrisii	UWBM 20671	carn	0.056	0.086	0.033	**0.825**	-	-
Scapanus orarius	UWBM 64808	sis	0.002	0.068	0.019	0.011	0.167	**0.733**
Scapanus orarius	UWBM 64811	sis	-	-	-	-	0.302	**0.698**
Scapanus orarius	UWBM 64820	sis	-	0.002	0.001	-	0.209	**0.788**
Sorex vagrans	UWBM 58640	ins	-	-	-	-	**0.911**	0.089
Sorex vagrans	UWBM 58646	ins	-	-	-	-	**0.858**	0.142
Sorex vagrans	UWBM 60640	ins	0.102	0.016	0.107	-	**0.721**	0.054
Spilogale putorius	UWBM 20192	ado	**0.675**	0.091	0.214	0.020	-	-
Spilogale putorius	UWBM 76080	ado	**0.543**	0.149	0.295	0.014	-	-
Tamias townsendii	UWBM 20077	pdo	0.087	**0.401**	0.173	0.276	0.007	0.056
Tamias townsendii	UWBM 43787	pdo	0.083	**0.515**	0.221	0.168	0.002	0.011
Tamias townsendii	UWBM 44335	pdo	0.101	**0.398**	0.172	0.321*	0.001	0.007
Thylamys elegans	UWBM 49007	ins	0.002	0.024	0.016	-	**0.541**	0.417
Thylamys elegans	UWBM 49057	ins	0.007	0.131	0.075	0.001	0.385*	**0.401**
Aenigmadelphys archeri	OMNH 20160	-	-	0.005	0.002	-	**0.522**	0.471*
Aenigmadelphys archeri	OMNH 23328	-	-	0.006	0.005	-	**0.724**	0.265
Albertatherium primum	UALVP 29611	-	-	0.005	0.004	-	**0.785**	0.205
Albertatherium primum	UALVP 29612	-	0.001	0.017	0.012	-	**0.698**	0.273
Albertatherium secundum	UALVP 29534	-	0.002	0.030	0.025	-	**0.662**	0.282
Alphadon halleyi	UCMP 130501	-	0.027	**0.526**	0.230	0.017	0.058	0.142
Alphadon marshi	UCMP 52450	-	0.001	0.017	0.015	-	**0.777**	0.191
Alphadon marshi	UCMP 53097	-	0.005	0.081	0.059	-	**0.549**	0.306
Alphadon sahnii	OMNH 20114	-	-	0.001	0.001	-	**0.850**	0.148

Alphadon wilsoni	UALVP 3532	-	0.028	**0.403**	0.209	0.010	0.123	0.227
Eoalphadon clemensi	MNA.V.5387	-	0.028	**0.369**	0.206	0.008	0.147	0.242
Eoalphadon lillegraveni	MNA.V.5835	-	0.080	0.417*	**0.452**	0.002	0.028	0.021
Eoalphadon woodburnei	UMNH VP 12842	-	0.004	0.086	0.064	-	**0.594**	0.253
Protalphadon foxi	UCMP 109031	-	0.015	**0.450**	0.163	0.015	0.098	0.259
Protalphadon lulli	UCMP 47446	-	0.011	0.295*	0.130	0.005	0.215	**0.345**
Protalphadon lulli	UCMP 47475	-	0.028	**0.410**	0.160	0.044	0.075	0.285
Turgidodon lillegraveni	OMNH 20117	-	0.069	**0.440**	0.258	0.035	0.053	0.144
Turgidodon madseni	OMNH 20538	-	-	0.002	0.002	-	**0.789**	0.207
Turgidodon praesagus	UALVP 55849	-	0.023	0.229	0.146	0.005	0.252*	**0.344**
Turgidodon praesagus	UCMP 122168	-	0.002	0.036	0.035	-	**0.714**	0.212
Turgidodon praesagus	UCMP 131345	-	0.004	0.220	0.073	0.003	0.243	**0.458**
Turgidodon rhaister	UCMP 47366	-	0.025	**0.341**	0.213	0.004	0.191	0.226
Turgidodon russelli	UALVP 55852	-	0.028	**0.278**	0.213	0.002	0.255*	0.225*
Turgidodon russelli	UALVP 6983	-	0.025	**0.320**	0.185	0.006	0.187	0.278*
Varalphadon creber	UALVP 29525	-	0.001	0.018	0.015	-	**0.679**	0.287
Varalphadon creber	UALVP 29527	-	0.002	0.037	0.024	-	**0.536**	0.400
Varalphadon creber	UALVP 5529	-	0.004	0.076	0.048	-	**0.502**	0.369
Varalphadon wahweapensis	UALVP 5544	-	0.008	0.125	0.072	0.002	0.357*	**0.435**
Atokatheridium boreni	OMNH 61623	-	0.019	0.214	0.069	0.108	0.075	**0.516**
Glasbius intricatus	UCMP 102111	-	0.198	**0.393**	0.374	0.027	0.003	0.006
Glasbius twitchelli	UCMP 153679	-	0.154	**0.439**	0.257	0.147	-	0.002
Glasbius twitchelli	UCMP 156143	-	0.094	**0.429**	0.412*	0.005	0.029	0.032
Glasbius twitchelli	UCMP 224090	-	0.122	**0.477**	0.342	0.034	0.007	0.018
Nortedelphys intermedius	UCMP 134776	-	0.008	0.146	0.080	0.002	0.342*	**0.422**

Nortedelphys jasoni	UCMP 174506	-	0.029	**0.331**	0.193	0.008	0.168	0.270*
Nortedelphys jasoni	UCMP 177838	-	0.005	0.111	0.060	0.001	0.411*	**0.412**
Nortedelphys magnus	UA 2846	-	0.003	0.042	0.032	-	**0.576**	0.347
Nortedelphys minimus	UCMP 52715	-	0.018	0.187	0.173	0.001	**0.414**	0.208
Nortedelphys minimus	UCMP 72211	-	0.002	0.019	0.020	-	**0.708**	0.251
Anchistodelphys archibaldi	OMNH 21033	-	-	0.003	0.003	-	**0.806**	0.188
Apistodon exiguus	UALVP 29693	-	0.019	**0.367**	0.232	0.002	0.201	0.179
Dakotadens morrowi	OMNH 49450	-	0.086	**0.451**	0.185	0.265	0.001	0.012
Hatcheritherium alpha	YPM.VP.014911	-	0.046	0.335*	**0.388**	0.001	0.161	0.069
Hatcheritherium alpha	YPM.VP.014912	-	0.003	0.020	0.029	-	**0.787**	0.161
Iugomortiferum thoringtoni	OMNH 20936	-	0.047	**0.454**	0.132	0.365*	-	0.003
Kokopellia juddi	OMMH 33248	-	0.010	0.150	0.094	0.001	**0.383**	0.362*
Iqualadelphis lactea	UALVP 22827	-	-	0.003	0.002	-	**0.650**	0.345
Iqualadelphis lactea	UALVP 29676	-	0.027	**0.283**	0.187*	0.005	0.224*	0.275*
Leptalestes cooki	UCMP 46306	-	0.001	0.009	0.011	-	**0.806**	0.173
Leptalestes cooki	UCMP 48351	-	0.017	0.148	0.099	0.003	0.324*	**0.408**
Leptalestes cooki	UCMP 51344	-	0.008	0.089	0.057	0.002	0.396*	**0.448**
Leptalestes krejcii	UCMP 47061	-	0.007	0.090	0.041	0.007	0.250	**0.605**
Leptalestes krejcii	UCMP 47552	-	-	0.011	0.004	-	0.429	**0.555**
Leptalestes krejcii	UCMP 52761	-	0.009	0.066	0.036	0.008	0.264	**0.618**
Leptalestes prokrejcii	UCMP 131341	-	0.017	0.123	0.072	0.010	0.250	**0.528**
Pediomys elegans	UCMP 168701	-	0.009	0.045	0.074	-	**0.731**	0.142
Pediomys elegans	UCMP 47558	-	0.008	0.085	0.070	-	**0.522**	0.315
Pediomys elegans	UCMP 51335	-	0.018	0.113	0.107	0.001	**0.457**	0.304
Protolambda clemensi	UALVP 55855	-	-	0.002	0.002	-	**0.802**	0.193

Protolambda clemensi	UCMP 122179	-	0.001	0.030	0.020	-	**0.613**	0.335
Protolambda clemensi	UCMP 131340	-	-	0.003	0.003	-	**0.661**	0.333
Protolambda florencae	UCMP 186770	-	0.004	0.031	0.028	-	**0.589**	0.347
Protolambda florencae	UCMP 48331	-	0.001	0.015	0.008	0.001	0.399	**0.577**
Protolambda florencae	UCMP 51389	-	0.001	0.012	0.012	-	**0.680**	0.295
Protolambda florencae	UCMP 52323	-	0.022	0.113	0.093	0.003	0.367*	**0.403**
Protolambda hatcheri	UCMP 46232	-	0.018	0.121	0.101	0.002	**0.401**	0.356*
Protolambda hatcheri	UCMP 47262	-	0.003	0.054	0.027	0.001	0.379	**0.536**
Protolambda hatcheri	UCMP 52404	-	0.013	0.137	0.057	0.025	0.165	**0.603**
Didelphodon vorax	UCMP 187607	-	0.202	0.330*	**0.437**	0.007	0.011	0.012
Didelphodon vorax	UCMP 47304	-	0.030	0.057	0.105	-	**0.616**	0.191
Pariadens kirklandi	MNA.V.5843	-	0.024	**0.489**	0.309	0.002	0.091	0.084

CHAPTER 5: CONCLUDING REMARKS

The studies of this dissertation use anatomical data and quantitative analyses to reassess the phylogenetic relationships among metatherian mammals and, more specifically, investigate evolutionary patterns of feeding ecologies of Late Cretaceous-aged North American metatherians. Metatherians diversified into a wide range of dietary niches during the Late Cretaceous—more so than other contemporaneous mammal groups or than has previously been appreciated. However, even with the addition of new data for *Alphadon*, our understanding of the origin of crown marsupials remains muddled. Taking into consideration the studies presented in the chapters above, important aspects of evolution and ecomorphology of this clade have been elucidated. Here, I summarize the major conclusions from each study.

Chapter 2

- The metatherian fossils from Egg Mountain represent some of the most complete skulls of any North American marsupialiform from the Cretaceous. Fourteen previously unknown character scores were updated for *Alphadon* and a subsequent parsimony analysis was conducted to reassess the phylogenetic relationships among metatherians.
- Much of the marsupialiform tree is unstable; we recover a different topology than the most recent analyses that focus on fossil metatherian taxa.
- *Holoclemensia*, a taxon most recently found to be at the base of the metatherian tree, is recovered as a stem eutherian or at the base of Eutheria.
- The Pediomyidae and Stagodontidae are phylogenetically robust; they are resolved as monophyletic groups, as in previous studies.

- Crown marsupials, North American marsupialiforms, and South American marsupialiforms are recovered as a polytomy; our results demonstrate the overall instability of the metatherian tree, and the origin of crown marsupials remains unclear.

Chapter 3

- *Eodelphis browni* was better suited to withstand dorsoventral forces and likely preyed on insects and small vertebrates. It likely was not capable of hard-object feeding, as it does not show any dorsoventral buttressing at the crushing locus or any mediolateral buttressing.
- *Eodelphis cutleri* was better suited for durophagy than *Eodelphis browni*, but less so than *Didelphodon*. *Eodelphis cutleri* shows patterns of dorsoventral buttressing from the canine to the p2–p3 and mediolateral buttressing in the anterior region of the dentary.
- There are two possible scenarios for the evolution of durophagy within the Stagodontidae: (1) a suite of morphological changes associated with durophagy evolved twice within stagodontids (once in *Eodelphis cutleri* and once in the most recent common ancestor of *Didelphodon coyi* and *Didelphodon vorax*; or (2) *Eodelphis* is paraphyletic, and a suite of morphological changes associated with durophagy evolved in the most recent common ancestor of *Eodelphis cutleri* and *Didelphodon*.
- Bending strength analysis of dentaries, which is independent of dental shape analyses, is an important tool for constraining dietary inferences of extinct mammals and should be considered when interpreting diet for fossil taxa.
- A broad range of morphologies of the dentary among Cretaceous metatherians was present that, at minimum, hint at a correspondingly broad range of biomechanical capabilities and feeding ecologies among these taxa. This study adds to the growing

consensus that Mesozoic mammals were more ecomorphologically diverse than previously thought.

Chapter 4

- Although three-dimensional dental topographic analysis has most often been applied to lower molars, we determined that this technique can also be reliably applied to upper molars.
- Our results show that many North American Late Cretaceous metatherians were insectivorous; however, the analyses also indicate that early metatherians exhibited a broad range of diets: insectivory, soft-insect specialists, carnivory, animal- and plant-dominated omnivory and likely frugivory.
- Dental disparity of metatherians did not significantly increase in the Late Cretaceous, contrary to our predictions.
- Our diet reconstructions and those from previous studies of taxa not sampled in our study show that NALK metatherians diversified into a wide range of dietary niches—more so than any other contemporary mammalian clade. Relative to other mammalian clades, both dental disparity and dietary diversity of metatherians were moderately high and stable throughout the Late Cretaceous.
- Metatherians underwent a pre-Cretaceous-Paleogene ecological diversification prior to the ecological diversification of angiosperms. We hypothesize that the metatherian ecological diversification was more correlated in time with the Cretaceous Terrestrial Revolution (ca. 125–80 Ma) and the mid-Cretaceous taxonomic diversification of angiosperms.